Metabolic Study of New Psychoactive Substances

by

Shimpei Watanabe

A thesis submitted for the

Degree of Doctor of Philosophy (Science)

University of Technology, Sydney

2018

Certificate of original authorship

I certify that the work in this thesis has not previously been submitted for a degree nor has it been submitted as part of requirements for a degree except as part of the collaborative doctoral degree and/or fully acknowledged within the text.

I also certify that the thesis has been written by me. Any help that I have received in my research work and the preparation of the thesis itself has been acknowledged. In addition, I certify that all information sources and literature used are indicated in the thesis.

Signature of Student: Shimpei Watanabe

Production Note:
Signature removed prior to publication.

Date: 10/01/2018

Acknowledgments

I would like to express my sincere gratitude to my supervisor Associate Professor Shanlin Fu for all your support and guidance. Your kind and cheerful manner was always encouraging and I would particularly like to thank you for the patience you had for me, which enabled me to finally reach the last stage of the challenging but rewarding journey.

To my co-supervisor, Dr Unnikrishnan Kuzhiumparambil, I would like to thank you for your various support in the lab, outside the lab and outside the university. You have been my mentor for research and beyond.

To the Swedish National Board of Forensic Medicine (Rättsmedicinalverket) and the Strategic Research Area Forensic Sciences (Strategiområdet Forensiska Vetenskaper) at Linköping University, particularly Dr Ariane Wohlfarth, Dr Robert Kronstrand, Dr Svante Vikingsson and Dr Henrik Green, I wish to thank you for the warm welcome in Sweden. The opportunity gave a whole new dimension to my project and enriched my cultural experience.

I would like to thank Advanced Chemistry Development (ACD/Labs) for providing MetaSense™ software as well as Richard Lee and Edward Milton for their help.

I thank you to all the academic and professional staff at UTS who supported me throughout my candidature. I wish to thank Jane Cameron and Zofia Winiarski for the support with the fungus study and allowing me the access to the incubation facility. Thank you to Dr Ronald Shimmon for providing the knowledge of synthetic techniques and support with the NMR and the laboratories. I also wish to thank Dr David Bishop and Dr Verena Taudte for the technical support with LC-MS instruments.

To Mahmoud El Safadi, thank you for the support with the synthesis. To Dr Susan Luong and Dr Anna Molnar, thank you for the tips for LC-MS use and PhD life. I also wish to thank Daniel Pasin, Morgan Philp and the forensic toxicology research group for providing valuable feedback at a number of occasions.

I would also like to thank Professor Claude Roux and Centre for Forensic Science for providing support, particularly with the attendance of conferences.

Finally, to all my friends and family, thank you for all your support, encouragement and fun times.

Publications

The following publications are reproduced in this thesis with the permission from the publishers (1. License Number, 4164621167361; 2. Creative Commons Attribution License (CC BY), https://creativecommons.org/licenses/by/4.0/; 3. License Number, 4164631017507; 4. License Number, 4164640139178):

For Chapter 2

1. Watanabe S, Kuzhiumparambil U, Winiarski Z, Fu S. Biotransformation of synthetic cannabinoids JWH-018, JWH-073 and AM2201 by Cunninghamella elegans. Forensic Sci Int. 2016;261:33-42. doi:http://dx.doi.org/10.1016/j.forsciint.2015.12.023.

2. Watanabe S, Kuzhiumparambil U, Winiarski Z, Fu S. Data on individual metabolites of synthetic cannabinoids JWH-018, JWH-073 and AM2201 by Cunninghamella elegans. Data Brief. 2016;7:332-40. doi:10.1016/j.dib.2016.02.039.

For Chapter 3

3. Watanabe S, Kuzhiumparambil U, Nguyen MA, Cameron J, Fu S. Metabolic Profile of Synthetic Cannabinoids 5F-PB-22, PB-22, XLR-11 and UR-144 by Cunninghamella elegans. AAPS Journal. 2017;19(4):1148-62. doi:10.1208/s12248-017-0078-4.

For Chapter 6

4. Watanabe S, Vikingsson S, Roman M, Green H, Kronstrand R, Wohlfarth A. In Vitro and In Vivo Metabolite Identification Studies for the New Synthetic Opioids Acetylfentanyl, Acrylfentanyl, Furanylfentanyl, and 4-Fluoro-Isobutyrylfentanyl. AAPS Journal. 2017;19(4):1102-22. doi:10.1208/s12248-017-0070-z.

Table of Contents

Certificate of original authorship ii

Acknowledgments iii

Publications v

List of figures xi

List of tables xiv

Abstract xvii

Chapter 1: Introduction 1

1.1 New Psychoactive Substances 2

1.1.1 Synthetic cannabinoids 3

1.1.2 Fentanyl analogues 7

1.2 Metabolism 8

1.2.1 Metabolism models 8

1.2.2 Metabolism studies 10

1.2.2.1 JWH-018 10

1.2.2.2 JWH-073 11

1.2.2.3 JWH-081 11

1.2.2.4 JWH-122 12

1.2.2.5 JWH-210 12

1.2.2.6 JWH-250 12

1.2.2.7 HU-210 12

1.2.2.8 RCS-4 12

1.2.2.9 AM2201 and UR-144 13

1.2.2.10 Potential common metabolite 13

1.3 Instruments 15

1.3.1 Liquid chromatography – mass spectrometry 15

1.3.2 Nuclear magnetic resonance spectroscopy 15

1.3.3 Detection of synthetic cannabinoids and their metabolites 16

1.4 Aims of this project 18

1.4 References 20

Chapter 2: Biotransformation of synthetic cannabinoids JWH-018, JWH-073 and AM2201 by *Cunninghamella elegans* 30

2.1 Abstract ... 31
2.2 Introduction ... 33
2.3 Materials and Methods ... 35
2.3.1 Chemicals ... 35
2.3.2 Microbial Culture and Biotransformation Conditions ... 35
2.3.3 Extraction, Isolation, and Identification of Metabolites ... 36
2.4 Results ... 38
2.4.1 JWH-018 ... 40
2.4.2 JWH-073 ... 41
2.4.3 AM2201 ... 45
2.5 Discussion ... 49
2.6 Conclusion ... 53
2.7 References ... 54
2.8. Appendices ... 59
Chapter 3: Metabolic profile of synthetic cannabinoids 5F-PB-22, PB-22, XLR-11 and UR-144 by *Cunninghamella elegans* ... 75
3.1 Abstract ... 76
3.2 Introduction ... 78
3.3 Materials and Methods ... 81
3.3.1 Chemicals and reagents ... 81
3.3.2 Biotransformation by fungus and sample preparation ... 81
3.3.3 LC-QTOF analysis ... 82
3.3.4 LC-QqQ analysis ... 83
3.4 Results ... 84
3.4.1 5F-PB-22 ... 84
3.4.2 PB-22 ... 84
3.4.3 XLR-11 ... 90
3.4.4 UR-144 ... 93
3.5 Discussion ... 96
3.5.1 Metabolite identification ... 96
3.5.1.1 5F-PB-22 ... 96
3.5.1.2 PB-22 ... 97
3.5.1.3 XLR-11 ... 99
3.5.1.4 UR-144 ... 101
3.5.2 Comparison of fungal metabolites with reported human metabolites ... 102

3.5.3 Comparison of fungal model with *in vitro* human models 104
3.6 Conclusion 106
3.7 References 107
3.8. Appendices 114
Chapter 4: Structural elucidation of metabolites of synthetic cannabinoid UR-144 by *Cunninghamella elegans* using nuclear magnetic resonance spectroscopy 121
4.1 Abstract 122
4.2 Introduction 124
4.3 Materials and methods 127
4.3.1 Chemicals and reagents 127
4.3.2 Fungus metabolite characterisation 127
4.3.2.1 Fungus incubation 127
4.3.2.2 Preparative high performance liquid chromatography (HPLC) 127
4.3.2.3 NMR spectroscopy 128
4.3.2.4 Liquid chromatography – quadrupole time-of-flight mass spectrometry (LC-QTOF-MS) 128
4.3.3 HLM metabolite characterisation 129
4.3.3.1 HLM incubation 129
4.3.3.2 LC-QTOF-MS 129
4.4 Results 130
4.4.1 Fungus metabolite characterisation 130
4.4.1.1 NMR analysis 131
4.4.2 HLM metabolite characterisation 131
4.5 Discussion 136
4.5.1 Fungus metabolite characterisation 136
4.5.1.1 NMR analysis 136
4.5.1.1.1 UR-144 136
4.5.1.1.2 Dihydroxy metabolites M1-3 (U7) 136
4.5.1.1.3 Hydroxy and ketone metabolite M7 (U14) 138
4.5.1.1.4 Carboxy and hydroxy metabolites M4-6 (U10) and M8-9 (U15) 138
4.5.1.1.5 Carboxy and ketone metabolite M10 (U17) 139
4.5.2 HLM metabolite characterisation 140
4.5.3 Advantages and disadvantages of the fungus metabolism 140
4.6 Conclusion 142

4.7 References 143

Chapter 5: *In vitro* metabolism of synthetic cannabinoid AM1220 by human liver microsomes and *Cunninghamella elegans* using liquid chromatography coupled with high resolution mass spectrometry 146

5.1 Abstract 147
5.2 Introduction 149
5.3 Materials and Methods 151
5.3.1 Chemicals and reagents 151
5.3.2 Metabolic stability 151
5.3.3 Metabolite identification 153
5.3.3.1 *Human liver microsomes incubation* 153
5.3.3.2 *Fungus incubation* 153
5.3.3.3 *LC-QTOF-MS* 153
5.4 Results 155
5.4.1 Metabolic stability 155
5.4.2 Metabolite identification 155
5.4.2.1 *AM1220 identification by LC-QTOF-MS* 157
5.4.2.2 *Human liver microsomes* 159
5.4.2.3 *Fungus C. elegans* 159
5.5 Discussion 160
5.5.1 Metabolic stability 160
5.5.2 Metabolite identification 160
5.5.2.1 Hydroxylation 160
5.5.2.2 Dihydroxylation 161
5.5.2.3 Dihydrodiol formation 161
5.5.2.4 Demethylation 161
5.5.2.5 Dihydrodiol formation and demethylation 162
5.5.3 Comparison of AM1220 metabolites in HLM and *C. elegans* with *in vivo* human metabolites 162
5.5.4 Suggested biomarkers 163
5.6 Conclusion 164
5.7 References 165

Chapter 6: *In vitro* and *in vivo* metabolite identification studies for the new synthetic opioids acetylfentanyl, acrylfentanyl, furanylfentanyl, and 4-fluoro-isobutyrylfentanyl 170

6.1 Abstract 171

6.2 Introduction 173
6.3 Materials and Methods 175
6.3.1 Chemicals and reagents 175
6.3.2 Incubation with human hepatocytes and sample preparation 176
6.3.3 Authentic human urine specimens and sample preparation 176
6.3.4 LC-QTOF analysis 177
6.3.5 Manual and software-assisted data analysis 177
6.4 Results 179
6.4.1 Metabolic profile of acetylfentanyl 179
6.4.2 Metabolic profile of acrylfentanyl 186
6.4.3 Metabolic profile of 4-fluoro-isobutyrylfentanyl 191
6.4.4 Metabolic profile of furanylfentanyl 191
6.5 Discussion 201
6.5.1 Structural elucidation of metabolites 201
6.5.1.1 Acetylfentanyl metabolites 201
6.5.1.2 Acrylfentanyl metabolites 204
6.5.1.3 4-Fluoro-isobutyrylfentanyl metabolites 205
6.5.1.4 Furanylfentanyl metabolites 206
6.5.2 How well did hepatocyte study results correlate with the findings in human urine samples? 207
6.5.3 Which metabolites are suitable analytical targets for urine analysis? 208
6.5.4 Is the metabolism of the new fentanyl analogues consistent with previous findings? 210
6.6 Conclusion 211
6.7 References 212
6.8 Appendices 216
Chapter 7: Conclusions and recommendations for further work 220

List of figures

Figure 1-1. Structures of some synthetic cannabinoids.

Figure 2-1. Product ion spectra (CE 20 eV) and the proposed fragmentation pathways for JWH-018, JWH-073, AM2201 and their most abundant metabolites (Ma15, Mb13 and Mc25).

Figure 2-2. Overlaid extracted ion chromatograms of all the metabolites identified in the fungus sample of JWH-018 at *m/z* 306, 340, 356, 358, 372, 374, 376, 390, 392 (**a**); JWH-073 at *m/z* 306, 326, 342, 344, 358, 360, 362, 376, 378 (**b**); and AM2201 at *m/z* 306, 328, 342, 358, 372, 374, 376, 388, 392, 394, 408, 410, 426, 472, 538, 554 (**c**). Only the major metabolites are labelled for AM2201 (**c**).

Figure 2-3. Proposed metabolic pathway of JWH-018 in *C. elegans*.

Figure 2-4. Proposed metabolic pathway of JWH-073 in *C. elegans*.

Figure 2-5. Proposed metabolic pathway of AM2201 in *C. elegans*. Parentheses indicate intermediate metabolites that were not detected in the study.

Figure 3-1. MS/MS spectra obtained with CE 20 eV and structures with the suggested fragmentation patterns and their exact masses for the parent drugs (5F-PB-22, PB-22, XLR-11 and UR-144) and their most abundant fungal metabolites based on peak area (F10, P13, X21 and U7). The exact position of the dihydrodiol structure within quinoline moiety in F10 is not determined.

Figure 3-2. Combined extracted ion chromatograms of all metabolites and their respective parent drugs for (**a)** 5F-PB-22, (**b)** PB-22, (**c**) XLR-11, and (**d)** UR-144 after incubation with *C. elegans*.

Figure 3-3. Proposed metabolic pathway of 5F-PB-22 by *C. elegans*. Blue colour denotes a Phase II metabolite. Parenthesis represents a possible intermediate metabolite that was not detected in the study. For the metabolites with dihydrodiol structure, only one possible isomer is shown as a representative.

Figure 3-4. Proposed metabolic pathway of PB-22 by *C. elegans*. Blue colour denotes Phase II metabolites. Parentheses represent possible intermediate metabolites that were

not detected in the study. For the metabolites with dihydrodiol structure, only one possible isomer is shown as a representative.

Figure 3-5. Proposed metabolic pathway of XLR-11 by *C. elegans*. Blue colour denotes Phase II metabolites.

Figure 3-6. Proposed metabolic pathway of UR-144 by *C. elegans*.

Figure 4-1. The structures of UR-144 and the metabolites analysed in this study. Brackets indicate the metabolite ID in chapter 3 [14]. Arrows indicate partial metabolic pathways. M2 and M3, M5 and M6, and M8 and M9 are diastereomers, respectively, and share the same structures apart from the spatial configurations at the stereo centres.

Figure 4-2. Preparative HPLC chromatogram showing separation of fractions 1-6. Fraction 2 and 3 partially coeluted.

Figure 4-3. Gradient correlation spectroscopy (gCOSY), gradient heteronuclear multiple bond correlation (gHMBC) and selected nuclear overhauser effect (NOE) correlations of UR-144 and the metabolites analysed in the study.

Figure 5-1. Combined extracted ion chromatograms of AM1220 and its metabolites in HLM and fungus incubation.

Figure 5-2. MS/MS spectra of AM1220 and its metabolites at collision energy of 20 eV, and proposed metabolite structures with exact masses of fragmentation. Metabolites in brackets did not show all the product ions. The exact location of dihydrodiol is not determined.

Figure 5-3. Proposed metabolic pathway of AM1220 in HLM and fungus *C. elegans* incubation in comparison with postmortem human data from the literature [10]. HP and HU refer to human plasma and human urine samples while asterisk indicates that the origin of the metabolite is not confirmed to be AM1220. The exact position of dihydrodiol is not determined.

Figure 6-1. Structures of fentanyl and analogues that have approved medicinal use, others that have been abused for several decades, and those that appeared recently on the illicit drug market.

Figure 6-2. Proposed metabolic pathway of acetylfentanyl combining both human hepatocyte and human urine metabolites. Markush structures are used where the exact

position of functional groups cannot be determined. Enclosed metabolites are the major metabolites detected in hydrolysed human urine samples; metabolites in italics were only found in either the *in vitro* or *in vivo* experiment.

Figure 6-3. Proposed metabolic pathway of acrylfentanyl combining both human hepatocyte and human urine metabolites. Markush structures are used where the exact position of functional groups cannot be determined. Enclosed metabolites are the major metabolites detected in hydrolysed human urine samples, metabolite in italics were only found in either the *in vitro* or *in vivo* experiment.

Figure 6-4. Proposed metabolic pathway of 4-fluoro-isobutyrylfentanyl combining both human hepatocyte and human urine metabolites. Markush structures are used where the exact position of functional groups cannot be determined. Enclosed metabolites are the major metabolites detected in hydrolysed human urine samples, metabolite in italics were only found in either the *in vitro* or *in vivo* experiment.

Figure 6-5. Proposed metabolic pathway of furanylfentanyl combining both human hepatocyte and human urine metabolites. Markush structures are used where the exact position of functional groups cannot be determined. Enclosed metabolites are the major metabolites detected in hydrolysed human urine samples, metabolite in italics were only found in either the *in vitro* or *in vivo* experiment.

Supplementary Figure 6-1. MS/MS spectra and proposed fragmentation pattern of acetylfentanyl and its major metabolites in hydrolysed human urine samples.

Supplementary Figure 6-2. MS/MS spectra and proposed fragmentation pattern of acrylfentanyl and its major metabolites in hydrolysed human urine samples.

Supplementary Figure 6-3. MS/MS spectra and proposed fragmentation pattern of 4-fluoroisobutyryllfentanyl and its major metabolites in hydrolysed human urine samples.

Supplementary Figure 6-4. MS/MS spectra and proposed fragmentation pattern of furanylfentanyl and its major metabolites in hydrolysed human urine samples.

List of tables

Table 2-1. Metabolites of JWH-018 after *C. elegans* incubation in comparison with metabolites from other sources (human urine, human liver microsomes and rat urine) reported in literature, in alphabetical order. Square brackets in the metabolites column indicate the corresponding fungal metabolites in Fig. 2-3.

Table 2-2. Metabolites of JWH-073 after *C. elegans* incubation in comparison with metabolites from other sources (human urine and human liver microsomes) reported in literature, in alphabetical order. Square brackets in the metabolites column indicate the corresponding fungal metabolites in Fig. 2-4.

Table 2-3. Metabolites of AM2201 after *C. elegans* incubation in comparison with metabolites from other sources (human urine, human postmortem heart blood, human liver microsomes and rat urine) reported in literature, in alphabetical order. Square brackets in the metabolites column indicate the corresponding fungal metabolites in Fig. 2-5.

Supplementary Table 2-1. Metabolites of JWH-018 after *C. elegans* incubation.

Supplementary Table 2-2. Key diagnostic product ions and their tentative structures used in elucidating biotransformation pathways of JWH-018 after *C. elegans* incubation.

Supplementary Table 2-3. Metabolites of JWH-073 after *C. elegans* incubation.

Supplementary Table 2-4. Key diagnostic product ions and their tentative structures used in elucidating biotransformation pathways of JWH-073 after *C. elegans* incubation.

Supplementary Table 2-5. Metabolites of AM2201 after *C. elegans* incubation.

Supplementary Table 2-6. Key diagnostic product ions and their tentative structures used in elucidating biotransformation pathways of AM2201 after *C. elegans* incubation. Square brackets indicate phase II metabolism.

Table 3-1. Comparison of 5F-PB-22 metabolites formed by fungus, *Cunninghamella elegans*, with those by human hepatocytes and human liver microsomes reported in literature.

Table 3-2. Comparison of PB-22 metabolites formed by fungus, *Cunninghamella elegans*, with those by human hepatocytes and human liver microsomes reported in literature.

Table 3-3. Comparison of XLR-11 metabolites formed by fungus, *Cunninghamella elegans*, with those in human urine and human liver microsomes reported in literature.

Table 3-4. Comparison of UR-144 metabolites formed by fungus, *Cunninghamella elegans*, with those in human urine and human liver microsomes reported in literature.

Supplementary Table 3-1. 5F-PB-22 metabolites with retention time, elemental composition, exact mass, accurate mass, mass error and diagnostic product ions.

Supplementary Table 3-2. PB-22 metabolites with retention time, elemental composition, exact mass, accurate mass, mass error and diagnostic product ions.

Supplementary Table 3-3. XLR-11 metabolites with retention time, elemental composition, exact mass, accurate mass, mass error and diagnostic product ions.

Supplementary Table 3-4. UR-144 metabolites with retention time, elemental composition, exact mass, accurate mass, mass error and diagnostic product ions.

Table 4-1. ^{1}H and ^{13}C NMR data for UR-144 and fraction 1 containing dihydroxy metabolites (M1-3) in $CDCl_3$.

Table 4-2. ^{1}H and ^{13}C NMR data for carboxy and hydroxy metabolites (M4-6 and M8-9) in $CDCl_3$.

Table 4-3. ^{1}H and ^{13}C NMR data for a hydroxy and ketone metabolite (M7) and a carboxy and ketone metabolite (M10) in $CDCl_3$.

Table 5-1. AM1220 metabolites after HLM and fungus *C. elegans* incubation.

Table 6-1. Acetylfentanyl metabolites with proposed biotransformation, retention time, elemental composition, accurate mass of protonated molecule, mass error of proposed metabolite, MS peak areas in hepatocyte samples (0h, 1h, 3h and 5h) and in five urine samples (hydrolysed and non-hydrolysed), and diagnostic product ions (masses and mass errors taken from sample #3, and #5 in case of saturation).

Table 6-2. Acrylfentanyl metabolites with proposed biotransformation, retention time, elemental composition, accurate mass of protonated molecule, mass error of proposed metabolite, MS peak areas in hepatocyte samples (0h, 1h, 3h and 5h) and in five urine

samples (hydrolysed and non-hydrolysed), and diagnostic product ions (masses and mass errors generally taken from sample #3, except for B12 (#2), B1 and B14 (#5) and B10 (hepatocytes).

Table 6-3. 4-Fluoro-isobutyrylfentanyl metabolites with proposed biotransformation, retention time, elemental composition, accurate mass of protonated molecule, mass error of proposed metabolite, MS peak areas in hepatocyte samples (0h, 1h, 3h and 5h) and in five urine samples (hydrolysed and non-hydrolysed), and diagnostic product ions (masses and mass errors generally taken from sample #3, except for C2 (#1) and C8, C14, C16 and C17 (hepatocytes).

Table 6-4. Furanylfentanyl metabolites with proposed biotransformation, retention time, elemental composition, accurate mass of protonated molecule, mass error of proposed metabolite, MS peak areas in hepatocyte samples (0h, 1h, 3h and 5h) and in five urine samples (hydrolysed and non-hydrolysed), and diagnostic product ions (masses and mass errors generally taken from sample #5, except for D6, D9, D11, D12 and D13 (hepatocytes).

Abstract

The rapid and continuous emergence of new psychoactive substances has been a trend of the recreational drug market over the last decade. The sheer number of the new drugs has posed a challenge for the forensic and clinical laboratories to detect the consumption of the drugs in urine drug testing, especially when the metabolism of the drugs is unknown. This thesis aims to demonstrate that the fungus *Cunninghamella elegans* is a suitable model for metabolism studies of synthetic cannabinoids, as well as to provide new knowledge on metabolism of several new psychoactive substances to aid the forensic and clinical laboratories in detection of these drugs in urine testing.

Seven synthetic cannabinoids JWH-018, JWH-073, AM2201, 5F-PB-22, PB-22, XLR-11 and UR-144 were incubated with *C. elegans* for 72 h and the obtained metabolites were analysed by liquid chromatography–high resolution mass spectrometry (LC-HRMS). The cannabinoids underwent various biotransformations including, either alone or in combination, carboxylation, defluorination, dehydrogenation, demethylation, dihydrodiol formation, dihydroxylation, ester hydrolysis, hydroxylation, ketone formation, *N*-dealkylation, oxidative defluorination, oxidative defluorination to carboxylic acid, and trihydroxylation. Glucosidation and sulfation were the observed phase II biotransformations, although uncommon. The fungal metabolites were generally consistent with the human-relevant metabolites of these drugs reported in literature, except that glucuronidation is the common phase II human metabolic pathway instead of glucosidation and that the prevalence of the fungal metabolites was not always reflective of the human metabolite prevalence.

Large amounts of fungal metabolites of UR-144 were obtained in an upscaled experiment and analysed by nuclear magnetic resonance (NMR) spectroscopy after isolating several metabolites by preparative high performance liquid chromatography (HPLC). Ten metabolites were characterised including dihydroxy metabolites, carboxy and hydroxy metabolites, a hydroxy and ketone metabolite, and a carboxy and ketone metabolite. Use of these metabolites as reference standards for the UR-144 metabolites after human liver

microsomes (HLM) incubation indicated that a dihydroxy metabolite, carboxy and hydroxy metabolites, and a hydroxy and ketone metabolite generated by the fungus were also produced by HLM.

The metabolism of the synthetic cannabinoid AM1220 was investigated after incubation with HLM and the fungus using liquid chromatography–tandem mass spectrometry (LC-MS/MS) and LC-HRMS. AM1220 was found to be a high clearance drug and hydroxylation, demethylation and dihydrodiol formation were the major biotransformations.

The metabolism of acetylfentanyl, acrylfentanyl, 4-fluoro-isobutyrylfentanyl, and furanylfentanyl was studied in authentic human urine and human hepatocytes samples using LC-HRMS. *N*-dealkylation, hydroxylation, and hydroxylation and methoxylation were the major biotransformations for all but furanylfentanyl, which was mainly transformed by amide hydrolysis and dihydrodiol formation. It illustrates the need to examine the metabolism of individual drugs rather than predicting them based on the previous knowledge.

In conclusion, *C. elegans* has the ability to mimic human metabolism and, by allowing large production of metabolites, enables more comprehensive characterisation of metabolites by NMR analysis. Therefore, the fungus can be a useful complementary model for metabolism of synthetic cannabinoids.

Chapter 1: Introduction

Chapter 1: Introduction

1.1 New Psychoactive Substances

According to the United Nations Office on Drugs and Crime, new psychoactive substances (NPS) are defined as "substances of abuse, either in a pure form or a preparation, that are not controlled by the 1961 Single Convention on Narcotic Drugs or the 1971 Convention on Psychotropic Substances, but which may pose a public health threat" [1]. As the term "new" suggests, NPS are relatively newly emerging drugs of abuse in the recreational drug market. However, they are not necessarily new in terms of when they were first synthesised. Many of them were synthesised in the early 1970s and an early detection of NPS dates back to the beginning of the 1980 when ketamine was abused in the United States [1]. By the end of 2016, more than 620 NPS had emerged and had been monitored in Europe [2]. Notably, approximately 70% of those NPS appeared during the last 5 years, indicating that NPS are mostly a recent phenomenon. NPS comprise several different classes of drugs including synthetic cannabinoids, synthetic cathinones, synthetic opioids, phenethylamines and benzodiazepines.

Often manufactured in China, NPS get shipped to the destination countries and sold frequently with a packaging labelled as "not for human consumption" [2, 3]. At the initial appearance, these substances hold a "legal" status as they are new drugs of abuse and are sold as a legal alternative to classic drugs of abuse [2]. When these substances are controlled, manufacturers generally replace the controlled drugs with "new" drugs with slight structural modifications so that the products can retain a legal status [3]. This explains the appearance of a large number of NPS and makes it difficult to keep up with the detection of these drugs and analysis of the toxicological properties of the drugs. Although these substances usually disappear from the market once they are regulated, the reappearance of then illegal drug has been observed [4]. In Germany, JWH-018, a first generation synthetic cannabinoid, was banned in 2009 and subsequently disappeared from the market. The drug surprisingly came back to the market almost 3 years after the ban. This observation illustrates the need to keep monitoring the drugs even after scheduling and apparent disappearance of the drugs. Regulation of these substances does not occur simultaneously throughout the world, instead varies among different

jurisdictions. For example, UR-144, another synthetic cannabinoid, was controlled as a designated substance in Japan in 2012 and as a schedule 1 drug in NSW, Australia and in the US in 2013, while it was controlled in Poland in 2015 [5-8]. As a result, UR-144 soon ceased to be detected in Japan in 2012 while it was a popular drug in Poland until 2015 when the ban took place [5, 8].

1.1.1 Synthetic cannabinoids

Cannabinoids are a class of compounds that bind to cannabinoid receptors in the central and/or peripheral nervous system and activate the receptors [3]. Cannabinoids can be classified as endocannabinoids, phytocannabinoids or synthetic cannabinoids [9]. Endocannabinoids are compounds naturally present in humans while phytocannabinoids are derived from the plant cannabis.

Cannabis contains more than 100 cannabinoids and the main active components are delta-9-tetrahydrocannabinol (THC) and cannabidiol (CBD) [10]. THC is a partial agonist at cannabinoid receptor 1 (CB_1 receptor) and cannabinoid receptor 2 (CB_2 receptor) and is the major contributor to the psychoactive effects due to the affinity to CB_1 receptors [9]. CBD, on the other hand, has little affinity to CB_1 receptors and is therefore not psychoactive, but interestingly modulates the adverse effects of THC by antagonising CB_1 receptors [10, 11]. Cannabis has been long abused for its euphoric and relaxing effects and as of 2014 it was the most prevalent drug of abuse globally [12].

Synthetic cannabinoids were initially synthesised in laboratories to investigate the potential as therapeutic drugs [3]. However, since 2004 they started to appear in the recreational drug market as a legal alternative to cannabis [3]. Initially, they were sold as herbal products often known as “Spice”, which consisted of dried plant materials onto which synthetic cannabinoid solution was sprayed [2]. Recently, synthetic cannabinoids have also been available in the form of powder as “research chemicals” and in solution to be used for an e-cigarette [9].

Synthetic cannabinoids can be structurally classified into many classes as below [13]:

I. Classical cannabinoids (THC and their analogues)
II. Non-classical cannabinoids (cyclohexylphenols)
III. Hybrid cannabinoids (compounds with structural features of both classical and nonclassical cannabinoids)
IV. Aminoalkylindoles (naphthoylindoles, phenylacetylindoles, naphthylmethylindoles and benzoylindoles)
V. Eicosanoids (endocannabinoids and their analogues)
VI. Others (diarylpyrazoles, naphthoylpyrroles, naphthylmethylindenes, etc.)

Initially, most of the synthetic cannabinoids that appeared in spice products were limited to JWH compounds, CP compounds (cyclohexylphenols) and HU-210. The JWH compounds, named after the synthesiser John W. Huffman, mostly consist of aminoalkylindoles and are the most common additives in spice. The CP compounds are non-classical cannabinoids made by Pfizer and HU-210 is a classical cannabinoid made by Hebrew University [3]. The structures of some synthetic cannabinoids found in herbal products are shown in Fig. 1-1.

Synthetic cannabinoids are the largest group of drugs among NPS that are monitored by the European Monitoring Centre for Drugs and Drug Addiction [2]. A total of 169 compounds have been detected by 2016 and synthetic cannabinoids accounted for 29% of the seizures of NPS reported in Europe in 2015. The prevalence of synthetic cannabinoids has been investigated in some studies. A survey of 3,928 high school students in Nevada, the US, in 2013 has revealed 17.3% of students reported to have used synthetic cannabinoids at least once and 4.3% have used more than 10 times [14]. Another study surveying 11,863 high school students throughout the US over 2011 to 2013 indicated that 10.1% of the students used synthetic cannabinoids within the last 12 months period while 3.2% used them 6 times or more [15]. In the study where 20,017 US military urine specimens were analysed by liquid chromatography – tandem mass spectrometry (LC-MS/MS) from 2011 to 2012, 1.4% was confirmed to be positive for synthetic cannabinoid use [16].

I. Classical cannabinoid

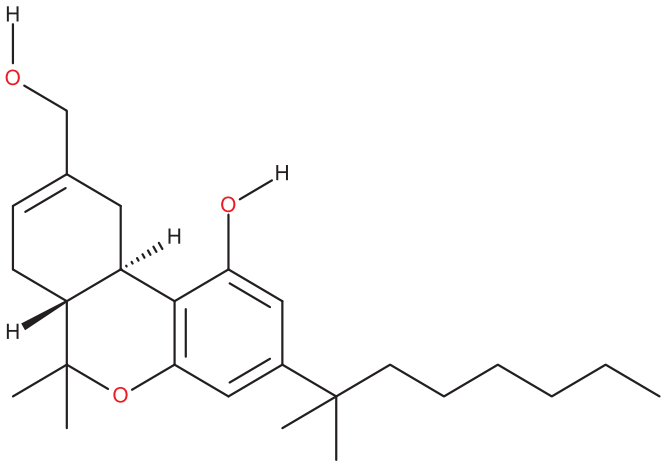

HU-210

II. Nonclassical cannabinoids

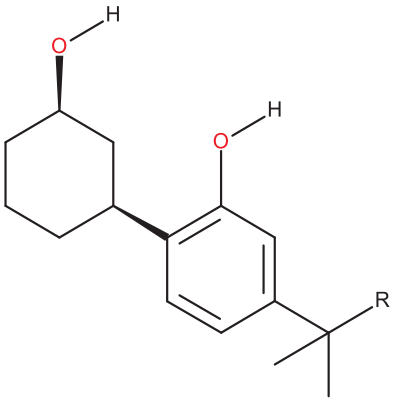

CP-47,497: R = C_6H_{13}
CP-47,497-C8: R = C_7H_{15}

IV. Naphthoylindoles

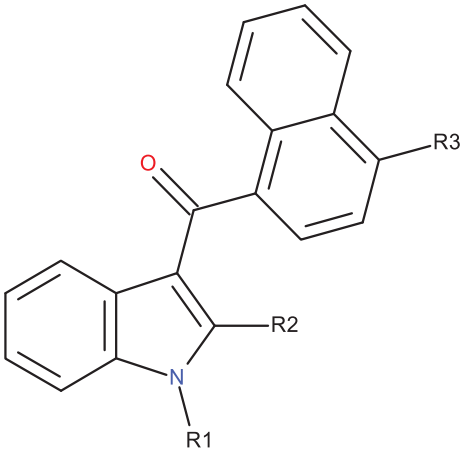

JWH-007: R1 = C_5H_{11}, R2 = CH_3, R3 = H
JWH-015: R1 = C_3H_7, R2 = CH_3, R3 = H
JWH-018: R1 = C_5H_{11}, R2 = R3 = H
JWH-019: R1 = C_6H_{13}, R2 = R3 = H
JWH-073: R1 = C_4H_9, R2 = R3 = H
JWH-081: R1 = C_5H_{11}, R2 = H, R3 = OCH_3
JWH-122: R1 = C_5H_{11}, R2 = H, R3 = CH_3
JWH-200: R1 = 2-(4-morpholinyl)ethyl, R2 = R3 = H
JWH-210: R1 = C_5H_{11}, R2 = H, R3 = C_2H_5
JWH-398: R1 = C_5H_{11}, R2 = H, R3 = Cl

IV. Phenylacetylindoles

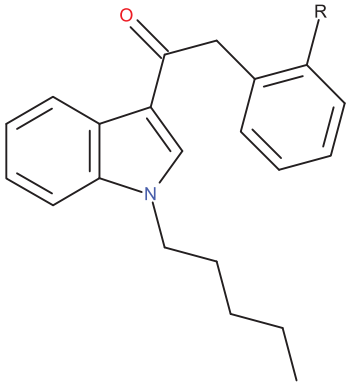

JWH-203: R = Cl
JWH-250: R = OCH_3

IV. Benzoylindoles

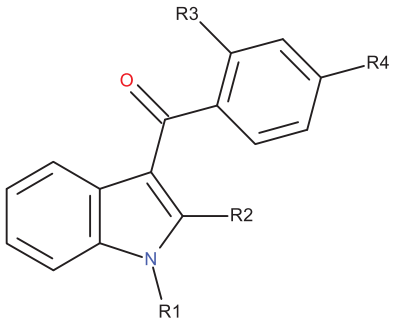

AM-694: R1 = $C_5H_{10}F$, R2 = H, R3 = I, R4 = H
RCS-4: R1 = C_5H_{11}, R2 = R3 = H, R4 = OCH_3
WIN-48,098: R1 = 2-(4-morpholinyl)ethyl, R2 = CH_3, R3 = H, R4 = OCH_3

Figure 1-1. Structures of some synthetic cannabinoids.

Although synthetic cannabinoids emerged as an alternative to cannabis, they are generally much more potent than THC, the major active component of cannabis. As mentioned earlier, THC is a partial agonist at CB_1 receptors, which means that it does not activate the receptor fully and therefore the effects generated from the activation are only partial compared to the maximum effects that can be obtained [9]. On the other hand, a study has shown that two synthetic cannabinoids JWH-018 and AM2201 have full agonist activity at CB_1 receptors, indicating that the use of synthetic cannabinoids can result in more adverse health effects [17].

When comparing the potency of drugs, the potency of their metabolites also needs to be taken into account because some metabolites lose the potency while others retain it. In case of THC, metabolism leads to only one major active metabolite, 11-hydroxy-THC, albeit with less affinity to CB_1 receptors [18]. In contrast, 4-hydroxy metabolites of both JWH-018 and AM2201 were shown to exhibit full agonist activity at CB_1 receptors [17]. Therefore, synthetic cannabinoids can have a higher potency not only for the parent drugs, but also for their metabolites.

The higher potency of synthetic cannabinoids makes them a greater health threat than cannabis, but the health risk posed by the herbal products containing synthetic cannabinoids is further complicated by the unknown nature of the products. Monitoring of more than 140 herbal products from 2008 to 2009 in Germany found that the products with the same brand name can vary in composition over time, containing different synthetic cannabinoids in an effort to circumvent the new prohibition of the drugs [19]. When the herbal products first emerged on the drug market, most of them contained only synthetic cannabinoids and they contained only 1 or 2 synthetic compounds in each product [20]. However, in later years, products containing other NPS such as synthetic cathinones and tryptamines became more common [12, 20]. As expected, the concentrations of synthetic cannabinoids are different in products with different brand names [21], but even among the products with the same brand the concentrations were found to vary [22]. All these variations in the products make them a huge risk for accidental overdose.

1.1.2 Fentanyl analogues

Opioids are compounds that act on opioid receptors either as agonists or antagonists and include endogenous opioids, opiates derived from opium of the poppy plant such as morphine and codeine, and synthetic opioids [23]. The main effect produced by opioids is analgesia and other effects include respiratory depression, miosis and euphoria.

Fentanyl is a synthetic opioid, which is estimated to be at least 50 times more potent than morphine [24]. Due to the analgesic effects, fentanyl is used therapeutically but is also abused for its euphoric effects, and as a result, accidental fatalities continuously occur [25].

Recently, fentanyl analogues have been appearing as NPS and a total of 18 analogues has been detected in Europe since 2009 [2]. Similar to fentanyl, fentanyl analogues are highly potent drugs with acetylfentanyl being 16 times more potent than morphine, posing a serious risk of health effects [24]. Overdose deaths associated with acetylfentanyl have been reported in Europe since 2013 (Sweden: at least 27 deaths, Germany: 2 deaths, the UK: 2 deaths: Poland: 1 death) [26, 27], the US since 2013 (at least 52 deaths) [28, 29], Russia in 2012 (12 deaths) [30] and Japan (1 death) [31]. Since adverse reactions of fentanyl analogues may be reversed by naloxone, a μ-opioid receptor antagonist [32], it is important to have the methods of detection for these analogues in drug testing.

1.2 Metabolism

When drugs are administered to humans, metabolism of the drugs takes place. Metabolism is a process in which drugs are structurally modified by chemical reactions, facilitated by enzymes in the body [33]. It generally leads to more polar compounds than the parent drugs, making it easier to excrete the compounds in urine or bile [33]. As a result of metabolic transformation, the toxicity and potency of drugs are decreased in some cases, but could also be increased in other cases [34].

There are two types of metabolic biotransformations; hydrolysis, oxidation, and reduction are known as phase I reactions, while conjugation reactions are called phase II reactions. Phase I reactions are predominantly catalysed by the cytochrome P450 (CYP) enzymes, which are mainly present in the liver [33]. Phase II metabolism is catalysed by phase II enzymes such as uridine diphosphoglucuronosyl transferases (UGT) for glucuronidation and sulfotransferases for sulfation [34].

1.2.1 Metabolism models

Metabolism of drugs is generally studied with *in vivo* systems using whole animals such as mice and rats or *in vitro* systems using human/animal microsomal fractions or hepatocytes [35]. There are both advantages and disadvantages for these models. *In vivo* metabolism studies can be performed by administering drugs, for example, to rats via gastric intubation and analysing the metabolites in urine collected [36]. Thus, i*n vivo* systems can simulate absorption, distribution, metabolism and excretion of drugs in humans. This provides an advantage, firstly because metabolism of drugs can occur outside of the liver such as the kidneys, skin, lungs and intestine, although the liver is the main site responsible for metabolic transformation of drugs including phase I and phase II metabolism [34, 35]. Secondly, interaction of drugs with organs and tissues may reflect the *in vivo* human metabolism more truthfully. With the use of animals, however, there is an ever-increasing concern for ethical issues. In addition, the cost of animals including their maintenance can be expensive. Species differences can also be a major disadvantage, producing irrelevant metabolites for human metabolism [33].

For *in vitro* metabolism studies, human liver preparations are often used. The obvious advantage of using human liver preparations over animals is that human liver preparations are not subject to species differences and therefore the metabolites obtained are relevant to humans. These models are prepared from livers that are unsuitable for transplantation purposes or liver sections obtained from biopsies. The metabolic transformations by human liver preparations are greatly influenced by the quality of the liver used [34]. Among the liver preparations, human liver microsomes (HLM) are particularly popular since they are easy to handle and cheaper than animal models and other *in vitro* models [34, 37]. HLM mostly contain CYP and UGT enzymes only, and NADPH regenerating system and UDPGA are required as cofactors for CYP and UGT enzyme activity, respectively. HLM, however, lack enzymes such as *N*-acetyl transferase (NAT), glutathione *S*-transferase (GST) and sulfotransferase (ST) [34]. The lack of some liver enzymes indicates that some *in vivo* metabolites may not be produced by HLM and that the extent of biotransformation observed in HLM metabolism may be heavily inclined to the CYP and/or UGT reactions without the competition with other enzymes and thus may not reflect *in vivo* human metabolism quantitatively. Furthermore, the UGT enzymes are located on the inside of the endoplasmic reticulum of the microsomes and an addition of alamethicin may be necessary for facilitating the interaction between drugs and the UGT enzymes [38].

Hepatocytes are a well-established model, which shows good correlation with *in vivo* human liver [34]. Primary hepatocytes can be usable for a few hours after isolation while cultured hepatocytes can last for 4 weeks. One advantage of primary hepatocytes is that they can be cryopreserved while still capable of most phase I and II enzyme activity [34]. A disadvantage of hepatocytes as with other *in vitro* models is the inter-individual variation. However, this can be overcome by pooling hepatocytes from multiple donors.

The potential for the use of microbial systems for drug metabolism studies was described by Smith and Rosazza and remarkable similarity between microbial metabolites and *in vitro*/*in vivo* mammalian metabolites was noted [39]. There have been a number of studies on the use of microorganisms for drug metabolism since, and *in vitro* microbial systems were found to be free from most of the issues encountered with *in vivo* animal systems and *in vitro* human/animal systems. Most notable is the significantly larger quantity of

metabolites in cleaner extracts that can be produced by microorganisms than other systems. This allows detection, isolation, and identification of metabolites easily. Also, the relative ease of handling microorganisms and its low cost are noteworthy. Although the use of microbial systems is not to replace the whole *in vivo* animal studies, it can reduce the number of animals sacrificed by serving as a tentative model [35, 40].

Among the microorganisms used in metabolism studies, the fungi, *Cunninghamella* species, have been demonstrated to produce regiospecific and stereospecific metabolites of a number of xenobiotics similar to those produced by mammalian systems. They are capable of producing both phase I and phase II metabolites using cytochrome P450 monooxygenase systems and phase II metabolism enzymes, respectively. There are 14 species within the genus *Cunninghamella* and the species, *Cunninghamella elegans*, has been shown to have agreement with mammalian metabolism for more drugs than any other species [33].

1.2.2 Metabolism studies

In general, the major metabolites of the JWH compounds are monohydroxy metabolites. Due to the absence of reference standards for most of the metabolites, the positions of the functional groups such as hydroxy and carboxy groups are usually only indicated within moieties, e.g. indole moiety, by fragment patterns of mass spectra and thus the exact positions are usually not elucidated. The parent drug is usually not detected in urine or detected at significantly lower concentrations than its metabolites. The absence of the parent drug is significant as it requires the detection of the metabolites in urine samples to monitor the use of the drug. Metabolism of individual cannabinoids is described in more detail below.

1.2.2.1 JWH-018

The metabolic pathways of JWH-018 in rats and humans were found to be different. *N*-dealkylated and *N*-dealkylated monohydroxylated metabolites were found in rats. In contrast, in humans the monohydroxylated metabolites were the most abundant along with smaller quantities of dihydroxylated, carboxylated, *N*-dealkylated, *N*-dealkylated

monohydroxylated, dihydrodiol, and monohydroxylated dihydrodiol metabolites. The parent compound, JWH-018, was not found in urine [41-43]. Among the major monohydroxy and carboxy metabolites, the decreasing order of *in vivo* concentration was found to be *N*-(4-hydroxypentyl) > *N*-(5-hydroxypentyl) > *N*-pentanoic acid [44]. Moran *et al*. [45] found JWH-073 *N*-butanoic acid metabolite in two urine specimens of subjects that consumed JWH-018 only. These two subjects may have consumed JWH-073 unlike their claims. However, JWH-073 *N*-butanoic acid metabolite was again found in urine reportedly after JWH-018 consumption despite the absence of other major metabolites of JWH-073 [44]. Moreover, Hutter *et al*. also reported the presence of JWH-073 *N*-butanoic acid metabolite in urine samples of the subjects whose serum samples were positive for JWH-018 but clear of JWH-073. The metabolite may be a result of enzymatic decarboxylation of the carboxylated JWH-018 metabolite [46]. In a study where urine samples were tested for JWH-018 and JWH-073 metabolites, all the 21 positive samples for JWH-018 contained JWH-073 *N*-butanoic acid metabolite while other JWH-073 metabolites were found in only 12 samples usually with much less concentrations [47]. Considering that monohydroxylated metabolites are the major metabolites of JWH-073 [41], the higher frequency and concentration of JWH-073 *N*-butanoic acid metabolite found in the study could be attributable to the formation from JWH-018.

1.2.2.2 JWH-073

Monohydroxylated (at either the *N*-butyl group or the indole moiety) and carboxylated metabolites of JWH-073 were found in humans [46]. The parent compound was not observed in urine [41].

1.2.2.3 JWH-081

In vivo, three monohydroxy metabolites (at the *N*-pentyl group, the indole moiety or the naphthalene moiety) were identified in urine. A carboxylated metabolite was not found unlike JWH-018 and JWH-073 [46].

1.2.2.4 JWH-122

As with JWH-081, only three monohydroxy metabolites (at the *N*-pentyl group, the indole moiety or the naphthalene moiety) were found as major metabolites *in vivo* [46].

1.2.2.5 JWH-210

Three monohydroxy metabolites (at the *N*-pentyl group, the indole moiety or the naphthalene moiety) were the major *in vivo* metabolites [46].

1.2.2.6 JWH-250

The metabolites of JWH-250 in human urine samples were found to be monohydroxylated, dihydroxylated, trihydroxylated, trihydroxylated dehydrated, and *N*-dealkylated monohydroxylated metabolites. Some monohydroxylated and dihydroxylated metabolites were also detected in human serum samples. In rats, however, *N*-dealkylated, *N*-dealkylated monohydroxylated, dihydroxylated, and trihydroxylated metabolites were found. The major metabolites in humans and rats were monohydroxylated and *N*-dealkylated monohydroxylated metabolites, respectively. The parent compound was not detected in urine samples by GC-MS analysis [48].

1.2.2.7 HU-210

In vitro metabolites of HU-210 using human liver microsomes were identified to be monooxygenated, monohydroxylated, dioxygenated, dihydroxylated metabolites by LC-MS/MS analysis [49].

1.2.2.8 RCS-4

Three monohydroxylated metabolites (one at the indole moiety and two at the phenyl moiety) were found in urine samples [46].

1.2.2.9 AM2201 and UR-144

The metabolites of AM2201 and UR-144 were reported by Sobolevsky *et al*. both *in vitro* and *in vivo* [50]. The metabolites of AM2201 were found to be *N*-desfluoropentyl, hydroxy, dihydroxy, and dihydrodiol metabolites as well as JWH-018 *N*-(5-hydroxypentyl) and JWH-018 *N*-pentanoic acid metabolites. JWH-018 metabolites were produced as a result of the enzymatic defluorination, since AM2201 has a structure of JWH-018 with a terminal hydrogen on *N*-pentyl chain replaced by fluorine. The major metabolites were monohydroxy and dihydrodiol. UR-144 metabolites were identified as *N*-despentyl, hydroxy, dihydroxy, dehydrated hydroxy, and *N*-despentylhydroxy metabolites (the last two were not detected *in vivo*). For both cannabinoids, the concentration of the parent compound was low and the majority of the metabolites were excreted as glucuronides.

1.2.2.10 Potential common metabolite

While screening the urine samples for the four metabolites, JWH-018 *N*-(4-hydroxypentyl), JWH-018 *N*-pentanoic acid, JWH-073 *N*-(3-hydroxybutyl), and JWH-073 *N*-butanoic acid, Lovett *et al*. discovered an unidentified peak in all the samples that were found positive for one or more of the above-mentioned metabolites [51]. The peak was detected in the multiple reaction monitoring mode with the parameters chosen for JWH-073 *N*-(3-hydroxybutyl) metabolite in LC-MS/MS. This led the authors to speculate that the unknown peak was a metabolite of JWH compounds and subsequent investigation revealed it to be JWH-072 *N*-propanoic acid metabolite. In 38 out of the 49 positive samples, the concentration of JWH-072 *N*-propanoic acid metabolite was found to be the greatest among the quantified metabolites; JWH-018 *N*-(4-hydroxypentyl), JWH-018 *N*-(5-hydroxypentyl), JWH-018 *N*-pentanoic acid, JWH-073 *N*-butanoic acid, and JWH-072 *N*-propanoic acid. In the other 11 samples, it was still the second major metabolite. This new metabolite may have resulted from JWH-072 added to Spice. However, the authors concluded that this new metabolite seems to be a common and major metabolite of JWH-018, JWH-073, and AM2201. This assumption is reasonable considering that JWH-072 has a significantly low affinity for the CB_1 receptor with the K_i value of 1050 nM [52] and hence it is not likely that JWH-072, much less potent than the other already

circulating cannabinoids, is used in Spice. Furthermore, the previous report on JWH-073 *N*-butanoic acid as a JWH-018 metabolite suggests the possibility of JWH-072 *N*-propanoic acid formation from JWH-073 and thus from JWH-018 [45, 46]. Since the presence or absence of JWH-072 in Spice smoked by the users tested positive for the urine samples cannot be confirmed, further investigations are necessary to draw a conclusion. Nevertheless, it would be a useful biomarker if it can be determined to be a common metabolite.

1.3 Instruments

1.3.1 Liquid chromatography – mass spectrometry

Liquid chromatography – mass spectrometry (LC-MS) is a useful technique for separating compounds in complex matrices and identifying the compounds, since a variety of compounds can be analysed as long as they are soluble in suitable solvents and mobile phases of the LC system. The ability of LC-MS, containing a single mass spectrometry, to characterise compounds is relatively weak, as fragments of compounds cannot be analysed. However, as liquid chromatography coupled to tandem mass spectrometry (MS/MS) became commonly available in laboratories allowing the analysis of fragment ions of analytes, LC-MS has become an indispensable tool for characterising many compounds including drugs and metabolites.

Recent advance in high resolution mass spectrometry (HR-MS) is of particular importance to the ability to characterise isobaric compounds. Isobaric compounds are those with the same nominal mass, which cannot be differentiated by low resolution mass spectrometers such as quadrupole mass spectrometer. In contrast, HR-MS can accurately measure the mass of analytes down to fourth decimal place, which provides elemental composition of the analytes, allowing differentiation of isobaric compounds [53].

1.3.2 Nuclear magnetic resonance spectroscopy

Nuclear magnetic resonance (NMR) spectroscopy is a powerful technique for elucidating the structures of unknown compounds. In contrast to LC-MS/MS including HR-MS, NMR analysis can, in most cases, lead to the complete structures of the analytes. ^{1}H NMR shows the number and chemical environment of protons present in the analytes, whereas ^{13}C NMR shows the number and chemical environment of carbon atoms present in the analytes. When these data are correlated by two-dimensional (2D) NMR techniques, the structures can be unambiguously identified. Common 2D NMR techniques include COSY, HSQC, HMBC and NOESY. COSY experiments show the correlations of protons on adjacent carbon atoms. HSQC indicates the connections of protons and carbon atoms. HMBC can show the correlations between protons and carbon atoms that are two to three

bonds away. NOSEY experiments give correlations for spatially close protons regardless of bonding, allowing the determination of stereochemistry of protons.

1.3.3 Detection of synthetic cannabinoids and their metabolites

Synthetic cannabinoids have been detected in Spice products using gas chromatography–mass spectrometry (GC-MS) [19, 21, 54-57], and LC-MS [21, 55, 56, 58]. The matrices used for monitoring of synthetic cannabinoids include serum, blood, oral fluid, and hair. The serum samples are analysed by LC-MS/MS [59-61] and a recent method by Hess *et al*. can detect as many as 93 synthetic cannabinoids simultaneously [62]. The method by Dziadosz *et al*. can monitor 16 synthetic cannabinoids and 20 new designer drugs that do not belong to synthetic cannabinoids simultaneously, which would be useful when the people suspected of abusing drugs have used multiple drugs [63]. The blood samples are also monitored by LC-MS/MS [64, 65]. Serum and blood samples are convenient in that metabolites of the parent drugs do not need to be determined, and hence they can be analysed as long as the method to detect the parent drugs is established. In spite of the strength, the other matrices are more favourable for routine work due to the invasive nature.

Several detection methods of synthetic cannabinoids in oral fluid samples have been reported [66-70]. These methods utilise LC-MS/MS and the method by Kneisel *et al*. can detect and quantify 28 synthetic cannabinoids in neat oral fluid samples. The presence of synthetic cannabinoids in the oral fluid was suggested to be a result of smoke contamination in the oral cavity rather than the drugs absorbed into the blood and excreted through salivary glands, and the quantity of the cannabinoids contamination drops significantly within half an hour, leading to a short detection window of up to 2 days [69]. Thus, oral fluid samples can be analysed for recent use of cannabinoids and may particularly be useful for roadside testing. Due to the lipophilic nature, the drugs in oral fluid samples were found to adsorb to containers used for collection at room temperature. As a result, it is necessary to store the samples cooled during the transporting until the analysis in order to prevent the unintended loss of the drugs [71].

In contrast to oral fluid, human hair samples can be an evidence of former use up to several months as well as recent use depending on the position of the hair containing the cannabinoids. However, similarly to the oral fluid samples, the major route of the drug to hair is not via systemic circulation but through side-stream smoke. Hence, care must be taken when interpreting such samples. Hair samples have been analysed by LC-MS/MS [72] and ultra-high performance liquid chromatography–tandem mass spectrometry (UHPLC-MS/MS) with 23 synthetic cannabinoids monitored by a method by Salomone *et al*. [73, 74].

Urine samples are also used to establish the consumption of synthetic cannabinoids. However, as most of the parent compounds are extensively metabolised, the presence of metabolites is monitored by GC-MS [41, 42, 75] and LC-MS/MS [41-46, 50, 76-79]. For the detection of minor metabolites, LC-MS/MS is suggested to be more useful. The method developed by Scheidweiler *et al*. can detect 47 metabolites from 21 synthetic cannabinoids [80].

1.4 Aims of this project

This study is divided into two main parts. The first part mainly aims to demonstrate that the fungus *Cunninghamella elegans* can be a useful model for synthetic cannabinoids metabolism studies, complementary to other models commonly employed. In order for the fungus to be a suitable model for human-relevant metabolism, it needs to be shown that at least some of the metabolites produced by the fungus, if not all, are the same as those produced in humans, ideally in similar prevalence to human metabolites. In addition, it should be demonstrated that the fungus has a specific advantage over other models: the ease with production of large amounts of metabolites, which allows NMR characterisation of metabolites. An evaluation of the fungus model as a valuable tool to complement other metabolism models has been carried out. The second part discusses the identification of fentanyl analogues metabolites obtained from authentic human urine specimens as well as human hepatocytes samples to illustrate the importance of metabolism studies.

The specific aims of each chapter were to:

1. Identify the metabolites of three synthetic cannabinoids JWH-018, JWH-073 and AM2201 after *C. elegans* incubation using liquid chromatography–triple quadrupole mass spectrometry (LC-QqQ-MS) and liquid chromatography–quadrupole time-of-flight mass spectrometry (LC-QTOF-MS) and compare the fungal metabolites with human-relevant metabolites reported in literature.

2. Further demonstrate the relevance of the fungus model to human metabolism by determining the fungal metabolites of four other synthetic cannabinoids 5F-PB-22, PB-22, XLR-11 and UR-144 using LC-QTOF-MS and comparing the fungal metabolites with human-relevant metabolites reported in literature.

3. Unambiguously characterise the major metabolites of UR-144 by NMR spectroscopy and use them as reference standards for the analysis of a UR-144 metabolite sample obtained from HLM incubation using LC-QTOF-MS.

4. Determine the metabolites of the synthetic cannabinoid AM1220 after HLM and *C. elegans* incubation using LC-QTOF-MS, and suggest suitable biomarkers for urine drug testing to prove the drug consumption. The metabolic stability of AM1220 by HLM incubation was also estimated using LC-QqQ-MS.

5. Identify the metabolites of four fentanyl analogues in authentic human urine specimens as well as in human hepatocytes samples using LC-QTOF-MS, and suggest suitable biomarkers for urine drug testing.

1.4 References

1. UNODC. The Challenge of New Psychoactive Substances. 2013. Available from: http://www.unodc.org/documents/scientific/NPS_2013_SMART.pdf. Accessed 05 August 2017.

2. European Monitoring Centre for Drugs and Drug Addiction. European Drug Report 2017: Trends and Developments. Luxembourg: Publications Office of the European Union 2017.

3. Seely KA, Lapoint J, Moran JH, Fattore L. Spice drugs are more than harmless herbal blends: a review of the pharmacology and toxicology of synthetic cannabinoids. Prog Neuropsychopharmacol Biol Psychiatry. 2012;39(2):234-43. doi:10.1016/j.pnpbp.2012.04.017.

4. Ernst L, Krüger K, Lindigkeit R, Schiebel H-M, Beuerle T. Synthetic cannabinoids in "spice-like" herbal blends: First appearance of JWH-307 and recurrence of JWH-018 on the German market. Forensic Sci Int. 2012;222(1):216-22. doi:http://dx.doi.org/10.1016/j.forsciint.2012.05.027.

5. Kikura-Hanajiri R, Kawamura NU, Goda Y. Changes in the prevalence of new psychoactive substances before and after the introduction of the generic scheduling of synthetic cannabinoids in Japan. Drug Test Anal. 2014;6(7-8):832-9. doi:10.1002/dta.1584.

6. Drug Misuse and Trafficking Amendment (Prohibited Substances) Regulation 2013 New South Wales2013. Available from: https://www.legislation.nsw.gov.au/regulations/2013-556.pdf. Accessed 06 August 2017.

7. Drug Enforcement Administration. Schedules of Controlled Substances: Temporary Placement of Three Synthetic Cannabinoids Into Schedule I 2013. Available from: https://www.federalregister.gov/documents/2013/05/16/2013-11593/schedules-of-controlled-substances-temporary-placement-of-three-synthetic-cannabinoids-into-schedule. Accessed 06 August 2017.

8. Adamowicz P, Gieroń J, Gil D, Lechowicz W, Skulska A, Tokarczyk B. The effects of synthetic cannabinoid UR-144 on the human body—A review of 39 cases. Forensic Sci Int. 2017;273:e18-e21. doi:http://dx.doi.org/10.1016/j.forsciint.2017.02.031.

9. Le Boisselier R, Alexandre J, Lelong-Boulouard V, Debruyne D. Focus on cannabinoids and synthetic cannabinoids. Clin Pharmacol Ther. 2017;101(2):220-9. doi:10.1002/cpt.563.

10. Russo EB. Taming THC: potential cannabis synergy and phytocannabinoid-terpenoid entourage effects. Br J Pharmacol. 2011;163(7):1344-64. doi:10.1111/j.1476-5381.2011.01238.x.

11. Robson PJ. Therapeutic potential of cannabinoid medicines. Drug Test Anal. 2014;6(1-2):24-30. doi:10.1002/dta.1529.

12. United Nations Office on Drugs and Crime. World Drug Report 2016. 2016. Available from: http://www.unodc.org/doc/wdr2016/WORLD_DRUG_REPORT_2016_web.pdf. Accessed 07 August 2017.

13. UNODC. Synthetic Cannabinoids in Herbal Products. 2011. Available from: http://www.unodc.org/unodc/en/scientists/synthetic-cannabinoids-in-herbal-products.html. Accessed 28 September 2013.

14. Clements-Nolle K, Lensch T, Larson S, Yang W. Prevalence and Correlates of Any and Frequent Synthetic Cannabinoid Use in a Representative Sample of High School Students. Subst Use Misuse. 2016;51(9):1139-46. doi:10.3109/10826084.2016.1160121.

15. Palamar JJ, Acosta P. Synthetic cannabinoid use in a nationally representative sample of US high school seniors. Drug Alcohol Depend. 2015;149:194-202. doi:https://doi.org/10.1016/j.drugalcdep.2015.01.044.

16. Wohlfarth A, Scheidweiler Karl B, Castaneto M, Gandhi Adarsh S, Desrosiers Nathalie A, Klette Kevin L, et al. Urinary prevalence, metabolite detection rates, temporal patterns and evaluation of suitable LC-MS/MS targets to document synthetic cannabinoid intake in US military urine specimens. Clin Chem Lab Med. 2015;53(3):423-34. doi:10.1515/cclm-2014-0612.

17. Chimalakonda KC, Seely KA, Bratton SM, Brents LK, Moran CL, Endres GW, et al. Cytochrome P450-mediated oxidative metabolism of abused synthetic cannabinoids found in K2/Spice: identification of novel cannabinoid receptor ligands. Drug Metab Dispos. 2012;40(11):2174-84. doi:10.1124/dmd.112.047530.

18. Fantegrossi WE, Moran JH, Radominska-Pandya A, Prather PL. Distinct pharmacology and metabolism of K2 synthetic cannabinoids compared to Delta(9)-THC: mechanism underlying greater toxicity? Life Sci. 2014;97(1):45-54. doi:10.1016/j.lfs.2013.09.017.

19. Dresen S, Ferreiros N, Putz M, Westphal F, Zimmermann R, Auwarter V. Monitoring of herbal mixtures potentially containing synthetic cannabinoids as psychoactive compounds. J Mass Spectrom. 2010;45(10):1186-94. doi:10.1002/jms.1811.

20. Kikura-Hanajiri R, Uchiyama N, Kawamura M, Goda Y. Changes in the prevalence of synthetic cannabinoids and cathinone derivatives in Japan until early 2012. Forensic Toxicol. 2013;31(1):44-53. doi:10.1007/s11419-012-0165-2.

21. Uchiyama N, Kikura-Hanajiri R, Ogata J, Goda Y. Chemical analysis of synthetic cannabinoids as designer drugs in herbal products. Forensic Sci Int. 2010;198(1-3):31-8. doi:10.1016/j.forsciint.2010.01.004.

22. Lindigkeit R, Boehme A, Eiserloh I, Luebbecke M, Wiggermann M, Ernst L, et al. Spice: A never ending story? Forensic Sci Int. 2009;191(1):58-63. doi:http://dx.doi.org/10.1016/j.forsciint.2009.06.008.

23. Silberstein S, McCrory D. Opioids. Cephalalgia. 2000;20(10):854-64. doi:10.1046/j.1468-2982.2000.00149.x.

24. Higashikawa Y, Suzuki S. Studies on 1-(2-phenethyl)-4-(N-propionylanilino)piperidine (fentanyl) and its related compounds. VI. Structure-analgesic activity relationship for fentanyl, methyl-substituted fentanyls and other analogues. Forensic Toxicol. 2008;26(1):1-5. doi:10.1007/s11419-007-0039-1.

25. Nelson L, Schwaner R. Transdermal fentanyl: Pharmacology and toxicology. J Med Toxicol. 2009;5(4):230-41. doi:10.1007/bf03178274.

26. Addiction EMCfDaD. EMCDDA–Europol Joint Report on a new psychoactive substance: N-phenyl-N-[1-(2-phenylethyl)piperidin-4-yl]acetamide (acetylfentanyl), Joint Reports. 2016. Available from: http://www.emcdda.europa.eu/publications/joint-reports/acetylfentanyl. Accessed 03 October 2016.

27. Helander A, Backberg M, Beck O. Intoxications involving the fentanyl analogs acetylfentanyl, 4-methoxybutyrfentanyl and furanylfentanyl: results from the Swedish

STRIDA project. Clin Toxicol (Phila). 2016;54(4):324-32. doi:10.3109/15563650.2016.1139715.

28. Lozier MJ, Boyd M, Stanley C, Ogilvie L, King E, Martin C, et al. Acetyl Fentanyl, a Novel Fentanyl Analog, Causes 14 Overdose Deaths in Rhode Island, March-May 2013. J Med Toxicol. 2015;11(2):208-17. doi:10.1007/s13181-015-0477-9.

29. Organization WH. Acetylfentanyl. Critical Review Report. Agenda item 5.2. 2015. Available from: http://www.who.int/medicines/access/controlled-substances/5.2_Acetylfentanyl_CRev.pdf. Accessed 04 October 2016.

30. Melent'ev AB, Kataev SS, Dvorskaya ON. Identification and analytical properties of acetyl fentanyl metabolites. J Anal Chem. 2015;70(2):240-8. doi:10.1134/s1061934815020124.

31. Yonemitsu K, Sasao A, Mishima S, Ohtsu Y, Nishitani Y. A fatal poisoning case by intravenous injection of "bath salts" containing acetyl fentanyl and 4-methoxy PV8. Forensic Sci Int. 2016. doi:10.1016/j.forsciint.2016.08.025.

32. Marquardt KA, Steven Tharratt R. Inhalation Abuse of Fentanyl Patch. J Toxicol Clin Toxicol. 1994;32(1):75-8. doi:10.3109/15563659409000433.

33. Asha S, Vidyavathi M. Cunninghamella--a microbial model for drug metabolism studies--a review. Biotechnol Adv. 2009;27(1):16-29. doi:10.1016/j.biotechadv.2008.07.005.

34. Brandon EFA, Raap CD, Meijerman I, Beijnen JH, Schellens JHM. An update on in vitro test methods in human hepatic drug biotransformation research: pros and cons. Toxicol Appl Pharmacol. 2003;189(3):233-46. doi:https://doi.org/10.1016/S0041-008X(03)00128-5.

35. Clark AM, McChesney JD, Hufford CD. The use of microorganisms for the study of drug metabolism. Med Res Rev. 1985;5(2):231-53. doi:10.1002/med.2610050203.

36. Meyer MR, Dinger J, Schwaninger AE, Wissenbach DK, Zapp J, Fritschi G, et al. Qualitative studies on the metabolism and the toxicological detection of the fentanyl-derived designer drugs 3-methylfentanyl and isofentanyl in rats using liquid chromatography–linear ion trap–mass spectrometry (LC-MSn). Anal Bioanal Chem. 2012;402(3):1249-55. doi:10.1007/s00216-011-5528-8.

37. Meyer MR, Maurer HH. Current applications of high-resolution mass spectrometry in drug metabolism studies. Anal Bioanal Chem. 2012;403(5):1221-31. doi:10.1007/s00216-012-5807-z.

38. Fisher MB, Campanale K, Ackermann BL, VandenBranden M, Wrighton SA. In Vitro Glucuronidation Using Human Liver Microsomes and The Pore-Forming Peptide Alamethicin. Drug Metab Dispos. 2000;28(5):560-6.

39. Smith RV, Rosazza JP. Microbial models of mammalian metabolism. Aromatic hydroxylation. Arch Biochem Biophys. 1974;161(2):551-8. doi:http://dx.doi.org/10.1016/0003-9861(74)90338-5.

40. Clark AM, Hufford CD. Use of microorganisms for the study of drug metabolism: An update. Med Res Rev. 1991;11(5):473-501. doi:10.1002/med.2610110503.

41. Grigoryev A, Savchuk S, Melnik A, Moskaleva N, Dzhurko J, Ershov M, et al. Chromatography-mass spectrometry studies on the metabolism of synthetic cannabinoids JWH-018 and JWH-073, psychoactive components of smoking mixtures. J Chromatogr B. 2011;879(15-16):1126-36. doi:10.1016/j.jchromb.2011.03.034.

42. Sobolevsky T, Prasolov I, Rodchenkov G. Detection of JWH-018 metabolites in smoking mixture post-administration urine. Forensic Sci Int. 2010;200(1-3):141-7. doi:10.1016/j.forsciint.2010.04.003.

43. Moller I, Wintermeyer A, Bender K, Jubner M, Thomas A, Krug O, et al. Screening for the synthetic cannabinoid JWH-018 and its major metabolites in human doping controls. Drug Test Anal. 2011;3(9):609-20. doi:10.1002/dta.158.

44. Chimalakonda KC, Moran CL, Kennedy PD, Endres GW, Uzieblo A, Dobrowolski PJ, et al. Solid-phase extraction and quantitative measurement of omega and omega-1 metabolites of JWH-018 and JWH-073 in human urine. Anal Chem. 2011;83(16):6381-8. doi:10.1021/ac201377m.

45. Moran CL, Le VH, Chimalakonda KC, Smedley AL, Lackey FD, Owen SN, et al. Quantitative measurement of JWH-018 and JWH-073 metabolites excreted in human urine. Anal Chem. 2011;83(11):4228-36. doi:10.1021/ac2005636.

46. Hutter M, Broecker S, Kneisel S, Auwarter V. Identification of the major urinary metabolites in man of seven synthetic cannabinoids of the aminoalkylindole type present

as adulterants in 'herbal mixtures' using LC-MS/MS techniques. J Mass Spectrom. 2012;47(1):54-65. doi:10.1002/jms.2026.

47. Jang M, Yang W, Choi H, Chang H, Lee S, Kim E, et al. Monitoring of urinary metabolites of JWH-018 and JWH-073 in legal cases. Forensic Sci Int. 2013;231(1-3):13-9. doi:10.1016/j.forsciint.2013.03.053.

48. Grigoryev A, Melnik A, Savchuk S, Simonov A, Rozhanets V. Gas and liquid chromatography-mass spectrometry studies on the metabolism of the synthetic phenylacetylindole cannabimimetic JWH-250, the psychoactive component of smoking mixtures. J Chromatogr B Analyt Technol Biomed Life Sci. 2011;879(25):2519-26. doi:10.1016/j.jchromb.2011.07.004.

49. Kim U, Jin MJ, Lee J, Han SB, In MK, Yoo HH. Tentative identification of phase I metabolites of HU-210, a classical synthetic cannabinoid, by LC-MS/MS. J Pharm Biomed Anal. 2012;64-65:26-34. doi:10.1016/j.jpba.2012.02.007.

50. Sobolevsky T, Prasolov I, Rodchenkov G. Detection of urinary metabolites of AM-2201 and UR-144, two novel synthetic cannabinoids. Drug Test Anal. 2012;4(10):745-53. doi:10.1002/dta.1418.

51. Lovett DP, Yanes EG, Herbelin TW, Knoerzer TA, Levisky JA. Structure elucidation and identification of a common metabolite for naphthoylindole-based synthetic cannabinoids using LC-TOF and comparison to a synthetic reference standard. Forensic Sci Int. 2013;226(1-3):81-7. doi:10.1016/j.forsciint.2012.12.012.

52. Huffman JW, Zengin G, Wu MJ, Lu J, Hynd G, Bushell K, et al. Structure-activity relationships for 1-alkyl-3-(1-naphthoyl)indoles at the cannabinoid CB(1) and CB(2) receptors: steric and electronic effects of naphthoyl substituents. New highly selective CB(2) receptor agonists. Bioorg Med Chem. 2005;13(1):89-112. doi:10.1016/j.bmc.2004.09.050.

53. Maurer HH, Meyer MR. High-resolution mass spectrometry in toxicology: current status and future perspectives. Arch Toxicol. 2016;90(9):2161-72. doi:10.1007/s00204-016-1764-1.

54. Auwarter V, Dresen S, Weinmann W, Muller M, Putz M, Ferreiros N. 'Spice' and other herbal blends: harmless incense or cannabinoid designer drugs? J Mass Spectrom. 2009;44(5):832-7. doi:10.1002/jms.1558.

55. Uchiyama N, Kikura-Hanajiri R, Goda Y. Identification of a Novel Cannabimimetic Phenylacetylindole, Cannabipiperidiethanone, as a Designer Drug in a Herbal Product and Its Affinity for Cannabinoid CB₁ and CB₂ Receptors. Chem Pharm Bull. 2011;59(9):1203-5.

56. Uchiyama N, Kawamura M, Kikura-Hanajiri R, Goda Y. Identification and quantitation of two cannabimimetic phenylacetylindoles JWH-251 and JWH-250, and four cannabimimetic naphthoylindoles JWH-081, JWH-015, JWH-200, and JWH-073 as designer drugs in illegal products. Forensic Toxicol. 2010;29(1):25-37. doi:10.1007/s11419-010-0100-3.

57. Zuba D, Byrska B, Maciow M. Comparison of "herbal highs" composition. Anal Bioanal Chem. 2011;400(1):119-26. doi:10.1007/s00216-011-4743-7.

58. Uchiyama N, Kawamura M, Kikura-Hanajiri R, Goda Y. URB-754: a new class of designer drug and 12 synthetic cannabinoids detected in illegal products. Forensic Sci Int. 2013;227(1-3):21-32. doi:10.1016/j.forsciint.2012.08.047.

59. Dresen S, Kneisel S, Weinmann W, Zimmermann R, Auwarter V. Development and validation of a liquid chromatography-tandem mass spectrometry method for the quantitation of synthetic cannabinoids of the aminoalkylindole type and methanandamide in serum and its application to forensic samples. J Mass Spectrom. 2011;46(2):163-71. doi:10.1002/jms.1877.

60. Teske J, Weller JP, Fieguth A, Rothamel T, Schulz Y, Troger HD. Sensitive and rapid quantification of the cannabinoid receptor agonist naphthalen-1-yl-(1-pentylindol-3-yl)methanone (JWH-018) in human serum by liquid chromatography-tandem mass spectrometry. J Chromatogr B Analyt Technol Biomed Life Sci. 2010;878(27):2659-63. doi:10.1016/j.jchromb.2010.03.016.

61. Kneisel S, Auwarter V. Analysis of 30 synthetic cannabinoids in serum by liquid chromatography-electrospray ionization tandem mass spectrometry after liquid-liquid extraction. J Mass Spectrom. 2012;47(7):825-35. doi:10.1002/jms.3020.

62. Hess C, Murach J, Krueger L, Scharrenbroch L, Unger M, Madea B, et al. Simultaneous detection of 93 synthetic cannabinoids by liquid chromatography-tandem mass spectrometry and retrospective application to real forensic samples. Drug Test Anal. 2017;9(5):721-33. doi:10.1002/dta.2030.

63. Dziadosz M, Weller JP, Klintschar M, Teske J. Scheduled multiple reaction monitoring algorithm as a way to analyse new designer drugs combined with synthetic cannabinoids in human serum with liquid chromatography-tandem mass spectrometry. J Chromatogr B Analyt Technol Biomed Life Sci. 2013;929:84-9. doi:10.1016/j.jchromb.2013.04.017.

64. Ammann J, McLaren JM, Gerostamoulos D, Beyer J. Detection and Quantification of New Designer Drugs in Human Blood: Part 1 – Synthetic Cannabinoids. J Anal Toxicol. 2012;36(6):372-80. doi:10.1093/jat/bks048.

65. Kacinko SL, Xu A, Homan JW, McMullin MM, Warrington DM, Logan BK. Development and Validation of a Liquid Chromatography-Tandem Mass Spectrometry Method for the Identification and Quantification of JWH-018, JWH-073, JWH-019, and JWH-250 in Human Whole Blood. J Anal Toxicol. 2011;35(7):386-93. doi:10.1093/anatox/35.7.386.

66. de Castro A, Pineiro B, Lendoiro E, Cruz A, Lopez-Rivadulla M. Quantification of selected synthetic cannabinoids and Delta9-tetrahydrocannabinol in oral fluid by liquid chromatography-tandem mass spectrometry. J Chromatogr A. 2013;1295:99-106. doi:10.1016/j.chroma.2013.04.035.

67. Coulter C, Garnier M, Moore C. Synthetic Cannabinoids in Oral Fluid. J Anal Toxicol. 2011;35(7):424-30. doi:10.1093/anatox/35.7.424.

68. Strano-Rossi S, Anzillotti L, Castrignano E, Romolo FS, Chiarotti M. Ultra high performance liquid chromatography-electrospray ionization-tandem mass spectrometry screening method for direct analysis of designer drugs, "spice" and stimulants in oral fluid. J Chromatogr A. 2012;1258:37-42. doi:10.1016/j.chroma.2012.07.098.

69. Kneisel S, Speck M, Moosmann B, Corneillie TM, Butlin NG, Auwarter V. LC/ESI-MS/MS method for quantification of 28 synthetic cannabinoids in neat oral fluid and its application to preliminary studies on their detection windows. Anal Bioanal Chem. 2013;405(14):4691-706. doi:10.1007/s00216-013-6887-0.

70. Kneisel S, Auwarter V, Kempf J. Analysis of 30 synthetic cannabinoids in oral fluid using liquid chromatography-electrospray ionization tandem mass spectrometry. Drug Test Anal. 2013;5(8):657-69. doi:10.1002/dta.1429.

71. Kneisel S, Speck M, Moosmann B, Auwarter V. Stability of 11 prevalent synthetic cannabinoids in authentic neat oral fluid samples: glass versus polypropylene containers at different temperatures. Drug Test Anal. 2013;5(7):602-6. doi:10.1002/dta.1497.

72. Hutter M, Kneisel S, Auwarter V, Neukamm MA. Determination of 22 synthetic cannabinoids in human hair by liquid chromatography-tandem mass spectrometry. J Chromatogr B Analyt Technol Biomed Life Sci. 2012;903:95-101. doi:10.1016/j.jchromb.2012.07.002.

73. Salomone A, Gerace E, D'Urso F, Di Corcia D, Vincenti M. Simultaneous analysis of several synthetic cannabinoids, THC, CBD and CBN, in hair by ultra-high performance liquid chromatography tandem mass spectrometry. Method validation and application to real samples. J Mass Spectrom. 2012;47(5):604-10. doi:10.1002/jms.2988.

74. Salomone A, Luciano C, Di Corcia D, Gerace E, Vincenti M. Hair analysis as a tool to evaluate the prevalence of synthetic cannabinoids in different populations of drug consumers. Drug Test Anal. 2014;6(1-2):126-34. doi:10.1002/dta.1556.

75. Emerson B, Durham B, Gidden J, Lay JO, Jr. Gas chromatography-mass spectrometry of JWH-018 metabolites in urine samples with direct comparison to analytical standards. Forensic Sci Int. 2013;229(1-3):1-6. doi:10.1016/j.forsciint.2013.03.006.

76. de Jager AD, Warner JV, Henman M, Ferguson W, Hall A. LC-MS/MS method for the quantitation of metabolites of eight commonly-used synthetic cannabinoids in human urine--an Australian perspective. J Chromatogr B Analyt Technol Biomed Life Sci. 2012;897:22-31. doi:10.1016/j.jchromb.2012.04.002.

77. Beuck S, Moller I, Thomas A, Klose A, Schlorer N, Schanzer W, et al. Structure characterisation of urinary metabolites of the cannabimimetic JWH-018 using chemically synthesised reference material for the support of LC-MS/MS-based drug testing. Anal Bioanal Chem. 2011;401(2):493-505. doi:10.1007/s00216-011-4931-5.

78. ElSohly MA, Gul W, ElSohly KM, Murphy TP, Madgula VLM, Khan SI. Liquid Chromatography-Tandem Mass Spectrometry Analysis of Urine Specimens for K2 (JWH-018) Metabolites. J Anal Toxicol. 2011;35(7):487-95. doi:10.1093/anatox/35.7.487.

79. Kronstrand R, Brinkhagen L, Birath-Karlsson C, Roman M, Josefsson M. LC-QTOF-MS as a superior strategy to immunoassay for the comprehensive analysis of synthetic cannabinoids in urine. Anal Bioanal Chem. 2014;406(15):3599-609. doi:10.1007/s00216-013-7574-x.

80. Scheidweiler KB, Jarvis MJ, Huestis MA. Nontargeted SWATH acquisition for identifying 47 synthetic cannabinoid metabolites in human urine by liquid chromatography-high-resolution tandem mass spectrometry. Anal Bioanal Chem. 2015;407(3):883-97. doi:10.1007/s00216-014-8118-8.

Chapter 2: Biotransformation of synthetic cannabinoids JWH-018, JWH-073 and AM2201 by *Cunninghamella elegans*

Chapter 2: Biotransformation of synthetic cannabinoids JWH-018, JWH-073 and AM2201 by *Cunninghamella elegans*

2.1 Abstract

Being marketed as "legal" smoking blends or mixtures, synthetic cannabinoids are abused widely owing to their cannabis-like effect. Due to the rapid introduction of new generation analogues of synthetic cannabinoids to escape from legislative/judicial control, the investigation of the metabolic pathways of these substances is of particular importance for drug control, abstinence and forensic toxicology purposes. In this study, the *in vitro* metabolism of JWH-018, JWH-073 and AM2201 by the fungus *Cunninghamella elegans* has been investigated with the purpose of validating its potential as a complementary model for investigating synthetic cannabinoid metabolism. JWH-018, JWH-073 and AM2201 were incubated for 72 h with *C. elegans*. Detection of metabolites was based on liquid chromatography–tandem mass spectrometry and high resolution mass spectrometry analysis. *C. elegans* was found capable of producing the majority of the phase I metabolites observed in earlier *in vitro* and *in vivo* mammalian studies as a result of monohydroxylation, dihydroxylation, carboxylation, dehydrogenation, ketone formation, dihydrodiol formation, dihydrodiol formation with *N*-dealkylation and combinations thereof. *C. elegans* can thus be a useful and economic model for studying synthetic cannabinoid metabolism.

Keywords: Synthetic cannabinoids, metabolism, *Cunninghamella elegans*, JWH-018, JWH-073, AM2201

Abbreviations

AM2201	[1-(5-fluoropentyl)-1H-indol-3-yl]-1-naphthalenyl-methanone
CB_1	Cannabinoid receptor type 1
C. elegans	*Cunninghamella elegans*
ESI	Electrospray ionisation
HRQToFMS	High resolution quadrupole time-of-flight mass spectrometry
JWH-018	(1-pentyl-1H-indol-3-yl)-1-naphthalenyl-methanone
JWH-073	(1-butyl-1H-indol-3-yl)-1-naphthalenyl-methanone
MS	Mass spectrometry
NMR	Nuclear magnetic resonance

2.2 Introduction

Abusive consumption of synthetic cannabinoids that are agonists at cannabinoid CB_1 receptors has been commonly reported since 2008 [1]. Usually sold as herbal blends or research chemicals in powder, synthetic cannabinoids mimic psychoactive effects of cannabis. However, unlike cannabis some synthetic cannabinoids are reported to be full agonists and thus create more serious public health issues [2]. When a synthetic cannabinoid is scheduled due to increased prevalence and health concerns, new molecules with similar or even stronger psychoactive effects are synthesized by slight structural modifications to bypass the laws [3, 4]. The lack of metabolism data of these new psychoactive molecules together with the lack of reference standards has made optimized detection in biological matrices, especially urine, difficult.

Due to rapid changes in product composition and continuous emergence of new compounds, identifying the unique fingerprint of drug metabolites is of vital importance for forensic-toxicological, clinical-toxicological and doping analysis. Several *in vivo* and *in vitro* models are being used to identify metabolites of synthetic cannabinoids. *In vivo* studies involving the researcher himself administering drug have been reported [5]. Despite the reliability of data obtained from such experiments, the adverse effects of these drugs are unknown and due to both health and ethical reasons it is difficult to perform *in vivo* human excretion studies to investigate the metabolism.

Other *in vivo* animal systems such as mouse, rat, and primates can be used as alternatives to human administration in metabolism studies. Unfortunately these models suffer from a number of limitations such as ethical constraints, cost of experimental models, time that must be spent on breeding animals etc. [6]. Moreover species differences in the excretory pathway may make the extrapolation from experimental animals to humans difficult [7]. Recently *in vivo* chimeric mouse models based upon the transplantation of primary human hepatocytes in uPA-SCID mice that suffer from a transgene-induced liver disease have been evaluated. This model proved to be an efficient alternative for human administration studies for the investigation of steroid metabolism and was recently used to reveal both phase I and phase II metabolism of synthetic cannabinoids, JWH-200 and JWH-122 [8-10]. Although the chimeric mouse is a promising model with respect to the array of

metabolic pathways, the cost and complexity involved in the development of such a model with a high level of hepatocyte repopulation, low amount of urine that can be collected and the concentrated mouse urine matrix are some inherent limitations [10, 11].

In vitro platforms like perfused liver, hepatocytes or human liver microsomes are other valuable models for the elucidation of drug metabolism [6]. In particular, primary human hepatocytes give the closest metabolic profile of a drug to that of *in vivo* humans and are hence considered as the 'gold standard' for predicting *in vivo* metabolic pathways of drugs [12]. Metabolic defects, restricted accessibility to suitable liver samples, unsuitability for quantitative estimations, inability of the cells to proliferate, quick degradation of P450 enzyme activities during culture and the requirement for specific culturing conditions are limitations of these *in vitro* models [10, 13].

The concept of using microorganisms, and in particular *Cunninghamella elegans*, as models of mammalian metabolism has been well documented [14-16]. It has been proven that *C. elegans* has CYP509A1 enzymes that are synonymous to that involved in xenobiotic detoxification in mammals [17] and can metabolise a wide variety of xenobiotics in a regio- and stereo-selective manner similar to mammalian enzyme systems [14, 15]. A recent review on *C. elegans* reports that the fungus shows similarities with mammalian metabolism for a wide variety of drugs [15]. It is highly efficient in its production of metabolites, especially from antidepressants, antibiotics, steroids, alkaloids and related drugs [15]. The cultures of the fungus can be grown by transferring to new agar plates without complexity, adding to advantages of the model [18].

The aim of the study was to elucidate the metabolite profile of (1-pentyl-1H-indol-3-yl)-1-naphthalenyl-methanone (JWH-018), (1-butyl-1H-indol-3-yl)-1-naphthalenyl-methanone (JWH-073) and [1-(5-fluoropentyl)-1H-indol-3-yl]-1-naphthalenyl-methanone (AM2201), three amino alkyl indoles with well-defined metabolic profiles, using the *C. elegans* model and to compare with previously reported *in vivo* and *in vitro* data to examine the potential of this model [19-23].

2.3 Materials and Methods

2.3.1 Chemicals

JWH-018 and JWH-073 were synthesized in-house following previously reported methods and characterised by mass spectrometry (MS) and nuclear magnetic resonance (NMR) spectroscopy with no evidence of cross contamination [24, 25]. AM2201 (purity 99.4%) was obtained from the National Measurement Institute (North Ryde, NSW, Australia). Reference standards of JWH-018 metabolites namely JWH-018 *N*-(4-hydroxypentyl), JWH-018 *N*-(5-hydroxypentyl) and JWH-018 *N*-pentanoic acid and JWH-073 metabolites namely JWH-073 *N*-(3-hydroxybutyl), JWH-073 *N*-(4-hydroxybutyl) and JWH-073 *N*-butanoic acid were obtained from PM separations (Capalaba, QLD, Australia). Reagent grade dichloromethane and LC grade acetonitrile and methanol were obtained from Chemsupply (Gilman, SA, Australia). Potato dextrose agar, glucose, peptone, and yeast extract were purchased from Oxoid Australia (Adelaide, SA, Australia).

2.3.2 Microbial Culture and Biotransformation Conditions

Cultures of *C. elegans* ATCC 10028b (Cryosite Ltd, South Granville, NSW, Australia) were propagated on potato dextrose agar plates [26] at 27 °C for 5 days. The mycelia from five plates were then transferred to 20 mL of sterile physiological saline solution and homogenised for 5 min. Approximately 3 mL aliquots of the homogenate were used to inoculate 250 mL Erlenmeyer flasks containing 100 mL of growth media prepared according to the methods in [18]. The cultures were incubated for 48 h at 26 °C on an Infors HT Multitron rotary shaker (In vitro Technologies, Noble Park North, VIC, Australia) operating at 180 rpm. After 48 h, 10 mg of JWH-018, JWH-073 or AM2201 dissolved in 0.5 mL of methanol was added to the culture and incubated for further 72 h [18]. Control experiments consisted of cultures without cannabinoids and flasks containing only media and cannabinoid [27, 28].

2.3.3 Extraction, Isolation, and Identification of Metabolites

After 72 h of incubation, the contents of each flask, including the controls, were filtered through Buchner funnel into a separating funnel and extracted with three aliquots of dichloromethane (3 × 50 mL). The combined organic extracts were evaporated to dryness under vacuum at 40 °C using a Buchi rotary evaporator (In vitro Technologies, Noble Park North, VIC, Australia) and placed under high vacuum to remove traces of moisture. The residue was dissolved in acetonitrile to prepare 1 mg/mL stock solution and was filtered through 0.22 μM syringe filter before analysis. Cannabinoid parent drugs and metabolites were chromatographically separated using an Agilent Zorbax Eclipse XDB-C18 analytical column (150 × 4.6 mm, 5 μm). Mobile phases consisted of 0.1 % formic acid in water (mobile phase A) and acetonitrile (mobile phase B). The gradient used consisted of 30 % B (0-2 min), linear gradient from 30 % B to 50 % B (2-5 min), 50 % B to 90 % B (5-30 min, hold for 5 min) and 90 % B to 30 % B (35-40 min) run at 0.4 mL/min. MS data were acquired on an Agilent 6490 Triple Quadrupole mass spectrometer with an electrospray ionisation (ESI) source (positive ion mode), interfaced with an Agilent 1290 LC system. Samples prepared were injected in 2 μL volume to obtain full scan and product ion scan spectra. Product ion scan experiments were conducted on precursor ions that were presumed to be metabolites based on the comparison of full scan spectra of the samples and controls. A fragmentor voltage of 380 V with discrete collision energy of 10, 20, 30 and 40 eV (for product ion scan) was applied. The scanning mass range was set at *m/z* 100-1000 (scan time = 500 ms). The sheath gas temperature and flow were set to 250 °C and 11 L/min, respectively. The capillary and nozzle voltages were 3000 V and 1500 V, respectively.

High resolution quadrupole time-of-flight mass spectrometry (HRQToFMS) experiments were carried out on an Agilent 6510 Accurate Mass QToF Mass Spectrometer, equipped with ESI source operated in positive ion mode, in order to determine accurate masses of the metabolites. The following operation parameters were used: injection volume 2μL (full scan) and 10 μL (product ion scan); capillary voltage 3500 V; nebulizer pressure 40 psi (275,790 Pa); drying gas 10.0 L/min; gas temperature 350 °C; fragmentor voltage 160 V; collision energy 10, 20 and 40 eV; skimmer voltage 60 V. HRQToFMS accurate mass spectra were recorded across the range from *m/z* 100 to *m/z* 1000. The mass axis was

calibrated using the mixture provided by the manufacturer over the *m/z* 50-3200 range. A second orthogonal sprayer with a reference solution was used as a continuous calibration using the following reference masses: *m/z* 121.0509 and *m/z* 922.0098. The chromatographic conditions and column used were same as described above. The controls were subjected to the same analysis. Analysis of the chromatographic and mass spectrometric data was conducted using MassHunter Workstation Software Qualitative Analysis (version B.06.00, Agilent). Peaks present in the fungus sample, but not in the controls, were manually identified and their fragmentation patterns and accurate masses were examined to identify the metabolites. The signal-to-noise ratio of all the identified metabolites was greater than 5.

2.4 Results

Fig. 2-1 shows the product ion mass spectra of JWH-018, JWH-073 and AM2201 and their fragmentation patterns. These fragmentation patterns were used as a basis for determining the structures of fungal metabolites of each drug as follows. The presence of a product ion at *m/z* 155 in a mass spectrum of a metabolite indicates that the naphthalene moiety of the metabolite has not been altered. If the ion at *m/z* 155 is absent, it suggests that the naphthalene moiety has undergone modification such as hydroxylation, dihydroxylation or dihydrodiol. The type of modification was deduced by the difference between the amu of the product ion of the parent drugs, i.e. *m/z* 155, and that of the product ion of the metabolite such as *m/z* 171 or *m/z* 189. A difference of 16 amu (*m/z* 171 – *m/z* 155) indicates an addition of an oxygen atom and hence the metabolite is considered to have undergone hydroxylation. Similarly, a difference of 34 amu (*m/z* 189 – *m/z* 155) suggests a formation of dihydrodiol. Product ions originating from other parts of metabolites, such as indole moiety or alkyl side chain, were analysed in the same way to deduce the whole structures of metabolites. The product ion mass spectra and their corresponding proposed fragmentation patterns of the most abundant metabolite for each drug (Ma15 for JWH-018, Mb13 for JWH-073 and Mc25 for AM2201) are shown in Fig. 2-1, illustrating the application of the above described approach in metabolite identification.

Overlaid extracted ion chromatograms of all the metabolites for each drug are shown in Fig. 2-2. The majority of phase I metabolites after incubation with *C. elegans* were oxidation products for all three drugs. In particular, hydroxylation was the most common transformation. Phase II metabolites due to glucosidation and sulfation were only detected for AM2201. The chromatograms of the control cultures without cannabinoids showed no metabolites or substrate present; those of the control flasks containing media and cannabinoid showed only the presence of the substrate. Metabolite identification was further supported by accurate mass data obtained from the high resolution quadrupole time-of-flight mass spectrometry analysis. These data are presented in Supplementary Tables 2-1, 2-3 and 2-5 in the appendix to this chapter [29].

JWH-018
Calculated *m/z*
342.1852
RT 31.4 min

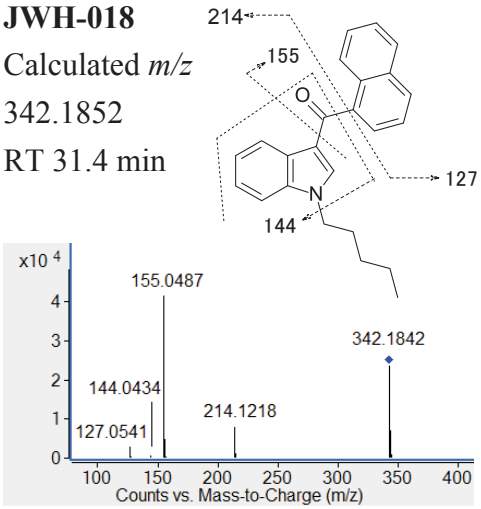

Ma15
Calculated *m/z*
358.1802
RT 17.6 min

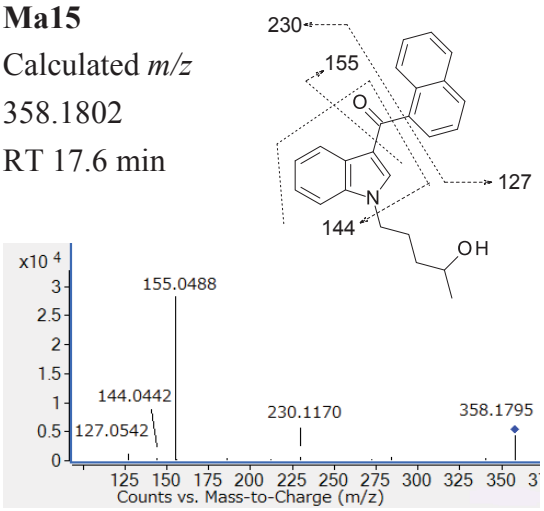

JWH-073
Calculated *m/z*
328.1696
RT 28.8 min

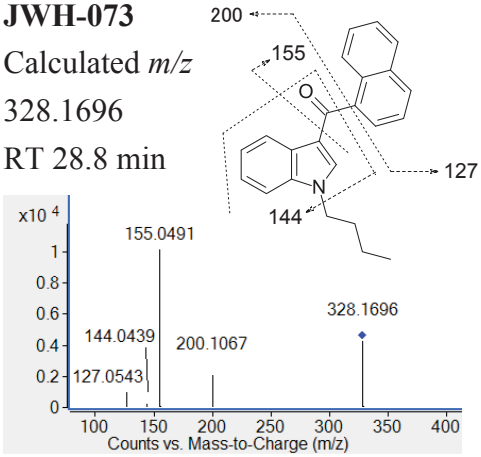

Mb13
Calculated *m/z*
344.1645
RT 17.1 min

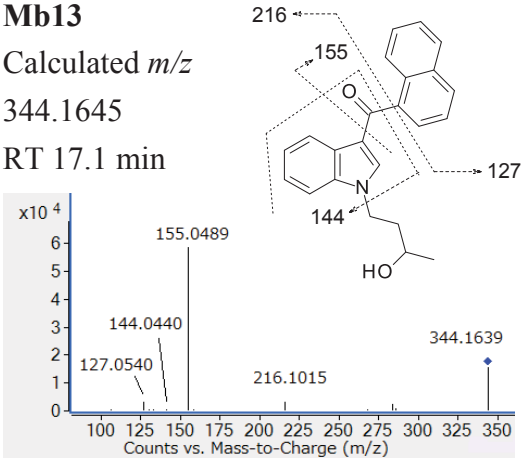

AM2201
Calculated *m/z*
360.1758
RT 25.6 min

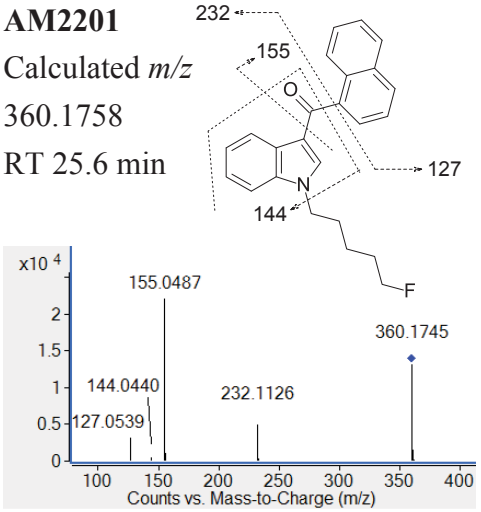

Mc25
Calculated *m/z*
394.1813
RT 12.5 min

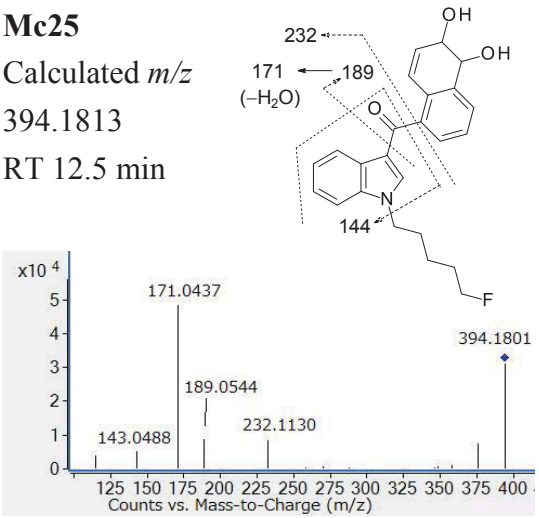

Figure 2-1. Product ion spectra (CE 20 eV) and the proposed fragmentation pathways for JWH-018, JWH-073, AM2201 and their most abundant metabolites (Ma15, Mb13 and Mc25).

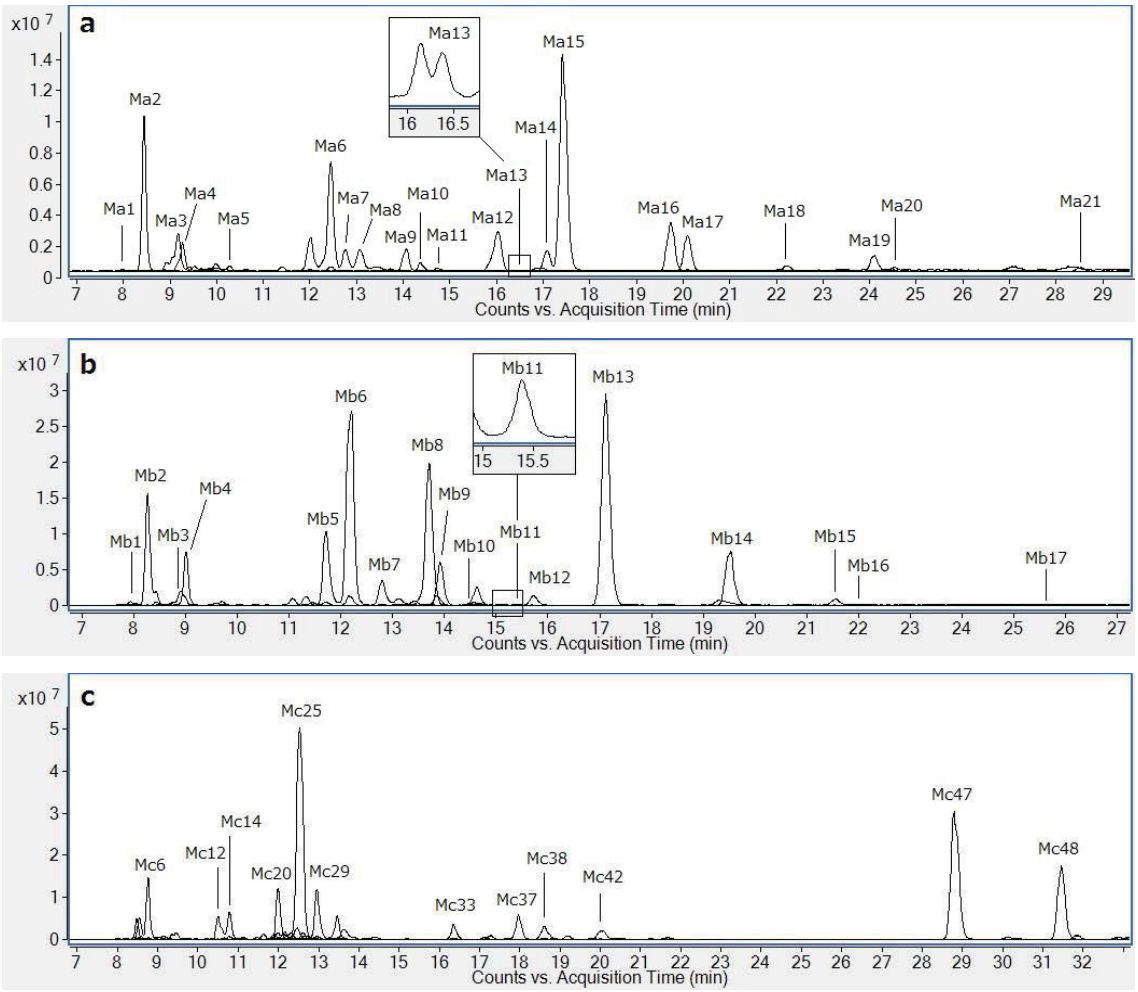

Figure 2-2. Overlaid extracted ion chromatograms of all the metabolites identified in the fungus sample of JWH-018 at *m/z* 306, 340, 356, 358, 372, 374, 376, 390, 392 (**a**); JWH-073 at *m/z* 306, 326, 342, 344, 358, 360, 362, 376, 378 (**b**); and AM2201 at *m/z* 306, 328, 342, 358, 372, 374, 376, 388, 392, 394, 408, 410, 426, 472, 538, 554 (**c**). Only the major metabolites are labelled for AM2201 (**c**). The parent drug peaks are not shown.

2.4.1 JWH-018

Twenty one phase I metabolites (Ma1 – Ma21) were detected (Fig. 2-2A). Supplementary Table 2-1 in the appendix to this chapter [29] lists all metabolites with suggested biotransformation, retention time, observed accurate mass, formula and major product ions. Supplementary Table 2-2 in the appendix to this chapter [29] tabulates the key diagnostic product ions and their tentative structures used in elucidating the biotransformation pathways. Hydroxylation, dihydroxylation, carboxylation, dihydrodiol formation, dehydrogenation, ketone formation, combinations of some of these transformations, and dihydrodiol formation with *N*-dealkylation were observed.

Phase II metabolites were not detected. Proposed metabolic pathway is given in Fig. 2-3. Hydroxylation and dihydroxylation were the most common transformations. The presence of the metabolites JWH-018 *N*-(4-hydroxypentyl) (Ma15), JWH-018 *N*-(5-hydroxypentyl) (Ma14) and JWH-018 *N*-pentanoic acid (Ma13) was confirmed by comparison with reference standards on retention time and product ion spectrum. The peak to the left of Ma13 in Fig. 2-2a has a *m/z* 372, but was found not to be a carboxylic acid metabolite based on the product ions. Mass errors of all metabolites in comparison with the calculated exact mass of proposed structures were all within 1.6 ppm. Comparison of metabolites obtained from *C. elegans* incubation in the present study with those obtained from human urine, human liver microsomes and rat urine samples in the literature is shown in Table 2-1. The majority of human urine metabolites reported in the literature were detected in the fungus sample including hydroxy and carboxy metabolites.

2.4.2 JWH-073

The metabolic transformation of JWH-073 was similar to that of JWH-018 except that there were fewer (seventeen, Mb1-Mb17) metabolites detected (Fig. 2-2b). Supplementary Table 2-3 in the appendix to this chapter [29] lists all metabolites with suggested biotransformation, retention time, observed accurate mass, formula and diagnostic product ions. Supplementary Table 2-4 in the appendix to this chapter [29] tabulates the key diagnostic product ions and their tentative structures used in elucidating the biotransformation pathways. Hydroxylation, dihydroxylation, carboxylation, dihydrodiol formation, dehydrogenation, ketone formation, combinations of some of these transformations, and dihydrodiol formation with *N*-dealkylation were observed. Phase II metabolites were not detected. Proposed metabolic pathway is given in Fig. 2-4. Hydroxylation was the most common transformation. The presence of the metabolites JWH-073 *N*-(3-hydroxybutyl) (Mb13), JWH-073 *N*-(4-hydroxybutyl) (Mb12) and JWH-073 *N*-butanoic acid (Mb11) was confirmed by comparison with reference standards on retention time and product ion spectrum. Mass errors of all metabolites in comparison with the calculated exact mass of proposed structures were all within 2.6 ppm. Comparison of metabolites obtained from *C. elegans* incubation in the present study with those obtained from human urine and human liver microsomes samples in the literature is shown in Table 2-2. Hydroxylation (human urine and human liver microsomes) and

carboxylation (human urine) were reported in the literature and both were observed for fungus metabolites.

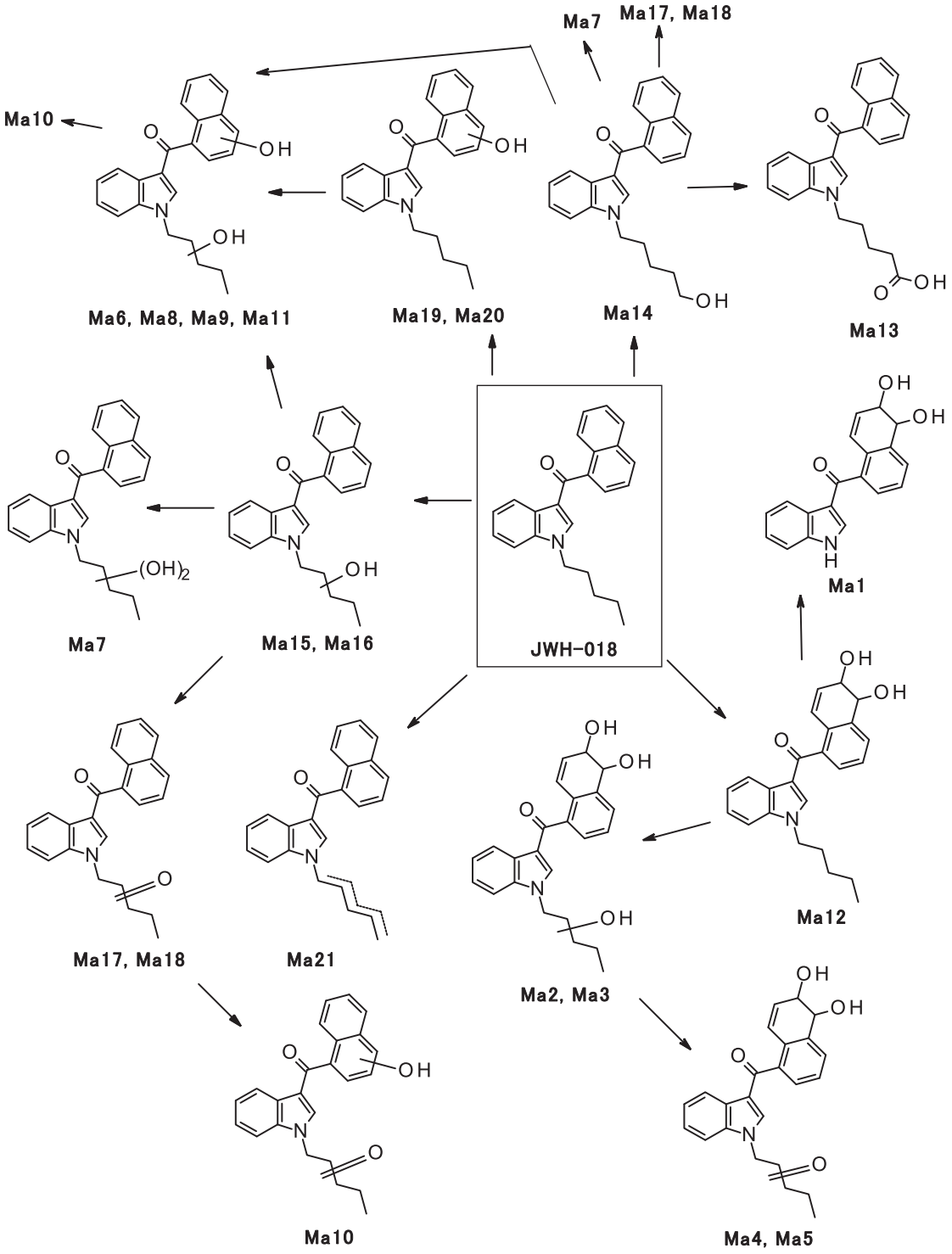

Figure 2-3. Proposed metabolic pathway of JWH-018 in *C. elegans*.

Table 2-1. Metabolites of JWH-018 after *C. elegans* incubation in comparison with metabolites from other sources (human urine, human liver microsomes and rat urine) reported in literature, in alphabetical order. Square brackets in the metabolites column indicate the corresponding fungal metabolites in Fig. 2-3.

Metabolites	*CE*[*]	HU[*]	HLM[*]	RU[*]
Carboxylation [Ma13]	√	√ [20, 23, 30-33]	√ [19]	
Dehydrogenation [Ma21]	√		√ [19]	
Demethylation + carboxylation (JWH-073 *N*-butanoic acid)		√ [33]		
Dihydrodiol formation [Ma12]	√	√ [30, 32]	√ [19]	
Dihydrodiol formation + dihydroxylation		√ [30]	√ [19]	
Dihydrodiol formation + hydroxylation [Ma2, Ma3]	√	√ [30, 32]	√ [19]	
Dihydrodiol formation + ketone formation [Ma4, Ma5]	√			
Dihydrodiol formation + *N*-dealkylation [Ma1]	√	√ [30]	√ [19]	
Dihydroxylation [Ma6 – Ma9, Ma11]	√	√ [20, 23, 30, 32]	√ [19]	
Hydroxylation [Ma14 – Ma16, Ma19, Ma20]	√	√ [20, 23, 30-33]	√ [19, 23]	
Ketone formation [Ma17, Ma18]	√	√ [30]	√ [19]	
Ketone formation + hydroxylation [Ma10]	√	√ [30]	√ [19]	
N-dealkylation			√ [19]	√ [20]
N-dealkylation + hydroxylation		√ [20, 30, 32]	√ [19]	√ [20]
Trihydroxylation		√ [23, 30]	√ [19]	

[*] Abbreviations: *CE*, *Cunninghamella elegans*; HU, human urine; HLM, human liver microsomes; RU, rat urine.

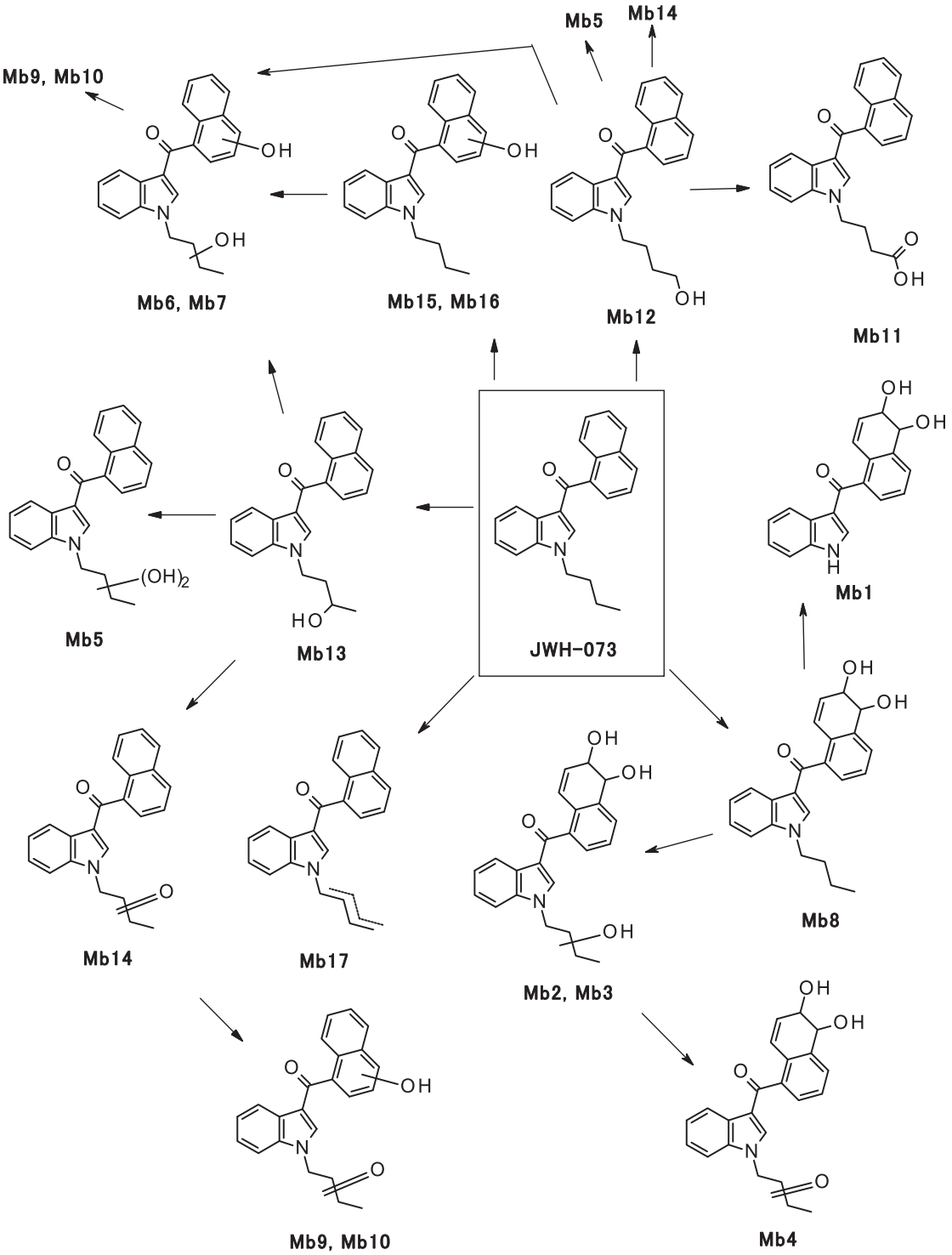

Figure 2-4. Proposed metabolic pathway of JWH-073 in *C. elegans*.

Table 2-2. Metabolites of JWH-073 after *C. elegans* incubation in comparison with metabolites from other sources (human urine and human liver microsomes) reported in literature, in alphabetical order. Square brackets in the metabolites column indicate the corresponding fungal metabolites in Fig. 2-4.

Metabolites	*CE*[*]	HU[*]	HLM[*]
Carboxylation [Mb11]	√	√ [31]	
Dehydrogenation [Mb17]	√		
Dihydrodiol formation [Mb8]	√		
Dihydrodiol formation + hydroxylation [Mb2, Mb3]	√		
Dihydrodiol formation + ketone formation [Mb4]	√		
Dihydrodiol formation + *N*-dealkylation [Mb1]	√		
Dihydroxylation [Mb5 – Mb7]	√		
Hydroxylation [Mb12, Mb13, Mb15, Mb16]	√	√ [20, 31]	√ [23]
Ketone formation [Mb14]	√		
Ketone formation + hydroxylation [Mb9, Mb10]	√		

[*] Abbreviations: *CE*, *Cunninghamella elegans*; HU, human urine; HLM, human liver microsomes.

2.4.3 AM2201

The biotransformation of AM2201 was similar to the other two drugs, but produced extra metabolites including phase II metabolites. Forty eight phase I and II metabolites (Mc1-Mc48) were detected. Supplementary Table 2-5 in the appendix to this chapter [29] lists all metabolites with suggested biotransformation, retention time, observed accurate mass, formula and diagnostic product ions. Supplementary Table 2-6 in the appendix to this chapter [29] tabulates the key diagnostic product ions and their tentative structures used in elucidating the biotransformation pathways. Hydroxylation, dihydroxylation, trihydroxylation, oxidative defluorination, dihydrodiol formation, ketone formation, *N*-dealkylation, defluorination and demethylation were observed either alone or in combination. Glucosidation of hydroxy and dihydroxy metabolites and sulfation of dihydroxy metabolites were detected as Phase II transformation. Although the retention of the sulfate metabolites on the C18 column used appears unusually long, similar observations were reported previously when the sulfate conjugates had a longer retention than the unconjugated metabolites [28]. In contrast, glucuronidation was not observed. This lack of detection of glucuronides is less likely due to the extraction conditions as the

similarly polar glucoside metabolites were successfully extracted and detected. Fig. 2-5 depicts the proposed metabolic pathways of AM2201 by *C. elegans*. Hydroxylation and dihydroxylation were the most common transformations. The presence of JWH-018 *N*-(5-hydroxypentyl) (Mc34) and JWH-018 *N*-pentanoic acid (Mc33) metabolites was confirmed by comparison with reference standards on retention time and product ion spectrum. Mass errors of all metabolites in comparison with the calculated exact mass of proposed structures were all within 1.4 ppm. Comparison of metabolites obtained from *C. elegans* incubation in the present study with those obtained from human urine, human postmortem heart blood, human liver microsomes and rat urine samples in the literature is shown in Table 2-3. The majority of human urine metabolites reported in the literature were detected in the fungus sample including JWH-018 *N*-(5-hydroxypentyl), JWH-018 *N*-pentanoic acid and AM2201 hydroxy metabolites.

AM2201 is a fluorinated analogue of JWH-018 at the terminal carbon of the pentyl side chain. Hence, in addition to the types of transformation observed for JWH-018 and JWH-073 metabolism, oxidative defluorination to form a terminal hydroxy or carboxy group was a common reaction.

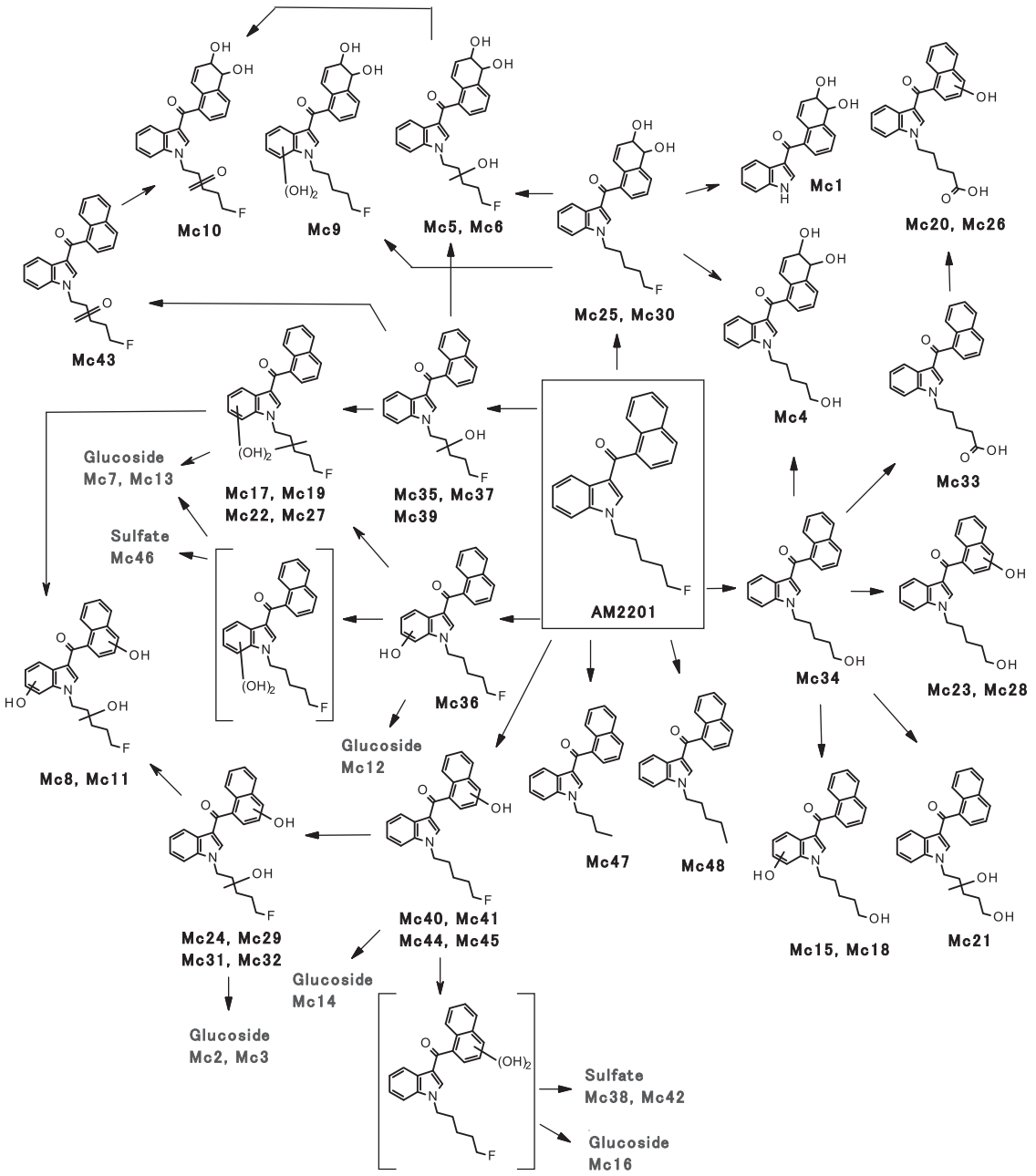

Figure 2-5. Proposed metabolic pathway of AM2201 in *C. elegans*. Parentheses indicate intermediate metabolites that were not detected in the study.

Table 2-3. Metabolites of AM2201 after *C. elegans* incubation in comparison with metabolites from other sources (human urine, human postmortem heart blood, human liver microsomes and rat urine) reported in literature, in alphabetical order. Square brackets in the metabolites column indicate the corresponding fungal metabolites in Fig. 2-5.

Metabolites	*CE*[*]	HU[*]	HPHB[*]	HLM[*]	RU[*]
Defluorination (JWH-018) [Mc48]	√				
Defluorination + Demethylation (JWH-073) [Mc47]	√				
Defluorination + hydroxylation (JWH-018 *N*-(4-hydroxypentyl))		√ [34]			
Dihydrodiol formation [Mc25, Mc30]	√	√ [35]		√ [35]	
Dihydrodiol formation + dihydroxylation [Mc9]	√				
Dihydrodiol formation + hydroxylation [Mc5, Mc6]	√				
Dihydrodiol formation + ketone formation [Mc10]	√				
Dihydrodiol formation + *N*-dealkylation [Mc1]	√				
Dihydroxylation [Mc2, Mc3, Mc7, Mc13, Mc16, Mc17, Mc19, Mc22, Mc24, Mc27, Mc29, Mc31, Mc32, Mc38, Mc42, Mc46]	√	√ [35]		√ [35]	
Hydroxylation [Mc12, Mc14, Mc35 – Mc37, Mc39 – Mc41, Mc44, Mc45]	√	√ [5, 34-36]	√ [37]	√ [35, 37]	√ [34]
Ketone formation [Mc43]	√				
N-dealkylation		√ [35]		√ [35]	
Oxidative defluorination (JWH-018 *N*-(5-hydroxypentyl)) [Mc34]	√	√ [5, 34, 35]	√ [37]	√ [35, 37]	√ [34]
Oxidative defluorination + dihydrodiol formation (JWH-018 dihydrodiol-hydroxy) [Mc4]	√	√ [35]		√ [35]	
Oxidative defluorination + hydroxylation (JWH-018 dihydroxy) [Mc15, Mc18, Mc21, Mc23, Mc28]	√				
Oxidative defluorination to carboxylic acid (JWH-018 *N*-pentanoic acid) [Mc33]	√	√ [5, 34, 35]	√ [37]	√ [35, 37]	√ [34]
Oxidative defluorination to carboxylic acid + decarboxylation + carboxylation (JWH-073 *N*-butanoic acid)		√ [5, 34]			√ [34]
Oxidative defluorination to carboxylic acid + decarboxylation + hydroxylation (JWH-073 *N*-(4-hydroxybutyl)		√ [5]			
Oxidative defluorination to carboxylic acid + hydroxylation [Mc20, Mc26]	√				
Trihydroxylation [Mc8, Mc11]	√				

[*] Abbreviations: *CE*, *Cunninghamella elegans*; HU, human urine; HLM, human liver microsomes; RU, rat urine.

2.5 Discussion

The metabolic transformation of JWH-018, JWH-073 and AM2201 by *C. elegans* was similar to one another as they are closely related structural analogues. The types of metabolic transformation detected were identical for JWH-018 and JWH-073, and they are carboxylation, dehydrogenation, dihydrodiol formation, dihydrodiol with hydroxylation, dihydrodiol with ketone formation, dihydrodiol with *N*-dealkylation, dihydroxylation, hydroxylation, ketone formation and ketone formation with hydroxylation. AM2201 showed all the transformations except carboxylation, dehydrogenation, and ketone formation with hydroxylation. AM2201 underwent additional transformation including defluorination and oxidative defluorination, unique to compounds with a fluorine atom, as well as phase II metabolism including glucosidation and sulfation. Due to oxidative defluorination, some of the AM2201 metabolites are the same as JWH-018 metabolites: Mc4 and Ma2, Mc33 and Ma13, Mc34 and Ma14. Mc23 and Mc28 also matched well with Ma6 and Ma8, respectively, on both retention times and fragmentation patterns. Mc21, on the other hand, was a structural isomer of Ma7. The number of metabolites and metabolic transformation observed for AM2201 was higher than that for JWH-018 and JWH-073, likely because AM2201 has a fluorine atom enabling additional metabolic pathways.

Comparison of the fungus metabolites from the present study with human metabolites reported in the literature shows good agreement. Out of the twelve kinds of human urine metabolites reported in the literature for JWH-018, eight metabolite types were also detected among the *C. elegans* metabolites (Table 2-1), including the major human urine metabolites, namely *N*-(4-hydroxypentyl), *N*-pentanoic acid and *N*-(5-hydroxypentyl) metabolites. Minor human urine metabolites [33] such as demethylation with carboxylation (JWH-073 *N*-butanoic acid), dihydrodiol formation with dihydroxylation, *N*-dealkylation with hydroxylation and trihydroxylation metabolites were not observed using this model.

For JWH-073, all the reported human urine and human liver microsomes metabolites, i.e. hydroxylated and carboxylated metabolites, were observed in the *C. elegans* sample (Table 2-2). Compared to JWH-018 metabolites, very few have been reported as human

urine or human liver microsomes metabolites. This may be because the detection of only the major metabolites was possible as the concentration of JWH-073 in the herbal products is usually low [38]. In any case, the fungus demonstrated the ability to produce the major human metabolites.

Among the ten human urine or human postmortem heart blood metabolites reported for AM2201, six metabolites were generated by the fungus (Table 2-3). Most importantly, these include the major human urine metabolites, JWH-018 *N*-(5-hydroxypentyl) and JWH-018 *N*-pentanoic acid metabolites [5], as well as JWH-018 *N*-(5-hydroxypentyl)-dihydrodiol, AM2201 hydroxy, AM2201 dihydroxy and AM2201 dihydrodiol metabolites. The four human urine metabolites that were not found in the fungus sample are *N*-dealkylation, JWH-018 *N*-(4-hydroxypentyl), JWH-073 *N*-butanoic acid and JWH-073 *N*-(4-hydroxybutyl) metabolites. The disagreement between the fungus and the human urine metabolites, however, may not be as significant. While JWH-018 *N*-(4-hydroxypentyl) metabolite was detected by Jang *et al*. [34], Hutter *et al*. [5] did not find its presence in authentic urine samples nor in self-administered urine samples. This may be such that JWH-018 *N*-(4-hydroxypentyl) metabolite detected by Jang *et al*. might come from unreported consumption of JWH-018 by the drug abusers. Also, despite the fact that JWH-073 metabolites were not observed in the present study, the fungus produced JWH-073 itself, suggesting the possibility that it can produce JWH-073 *N*-butanoic acid and JWH-073 *N*-(4-hydroxybutyl) metabolites if incubated longer. With regards to human postmortem heart blood metabolites, it is interesting to note that the reported metabolites are JWH-018 *N*-(5-hydroxypentyl), JWH-018 *N*-pentanoic acid and AM2201 *N*-(4-hydroxypentyl) metabolites and that the former two metabolites are the most abundant as with human urine metabolites [37]. Therefore, the fungus metabolites of AM2201 were consistent with not only human urine but also human postmortem heart blood metabolites.

Previously, the detection of JWH-018 itself as a metabolite of AM2201 has not been reported although JWH-018 metabolites, such as JWH-018 *N*-(5-hydroxypentyl) and JWH-018 *N*-pentanoic acid, derived from oxidative defluorination have been reported. If JWH-018 can be formed as a metabolite by humans, it would present difficulty in distinguishing AM2201 abusers from those who ingested both JWH-018 and AM2201. However, in a self-experiment where one of the authors ingested pure AM2201, the

absence of JWH-018 *N*-(4-hydroxypentyl) metabolite, a major human metabolite of JWH-018, was reported in both serum and urine samples [5]. This suggests that oxidative defluorination is the only pathway to JWH-018 metabolites in humans and that if JWH-018 is formed at all, the concentration is likely to be so low that it has virtually no effects on production of its metabolites.

Unlike JWH-018 and JWH-073, phase II metabolites of AM2201 were also detected in the fungus sample. However, glucuronides, which were determined to be the major phase II human urine metabolites [35], were not observed. Instead, glucosides and sulfates were found. A previous study on drug metabolism by *C. elegans* showed that glucosides and sulfates were formed for the drugs whose main phase II human and equine metabolites are sulfates and glucuronides [28]. Although *C. elegans* has been reported to have the ability to produce glucuronides [39], its capacity to produce glucuronides may be limited and therefore the fungus is not suitable for producing the human phase II metabolites of synthetic cannabinoids, whose main phase II metabolites are reported to be glucuronides [35, 40]. The cause for more extensive metabolism observed for AM2201 is unknown.

In the present study, the incubation time was not optimised to obtain the best metabolic profiles that mimic human metabolism in terms of the quantity (measured by peak area) of the metabolites formed. Under the conditions reported here, however, JWH-018 *N*-(4-hydroxypentyl) metabolite (Ma15) and JWH-073 *N*-(3-hydroxybutyl) metabolite (Mb13) were found to be the most abundant metabolite for JWH-018 and JWH-073, respectively, consistent with human metabolism. On the other hand, carboxy metabolites (Ma13, Mb11), were present in a relatively lower amount in the fungal system. With AM2201, the most abundant metabolite was a dihydrodiol metabolite (Mc25), while the abundance of human metabolites JWH-018 *N*-(5-hydroxypentyl) (Mc34) and JWH-018 *N*-pentanoic acid (Mc33) was relatively low. Two limitations for using peak area as the quantity of the metabolites in these experiments should be noted: different metabolites may have significant differences in extraction recoveries resulting in a different ratio of metabolites observed by mass spectrometry from the actual ratio in the sample and mass spectrometric responses can be different for each metabolite due to different ionisation efficiencies.

Metabolism study is important not only for drug testing purposes by Police and hospital scientists but also for understanding pharmacology of the new designer drugs. However, currently the identification of metabolites of synthetic cannabinoids is largely relying on the analysis by mass spectrometry and thus the exact structures of metabolites are inconclusive without the use of reference standards. Analysis of metabolites by nuclear magnetic resonance spectroscopy after isolating them will provide more concrete structural elucidation, but this is usually limited by the low amount of metabolites obtained by the common models such as human hepatocytes, human liver microsomes or rats. With *C. elegans*, it is easy to scale up the incubation and hence obtain a large amount of metabolites [15], indicating the potential for isolation and purification of new synthetic cannabinoid metabolites for NMR analysis.

2.6 Conclusion

Cunninghamella elegans produced a large number of metabolites of JWH-018, JWH-073 and AM2201. Although the fungus cannot be used to produce phase II metabolites consistent with those found in humans, it has demonstrated its ability to form the reported major human phase I metabolites of the investigated synthetic cannabinoids. Therefore, the fungus has the potential to be used as a complementary model to predict and characterise human metabolites of new synthetic cannabinoids.

2.7 References

1. EMCDDA. Understanding the 'Spice' phenomenon. Luxembourg: Office for Official Publications of the European Communities 2009.

2. Fantegrossi WE, Moran JH, Radominska-Pandya A, Prather PL. Distinct pharmacology and metabolism of K2 synthetic cannabinoids compared to Delta(9)-THC: mechanism underlying greater toxicity? Life Sci. 2014;97(1):45-54. doi:10.1016/j.lfs.2013.09.017.

3. Seely KA, Lapoint J, Moran JH, Fattore L. Spice drugs are more than harmless herbal blends: a review of the pharmacology and toxicology of synthetic cannabinoids. Prog Neuropsychopharmacol Biol Psychiatry. 2012;39(2):234-43. doi:10.1016/j.pnpbp.2012.04.017.

4. Kikura-Hanajiri R, Kawamura NU, Goda Y. Changes in the prevalence of new psychoactive substances before and after the introduction of the generic scheduling of synthetic cannabinoids in Japan. Drug Test Anal. 2014;6(7-8):832-9. doi:10.1002/dta.1584.

5. Hutter M, Moosmann B, Kneisel S, Auwarter V. Characteristics of the designer drug and synthetic cannabinoid receptor agonist AM-2201 regarding its chemistry and metabolism. J Mass Spectrom. 2013;48(7):885-94. doi:10.1002/jms.3229.

6. Pekala E, Kubowicz P, Lazewska D. Cunninghamella as a microbiological model for metabolism of histamine H(3) receptor antagonist 1-[3-(4-tert-butylphenoxy)propyl]piperidine. Appl Biochem Biotechnol. 2012;168(6):1584-93. doi:10.1007/s12010-012-9880-8.

7. Katoh M, Tateno C, Yoshizato K, Yokoi T. Chimeric mice with humanized liver. Toxicology. 2008;246(1):9-17. doi:10.1016/j.tox.2007.11.012.

8. De Brabanter N, Esposito S, Tudela E, Lootens L, Meuleman P, Leroux-Roels G, et al. In vivo and in vitro metabolism of the synthetic cannabinoid JWH-200. Rapid Commun Mass Spectrom. 2013;27(18):2115-26. doi:10.1002/rcm.6673.

9. De Brabanter N, Esposito S, Geldof L, Lootens L, Meuleman P, Leroux-Roels G, et al. In vitro and in vivo metabolisms of 1-pentyl-3-(4-methyl-1-naphthoyl)indole (JWH-122). Forensic Toxicol. 2013;31(2):212-22. doi:10.1007/s11419-013-0179-4.

10. Lootens L, Meuleman P, Pozo OJ, Van Eenoo P, Leroux-Roels G, Delbeke FT. uPA+/+-SCID mouse with humanized liver as a model for in vivo metabolism of exogenous steroids: methandienone as a case study. Clin Chem. 2009;55(10):1783-93. doi:10.1373/clinchem.2008.119396.

11. Lootens L, Van Eenoo P, Meuleman P, Pozo OJ, Van Renterghem P, Leroux-Roels G, et al. Steroid metabolism in chimeric mice with humanized liver. Drug Test Anal. 2009;1(11-12):531-7. doi:10.1002/dta.67.

12. Gómez-Lechón MJ, Castell JV, Donato MT. An update on metabolism studies using human hepatocytes in primary culture. Expert Opin Drug Metab Toxicol. 2008;4(7):837-54. doi:doi:10.1517/17425255.4.7.837.

13. Asha S, Vidyavathi M. Role of human liver microsomes in in vitro metabolism of drugs-a review. Appl Biochem Biotechnol. 2010;160(6):1699-722. doi:10.1007/s12010-009-8689-6.

14. Moody JD, Freeman JP, Cerniglia CE. Biotransformation of Doxepin by Cunninghamella elegans. Drug Metab Dispos. 1999;27(10):1157-64.

15. Asha S, Vidyavathi M. Cunninghamella--a microbial model for drug metabolism studies--a review. Biotechnol Adv. 2009;27(1):16-29. doi:10.1016/j.biotechadv.2008.07.005.

16. Murphy C. Drug metabolism in microorganisms. Biotechnol Lett. 2015;37(1):19-28. doi:10.1007/s10529-014-1653-8.

17. Wang R-F, Cao W-W, Khan AA, Cerniglia CE. Cloning, sequencing, and expression in Escherichia coli of a cytochrome P450 gene from Cunninghamella elegans. FEMS Microbiol Lett. 2000;188(1):55-61. doi:10.1111/j.1574-6968.2000.tb09168.x.

18. Choudhary MI, Khan NT, Musharraf SG, Anjum S, Atta ur R. Biotransformation of adrenosterone by filamentous fungus, Cunninghamella elegans. Steroids. 2007;72(14):923-9. doi:http://dx.doi.org/10.1016/j.steroids.2007.08.002.

19. Wintermeyer A, Moller I, Thevis M, Jubner M, Beike J, Rothschild MA, et al. In vitro phase I metabolism of the synthetic cannabimimetic JWH-018. Anal Bioanal Chem. 2010;398(5):2141-53. doi:10.1007/s00216-010-4171-0.

20. Grigoryev A, Savchuk S, Melnik A, Moskaleva N, Dzhurko J, Ershov M, et al. Chromatography-mass spectrometry studies on the metabolism of synthetic cannabinoids JWH-018 and JWH-073, psychoactive components of smoking mixtures. J Chromatogr B. 2011;879(15-16):1126-36. doi:10.1016/j.jchromb.2011.03.034.

21. Chimalakonda KC, Bratton SM, Le VH, Yiew KH, Dineva A, Moran CL, et al. Conjugation of synthetic cannabinoids JWH-018 and JWH-073, metabolites by human UDP-glucuronosyltransferases. Drug Metab Dispos. 2011;39(10):1967-76. doi:10.1124/dmd.111.040709.

22. Elsohly MA, Gul W, Wanas AS, Radwan MM. Synthetic cannabinoids: analysis and metabolites. Life Sci. 2014;97(1):78-90. doi:10.1016/j.lfs.2013.12.212.

23. ElSohly MA, Gul W, ElSohly KM, Murphy TP, Madgula VLM, Khan SI. Liquid Chromatography-Tandem Mass Spectrometry Analysis of Urine Specimens for K2 (JWH-018) Metabolites. J Anal Toxicol. 2011;35(7):487-95. doi:10.1093/anatox/35.7.487.

24. Nunomoto S, Kawakami Y, Yamashita Y, Takeuchi H, Eguchi S. Regioselectivity control in alkylation reactions of indolyl ambident anion. J Chem Soc, Perkin Trans 1. 1990(1):111-4. doi:10.1039/P19900000111.

25. Okauchi T, Itonaga M, Minami T, Owa T, Kitoh K, Yoshino H. A General Method for Acylation of Indoles at the 3-Position with Acyl Chlorides in the Presence of Dialkylaluminum Chloride. Org Lett. 2000;2(10):1485-7. doi:10.1021/ol005841p.

26. Botha A. Geotrichum. In: Batt CA, Tortorello ML, editors. Encyclopedia of Food Microbiology. 2. second ed. London: Elsevier; 2014. p. 90.

27. Choudhary MI, Siddiqui ZA, Musharraf SG, Nawaz SA, Atta Ur R. Microbial transformation of prednisone. Nat Prod Res. 2005;19(4):311-7. doi:10.1080/14786410410001729168.

28. Rydevik A, Thevis M, Krug O, Bondesson U, Hedeland M. The fungus Cunninghamella elegans can produce human and equine metabolites of selective

androgen receptor modulators (SARMs). Xenobiotica. 2013;43(5):409-20. doi:10.3109/00498254.2012.729102.

29. Watanabe S, Kuzhiumparambil U, Winiarski Z, Fu S. Data on individual metabolites of synthetic cannabinoids JWH-018, JWH-073 and AM2201 by *Cunninghamella elegans*. Data Brief. 2016;7:332-40. doi:10.1016/j.dib.2016.02.039.1.

30. Moller I, Wintermeyer A, Bender K, Jubner M, Thomas A, Krug O, et al. Screening for the synthetic cannabinoid JWH-018 and its major metabolites in human doping controls. Drug Test Anal. 2011;3(9):609-20. doi:10.1002/dta.158.

31. Hutter M, Broecker S, Kneisel S, Auwarter V. Identification of the major urinary metabolites in man of seven synthetic cannabinoids of the aminoalkylindole type present as adulterants in 'herbal mixtures' using LC-MS/MS techniques. J Mass Spectrom. 2012;47(1):54-65. doi:10.1002/jms.2026.

32. Sobolevsky T, Prasolov I, Rodchenkov G. Detection of JWH-018 metabolites in smoking mixture post-administration urine. Forensic Sci Int. 2010;200(1-3):141-7. doi:10.1016/j.forsciint.2010.04.003.

33. Moran CL, Le VH, Chimalakonda KC, Smedley AL, Lackey FD, Owen SN, et al. Quantitative measurement of JWH-018 and JWH-073 metabolites excreted in human urine. Anal Chem. 2011;83(11):4228-36. doi:10.1021/ac2005636.

34. Jang M, Yang W, Shin I, Choi H, Chang H, Kim E. Determination of AM-2201 metabolites in urine and comparison with JWH-018 abuse. Int J Legal Med. 2014;128(2):285-94. doi:10.1007/s00414-013-0884-x.

35. Sobolevsky T, Prasolov I, Rodchenkov G. Detection of urinary metabolites of AM-2201 and UR-144, two novel synthetic cannabinoids. Drug Test Anal. 2012;4(10):745-53. doi:10.1002/dta.1418.

36. Elian AA, Hackett J. Analysis of AM-2201 and metabolites in a drugs and driving case. Drug Test Anal. 2014;6(4):389-95. doi:10.1002/dta.1535.

37. Patton AL, Chimalakonda KC, Moran CL, McCain KR, Radominska-Pandya A, James LP, et al. K2 toxicity: fatal case of psychiatric complications following AM2201 exposure. J Forensic Sci. 2013;58(6):1676-80. doi:10.1111/1556-4029.12216.

38. Jang M, Yang W, Choi H, Chang H, Lee S, Kim E, et al. Monitoring of urinary metabolites of JWH-018 and JWH-073 in legal cases. Forensic Sci Int. 2013;231(1-3):13-9. doi:10.1016/j.forsciint.2013.03.053.

39. Zhang D, Yang Y, Leakey JEA, Cerniglia CE. Phase I and phase II enzymes produced by Cunninghamella elegans for the metabolism of xenobiotics. FEMS Microbiol Lett. 1996;138(2-3):221-6. doi:10.1111/j.1574-6968.1996.tb08161.x.

40. Chimalakonda KC, Moran CL, Kennedy PD, Endres GW, Uzieblo A, Dobrowolski PJ, et al. Solid-phase extraction and quantitative measurement of omega and omega-1 metabolites of JWH-018 and JWH-073 in human urine. Anal Chem. 2011;83(16):6381-8. doi:10.1021/ac201377m.

2.8. Appendices

Supplementary Table 2-1. Metabolites of JWH-018 after *C. elegans* incubation.

ID	Biotransformation	RT (min)	*m/z* $[M+H]^+$	Mass accuracy (ppm)	Formula	Major product ions
Ma1	Dihydrodiol formation + *N*-dealkylation	8.0	306.1123	-0.7	$C_{19}H_{15}NO_3$	143, 144, 171, 189
Ma2	Dihydrodiol formation + hydroxylation at pentyl side chain	8.5	392.1852	-1.0	$C_{24}H_{25}NO_4$	143, 144, 171, 189, 230, 374
Ma3	Dihydrodiol formation + hydroxylation at pentyl side chain	9.2	392.1850	-1.6	$C_{24}H_{25}NO_4$	143, 144, 171, 189, 230, 374
Ma4	Dihydrodiol formation + ketone formation at pentyl side chain	9.3	390.1694	-1.4	$C_{24}H_{23}NO_4$	143, 144, 171, 189, 228
Ma5	Dihydrodiol formation + ketone formation at pentyl side chain	10.3	390.1695	-1.1	$C_{24}H_{23}NO_4$	143, 144, 171, 189, 228
Ma6	Dihydroxylation at pentyl side chain and naphthalene moiety	12.5	374.1745	-1.5	$C_{24}H_{23}NO_3$	143, 144, 171, 230
Ma7	Dihydroxylation at pentyl side chain	12.8	374.1745	-1.6	$C_{24}H_{23}NO_3$	127, 144, 155, 246
Ma8	Dihydroxylation at pentyl side chain and naphthalene moiety	13.1	374.1746	-1.3	$C_{24}H_{23}NO_3$	143, 144, 171, 230
Ma9	Dihydroxylation at pentyl side chain and naphthalene moiety	14.1	374.1746	-1.3	$C_{24}H_{23}NO_3$	143, 144, 171, 230

ID	Biotransformation	RT (min)	*m/z* $[M+H]^+$	Mass accuracy (ppm)	Formula	Major product ions
Ma10	Ketone formation at pentyl side chain + hydroxylation at naphthalene moiety	14.5	372.1590	-1.0	$C_{24}H_{21}NO_3$	143, 144, 171, 228
Ma11	Dihydroxylation at pentyl side chain and naphthalene moiety	14.9	374.1745	-1.5	$C_{24}H_{23}NO_3$	143, 144, 171, 230
Ma12	Dihydrodiol formation	16.1	376.1901	-1.6	$C_{24}H_{25}NO_3$	143, 171, 189, 214
Ma13	Carboxylation (*N*-pentanoic acid)[a]	16.4	372.1591	-0.9	$C_{24}H_{21}NO_3$	127, 144 155 244
Ma14	Hydroxylation at pentyl side chain (5-hydroxypentyl)[a]	17.2	358.1796	-1.6	$C_{24}H_{23}NO_2$	127, 144, 155, 230
Ma15	Hydroxylation at pentyl side chain (4-hydroxypentyl)[a]	17.6	358.1798	-1.0	$C_{24}H_{23}NO_2$	127, 144, 155, 230
Ma16	Hydroxylation at pentyl side chain	19.9	358.1798	-1.1	$C_{24}H_{23}NO_2$	127, 144, 155, 230
Ma17	Ketone formation at pentyl side chain	20.2	356.1640	-1.6	$C_{24}H_{21}NO_2$	127, 144, 155, 228
Ma18	Ketone formation at pentyl side chain	22.4	356.1641	-1.2	$C_{24}H_{21}NO_2$	127, 144, 155, 228
Ma19	Hydroxylation at naphthalene moiety	24.3	358.1797	-1.3	$C_{24}H_{23}NO_2$	143, 171, 214
Ma20	Hydroxylation at naphthalene moiety	24.8	358.1797	-1.2	$C_{24}H_{23}NO_2$	143, 171, 214
Ma21	Dehydrogenation	28.7	340.1692	-1.1	$C_{24}H_{21}NO$	127, 144, 155, 212
	JWH-018	31.4	342.1851	-0.5	$C_{24}H_{23}NO$	127, 144, 155, 214

[a] Position confirmed by the use of reference standards

Supplementary Table 2-2. Key diagnostic product ions and their tentative structures used in elucidating biotransformation pathways of JWH-018 after *C. elegans* incubation.

Biotransformation	ID	Key diagnostic product ions (*m/z*) and tentative structures
Carboxylation at pentyl side chain	Ma13	144: unchanged indole, 244: carboxylated pentylindole
Dehydrogenation at pentyl side chain	Ma21	144: unchanged indole, 212: dehydrogenated *N*-pentylindole
Dihydrodiol formation at naphthalene moiety	Ma12	189: naphthalene with dihydrodiol
Dihydrodiol formation at naphthalene moiety + hydroxylation at pentyl side chain	Ma2, Ma3	144: unchanged indole, 189: naphthalene with dihydrodiol, 230: hydroxylated *N*-pentylindole
Dihydrodiol formation at naphthalene moiety + ketone formation at pentyl side chain	Ma4, Ma5	189: naphthalene with dihydrodiol, 228: *N*-pentylindole with ketone
Dihydrodiol formation at naphthalene moiety + *N*-dealkylation	Ma1	189: naphthalene with dihydrodiol
Dihydroxylation at pentyl side chain	Ma7	144: unchanged indole, 246: dihydroxylated *N*-pentylindole
Dihydroxylation at pentyl side chain and naphthalene moiety	Ma6, Ma8, Ma9, Ma11	144: unchanged indole, 171: hydroxylated naphthalene, 230: hydroxylated *N*-pentylindole
Hydroxylation at naphthalene moiety	Ma19, Ma20	171: hydroxylated naphthalene
Hydroxylation at pentyl side chain	Ma14 – Ma16	144: unchanged indole, 230: hydroxylated *N*-pentylindole
Ketone formation at pentyl side chain	Ma17, Ma18	144: unchanged indole, 228: *N*-pentylindole with ketone

Biotransformation	ID	Key diagnostic product ions (*m/z*) and tentative structures
Ketone formation at pentyl side chain + hydroxylation at naphthalene moiety	Ma10	144: unchanged indole, 171: hydroxylated naphthalene, 228: *N*-pentylindole with ketone

Supplementary Table 2-3. Metabolites of JWH-073 after *C. elegans* incubation.

ID	Biotransformation	RT (min)	*m/z* $[M+H]^+$	Mass accuracy (ppm)	Formula	Major product ions
Mb1	Dihydrodiol formation + *N*-dealkylation	8.0	306.1123	-0.5	$C_{19}H_{15}NO_3$	143, 144, 171
Mb2	Dihydrodiol formation + hydroxylation at butyl side chain	8.2	378.1700	-0.1	$C_{23}H_{23}NO_4$	143, 144, 171, 189, 216
Mb3	Dihydrodiol formation + hydroxylation at butyl side chain	8.9	378.1690	-2.6	$C_{23}H_{23}NO_4$	143, 144, 171, 189, 216
Mb4	Dihydrodiol formation + ketone formation at butyl side chain	9.0	376.1543	-0.1	$C_{23}H_{21}NO_4$	143, 144, 171, 189, 214
Mb5	Dihydroxylation at butyl side chain	11.7	360.1594	0.0	$C_{23}H_{21}NO_3$	127, 144, 155, 232
Mb6	Dihydroxylation at butyl side chain and naphthalene moiety	12.1	360.1595	0.1	$C_{23}H_{21}NO_3$	143, 144, 171, 216
Mb7	Dihydroxylation at butyl side chain and naphthalene moiety	12.8	360.1594	-0.1	$C_{23}H_{21}NO_3$	143, 144, 171, 216
Mb8	Dihydrodiol formation	13.7	362.1751	0.1	$C_{23}H_{23}NO_3$	143, 144, 171, 189, 200
Mb9	Ketone formation at butyl side chain + hydroxylation at naphthalene moiety	13.9	358.1438	0.0	$C_{23}H_{19}NO_3$	143, 144, 171, 214
Mb10	Ketone formation at butyl side chain + hydroxylation at naphthalene moiety	14.5	358.1438	0.0	$C_{23}H_{19}NO_3$	143, 144, 171, 214

ID	Biotransformation	RT (min)	*m/z* $[M+H]^+$	Mass accuracy (ppm)	Formula	Major product ions
Mb11	Carboxylation (*N*-butanoic acid)[a]	15.4	358.1437	-0.1	$C_{23}H_{19}NO_3$	127, 144, 155, 230
Mb12	Hydroxylation at butyl side chain (4-hydroxybutyl)[a]	15.7	344.1645	-0.2	$C_{23}H_{21}NO_2$	127, 144, 155, 216
Mb13	Hydroxylation at butyl side chain (3-hydroxybutyl)[a]	17.1	344.1646	0.3	$C_{23}H_{21}NO_2$	127, 144, 155, 216
Mb14	Ketone formation at butyl side chain	19.5	342.1488	0.0	$C_{23}H_{19}NO_2$	127, 144, 155, 214
Mb15	Hydroxylation at naphthalene moiety	21.5	344.1645	-0.1	$C_{23}H_{21}NO_2$	143, 144, 171, 200
Mb16	Hydroxylation at naphthalene moiety	22.0	344.1645	0.0	$C_{23}H_{21}NO_2$	143, 144, 171, 200
Mb17	Dehydrogenation	25.7	326.1539	-0.1	$C_{23}H_{19}NO$	127, 155, 198
	JWH-073	28.8	328.1697	0.3	$C_{23}H_{21}NO$	127, 144, 155, 200

[a] Position confirmed by the use of reference standards

Supplementary Table 2-4. Key diagnostic product ions and their tentative structures used in elucidating biotransformation pathways of JWH-073 after *C. elegans* incubation.

Biotransformation	ID	Key diagnostic product ions (*m/z*) and tentative structures
Carboxylation at butyl side chain	Mb11	144: unchanged indole, 230: carboxylated butylindole
Dehydrogenation	Mb17	198: dehydrogenated *N*-butylindole
Dihydrodiol formation at naphthalene moiety	Mb8	189: naphthalene with dihydrodiol
Dihydrodiol formation at naphthalene moiety + hydroxylation at butyl side chain	Mb2, Mb3	144: unchanged indole, 189: naphthalene with dihydrodiol, 216: hydroxylated *N*-butylindole
Dihydrodiol formation at naphthalene moiety + ketone formation at butyl side chain	Mb4	144: unchanged indole, 189: naphthalene with dihydrodiol, 214: *N*-butylindole with ketone
Dihydrodiol formation at naphthalene moiety + *N*-dealkylation	Mb1	171: hydroxylated naphthalene (resulting from naphthalene with dihydrodiol [1])
Dihydroxylation at butyl side chain	Mb5	144: unchanged indole, 232: dihydroxylated *N*-butylindole
Dihydroxylation at butyl chain and naphthalene moiety	Mb6, Mb7	144: unchanged indole, 171: hydroxylated naphthalene, 216: hydroxylated *N*-butylindole
Hydroxylation at butyl side chain	Mb12, Mb13	144: unchanged indole, 216: hydroxylated *N*-butylindole

Biotransformation	ID	Key diagnostic product ions (*m/z*) and tentative structures
Hydroxylation at naphthalene moiety	Mb15, Mb16	171: hydroxylated naphthalene
Ketone formation at butyl side chain	Mb14	144: unchanged indole, 214: *N*-butylindole with ketone
Ketone formation at butyl side chain + hydroxylation at naphthalene moiety	Mb9, Mb10	144: unchanged indole, 171: hydroxylated naphthalene, 214: *N*-butylindole with ketone

1. Sobolevsky T, Prasolov I, Rodchenkov G. Detection of urinary metabolites of AM-2201 and UR-144, two novel synthetic cannabinoids. Drug Test Anal. 2012;4(10):745-53. doi:10.1002/dta.1418.

Supplementary Table 2-5. Metabolites of AM2201 after *C. elegans* incubation.

ID	Biotransformation	RT (min)	*m/z* $[M+H]^+$	Mass accuracy (ppm)	Formula	Major product ions
Mc1	Dihydrodiol formation + *N*-dealkylation	8.0	306.1122	-1.0	$C_{19}H_{15}NO_3$	143, 144, 171, 189
Mc2	Dihydroxylation at pentyl side chain and naphthalene moiety + glucosidation	8.2	554.2185	0.0	$C_{30}H_{32}FNO_8$	143, 144, 171, 248, 392
Mc3	Dihydroxylation at pentyl side chain and naphthalene moiety + glucosidation	8.4	554.2186	0.2	$C_{30}H_{32}FNO_8$	143, 144, 171, 248, 392
Mc4	Oxidative defluorination + dihydrodiol formation (JWH-018 dihydrodiol-hydroxy)	8.5	392.1858	0.4	$C_{24}H_{25}NO_4$	143, 171, 189, 230
Mc5	Dihydrodiol formation + hydroxylation at pentyl side chain	8.5	410.1764	0.6	$C_{24}H_{24}FNO_4$	143, 144, 171, 189, 248
Mc6	Dihydrodiol formation + hydroxylation at pentyl side chain	8.7	410.1761	-0.2	$C_{24}H_{24}FNO_4$	143, 144, 171, 189, 248
Mc7	Dihydroxylation at pentyl side chain and/or indole moiety + glucosidation	9.0	554.2186	0.3	$C_{30}H_{32}FNO_8$	127, 155, 264, 392
Mc8	Trihydroxylation at pentyl side chain, indole moiety and naphthalene moiety	9.3	408.1606	0.1	$C_{24}H_{22}FNO_4$	143, 160, 171, 264
Mc9	Dihydrodiol formation + dihydroxylation at indole moiety	9.5	426.1712	0.1	$C_{24}H_{24}FNO_5$	143, 171, 176, 189, 264
Mc10	Dihydrodiol formation + ketone formation at pentyl side chain	9.7	408.1606	0.0	$C_{24}H_{22}FNO_4$	143, 171, 189, 246

ID	Biotransformation	RT (min)	*m/z* $[M+H]^+$	Mass accuracy (ppm)	Formula	Major product ions
Mc11	Trihydroxylation at pentyl side chain, indole moiety and naphthalene moiety	10.2	408.1606	0.0	$C_{24}H_{22}FNO_4$	143, 160, 171, 264
Mc12	Hydroxylation at indole moiety + glucosidation	10.5	538.2235	-0.1	$C_{30}H_{32}FNO_7$	127, 155, 160, 248, 376
Mc13	Dihydroxylation at pentyl side chain and/or indole moiety + glucosidation	10.7	554.2183	-0.3	$C_{30}H_{32}FNO_8$	127, 155, 264, 392
Mc14	Hydroxylation at naphthalene moiety + glucosidation	10.8	538.2234	-0.4	$C_{30}H_{32}FNO_7$	143, 144, 171, 232, 376
Mc15	Oxidative defluorination + hydroxylation at indole moiety (JWH-018 dihydroxy)	11.1	374.1751	0.2	$C_{24}H_{23}NO_3$	127, 155, 160, 246
Mc16	Dihydroxylation at naphthalene + glucosidation	11.5	554.2182	-0.4	$C_{30}H_{32}FNO_8$	187, 232, 392
Mc17	Dihydroxylation at indole moiety and pentyl side chain	11.5	392.1657	0.0	$C_{24}H_{22}FNO_3$	127, 155, 160, 264
Mc18	Oxidative defluorination + hydroxylation at indole moiety (JWH-018 dihydroxy)	11.8	374.1748	-0.8	$C_{24}H_{23}NO_3$	127, 155, 160, 246
Mc19	Dihydroxylation at indole moiety and pentyl side chain	11.9	392.1656	-0.2	$C_{24}H_{22}FNO_3$	127, 155, 160, 264
Mc20	Oxidative defluorination to carboxylic acid + hydroxylation at naphthalene moiety	12.0	388.1547	1.0	$C_{24}H_{21}NO_4$	143, 144, 171, 244
Mc21	Oxidative defluorination + hydroxylation at pentyl side chain (JWH-018 dihydroxy)	12.1	374.1751	0.2	$C_{24}H_{23}NO_3$	127, 144, 155, 246

ID	Biotransformation	RT (min)	*m/z* $[M+H]^+$	Mass accuracy (ppm)	Formula	Major product ions
Mc22	Dihydroxylation at indole moiety and pentyl side chain	12.2	392.1658	0.5	$C_{24}H_{22}FNO_3$	127, 155, 160, 264
Mc23	Oxidative defluorination + hydroxylation at naphthalene moiety (JWH-018 dihydroxy)	12.3	374.1749	-0.4	$C_{24}H_{23}NO_3$	143, 144, 171, 230
Mc24	Dihydroxylation at pentyl side chain and naphthalene moiety	12.5	392.1651	1.4	$C_{24}H_{22}FNO_3$	143, 144, 171, 248
Mc25	Dihydrodiol formation	12.5	394.1812	-0.3	$C_{24}H_{24}FNO_3$	143, 144, 171, 189, 232
Mc26	Oxidative defluorination to carboxylic acid + hydroxylation at naphthalene moiety	12.7	388.1544	0.3	$C_{24}H_{21}NO_4$	143, 144, 171, 244
Mc27	Dihydroxylation at indole moiety and pentyl side chain	12.7	392.1657	0.0	$C_{24}H_{22}FNO_3$	127, 155, 160, 264
Mc28	Oxidative defluorination + hydroxylation at naphthalene moiety (JWH-018 dihydroxy)	12.9	374.1750	-0.3	$C_{24}H_{23}NO_3$	143, 144, 171, 230
Mc29	Dihydroxylation at pentyl side chain and naphthalene moiety	13.0	392.1655	0.3	$C_{24}H_{22}FNO_3$	143, 144, 171, 248
Mc30	Dihydrodiol formation	13.5	394.1818	1.2	$C_{24}H_{24}FNO_3$	143, 144, 171, 189, 232
Mc31	Dihydroxylation at pentyl side chain and naphthalene moiety	13.6	392.1655	-0.3	$C_{24}H_{22}FNO_3$	143, 144, 171, 248
Mc32	Dihydroxylation at pentyl side chain and naphthalene moiety	14.4	392.1659	0.6	$C_{24}H_{22}FNO_3$	143, 144, 171, 248
Mc33	Oxidative defluorination to carboxylic acid (JWH-018 *N*-pentanoic acid)[a]	16.4	372.1592	-0.7	$C_{24}H_{21}NO_3$	127, 144, 155, 244

ID	Biotransformation	RT (min)	*m/z* $[M+H]^+$	Mass accuracy (ppm)	Formula	Major product ions
Mc34	Oxidative defluorination (JWH-018 *N*-(5-hydroxypentyl))[a]	17.1	358.1802	0.2	$C_{24}H_{23}NO_2$	127, 144, 155, 230
Mc35	Hydroxylation at pentyl side chain	17.3	376.1709	0.4	$C_{24}H_{22}FNO_2$	127, 144, 155, 248
Mc36	Hydroxylation at indole moiety	17.7	376.1707	-0.2	$C_{24}H_{22}FNO_2$	127, 155, 160, 248
Mc37	Hydroxylation at pentyl side chain	18.0	376.1708	0.1	$C_{24}H_{22}FNO_2$	127, 144, 155, 248
Mc38	Dihydroxylation at naphthalene moiety + sulfation	18.7	472.1222	-0.6	$C_{24}H_{22}FNO_6S$	144, 158, 159, 186, 187, 232, 391, 392
Mc39	Hydroxylation at pentyl side chain	18.8	376.1708	0.3	$C_{24}H_{22}FNO_2$	127, 144, 155, 248
Mc40	Hydroxylation at naphthalene moiety	19.2	376.1709	0.6	$C_{24}H_{22}FNO_2$	143, 144, 171, 232
Mc41	Hydroxylation at naphthalene moiety	19.8	376.1703	-1.2	$C_{24}H_{22}FNO_2$	143, 144, 171, 232
Mc42	Dihydroxylation at naphthalene moiety + sulfation	20.2	472.1224	-0.1	$C_{24}H_{22}FNO_6S$	144, 158, 159, 186, 187, 232, 391, 392
Mc43	Ketone formation at pentyl side chain	20.4	374.1549	-0.5	$C_{24}H_{20}FNO_2$	127, 144, 155, 246
Mc44	Hydroxylation at naphthalene moiety	20.6	376.1706	-0.3	$C_{24}H_{22}FNO_2$	143, 144, 171, 232
Mc45	Hydroxylation at naphthalene moiety	21.3	376.1707	-0.1	$C_{24}H_{22}FNO_2$	143, 144, 171, 232
Mc46	Dihydroxylation at indole moiety + sulfation	22.0	472.1223	-0.3	$C_{24}H_{22}FNO_6S$	127, 155, 175, 176, 264, 391, 392

ID	Biotransformation	RT (min)	*m/z* $[M+H]^+$	Mass accuracy (ppm)	Formula	Major product ions
	AM2201	25.6	360.1759	0.2	$C_{24}H_{22}FNO$	127, 144, 155, 232
Mc47	Defluorination + Demethylation (JWH-073)[a]	28.8	328.1695	-0.3	$C_{23}H_{21}NO$	127, 144, 155, 200
Mc48	Defluorination (JWH-018)[a]	31.5	342.1853	0.0	$C_{24}H_{23}NO$	127, 144, 155, 214

[a] Position confirmed by the use of reference standards

Supplementary Table 2-6. Key diagnostic product ions and their tentative structures used in elucidating biotransformation pathways of AM2201 after *C. elegans* incubation. Square brackets indicate phase II metabolism.

Biotransformation	**ID**	**Key diagnostic product ions (*m/z*) and tentative structures**
Defluorination (JWH-018)	Mc48	155: unchanged naphthalene, 214: unchanged *N*-pentylindole
Defluorination + Demethylation (JWH-073)	Mc47	155: unchanged naphthalene, 200: unchanged *N*- butylindole
Dihydrodiol formation at naphthalene moiety	Mc25, Mc30	189: naphthalene with dihydrodiol
Dihydrodiol formation at naphthalene moiety + dihydroxylation at indole moiety	Mc9	176: dihydroxylated indole, 189: naphthalene with dihydrodiol
Dihydrodiol formation at naphthalene moiety + hydroxylation at pentyl side chain	Mc5, Mc6	144: unchanged indole, 189: naphthalene with dihydrodiol, 248: hydroxylated *N*-fluoropentylindole
Dihydrodiol formation at naphthalene moiety + ketone formation at pentyl side chain	Mc10	144: unchanged indole, 189: naphthalene with dihydrodiol, 246: *N*-fluoropentylindole with ketone
Dihydrodiol formation at naphthalene moiety + *N*-dealkylation	Mc1	189: naphthalene with dihydrodiol
Dihydroxylation at indole moiety [+ sulfation]	[Sulfate Mc46]	176: dihydroxylation at indole, [392: dihydroxylated AM2201]
Dihydroxylation at indole moiety and pentyl side chain	Mc17, Mc19, Mc22, Mc27	160: hydroxylated indole, 264: dihydroxylated *N*-fluoropentylindole

Biotransformation	ID	Key diagnostic product ions (*m/z*) and tentative structures
Dihydroxylation at naphthalene moiety [+ glucosidation and sulfation]	[Glucoside Mc16, sulfates Mc38, Mc42]	187: dihydroxylated naphthalene, [392: dihydroxylated AM2201]
Dihydroxylation at naphthalene moiety and pentyl side chain [+ glucosidation]	Mc24, Mc29, Mc31, Mc32, [glucosides Mc2, Mc3]	144: unchanged indole, 171: hydroxylated naphthalene, 248: hydroxylated *N*-fluoropentylindole, [392: dihydroxylated AM2201]
Dihydroxylation at pentyl side chain and/or indole moiety [+ glucosidation]	[glucosides Mc7, Mc13]	264: dihydroxylated *N*-fluoropentylindole, [392: dihydroxylated AM2201]
Hydroxylation at indole moiety [+ glucosidation]	Mc36, [glucoside Mc12]	160: hydroxylated indole, 248: hydroxylated *N*-fluoropentylindole, [376: hydroxylated AM2201]
Hydroxylation at naphthalene moiety [+ glucosidation]	Mc40, Mc41, Mc44, Mc45, [glucoside Mc14]	171: hydroxylated naphthalene, [376: hydroxylated AM2201]
Hydroxylation at pentyl side chain	Mc35, Mc37 and Mc39	144: unchanged indole, 248: hydroxylated *N*-fluoropentylindole
Ketone formation at pentyl side chain	Mc43	144: unchanged indole, 246: *N*-fluoropentylindole with ketone
Oxidative defluorination (JWH-018 *N*-(5-hydroxypentyl))	Mc34	144: unchanged indole, 230: hydroxylated *N*-pentylindole

Biotransformation	ID	Key diagnostic product ions (*m/z*) and tentative structures
Oxidative defluorination + dihydrodiol formation (JWH-018 dihydrodiol-hydroxy)	Mc4	189: naphthalene with dihydrodiol, 230: hydroxylated *N*-pentylindole
Oxidative defluorination + hydroxylation at indole moiety (JWH-018 dihydroxy)	Mc15, Mc18	160: hydroxylated indole, 246: dihydroxylated *N*-pentylindole
Oxidative defluorination + hydroxylation at naphthalene moiety (JWH-018 dihydroxy)	Mc23, Mc28	144: unchanged indole , 171: hydroxylated naphthalene, 230: hydroxylated *N*-pentylindole
Oxidative defluorination + hydroxylation at pentyl side chain (JWH-018 dihydroxy)	Mc21	144: unchanged indole, 246: dihydroxylated *N*-pentylindole
Oxidative defluorination to carboxylic acid (JWH-018 *N*-pentanoic acid)	Mc33	144: unchanged indole, 244: carboxylated pentylindole
Oxidative defluorination to carboxylic acid + hydroxylation at naphthalene moiety.	Mc20, Mc26	144: unchanged indole, 171: hydroxylated naphthalene, 244: carboxylated pentylindole
Trihydroxylation at indole moiety, naphthalene moiety and pentyl side chain	Mc8, Mc11	160: hydroxylated indole, 171: hydroxylated naphthalene, 264: dihydroxylated *N*-fluoropentylindole

Chapter 3: Metabolic profile of synthetic cannabinoids 5F-PB-22, PB-22, XLR-11 and UR-144 by *Cunninghamella elegans*

Chapter 3: Metabolic profile of synthetic cannabinoids 5F-PB-22, PB-22, XLR-11 and UR-144 by *Cunninghamella elegans*

3.1 Abstract

Knowledge of the metabolic profile of synthetic cannabinoids is important for the detection of the drugs in urinalysis due to the typical absence or low abundance of parent cannabinoids in human urine. The fungus *Cunninghamella elegans* has been reported to be a useful tool for metabolism study and thus applicability to synthetic cannabinoids metabolism was examined. In this study, 8-quinolinyl 1-(5-fluoropentyl)-1H-indole-3-carboxylate (5F-PB-22), 8-quinolinyl 1-pentyl-1H-indole-3-carboxylate (PB-22), [1-(5-fluoropentyl)-1H-indol-3-yl](2,2,3,3-tetramethylcyclopropyl)methanone (XLR-11) and (1-pentyl-1H-indol-3-yl)(2,2,3,3-tetramethylcyclopropyl)methanone (UR-144) were incubated with *Cunninghamella elegans* and the metabolites were identified using liquid chromatography-quadrupole time-of-flight mass spectrometry. The obtained metabolites were compared with reported human metabolites to assess the suitability of the fungus to extrapolate human metabolism. 5F-PB-22 underwent dihydroxylation, dihydrodiol formation, oxidative defluorination, oxidative defluorination to carboxylic acid, ester hydrolysis and glucosidation, alone and/or in combination. The metabolites of PB-22 were generated by hydroxylation, dihydroxylation, trihydroxylation, dihydrodiol formation, ketone formation, carboxylation, ester hydrolysis and glucosidation, alone and/or in combination. XLR-11 was transformed through hydroxylation, dihydroxylation, aldehyde formation, carboxylation, oxidative defluorination, oxidative defluorination to carboxylic acid and glucosidation, alone and/or in combination. UR-144 was metabolised by hydroxylation, dihydroxylation, trihydroxylation, aldehyde formation, ketone formation, carboxylation, *N*-dealkylation and combinations. These findings were consistent with previously reported human metabolism except for the small extent of ester hydrolysis observed and absence of glucuronidation. Despite the limitations, *Cunninghamella elegans* demonstrated the capacity to produce a wide variety of metabolites including some major human metabolites of XLR-11 and UR-144 at high abundance, showing the potential for metabolism of newly emerging synthetic cannabinoids.

Key words: Synthetic cannabinoids, Metabolism, *Cunninghamella elegans*, 5F-PB-22, XLR-11

Abbreviations

CB_1	Cannabinoid type 1
CB_2	Cannabinoid type 2
C. elegans	*Cunninghamella elegans*
ESI	Electrospray ionisation
5F-PB-22	8-quinolinyl 1-(5-fluoropentyl)-1H-indole-3-carboxylate
5F-PI-COOH	5-fluoropentylindole-3-carboxylic acid
HLM	Human liver microsomes
LC-QqQ	Liquid chromatography-triple quadrupole
LC-QTOF-MS	Liquid chromatography-quadrupole time-of-flight mass spectrometry
MS	Mass spectrometry
NMR	Nuclear magnetic resonance
PB-22	8-quinolinyl 1-pentyl-1H-indole-3-carboxylate
PI-COOH	Pentylindole-3-carboxylic acid
TMCP	Tetramethylcyclopropyl
UR-144	(1-pentyl-1H-indol-3-yl)(2,2,3,3-tetramethylcyclopropyl)methanone
XLR-11	[1-(5-fluoropentyl)-1H-indol-3-yl](2,2,3,3-tetramethylcyclopropyl)methanone

3.2 Introduction

New psychoactive substances have been increasingly appearing on the drug market. In particular, synthetic cannabinoids are the major class of drugs and over 160 compounds have been detected since 2008 with 24 of them appearing for the first time in 2015 [1]. Synthetic cannabinoids are cannabinoid type 1 (CB_1) and type 2 (CB_2) receptor agonists like Δ^9-tetrahydrocannabinol, the active ingredient of cannabis, producing psychoactive effects but can be significantly more potent since cannabinoids and metabolites often have higher affinity and full agonist activity for both CB_1 and CB_2 receptor [2, 3]. As such, adverse health effects including seizures, psychosis, hallucinations, cardiotoxic effects, coma and deaths have been associated with the use of synthetic cannabinoids and it has become a serious public health concern [4].

Due to the emergence of many synthetic cannabinoids within a short period, understanding of their pharmacology including metabolism is still limited. Knowledge of metabolites is important for forensic and clinical cases to prove the consumption of particular cannabinoids in urinalysis because synthetic cannabinoids are generally extensively metabolised and are usually not found without modification or found in low abundance in urine, requiring abundant and specific metabolites to be targeted instead [5-14].

Different approaches have been taken for metabolite identification studies. While providing the most reliable data [15], self-administration of drugs is difficult due to possible side effects and ethical concerns and therefore other approaches are commonly taken such as *in vitro* human hepatocytes [7-9, 16-20] and human liver microsomes (HLM) [6, 14, 21-26], and *in vivo* animals [5, 25-27]. The combination of controlled experiments such as human hepatocytes and authentic human urine analysis particularly appears to be valuable [28, 29]. However, cost, maintenance, species differences and/or ethics can be an issue with these models [30]. Furthermore, quantity of metabolites obtained is usually not sufficient for isolation [30], limiting the analysis to the use of mass spectrometry. However, unambiguous structural elucidation may not be possible without techniques such as nuclear magnetic resonance (NMR) spectroscopy [29].

While less common, the potential of microbial models for metabolic studies has been investigated over the past few decades [30]. *Cunninghamella elegans* (*C. elegans*) is a fungus species known to metabolise many xenobiotics regio- and stereo-selectively, similar to mammalian metabolism [30]. The fungus has enzymatic activity for both phase I and II enzymes [31] and possesses cytochrome P450 enzymes known as CYP509A1, which are close to CYP51 family [32]. While little is known about the activity of CYP509A1, the fungus is capable of various reactions, such as hydroxylation, carboxylation, dihydrodiol formation, oxidative defluorination, *N*-dealkylation, glucosidation and sulfation [30, 33], including those catalysed by human CYP1A2, CYP2C9, CYP2C19 and CYP2D6 [2, 33-37]. CYP3A4 is reported to be the major enzyme involved in the metabolism of [1-(5-fluoropentyl)-1H-indol-3-yl](2,2,3,3-tetramethylcyclopropyl)methanone (XLR-11) and (1-pentyl-1H-indol-3-yl)(2,2,3,3-tetramethylcyclopropyl)methanone (UR-144), two of the drugs investigated in this study, while CYP1A2 has a minor influence. There is no literature on specific enzymes responsible for the metabolism of 8-quinolinyl 1-(5-fluoropentyl)-1H-indole-3-carboxylate (5F-PB-22) and 8-quinolinyl 1-pentyl-1H-indole-3-carboxylate (PB-22), the other two drugs investigated. Some of the advantages of *C. elegans* include low cost, no ethical concern involved, simple and cheap maintenance of stock fungal cultures that can be subcultured, high reproducibility, diverse metabolic profile and larger amounts of metabolite produced, which might result in more fragment ions in mass spectrometric analysis, facilitating structural elucidation [30, 38]. More importantly, production of large amounts of metabolites has allowed for the structural characterisation of metabolites by NMR spectroscopy [39, 40]. Therefore, *C. elegans* may prove useful for synthetic cannabinoids metabolism study, especially where reference standards for metabolites of new compounds are not available.

The purpose of the study was to identify the metabolites of 5F-PB-22, PB-22, XLR-11 and UR-144 by *C. elegans* and to compare the fungal metabolites with human *in vivo* and *in vitro* metabolites reported in literature to examine whether *C. elegans* might have the possibility to be used as a complementary model for metabolism studies of synthetic cannabinoids with production of appropriate human metabolites. We have previously investigated the metabolism of synthetic cannabinoids JWH-018, JWH-073 and AM2201 by *C. elegans* and their metabolic profiles were in good agreement with human

metabolism, producing the majority of the phase I human metabolites [33, 41]. The four synthetic cannabinoids were chosen because they have different structural classes from the cannabinoids in our previous study and human *in vivo* and/or *in vitro* metabolism data are available. Metabolites were analysed by liquid chromatography-quadrupole time-of-flight mass spectrometry (LC-QTOF-MS) with the aid of liquid chromatography-triple quadrupole (LC-QqQ) mass spectrometry. LC-QTOF-MS was mainly employed because it provides high-resolution mass spectrometric data, increasing the confidence of characterisation of metabolites by distinguishing isobaric compounds.

3.3 Materials and Methods

3.3.1 Chemicals and reagents

5F-PB-22 and PB-22 were obtained from PM separations (Capalaba, QLD, Australia) and XLR-11 and UR-144 were from the National Measurement Institute (North Ryde, NSW, Australia). Reagent grade dichloromethane, LC grade acetonitrile, acetone and sodium chloride were obtained from Chemsupply (Gilman, SA, Australia). LC-MS grade formic acid was obtained from Sigma–Aldrich (St. Louis, MO, USA). Glycerol and potassium dihydrogen orthophosphate were from Ajax Chemicals (Auburn, NSW, Australia). Potato dextrose agar, glucose, peptone, and yeast extract were purchased from Oxoid Australia (Adelaide, SA, Australia).

3.3.2 Biotransformation by fungus and sample preparation

C. elegans ATCC 10028b (Cryosite Ltd., South Granville, NSW, Australia) was cultured on potato dextrose agar plates at 27 °C for 5 days ensuring the whole plates were covered with mycelia. The mycelia were then transferred to sterile physiological saline solution (1 plate of mycelia per 5 mL) and homogenised for 5 min. Approximately 1.5 mL aliquots of the homogenate were inoculated into 100 mL growth media, prepared according to the methods in [42], in 250 mL Erlenmeyer flasks. The cultures were incubated for 48 h at 26 °C and 180 rpm on an Infors HT Multitron rotary shaker (In vitro Technologies, Noble Park North, VIC, Australia). After 48 h, 0.5 mL of 5F-PB-22, PB-22, XLR-11 or UR-144 in acetone (2 mg/mL) was added to the culture and incubated for further 72 h. Two control samples were also incubated and consisted of 1) media and fungus without drugs to determine compounds unrelated to the drugs and 2) media and drug without fungus.to determine degradation of the drugs.

After 72 h, fungus was removed by filtration using Buchner funnel and the remaining solution was extracted with dichloromethane (3 × 50 mL). The extracts were combined and evaporated to dryness using a Buchi rotary evaporator (In vitro Technologies, Noble Park North, VIC, Australia) followed by a vacuum pump. Each sample was reconstituted

in 2 mL acetonitrile and was further diluted in acetonitrile by 10-fold before injecting to LC-MS.

3.3.3 LC-QTOF analysis

Chromatographic separation of samples was performed using an Agilent 1290 LC system with an Agilent Zorbax Eclipse XDBC18 analytical column (150 mm × 4.6 mm, 5 µm). Mobile phases were 0.1% formic acid in water (A) and 0.1% formic acid in acetonitrile (B) at a flow rate of 0.4 mL/min. Due to the difference in polarity of the cannabinoids, two mobile phase gradients were used. For 5F-PB-22 and PB-22, 30% B was held until 1 min, ramped to 50% B at 3 min, 90% B at 20 min and held until 24 min, then ramped down to 30% B at 25 min and held for re-equilibration until 30 min. For XLR-11 and UR-144, 30% B was held until 1 min, ramped to 60% B at 3 min, to 90% B at 20 min and held until 24 min, and ramped down to 30% B at 25 min for re-equilibration until 30 min. Injection volume was 4 µL (MS mode) and 10 µL (targeted MS/MS mode).

Mass spectrometric data was acquired on an Agilent 6510 Accurate Mass Q-TOF Mass Spectrometer, equipped with an electrospray ionisation (ESI) source operated in positive ion mode. The following parameters were used: scanning mass range, *m/z* 100–1000 (MS), *m/z* 100–950 (MS/MS); capillary voltage, 3500 V; nebulizer pressure, 30 psig; gas flow, 5 L/min; gas temperature, 325 °C; fragmentor voltage, 160 V (XLR-11, UR-144), 80 V (5F-PB-22, PB-22); collision energy, 10, 20 and 40 eV; skimmer voltage, 65 V. Mass calibration was performed over the m/z 50–3200 range with the mixture provided by the manufacturer. Automated real-time calibration during runs was in place using the following reference masses: m/z 121.0509 and m/z 922.0098.

Chromatographic and mass spectrometric data was analysed using Agilent MassHunter Workstation Software Qualitative Analysis (version B.06.00) for MS scan both manually looking at peaks present in fungus samples but absent in controls and with a PCDL library created by Agilent MassHunter PCDL Manager (version B.04.00) with known metabolites of the drugs to search for the potential metabolites. MS/MS scans were performed on the precursor ions which were suspected to be metabolites. Search parameters were as follows: mass tolerance, 20 ppm; maximum number of matches, 8;

absolute peak area ≥ 5000. The criteria for metabolites were as follows: mass error of the protonated ion ≤ 5.1 ppm; consistent fragmentation pattern with proposed structure; reasonable retention time relative to other biotransformations; absence of the specific peak in controls.

3.3.4 LC-QqQ analysis

An Agilent 6490 Triple Quadrupole mass spectrometer with ESI source (positive ion mode) coupled with an Agilent 1290 LC system was used for product ion scans for a few PB-22 metabolites (*m/z* 405 and 409) where some fragment ions for the potential metabolites were absent in QTOF analysis. Data derived from QqQ analysis is indicated in Supplementary Table 3-2 in the appendix to this chapter. All the chromatographic conditions and column used were the same as for QTOF analysis except for the injection volume of 2 μL. The following mass spectrometric conditions were used: scanning mass range, *m/z* 85–500; fragmentor voltage, 380 V; collision energy, 10, 20, 30 and 40 eV; gas temperature, 200 °C; gas flow, 14 L/min; capillary voltage, 3000 V.

3.4 Results

5F-PB-22 metabolites found after fungus incubation are listed in Supplementary Table 3-1, in the appendix to this chapter, including proposed biotransformation, retention time, elemental composition, exact mass, accurate mass, mass error, and diagnostic product ions. Similarly, PB-22, XLR-11, and UR-144 metabolites are listed in Supplementary Tables 3-2, 3-3 and 3-4, respectively, in the appendix to this chapter. Fig. 3-1 shows MS/MS spectra as well as their structures with suggested fragmentation patterns of 5F-PB-22, PB-22, XLR-11 and UR-144 and their major metabolites.

3.4.1 5F-PB-22

Sixteen metabolites (labelled as F1 – F16 in the order of retention time) were detected after incubation with *C. elegans*. They eluted between 6.4 min and 12.6 min before the parent drug at 17.6 min (Fig. 3-2a). The metabolites were generated by dihydrodiol formation (F10) followed by hydroxylation (F3), dihydroxylation (F7-F9), hydroxylation (F14-F16), oxidative defluorination to carboxylic acid (F13) followed by hydroxylation (F5, F6, F11), oxidative defluorination with dihydrodiol (F1), ester hydrolysis resulting in 5-fluoropentylindole-3-carboxylic acid (5F-PI-COOH, F12) followed by glucosidation (F2) or hydroxylation (F4). The mass errors of the metabolites based on the proposed biotransformations were all within 1.39 ppm. The top three abundant metabolites based on peak area were dihydrodiol (F10), hydroxylation (F15) and oxidative defluorination to carboxylic acid (F13). Proposed metabolic pathway of 5F-PB-22 is shown in Fig. 3-3. Comparison of the fungal metabolites in this study with human hepatocytes and HLM metabolites in the literature is shown in Table 3-1.

3.4.2 PB-22

A total of 30 metabolites (P1-P30) were found to elute between 6.2 min and 15.1 min, all before the parent drug at 21.7 min (Fig. 3-2b). The following biotransformation was observed: carboxylation (P24) followed by hydroxylation (P12), dihydrodiol formation (P27) followed by hydroxylation (P3, P7) or ketone formation (P8, P14), dihydroxylation (P13, P15, P16, P19), hydroxylation (P26, P28), ketone formation (P29, P30) followed

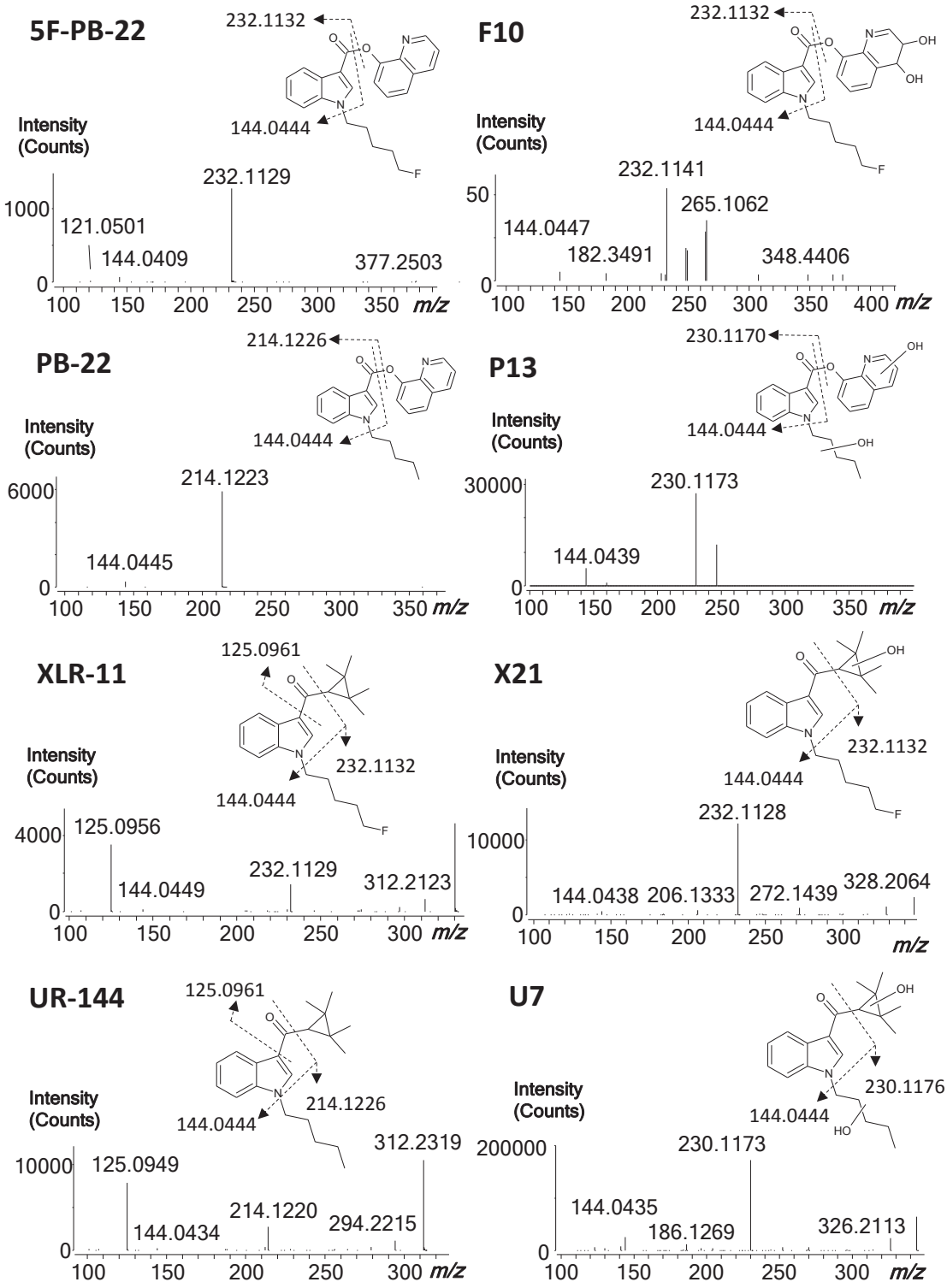

Figure 3-1. MS/MS spectra obtained with CE 20 eV and structures with the suggested fragmentation patterns and their exact masses for the parent drugs (5F-PB-22, PB-22, XLR-11 and UR-144) and their most abundant fungal metabolites based on peak area (F10, P13, X21 and U7). The exact position of the dihydrodiol structure within quinoline moiety in F10 is not determined.

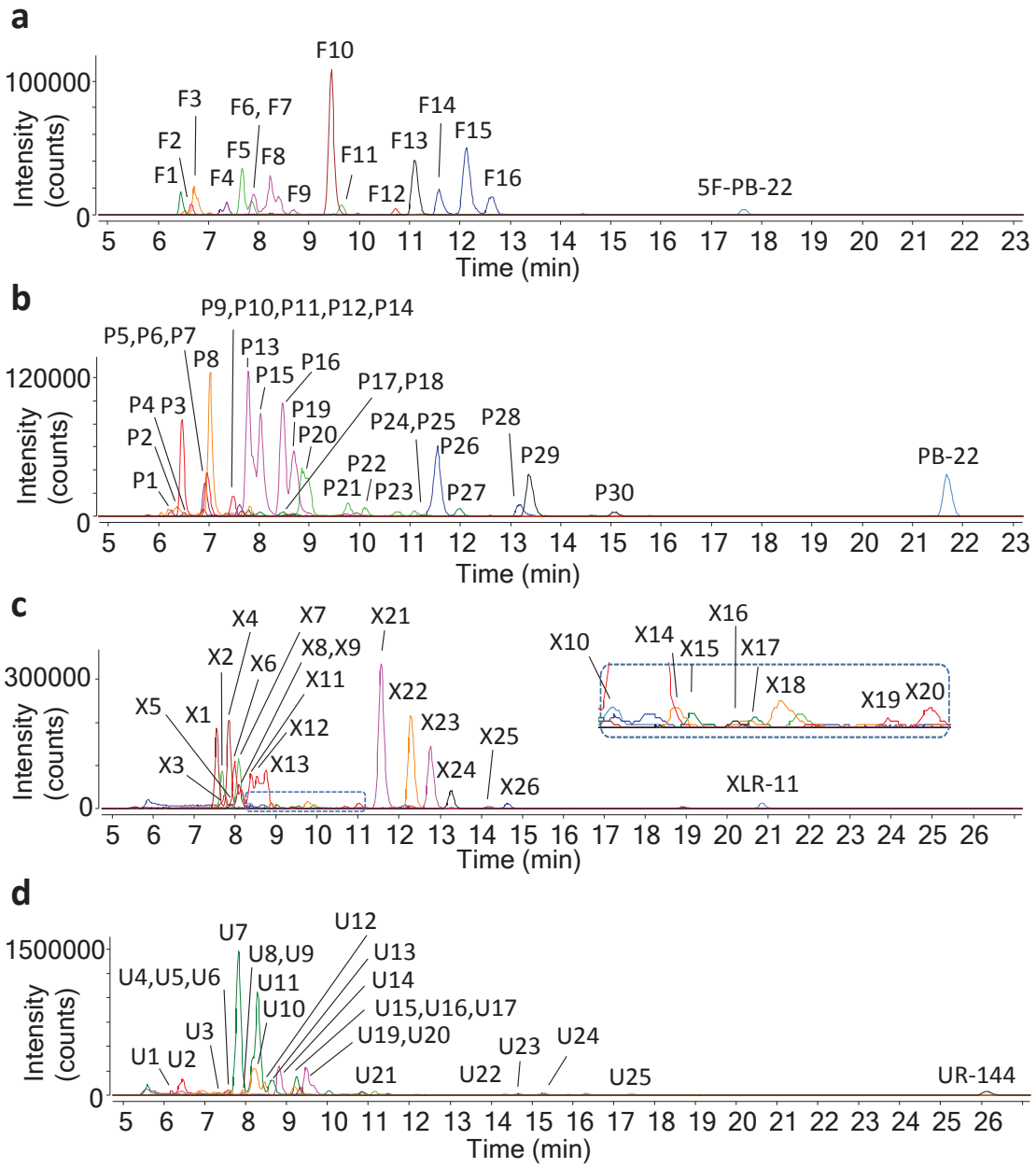

Figure 3-2. Combined extracted ion chromatograms of all metabolites and their respective parent drugs for (**a**) 5F-PB-22, (**b**) PB-22, (**c**) XLR-11, and (**d**) UR-144 after incubation with *C. elegans*.

by hydroxylation (P17, P20-P23, P25) and glucosidation (P1) or dihydroxylation (P4, P5, P9, P18), trihydroxylation (P2), ester hydrolysis leading to pentylindole-3-carboxylic acid (PI-COOH) followed by hydroxylation (P6, P11) or glucosidation (P10). The mass errors of all the metabolites were 2.51 ppm or less. Three major fungal metabolites were dihydroxylation (P13), dihydrodiol formation with ketone formation (P8) and dihydroxylation (P16). Proposed metabolic pathway of PB-22 is shown in Fig. 3-4.

Comparison of the fungal metabolites in this study with human hepatocytes and HLM metabolites in the literature is shown in Table 3-2.

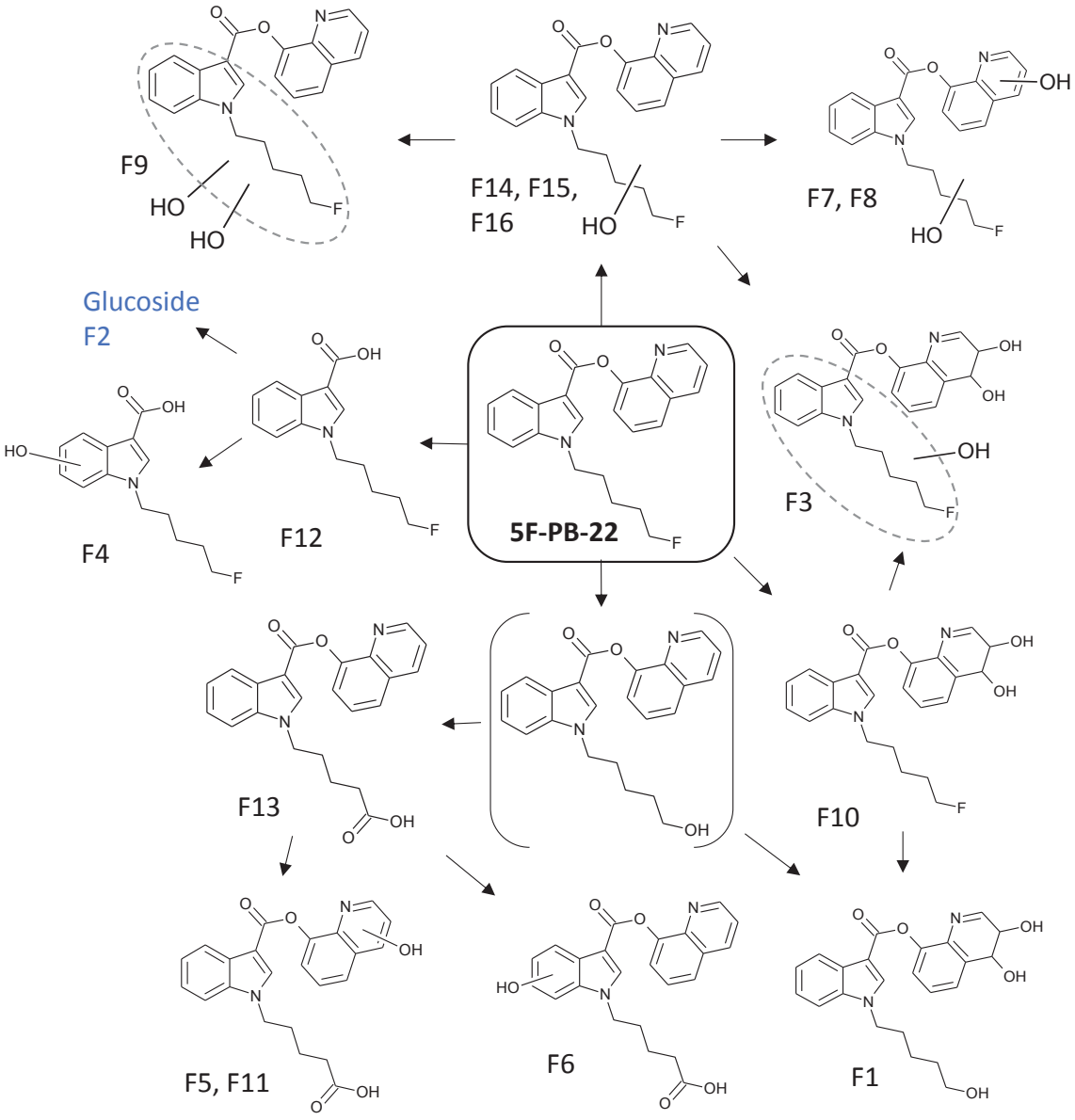

Figure 3-3. Proposed metabolic pathway of 5F-PB-22 by *C. elegans*. Blue colour denotes a Phase II metabolite. Parenthesis represents a possible intermediate metabolite that was not detected in the study. For the metabolites with dihydrodiol structure, only one possible isomer is shown as a representative.

Table 3-1. Comparison of 5F-PB-22 metabolites formed by fungus, *Cunninghamella elegans*, with those by human hepatocytes and human liver microsomes reported in literature.

Metabolites	CE	HHep	HLM
5F-PI-COOH [F12]	√	√ [17]	√ [22]
5F-PI-COOH + glucosidation [F2]	√		
5F-PI-COOH + glucuronidation		√ [17]	
5F-PI-COOH + cysteine conjugation		√ [17]	
5F-PI-COOH + hydroxylation [F4]	√	√ [17]	
5F-PI-COOH + hydroxylation + glucuronidation		√ [17]	
5F-PI-COOH + oxidative defluorination		√ [17]	
5F-PI-COOH + oxidative defluorination to carboxylic acid		√ [17]	
5F-PI-COOH + oxidative defluorination to carboxylic acid + glucuronidation		√ [17]	
Dihydrodiol formation [F10]	√	√ [17]	
Dihydrodiol formation + hydroxylation [F3]	√		
Dihydroxylation [F7-F9]	√		
Dihydroxylation + glucuronidation		√ [17]	
Hydroxylation [F14 - F16]	√	√ [17]	
Hydroxylation + glucuronidation		√ [17]	
Oxidative defluorination + dihydrodiol formation [F1]	√		
Oxidative defluorination + glucuronidation		√ [17]	
Oxidative defluorination to carboxylic acid [F13]	√	√ [17]	
Oxidative defluorination to carboxylic acid + glucuronidation		√ [17]	
Oxidative defluorination to carboxylic acid + hydroxylation [F5, F6, F11]	√		

CE Cunninghamella elegans; *HHep* Human hepatocytes; *HLM* Human liver microsomes

Square brackets in Metabolites column indicate the ID of corresponding fungal metabolites. Phase II metabolites are shown in blue colour.

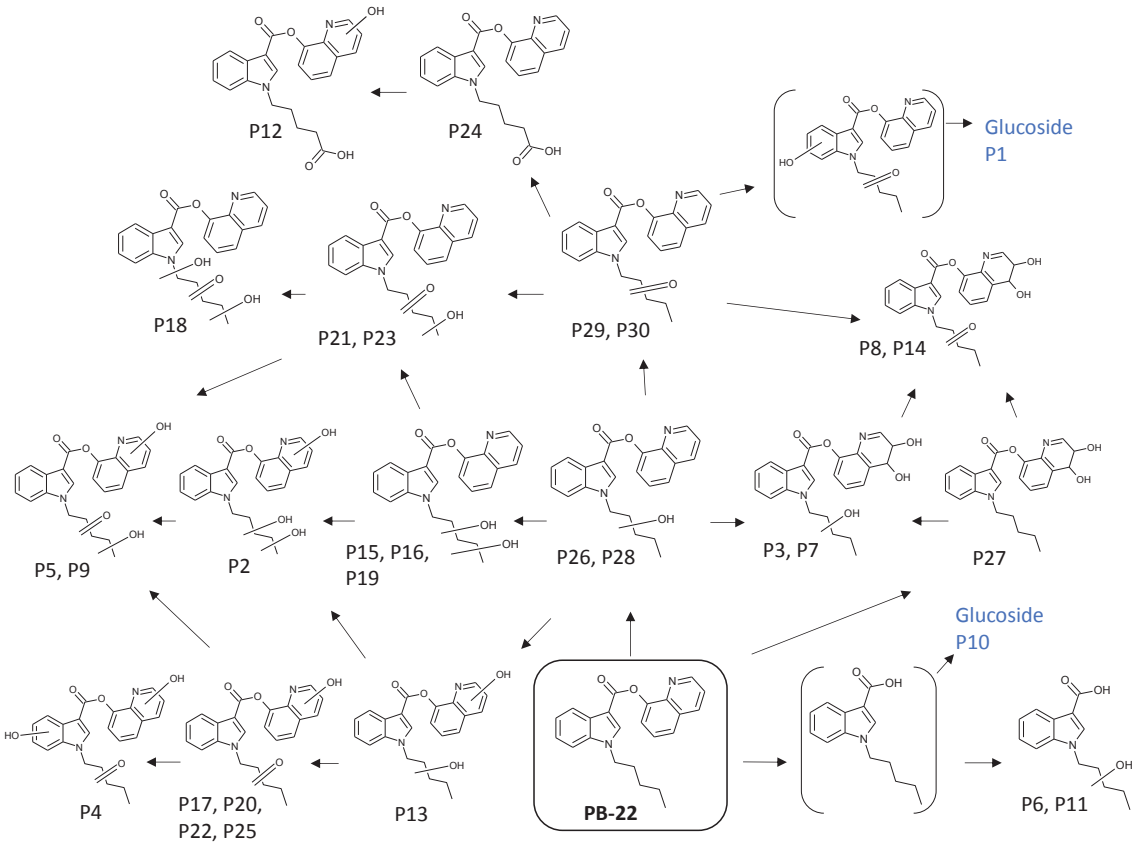

Figure 3-4. Proposed metabolic pathway of PB-22 by *C. elegans*. Blue colour denotes Phase II metabolites. Parentheses represent possible intermediate metabolites that were not detected in the study. For the metabolites with dihydrodiol structure, only one possible isomer is shown as a representative.

Table 3-2. Comparison of PB-22 metabolites formed by fungus, *Cunninghamella elegans*, with those by human hepatocytes and human liver microsomes reported in literature.

Metabolites	CE	HHep	HLM
Carboxylation [P24]	√	√ [17]	
Carboxylation + hydroxylation [P12]	√		
Dihydrodiol formation [P27]	√	√ [17]	
Dihydrodiol formation + hydroxylation [P3, P7]	√		
Dihydrodiol formation + ketone formation [P8, P14]	√		
Dihydroxylation [P13, P15, P16, P19]	√		
Hydroxylation [P26, P28]	√	√ [17]	
Hydroxylation + glucuronidation		√ [17]	
Ketone formation [P29, P30]	√	√ [17]	
Ketone formation + dihydroxylation [P4, P5, P9, P18]	√		
Ketone formation + hydroxylation [P17, P20 - P23, P25]	√		
Ketone formation + hydroxylation + glucosidation [P1]	√		
PI-COOH		√ [17]	√ [22]
PI-COOH + glucosidation [P10]	√		
PI-COOH + glucuronidation		√ [17]	
PI-COOH + carboxylation + glucuronidation		√ [17]	
PI-COOH + cysteine conjugation		√ [17]	
PI-COOH + hydroxylation [P6, P11]	√	√ [17]	
PI-COOH + hydroxylation + glucuronidation		√ [17]	
PI-COOH + ketone formation + glucuronidation		√ [17]	
Trihydroxylation [P2]	√		

CE Cunninghamella elegans; *HHep* Human hepatocytes; *HLM* Human liver microsomes

Square brackets in Metabolites column indicate the ID of corresponding fungal metabolites. Phase II metabolites are shown in blue colour.

3.4.3 XLR-11

Twenty six metabolites (X1-X26) were observed between 7.6 min and 14.6 min, with the parent drug eluting at 20.9 min (Fig. 3-2c). XLR-11 was found to undergo aldehyde formation (X26), carboxylation (X22) followed by glucosidation (X14, X18) or hydroxylation (X10), hydroxylation (X21, X23), dihydroxylation (X3, X6, X9, X11-X13, X19, X20), oxidative defluorination (X25) followed by aldehyde formation (X16) or carboxylation (X8) or hydroxylation (X2, X7), oxidative defluorination to carboxylic acid (X24) followed by aldehyde formation (X15, X17) or carboxylation (X5) or hydroxylation (X1, X4). The mass errors of all the metabolites were within 5.10 ppm. Three most abundant metabolites were hydroxylation (X21), carboxylation (X22) and hydroxylation (X23). Proposed metabolic pathway of XLR-11 is shown in Fig. 3-5. The

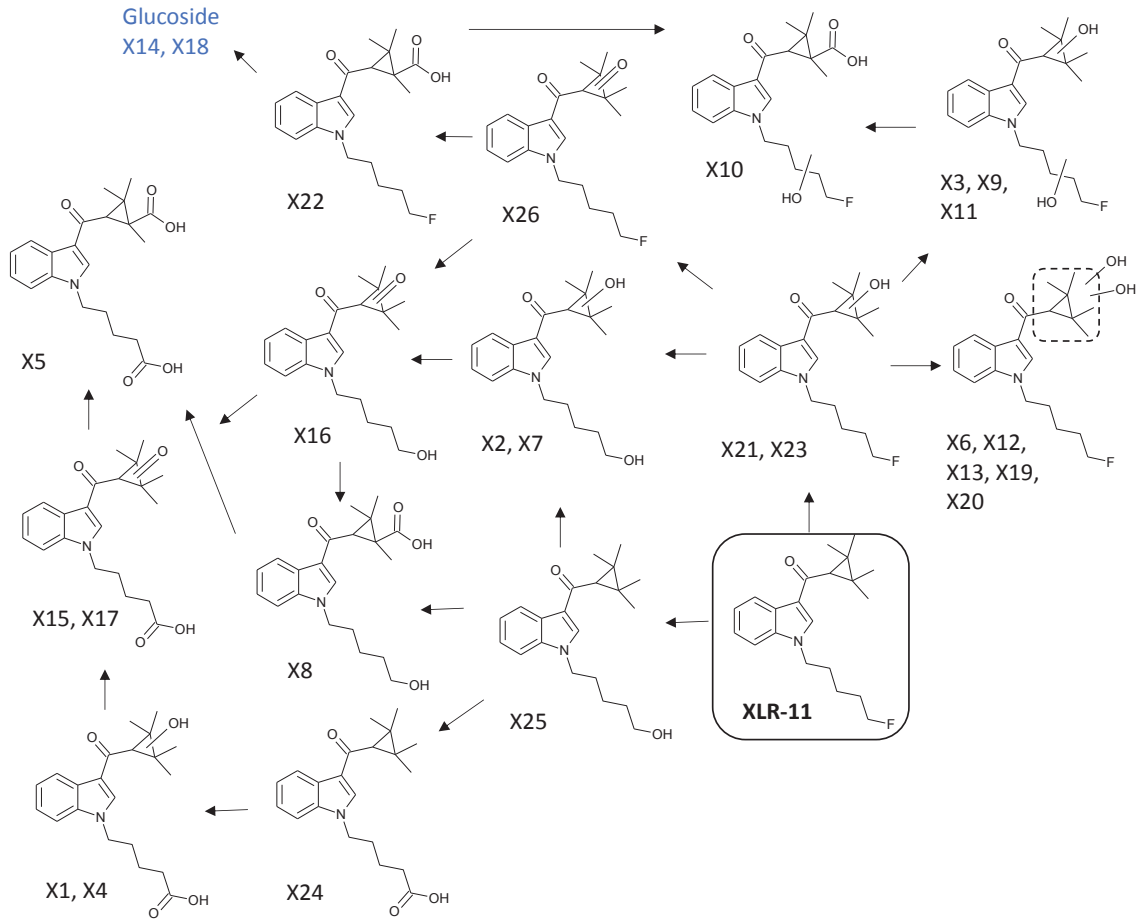

Figure 3-5. Proposed metabolic pathway of XLR-11 by *C. elegans*. Blue colour denotes Phase II metabolites.

fungal metabolites in this study are compared with the metabolites in human urine, human hair, human hepatocytes, HLM and HepaRG cells that have been reported in the literature (Table 3-3).

Table 3-3. Comparison of XLR-11 metabolites formed by fungus, *Cunninghamella elegans*, with those in human urine and human liver microsomes reported in literature.

Metabolites	CE	HU		HH	HHep	HLM	HRG	
		XLR-11	Pyrolysis product[a]				XLR-11	Pyrolysis product[a]
Aldehyde formation[b] [X26]	√				√ [16]	√ [43]		
Aldehyde formation + hydroxylation followed by hemiacetal formation + glucuronidation					√ [16]			
Carboxylation [X22]	√				√ [16]	√ [43]		
Carboxylation + glucosidation [X14, X18]	√							
Carboxylation + glucuronidation					√ [16]			
Carboxylation + hydroxylation [X10]	√				√ [16]			
Dihydroxylation [X3, X6, X9, X11-X13, X19, X20]	√		√ [44]				√ [44]	√ [44]
Dihydroxylation + glucuronidation		√ [45]	√ [45]		√ [16]			
Hydroxylation [X21, X23]	√	√ [46]	√ [44, 45]	√ [47]		√ [43]	√ [44]	√ [44]
Hydroxylation + glucuronidation					√ [16]			
***N*-dealkylation**						√ [43]		
Oxidative defluorination [X25]	√	√ [44, 45]	√ [44]	√ [47]	√ [16]	√ [43, 45]	√ [44]	√ [44]
Oxidative defluorination + glucuronidation		√ [45]	√ [45]		√ [16]			
Oxidative defluorination + aldehyde formation[b] [X16]	√					√ [43]		
Oxidative defluorination + carboxylation [X8]	√				√ [16]	√ [43]		
Oxidative defluorination + hydroxylation [X2, X7]	√		√ [44]			√ [43]	√ [44]	√ [44]
Oxidative defluorination + hydroxylation + glucuronidation			√ [45]		√ [16]			
Oxidative defluorination to carboxylic acid [X24]	√	√ [44, 45]	√ [44, 45]	√ [47]	√ [16]	√ [45]	√ [44]	√ [44]
Oxidative defluorination to carboxylic acid + glucuronidation			√ [45]		√ [16]			
Oxidative defluorination to carboxylic acid + aldehyde formation[b] [X15, X17]	√				√ [16]			
Oxidative defluorination to carboxylic acid + aldehyde formation + hydroxylation followed by hemiacetal formation					√ [16]			
Oxidative defluorination to carboxylic acid + aldehyde formation + hydroxylation followed by hemiacetal formation + glucuronidation					√ [16]			

Metabolites	CE	HU		HH	HHep	HLM	HRG	
		XLR-11	Pyrolysis product[a]				XLR-11	Pyrolysis product[a]
Oxidative defluorination to carboxylic acid + carboxylation [X5]	√	√ [45]	√ [45]		√ [16]			
Oxidative defluorination to carboxylic acid + carboxylation + glucuronidation					√ [16]			
Oxidative defluorination to carboxylic acid + hydroxylation [X1, X4]	√	√ [45]	√ [44, 45]		√ [16]		√ [44]	√ [44]
Oxidative defluorination to carboxylic acid + hydroxylation + dehydration		√ [45]	√ [45]					
Oxidative defluorination to carboxylic acid + hydroxylation + hemiketal formation					√ [16]			
Trihydroxylation + glucuronidation					√ [16]			

CE Cunninghamella elegans; *HU* Human urine; *HH* Human hair; *HHep* Human hepatocytes; *HLM* Human liver microsomes; *HRG* HepaRG cells

Square brackets in Metabolites column indicate the ID of corresponding fungal metabolites. Phase II metabolites are shown in blue colour.

[a] Metabolites of XLR-11 pyrolysis product are shown separately from those of non-pyrolysed XLR-11.

[b] The biotransformation proposed as 'dioxidation followed by internal dehydration' in the reference is included since it might be the same biotransformation.

3.4.4 UR-144

Twenty five metabolites (U1-U25) were detected, eluting between 6.2 min and 17.4 min before the parent drug at 26.1 min (Fig. 3-2d). The biotransformation included aldehyde formation followed by hydroxylation (U19) or ketone formation (U21), carboxylation followed by hydroxylation (U6, U8, U10, U12, U15), dihydroxylation (U7, U11, U13, U16), hydroxylation (U22-U25), ketone formation followed by carboxylation (U17, U20) or hydroxylation (U14, U18), *N*-dealkylation followed by hydroxylation (U4, U9), trihydroxylation (U1-U3, U5). The mass errors of the proposed metabolites were all within 2.04 ppm. Top three abundant metabolites were dihydroxylation (U7), dihydroxylation (U11) and carboxylation with hydroxylation (U10). Proposed metabolic pathway of XLR-11 is shown in Fig. 3-6. The observed fungal metabolites are compared with the metabolites in human urine and HLM reported in the literature (Table 3-4).

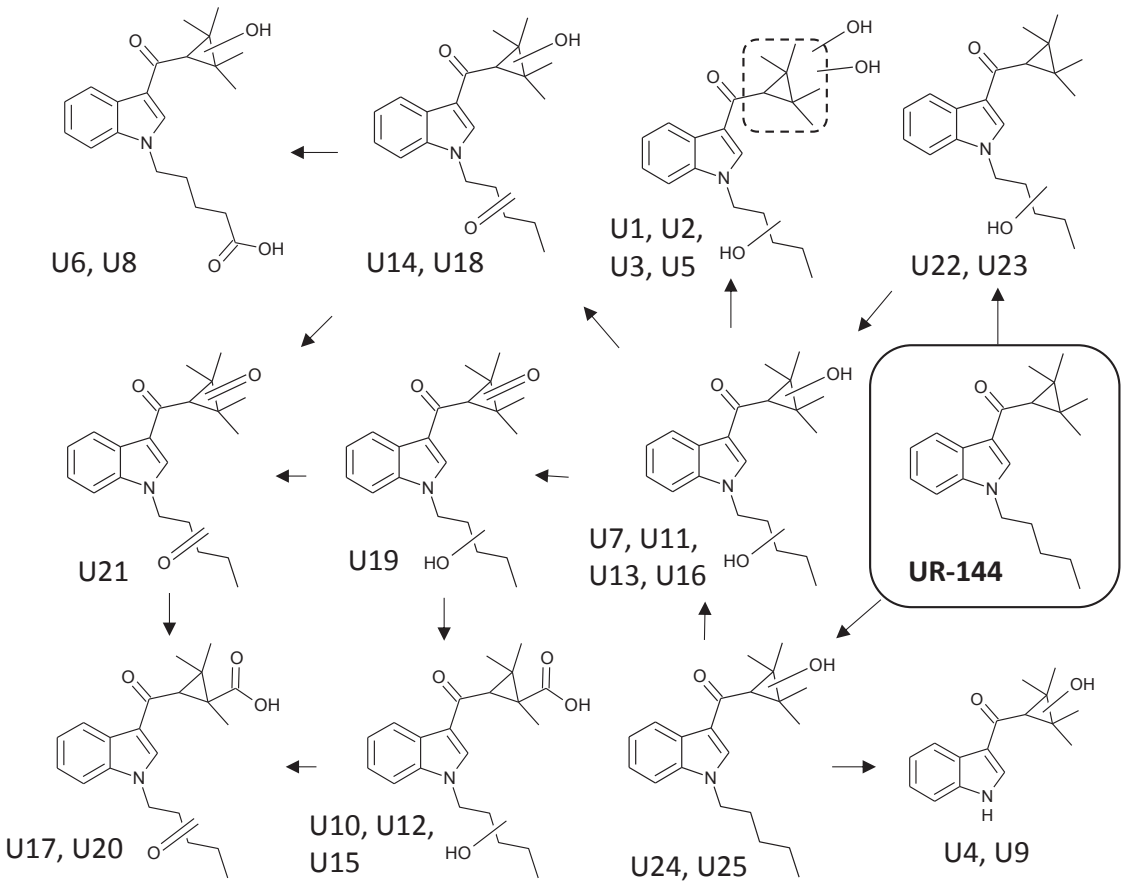

Figure 3-6. Proposed metabolic pathway of UR-144 by *C. elegans*.

Table 3-4. Comparison of UR-144 metabolites formed by fungus, *Cunninghamella elegans*, with those in human urine and human liver microsomes reported in literature.

Metabolites	CE	HU		HLM
		UR-144	Pyrolysis product[a]	
Aldehyde formation[b]				√ [6, 43]
Aldehyde formation[b] + hydroxylation [U19]	√			√ [43]
Aldehyde formation + ketone formation [U21]	√			
Carboxylation		√ [46]	√ [46, 48, 49]	√ [43]
Carboxylation + hydroxylation [U6, U8, U10, U12, U15]	√			√ [43]
Dihydroxylation [U7, U11, U13, U16]	√	√ [6, 48, 49]	√ [48, 49]	√ [6, 43]
Hydroxylation [U22 – U25]	√	√ [6, 46, 48]	√ [48, 49]	√ [6, 43]
Ketone formation				√ [6]
Ketone formation + carboxylation [U17, U20]	√			
Ketone formation + hydroxylation [U14, U18]	√	√ [48]	√ [48]	
N-dealkylation		√ [6]		√ [6]
N-dealkylation + hydroxylation [U4, U9]	√	√ [48]	√ [48]	√ [6]
Trihydroxylation [U1 - U3, U5]	√			

CE Cunninghamella elegans; *HU* Human urine; *HLM* Human liver microsomes

Square brackets in Metabolites column indicate the ID of corresponding fungal metabolites.

[a] Metabolites of UR-144 pyrolysis product are shown separately from those of non-pyrolysed UR-144.

[b] The biotransformation proposed as 'dioxidation followed by internal dehydration' or 'dehydrated hydroxy' in the reference is included since they might be the same biotransformation.

3.5 Discussion

3.5.1 Metabolite identification

3.5.1.1 5F-PB-22

In MS/MS scan, 5F-PB-22 was fragmented to the ions at *m/z* 144 (an unchanged indole moiety) and 232 (an unaltered 5-fluoropentylindole moiety) and they were used as the basis for determining the structures of the metabolites (Fig. 3-1**)**. All three hydroxy metabolites (*m/z* 393, F14-F16) were found to be hydroxylated at the fluoropentyl side chain indicated by the fragment ions at *m/z* 144 representing an unchanged indole ring and at *m/z* 248 representative of a hydroxylated fluoropentylindole moiety. Two dihydroxy metabolites (*m/z* 409, F7, F8) showed fragment ions at *m/z* 144 and 248 indicating hydroxylation once at the fluoropentyl side chain and another at the quinoline moiety. F9 was another dihydroxy metabolite, hydroxylated twice at the fluoropentylindole moiety as shown by the fragment ion at *m/z* 264. But the lack of fragment ions corresponding to the indole moiety limited further determination as to whether hydroxylation took place at the fluoropentyl side chain, the indole moiety or at both. A metabolite with dihydrodiol formation (*m/z* 411, F10) was characterised by the fragment ions at *m/z* 144 and 232 (Fig. 3-1), suggesting dihydrodiol formation at the quinoline moiety. Further hydroxylation of F10 led to the metabolite (*m/z* 427, F3) with a hydroxy group at the fluoropentylindole moiety as indicated by the fragment ion at *m/z* 248.

Oxidative defluorination to carboxylic acid (*m/z* 389, F13) was suggested by the fragment ions at *m/z* 144 (an unaltered indole ring) and 244 (a carboxylated pentylindole moiety). These fragments themselves only indicate that 5F-PB-22 was defluorinated and that the pentyl side chain has two additional oxygen atoms and two less hydrogen atoms. However, it is probably an *N*-pentanoic acid as it is reported to be a major metabolite of 5F-PB-22 in human hepatocytes studies by Wohlfarth *et al*. [17]. Also, oxidative defluorination to carboxylic acid is a biotransformation previously observed for a synthetic cannabinoid AM2201 by *C. elegans* [33]. Further hydroxylation of F13 resulted in F5, F6 and F11 (*m/z* 405). F5 and F11 were hydroxylated at the quinoline moiety as the fragment ions at

m/z 144 and 244 were still present. F6 was hydroxylated at the indole moiety, indicated by the fragment ions at *m/z* 160 (a hydroxylated indole ring) and 260 (a hydroxylated and carboxylated pentylindole). Although oxidative defluorination by itself was not observed, a metabolite with oxidative defluorination and dihydrodiol formation was indicated (*m/z* 409, F1). The only fragment ion detected was at *m/z* 230 suggesting a quinoline moiety with dihydrodiol formation and a pentylindole moiety with a hydroxy group. Despite the lack of the *m/z* 144 fragment ion, the position of the hydroxy group can be considered to be at the terminal carbon of the pentyl side chain since oxidative defluorination is a commonly reported pathway to simultaneously defluorinate and hydroxylate fluorinated synthetic cannabinoids [2, 6, 7, 16, 18, 19] and it has been reported for *C. elegans* [33].

Ester hydrolysis led to the 5F-PI-COOH metabolite (*m/z* 250, F12) as indicated by the fragment ions at *m/z* 118 and 232 suggesting an unchanged indole moiety and unmodified 5-fluoropentylindole moiety, respectively. There was another unknown peak with *m/z* 250 in the extracted ion chromatogram, but careful examination of mass spectrum in full scan mode revealed the presence of a coeluting protonated ion at *m/z* 412, which has mass error of 1.39 ppm for a glucoside of F12. Thus, it seems to be a glucoside of 5F-PI-COOH with in-source fragmentation (*m/z* 412, F2). In-source fragmentation of acyl glucuronides is reported for synthetic cannabinoid metabolites including 5F-PB-22 [16, 17] and is likely to occur with glucosides. A metabolite resulting from hydroxylation of F12 was shown by the fragment ions at *m/z* 248 indicating a 5-fluorohydroxypentylindole moiety and 134 corresponding to a hydroxyindole moiety (*m/z* 266, F4).

3.5.1.2 PB-22

PB-22 was fragmented similarly to 5F-PB-22 and resulted in two product ions at *m/z* 144 and 214 (Fig. 3-1), corresponding to an unchanged indole ring and an unaltered pentylindole moiety. Both hydroxy metabolites (*m/z* 375, P26, P28) underwent hydroxylation at the pentyl side chain as shown by the fragment ions at *m/z* 144 and 230 with the latter indicating a hydroxylated pentylindole moiety. A dihydroxy metabolite (*m/z* 391, P13) showed the fragment ions at *m/z* 144 and 230 (Fig. 3-1), indicating hydroxylation at both the pentyl side chain and the quinoline moiety while the other three dihydroxy metabolites (P15, P16, P19) were hydroxylated twice at the pentyl side chain

as suggested by the fragment ions at *m/z* 144 and 246. A trihydroxylated metabolite (*m/z* 407, P2) was indicated to have two hydroxy groups at the pentyl side chain and another at the quinoline moiety (*m/z* 144, 246). A metabolite with dihydrodiol formation at the quinoline moiety (*m/z* 393, P27) was suggested by the ions at *m/z* 144 and 214 representing an unchanged pentylindole moiety. Hydroxylation of P27 at the pentyl side chain resulted in (*m/z* 409, P3, P7) as indicated by the ions at *m/z* 144 and 230. The retention time and fragmentation pattern of P3 and F1 indicated they are identical, suggesting the position of hydroxylation at the terminal carbon. Notably, for P7 the fragment ion at *m/z* 230 was not observed likely because the ion suppression occurred due to the coeluting metabolite P8 (peaks at *m/z* 228 and 229 are seen in the MS/MS, data not shown). However, product ion scan by the LC-QqQ revealed a clear peak at *m/z* 230. Further oxidation of P3 and P7 appeared to form metabolites (*m/z* 407, P8, P14) with a ketone group at the pentyl side chain with dihydrodiol at the quinoline moiety as evidenced by the fragment ions at *m/z* 144 and 228.

Metabolites with a ketone group at the pentyl side chain (*m/z* 373, P29, P30) were characterised by the fragment ions at *m/z* 144 and 228, the latter indicating a pentylindole moiety with a ketone group. Further hydroxylation occurred at the quinoline moiety for P17, P20, P22 and P25 (*m/z* 389) indicated by the fragment ions at *m/z* 144 and 228 and at the pentyl side chain for P21 and P23 suggested by the fragment ions at *m/z* 144 and 244. A glucoside of a hydroxylated metabolite with ketone was detected (*m/z* 551, P1) but it was not a glucoside of any of the phase I metabolites found as the position of the hydroxylation for this metabolite was at the indole moiety (*m/z* 160, 244). Four metabolites with a ketone group at the side chain and dihydroxylation (*m/z* 405, P4, P5, P9, P18) were formed. P4 has a hydroxy group each at the indole ring and the quinoline moiety (*m/z* 160, 244), P5 and P9 at the pentyl side chain and the quinoline moiety (*m/z* 144, 244) and P18 twice at the pentyl side chain (*m/z* 144, 260). For P9 and P18, the fragment ion at *m/z* 144 was absent but was confirmed by the LC-QqQ analysis. P24 (*m/z* 389) showed the fragment ions at *m/z* 144, 244 and based on the retention time and fragmentation pattern it was considered to be identical to F13 and is proposed to be an *N*-pentanoic acid metabolite. Also, P12 (*m/z* 405) was determined to be identical to F5 and is proposed to be formed by hydroxylating P24 at the quinoline ring.

Similarly to 5F-PB-22, a glucoside of PI-COOH formed from ester hydrolysis (*m/z* 394, P10) was largely fragmented to *m/z* 232 by in-source fragmentation. Several fragment ions including *m/z* 118 and 214 suggested an unchanged pentylindole moiety. PI-COOH with hydroxylation at the pentyl side chain (*m/z* 248, P6, P11) was represented by the fragment ions at *m/z* 130 (an unaltered indole) and 230.

3.5.1.3 XLR-11

The structure of XLR-11 is similar to 5F-PB-22 with the quinoline moiety replaced by the tetramethylcyclopropyl (TMCP) ring. As such, the fragmentation pattern of XLR-11 was similar; *m/z* 144, 232 and additionally 125 (Fig. 3-1), corresponding to the TMCP moiety were observed. Hydroxylated metabolites (*m/z* 346, X21, X23) were found to have a hydroxy group at the TMCP ring as indicated by the fragment ions at *m/z* 144 and 232 (Fig. 3-1). The absence of the fragment ion at *m/z* 125 also indicated the modification at the TMCP ring. There are three possible positions of hydroxylation: the alpha carbon to the carbonyl group, two methyl groups on the same side of the cyclopropyl ring as the hydrogen atom on the alpha carbon, which is an (*E*)-isomer, and two methyl groups on the other side of the ring from the hydrogen, a (*Z*)-isomer. Wohlfarth *et al*. reported, in their human hepatocytes studies, three hydroxy glucuronides with the two diastereomers eluting closely [16]. Thus, it is possible that the diastereomers might have coeluted under the chromatographic condition employed, resulting in two apparent peaks. Eight dihydroxy metabolites (*m/z* 362, X3, X6, X9, X11-X13, X19, and X20) were detected. X3, X9 and X11 were hydroxylated once each at the fluoropentyl side chain and at the TMCP ring (*m/z* 144, 248) and X6, X12, X13, X19 and X20 twice at the TMCP ring (*m/z* 144, 232). Aldehyde formation at the TMCP ring (*m/z* 344, X26) was characterised by the fragment ions at *m/z* 144 and 232. In fact, aldehydes are highly reactive and might undergo subsequent reaction before being detected. However, intermediate aldehyde metabolite of ebastine is reported to be isolated and characterised along with subsequent carboxylic acid metabolite after incubation with *Cunninghamella blakesleeana*, another species of the genus *Cunninghamella* [50], and therefore aldehyde is tentatively proposed in this study.

Three metabolites (*m/z* 360, X14, X18, X22) were observed with the fragment ions at *m/z* 144 and 232 corresponding to carboxylic acid at the TMCP ring. Similar to hydroxylation of the TMCP ring, there appears to be two possible positions for carboxylation at methyl carbons generating (*E*)- and (*Z*)-isomers. However, this does not explain the presence of three metabolites. Therefore, it is likely that one or two of the three metabolites are phase II metabolites with in-source fragmentation. As the retention time of X22 is relatively late compared to the other two, it is possible that X22 is a carboxy metabolite and X14 and X18 are glucosides of carboxy metabolites. The reason for only one chromatographic peak for the carboxy metabolite may be explained by coelution whereas the phase II metabolites may have sufficient difference in property to be separated by chromatography under the condition employed. Wohlfarth *et al*. also reported the presence of single carboxy metabolite and it was the peak eluting last among the metabolites with *m/z* 360 and their glucuronides [16]. Alternatively, X14 or X18 may be hemiacetal formation as reported by Wohlfarth *et al*. [16]. Carboxylation followed by hydroxylation (*m/z* 376, X10) showed the fragments at *m/z* 144 and 248 indicating hydroxylation at the fluoropentyl side chain.

A metabolite with oxidative defluorination (*m/z* 328, X25) was characterised by the fragment ions at *m/z* 125, 144 and 230 indicating a hydroxylated pentyl side chain. Hydroxylation of X25 led to X2 and X7 (*m/z* 344) with the fragment ions at *m/z* 144 and 230 suggesting hydroxylation at the TMCP ring. Further oxidation of X2 or X7 formed an aldehyde metabolite (*m/z* 342, X16) and a carboxylated metabolite (*m/z* 358, X8) both with the fragment ions at *m/z* 144 and 230. Oxidative defluorination to carboxylic acid (*m/z* 342, X24) was indicated by the fragment ions at *m/z* 125, 144 and 244. X24 was subsequently hydroxylated at the TMCP ring (*m/z* 358, X1, X4), further oxidised to aldehyde (*m/z* 356, X15, X17) and carboxylic acid (*m/z* 372, X5), all with the fragment ions at *m/z* 144 and 244. Notably, if the two metabolites at *m/z* 356 (X15 and X17) are aldehydes as tentatively assigned, it would be the only case where the (*E*)- and (*Z*)-isomers do not coelute. Therefore, it is possible that one of them is a metabolite that underwent dihydroxylation followed by internal dehydration as previously reported [16].

3.5.1.4 UR-144

UR-144 is a defluorinated analogue of XLR-11. Hence, it showed the same fragment ions at *m/z* 125, 144 and the defluorinated ion at *m/z* 214, instead of 232 (Fig. 3-1). Hydroxylation (*m/z* 328) of UR-144 occurred at the pentyl side chain with the fragment ions at *m/z* 125, 144 and 230 (U22, U23) and at the TMCP ring with the ions at 144 and 214 (U24, U25). U22 matched well in retention time with X25 (oxidative defluorination metabolite of XLR-11), suggesting 5-hydroxypentyl metabolite. The position of hydroxylation for U23 cannot be determined but is likely to be 4-hydroxypentyl metabolite since (ω)-OH and (ω-1)-OH metabolites of alkyl side chain have been reported for some synthetic cannabinoids [33, 51]. Further hydroxylation of hydroxy metabolites resulted in dihydroxylation (*m/z* 344, U7, U11, U13, U16) with one hydroxy group at the pentyl side chain and another at the TMCP ring as indicated by the fragment ions at *m/z* 144 and 230 (Fig. 3-1). U7 and U11 agreed well with X2 and X7, respectively, indicating that the hydroxy group at the side chain is likely to be at the terminal carbon. Trihydroxylated metabolites (*m/z* 360, U1-U3, U5) were then formed with a hydroxy group at the pentyl side chain and two at the TMCP ring as shown by the fragment ions at *m/z* 144 and 230. *N*-dealkylation of U24 and U25 resulted in despentyl hydroxy metabolites (*m/z* 258, U4, U9) with the fragment ion at *m/z* 144.

Aldehyde formation at the TMCP ring followed by hydroxylation at the pentyl side chain (*m/z* 342, U19) was suggested by the fragment ions at *m/z* 144 and 230. Due to the close retention time with X16 (oxidative defluorination metabolite of XLR-11), U19 is likely to be hydroxylated at the 5-position of the pentyl side chain. Aldehyde at the TMCP ring followed by ketone at the pentyl side chain (*m/z* 340, U21) showed the fragment ions at the *m/z* 144 and 228 representing ketone formation at the pentyl side chain. Carboxylation at the pentyl side chain with hydroxylation at the TMCP ring (*m/z* 358, U6, U8) was suggested by the ions at *m/z* 144 and 244 indicative of *N*-pentanoic acid, which was supported by the matching retention time with X1 and X4, respectively. Similarly, carboxylation at the TMCP ring with hydroxylation at the pentyl side chain (*m/z* 358, U10, U12, U15) was indicated by the ions at *m/z* 144 and 230. U10 was considered to be the same metabolite as X8 and is expected to have been hydroxylated at the terminal carbon.

Ketone formation at the pentyl side chain with hydroxylation at the TMCP ring (*m/z* 342, U14, U18) was suggested by the fragment ions at *m/z* 144 and 228. Ketone at the pentyl side chain with carboxylation at the TMCP ring (*m/z* 356, U17, U20) was represented by the fragment ions at *m/z* 144 and 228.

3.5.2 Comparison of fungal metabolites with reported human metabolites

For 5F-PB-22 and PB-22, the fungal metabolites were generally in good agreement with reported human *in vitro* metabolites (Tables 3-1 and 3-2). Almost all types of individual biotransformations reported for the human metabolism were observed for the fungal metabolism though not necessarily in the same combinations; the only transformations that lacked with the fungus were cysteine conjugation and glucuronidation. The important difference, however, was that ester hydrolysis that forms 5F-PI-COOH/PI-COOH was the main pathway found by human hepatocytes [17] and HLM [22] while it was not a major pathway for *C. elegans*. In hepatocytes, three out of the five most abundant 5F-PB-22 metabolites are ester hydrolysis products with/without hydroxylation or glucuronidation whereas all seven major metabolites of PB-22 are ester hydrolysis products with/without hydroxylation, ketone formation and/or glucuronidation [17]. In contrast, all the fungal metabolites with ester hydrolysis were among the minor metabolites.

Since publication of this work, human *in vivo* metabolites of 5F-PB-22 and PB-22 obtained from authentic urine samples were reported. Cannaert *et al*. found 5F-PI-COOH/PI-COOH as the most abundant metabolite of 5F-PB-22/PB-22 in human urine samples and 5-pentylhydroxy/4-pentylhydroxy metabolite as the second most prevalent metabolite [52]. *N*-pentanoic acid metabolite was also reported to be present in most cases. Minakata *et al*. also reported 5F-PB-22 metabolites in urine and similar observations were made, except that *N*-pentanoic acid metabolite was the second most abundant metabolite instead of 5-pentylhydroxy metabolite [53]. These results are comparable to those of the *in vitro* studies as well as the fungus, apart from the quantitative differences between fungal and human metabolites as described previously.

The majority of the human metabolites for XLR-11 and UR-144 were observed in the fungus samples (Tables 3-3 and 3-4). For XLR-11, hemiacetal, *N*-dealkylation, dehydration, hemiketal, trihydroxylation and glucuronidation were the only individual transformations found in both *in vivo* and *in vitro* human metabolism that were not generated by the fungus. The major human urine metabolites have been reported to be oxidative defluorination and oxidative defluorination to carboxylic acid with/without hydroxylation [44, 45], mostly of the pyrolysis product formed from thermal degradation due to smoking. All these metabolites were found in the fungus culture, though not of the pyrolysis product as the process of heating was not involved in this study, and metabolites with oxidative defluorination to carboxylic acid with hydroxylation (X1 and X4) were the fourth and fifth abundant fungal metabolites among 26 metabolites indicating good correlation in abundance. With UR-144, although metabolites with aldehyde, carboxylation, ketone or *N*-dealkylation alone were absent, all the reported individual human biotransformations including the four aforementioned were detected in fungal metabolism. Hydroxylation and dihydroxylation are reported major human urine metabolites [6, 48] and two dihydroxylated metabolites (U7 and U11) were found to be the two most abundant fungal metabolites.

These findings demonstrate that *C. elegans* is capable of most biotransformations observed for the four synthetic cannabinoids in humans, which is consistent with the previous studies on JWH-018, JWH-073 and AM2201 [33]. Hence, it shows the potential to be used to predict metabolism of future cannabinoids, complementary to other models, and to characterise metabolites by NMR analysis. However, two distinct differences between the fungus and human metabolism seem to exist. One is that glucuronides were not observed in this study and instead glucosides were generated by the fungus. This finding agrees with the study on the synthetic cannabinoid AM2201 that glucosidation and sulfation are the only phase II reactions observed for *C. elegans* metabolism while glucuronidation is the major phase II transformation in humans [33]. Similarly, for some other drugs, glucosidation and sulfation are reported to be the phase II reactions of *C. elegans* while the same drugs are glucuronidated and sulfated in humans [38, 54]. The latter experiments did not involve extraction step as a sample preparation, supporting that poor recovery of glucuronides in dichloromethane is not likely a reason for the absence of glucuronides in this study. Furthermore, the retention time of the glucosides observed

in this study was between 6 and 10 min. If glucuronides of corresponding aglycones were present in the culture, they would likely have been extracted by dichloromethane, which did extract polar compounds derived from matrix eluting between 3 and 6 min. This indicates that phase II metabolites produced by the fungus, particularly glucosides, may be irrelevant and need to be interpreted with caution, if hydrolysis step is not included in sample preparation before urinalysis. The other difference is that ester hydrolysis was clearly not a favoured pathway in the fungal metabolism. Previously, incubation of steroidal drug, ethynodiol diacetate containing two ester groups, with *C. elegans* and *Ocimum basilicum* has been reported [55] and while ester hydrolysis did not occur with *C. elegans*, three of the four metabolites by *Ocimum basilicum* underwent hydrolysis suggesting that *C. elegans* may not favour ester hydrolysis in general. Some of the other discrepancies between the fungal and human metabolites may be due to dosages, possible co-administration of drugs in authentic human samples, incubation/sampling time. Finally, there are limitations of the comparison method. Each biotransformation observed for fungus and human metabolism was compared in this study. While this method provides useful information on the major metabolic pathways, specific isomers found in fungal metabolism may not always be the exact isomers found in human metabolism, e.g. 2-pentylhydroxy isomer in fungus vs. 4-pentylhydroxy isomer in human urine. This limitation is inherent to the mass spectrometry technique used and highlights the need to use other complimentary techniques such as NMR to aid unambiguous structural elucidation of metabolites and to facilitate more accurate comparison.

3.5.3 Comparison of fungal model with *in vitro* human models

One of the incentives to use the fungus is the cost efficiency of the model. Unlike human hepatocytes or HLM, fungus can be repeatedly subcultured as required for new experiments. Therefore, once the stock culture of the fungus is obtained, potato dextrose agar plates for subculturing will essentially be the only cost associated for the subsequent use of fungus.

Regarding extrapolation of metabolic profiles to human metabolism, human hepatocytes appear to best serve the purpose as the biotransformations observed are most closely aligned to human metabolites including the phase II metabolites as observed for XLR-11

(Table 3-3) and the metabolite abundance is often closer to *in vivo* human metabolites [8]. While *C. elegans* did not match the human metabolites for XLR-11 as well as hepatocytes, it seems just as useful as HLM, generating most of the HLM metabolites in addition to those not produced by HLM (Tables 3-1 – 3-4).

As previously mentioned, the fungus metabolism can be scaled up to produce amounts of metabolites sufficient for NMR analysis. This is useful because it allows for more definitive characterisation of metabolites. Metabolites/isomers found in human urine and *in vitro* studies are not always conclusively characterised since commercially available reference standards do not cover all the potential metabolites and isomers. With upscaling of fungus metabolism followed by NMR analysis, the obtained metabolites could act as reference standards and in conjunction with human metabolism studies, appropriate biomarkers can be suggested. The quantity of drugs and volume of the media required for upscaling will depend on how much drug is metabolised, how many metabolites are to be analysed, abundance of major metabolites among all the metabolites, recovery of the metabolites in extraction and sensitivity of NMR spectrometer. In this study, these parameters were not quantified, and consequently it is difficult to estimate the quantity and volume required. Previous studies report that as little as 0.9 mg of 18-nor-oxandrolone in 30 mL of media is sufficient for analysis of two metabolites [39] while five metabolites of adrenosterone were generated from 450 mg in 3 L, indicating the variability of the quantity and volume from case to case.

3.6 Conclusion

The metabolism of four synthetic cannabinoids, 5F-PB-22, XLR-11 and their defluorinated analogues PB-22 and UR-144 respectively, was investigated using the fungus *C. elegans*. The phase I and II metabolites were identified based on LC-QTOF analysis and their metabolic pathways were proposed. Hydroxylation, dihydroxylation, dihydrodiol formation, oxidative defluorination, oxidative defluorination to carboxylic acid, ester hydrolysis, glucosidation and combinations of these were observed for 5F-PB-22 with some of them only appearing as combinations. For PB-22, transformations were similar, but trihydroxylation, ketone formation and carboxylation were found instead of oxidative defluorination (to carboxylic acid). XLR-11 underwent hydroxylation, dihydroxylation, aldehyde formation, carboxylation, oxidative defluorination, oxidative defluorination to carboxylic acid and glucosidation either alone or in combinations. With UR-144, trihydroxylation, ketone formation and *N*-dealkylation were observed instead of oxidative defluorination (to carboxylic acid) and glucosidation. Comparison of the fungal metabolites with reported human metabolites showed that while *C. elegans* has limitations, such as low abundance of ester hydrolysis and absence of glucuronidation, overall the metabolic profiles were in good agreement. Therefore, it might have the potential to be a complementary model for synthetic cannabinoid metabolism.

3.7 References

1. European Monitoring Centre for Drugs and Drug Addiction. European Drug Report 2016: Trends and Developments. Luxembourg: Publications Office of the European Union 2016.

2. Chimalakonda KC, Seely KA, Bratton SM, Brents LK, Moran CL, Endres GW, et al. Cytochrome P450-mediated oxidative metabolism of abused synthetic cannabinoids found in K2/Spice: identification of novel cannabinoid receptor ligands. Drug Metab Dispos. 2012;40(11):2174-84. doi:10.1124/dmd.112.047530.

3. Fantegrossi WE, Moran JH, Radominska-Pandya A, Prather PL. Distinct pharmacology and metabolism of K2 synthetic cannabinoids compared to Delta(9)-THC: mechanism underlying greater toxicity? Life Sci. 2014;97(1):45-54. doi:10.1016/j.lfs.2013.09.017.

4. Trecki J, Gerona RR, Schwartz MD. Synthetic Cannabinoid–Related Illnesses and Deaths. N Engl J Med. 2015;373(2):103-7. doi:doi:10.1056/NEJMp1505328.

5. Grigoryev A, Savchuk S, Melnik A, Moskaleva N, Dzhurko J, Ershov M, et al. Chromatography-mass spectrometry studies on the metabolism of synthetic cannabinoids JWH-018 and JWH-073, psychoactive components of smoking mixtures. J Chromatogr B. 2011;879(15-16):1126-36. doi:10.1016/j.jchromb.2011.03.034.

6. Sobolevsky T, Prasolov I, Rodchenkov G. Detection of urinary metabolites of AM-2201 and UR-144, two novel synthetic cannabinoids. Drug Test Anal. 2012;4(10):745-53. doi:10.1002/dta.1418.

7. Wohlfarth A, Castaneto MS, Zhu M, Pang S, Scheidweiler KB, Kronstrand R, et al. Pentylindole/Pentylindazole Synthetic Cannabinoids and Their 5-Fluoro Analogs Produce Different Primary Metabolites: Metabolite Profiling for AB-PINACA and 5F-AB-PINACA. AAPS J. 2015;17(3):660-77. doi:10.1208/s12248-015-9721-0.

8. Diao X, Scheidweiler KB, Wohlfarth A, Pang S, Kronstrand R, Huestis MA. In Vitro and In Vivo Human Metabolism of Synthetic Cannabinoids FDU-PB-22 and FUB-PB-22. AAPS J. 2016;18(2):455-64. doi:10.1208/s12248-016-9867-4.

9. Castaneto MS, Wohlfarth A, Pang S, Zhu M, Scheidweiler KB, Kronstrand R, et al. Identification of AB-FUBINACA metabolites in human hepatocytes and urine using high-resolution mass spectrometry. Forensic Toxicol. 2015;33(2):295-310. doi:10.1007/s11419-015-0275-8.

10. Vikingsson S, Green H, Brinkhagen L, Mukhtar S, Josefsson M. Identification of AB-FUBINACA metabolites in authentic urine samples suitable as urinary markers of drug intake using liquid chromatography quadrupole tandem time of flight mass spectrometry. Drug Test Anal. 2016;8(9):950-6. doi:10.1002/dta.1896.

11. Sobolevsky T, Prasolov I, Rodchenkov G. Detection of JWH-018 metabolites in smoking mixture post-administration urine. Forensic Sci Int. 2010;200(1-3):141-7. doi:10.1016/j.forsciint.2010.04.003.

12. Kavanagh P, Grigoryev A, Melnik A, Savchuk S, Simonov A, Rozhanets V. Detection and tentative identification of urinary phase I metabolites of phenylacetylindole cannabimimetics JWH-203 and JWH-251, by GC–MS and LC–MS/MS. J Chromatogr B. 2013;934:102-8. doi:http://dx.doi.org/10.1016/j.jchromb.2013.07.005.

13. Zaitsu K, Nakayama H, Yamanaka M, Hisatsune K, Taki K, Asano T, et al. High-resolution mass spectrometric determination of the synthetic cannabinoids MAM-2201, AM-2201, AM-2232, and their metabolites in postmortem plasma and urine by LC/Q-TOFMS. Int J Legal Med. 2015;129(6):1233-45. doi:10.1007/s00414-015-1257-4.

14. Sobolevsky T, Prasolov I, Rodchenkov G. Study on the phase I metabolism of novel synthetic cannabinoids, APICA and its fluorinated analogue. Drug Test Anal. 2015;7(2):131-42. doi:10.1002/dta.1756.

15. Hutter M, Moosmann B, Kneisel S, Auwarter V. Characteristics of the designer drug and synthetic cannabinoid receptor agonist AM-2201 regarding its chemistry and metabolism. J Mass Spectrom. 2013;48(7):885-94. doi:10.1002/jms.3229.

16. Wohlfarth A, Pang S, Zhu M, Gandhi AS, Scheidweiler KB, Liu HF, et al. First metabolic profile of XLR-11, a novel synthetic cannabinoid, obtained by using human hepatocytes and high-resolution mass spectrometry. Clin Chem. 2013;59(11):1638-48. doi:10.1373/clinchem.2013.209965.

17. Wohlfarth A, Gandhi AS, Pang S, Zhu M, Scheidweiler KB, Huestis MA. Metabolism of synthetic cannabinoids PB-22 and its 5-fluoro analog, 5F-PB-22, by human hepatocyte incubation and high-resolution mass spectrometry. Anal Bioanal Chem. 2014;406(6):1763-80. doi:10.1007/s00216-014-7668-0.

18. Diao X, Scheidweiler KB, Wohlfarth A, Zhu M, Pang S, Huestis MA. Strategies to distinguish new synthetic cannabinoid FUBIMINA (BIM-2201) intake from its isomer THJ-2201: metabolism of FUBIMINA in human hepatocytes. Forensic Toxicol. 2016;34:256-67. doi:10.1007/s11419-016-0312-2.

19. Diao X, Wohlfarth A, Pang S, Scheidweiler KB, Huestis MA. High-Resolution Mass Spectrometry for Characterizing the Metabolism of Synthetic Cannabinoid THJ-018 and Its 5-Fluoro Analog THJ-2201 after Incubation in Human Hepatocytes. Clin Chem. 2016;62(1):157-69. doi:10.1373/clinchem.2015.243535.

20. Gandhi AS, Zhu M, Pang S, Wohlfarth A, Scheidweiler KB, Liu HF, et al. First characterization of AKB-48 metabolism, a novel synthetic cannabinoid, using human hepatocytes and high-resolution mass spectrometry. AAPS J. 2013;15(4):1091-8. doi:10.1208/s12248-013-9516-0.

21. Wintermeyer A, Moller I, Thevis M, Jubner M, Beike J, Rothschild MA, et al. In vitro phase I metabolism of the synthetic cannabimimetic JWH-018. Anal Bioanal Chem. 2010;398(5):2141-53. doi:10.1007/s00216-010-4171-0.

22. Takayama T, Suzuki M, Todoroki K, Inoue K, Min JZ, Kikura-Hanajiri R, et al. UPLC/ESI-MS/MS-based determination of metabolism of several new illicit drugs, ADB-FUBINACA, AB-FUBINACA, AB-PINACA, QUPIC, 5F-QUPIC and alpha-PVT, by human liver microsome. Biomed Chromatogr. 2014;28(6):831-8. doi:10.1002/bmc.3155.

23. Jang M, Shin I, Yang W, Chang H, Yoo HH, Lee J, et al. Determination of major metabolites of MAM-2201 and JWH-122 in in vitro and in vivo studies to distinguish their intake. Forensic Sci Int. 2014;244:85-91. doi:10.1016/j.forsciint.2014.08.008.

24. Vikingsson S, Josefsson M, Green H. Identification of AKB-48 and 5F-AKB-48 Metabolites in Authentic Human Urine Samples Using Human Liver Microsomes and Time of Flight Mass Spectrometry. J Anal Toxicol. 2015;39(6):426-35. doi:10.1093/jat/bkv045.

25. De Brabanter N, Esposito S, Geldof L, Lootens L, Meuleman P, Leroux-Roels G, et al. In vitro and in vivo metabolisms of 1-pentyl-3-(4-methyl-1-naphthoyl)indole (JWH-122). Forensic Toxicol. 2013;31(2):212-22. doi:10.1007/s11419-013-0179-4.

26. De Brabanter N, Esposito S, Tudela E, Lootens L, Meuleman P, Leroux-Roels G, et al. In vivo and in vitro metabolism of the synthetic cannabinoid JWH-200. Rapid Commun Mass Spectrom. 2013;27(18):2115-26. doi:10.1002/rcm.6673.

27. Schaefer N, Helfer AG, Kettner M, Laschke MW, Schlote J, Ewald AH, et al. Metabolic patterns of JWH-210, RCS-4, and THC in pig urine elucidated using LC-HR-MS/MS: Do they reflect patterns in humans? Drug Test Anal. 2016. doi:10.1002/dta.1995.

28. Maurer HH, Meyer MR. High-resolution mass spectrometry in toxicology: current status and future perspectives. Arch Toxicol. 2016;90(9):2161-72. doi:10.1007/s00204-016-1764-1.

29. Diao X, Huestis MA. Approaches, Challenges, and Advances in Metabolism of New Synthetic Cannabinoids and Identification of Optimal Urinary Marker Metabolites. Clin Pharmacol Ther. 2017;101(2):239-53. doi:10.1002/cpt.534.

30. Asha S, Vidyavathi M. Cunninghamella--a microbial model for drug metabolism studies--a review. Biotechnol Adv. 2009;27(1):16-29. doi:10.1016/j.biotechadv.2008.07.005.

31. Zhang D, Yang Y, Leakey JEA, Cerniglia CE. Phase I and phase II enzymes produced by Cunninghamella elegans for the metabolism of xenobiotics. FEMS Microbiol Lett. 1996;138(2-3):221-6. doi:10.1111/j.1574-6968.1996.tb08161.x.

32. Wang R-F, Cao W-W, Khan AA, Cerniglia CE. Cloning, sequencing, and expression in Escherichia coli of a cytochrome P450 gene from Cunninghamella elegans. FEMS Microbiol Lett. 2000;188(1):55-61. doi:10.1111/j.1574-6968.2000.tb09168.x.

33. Watanabe S, Kuzhiumparambil U, Winiarski Z, Fu S. Biotransformation of synthetic cannabinoids JWH-018, JWH-073 and AM2201 by Cunninghamella elegans. Forensic Sci Int. 2016;261:33-42. doi:http://dx.doi.org/10.1016/j.forsciint.2015.12.023.

34. Kaminsky LS, Zhang Z-Y. Human P450 metabolism of warfarin. Pharmacol Ther. 1997;73(1):67-74. doi:http://dx.doi.org/10.1016/S0163-7258(96)00140-4.

35. Wong YWJ, Davis PJ. Microbial Models of Mammalian Metabolism: Stereoselective Metabolism of Warfarin in the Fungus Cunninghamella elegans. Pharm Res. 1989;6(11):982-7. doi:10.1023/a:1015905832184.

36. Olesen OV, Linnet K. Metabolism of the Tricyclic Antidepressant Amitriptyline by cDNA-Expressed Human Cytochrome P450 Enzymes. Pharmacology. 1997;55(5):235-43. doi:10.1159/000139533.

37. Zhang D, Evans FE, Freeman JP, Duhart B, Cerniglia CE. Biotransformation of amitriptyline by Cunninghamella elegans. Drug Metab Dispos. 1995;23(12):1417-25.

38. Hansson A, Thevis M, Cox H, Miller G, Eichner D, Bondesson U, et al. Investigation of the metabolites of the HIF stabilizer FG-4592 (roxadustat) in five different in vitro models and in a human doping control sample using high resolution mass spectrometry. J Pharm Biomed Anal. 2017;134:228-36. doi:10.1016/j.jpba.2016.11.041.

39. Guddat S, Fußhöller G, Beuck S, Thomas A, Geyer H, Rydevik A, et al. Synthesis, characterization, and detection of new oxandrolone metabolites as long-term markers in sports drug testing. Anal Bioanal Chem. 2013;405(25):8285-94. doi:10.1007/s00216-013-7218-1.

40. Tian J-L, Chen Y, Wang Y-X, Huang X-X, Sun X, Liu K-C, et al. Microbial transformation of methyl cyperenoate by Cunninghamella elegans AS 3.2028 and the antithrombotic activities of its metabolites. RSC Adv. 2016;6(113):112712-20. doi:10.1039/c6ra24332k.

41. Watanabe S, Kuzhiumparambil U, Winiarski Z, Fu S. Data on individual metabolites of synthetic cannabinoids JWH-018, JWH-073 and AM2201 by Cunninghamella elegans. Data Brief. 2016;7:332-40. doi:10.1016/j.dib.2016.02.039.

42. Choudhary MI, Khan NT, Musharraf SG, Anjum S, Atta ur R. Biotransformation of adrenosterone by filamentous fungus, Cunninghamella elegans. Steroids. 2007;72(14):923-9. doi:http://dx.doi.org/10.1016/j.steroids.2007.08.002.

43. Nielsen LM, Holm NB, Olsen L, Linnet K. Cytochrome P450-mediated metabolism of the synthetic cannabinoids UR-144 and XLR-11. Drug Test Anal. 2016;8(8):792-800. doi:10.1002/dta.1860.

44. Kanamori T, Kanda K, Yamamuro T, Kuwayama K, Tsujikawa K, Iwata YT, et al. Detection of main metabolites of XLR-11 and its thermal degradation product in human hepatoma HepaRG cells and human urine. Drug Test Anal. 2015;7(4):341-5. doi:10.1002/dta.1765.

45. Jang M, Kim IS, Park YN, Kim J, Han I, Baeck S, et al. Determination of urinary metabolites of XLR-11 by liquid chromatography-quadrupole time-of-flight mass spectrometry. Anal Bioanal Chem. 2016;408(2):503-16. doi:10.1007/s00216-015-9116-1.

46. Scheidweiler KB, Jarvis MJ, Huestis MA. Nontargeted SWATH acquisition for identifying 47 synthetic cannabinoid metabolites in human urine by liquid chromatography-high-resolution tandem mass spectrometry. Anal Bioanal Chem. 2015;407(3):883-97. doi:10.1007/s00216-014-8118-8.

47. Park M, Yeon S, Lee J, In S. Determination of XLR-11 and its metabolites in hair by liquid chromatography-tandem mass spectrometry. J Pharm Biomed Anal. 2015;114:184-9. doi:10.1016/j.jpba.2015.05.022.

48. Grigoryev A, Kavanagh P, Melnik A, Savchuk S, Simonov A. Gas and liquid chromatography-mass spectrometry detection of the urinary metabolites of UR-144 and its major pyrolysis product. J Anal Toxicol. 2013;37(5):265-76. doi:10.1093/jat/bkt028.

49. Adamowicz P, Zuba D, Sekula K. Analysis of UR-144 and its pyrolysis product in blood and their metabolites in urine. Forensic Sci Int. 2013;233(1-3):320-7. doi:10.1016/j.forsciint.2013.10.005.

50. Schwartz H, Liebig-Weber A, Hochstätter H, Böttcher H. Microbial oxidation of ebastine. Appl Microbiol Biotechnol. 1996;44(6):731-5. doi:10.1007/bf00178610.

51. Chimalakonda KC, Moran CL, Kennedy PD, Endres GW, Uzieblo A, Dobrowolski PJ, et al. Solid-phase extraction and quantitative measurement of omega and omega-1 metabolites of JWH-018 and JWH-073 in human urine. Anal Chem. 2011;83(16):6381-8. doi:10.1021/ac201377m.

52. Cannaert A, Storme J, Franz F, Auwärter V, Stove CP. Detection and Activity Profiling of Synthetic Cannabinoids and Their Metabolites with a Newly Developed Bioassay. Anal Chem. 2016;88(23):11476-85. doi:10.1021/acs.analchem.6b02600.

53. Minakata K, Hasegawa K, Yamagishi I, Nozawa H, Kikura-Hanajiri R, Suzuki M, et al. Sensitive quantification of 5F-PB-22 and its three metabolites 5F-PB-22 3-carboxyindole, B-22 N-5-hydroxypentyl and PB-22 N-pentanoic acid in authentic urine specimens obtained from four individuals by liquid chromatography–tandem mass spectrometry. Forensic Toxicol. 2017. doi:10.1007/s11419-017-0395-4.

54. Rydevik A, Thevis M, Krug O, Bondesson U, Hedeland M. The fungus Cunninghamella elegans can produce human and equine metabolites of selective androgen receptor modulators (SARMs). Xenobiotica. 2013;43(5):409-20. doi:10.3109/00498254.2012.729102.

55. Zafar S, Yousuf S, Kayani HA, Saifullah S, Khan S, Al-Majid AM, et al. Biotransformation of oral contraceptive ethynodiol diacetate with microbial and plant cell cultures. Chem Cent J. 2012;6(1):109. doi:10.1186/1752-153x-6-109.

3.8 Appendices

Supplementary Table 3-1. 5F-PB-22 metabolites with retention time, elemental composition, exact mass, accurate mass, mass error and diagnostic product ions.

ID	Metabolites	RT (min)	Elemental composition [M+H]	Exact mass	Accurate mass	Mass error (ppm)	Diagnostic product ions
F1	Oxidative defluorination + dihydrodiol formation	6.4	C23H25N2O5	409.1758	409.1761	0.76	230
F2	5F-PI-COOH + glucosidation	6.6	C20H27FNO7	412.1766	412.1772	1.39	118, 132, 144, 206, 232, 250
F3	Dihydrodiol formation + hydroxylation	6.7	C23H24FN2O5	427.1664	427.1665	0.35	248
F4	5F-PI-COOH + hydroxylation	7.4	C14H17FNO3	266.1187	266.1191	1.12	134, 148, 174, 222, 248
F5	Oxidative defluorination to carboxylic acid + hydroxylation	7.7	C23H21N2O5	405.1445	405.1448	0.71	144, 244
F6	Oxidative defluorination to carboxylic acid + hydroxylation	7.9	C23H21N2O5	405.1445	405.1447	0.53	160, 260
F7	Dihydroxylation	7.9	C23H22FN2O4	409.1558	409.1560	0.52	144, 248
F8	Dihydroxylation	8.2	C23H22FN2O4	409.1558	409.1557	-0.36	144, 158, 248
F9	Dihydroxylation	8.7	C23H22FN2O4	409.1558	409.1561	0.77	264
F10	Dihydrodiol formation	9.4	C23H24FN2O4	411.1715	411.1715	0.09	144, 232
F11	Oxidative defluorination to carboxylic acid + hydroxylation	9.6	C23H21N2O5	405.1445	405.1449	0.91	144, 244
F12	5F-PI-COOH	10.7	C14H17FNO2	250.1238	250.1240	0.73	118, 132, 144, 206, 232
F13	Oxidative defluorination to carboxylic acid	11.1	C23H21N2O4	389.1496	389.1498	0.54	144, 244
F14	Hydroxylation	11.6	C23H22FN2O3	393.1609	393.1612	0.75	144, 248
F15	Hydroxylation	12.1	C23H22FN2O3	393.1609	393.1612	0.72	144, 158, 248
F16	Hydroxylation	12.6	C23H22FN2O3	393.1609	393.1610	0.32	144, 248
Parent	5F-PB-22	17.6	C23H22FN2O2	377.1660	377.1664	1.17	144, 232

Supplementary Table 3-2. PB-22 metabolites with retention time, elemental composition, exact mass, accurate mass, mass error and diagnostic product ions.

ID	Metabolites	RT (min)	Elemental composition [M+H]	Exact mass	Accurate mass	Mass error (ppm)	Diagnostic product ions
P1	Ketone formation + hydroxylation + glucosidation	6.2	C29H31N2O9	551.2024	551.2028	0.69	160, 244
P2	Trihydroxylation	6.4	C23H23N2O5	407.1601	407.1599	-0.56	144, 246
P3	Dihydrodiol formation + hydroxylation	6.5	C23H25N2O5	409.1758	409.1763	1.13	144, 230
P4	Ketone formation + dihydroxylation	6.5	C23H21N2O5	405.1445	405.1449	0.97	160, 244
P5	Ketone formation + dihydroxylation	6.9	C23H21N2O5	405.1445	405.1449	1.08	144, 244
P6	PI-COOH + hydroxylation	6.9	C14H18NO3	248.1281	248.1284	1.26	130, 144, 158, 174, 230
P7	Dihydrodiol formation + hydroxylation	7.0	C23H25N2O5	409.1758	409.1748	-2.51	144, 158 (230 is missing in QTOF but present in QqQ)
P8	Dihydrodiol formation + ketone formation	7.0	C23H23N2O5	407.1601	407.1603	0.36	144, 228
P9	Ketone formation + dihydroxylation	7.4	C23H21N2O5	405.1445	405.1448	0.62	244 (144 is missing in QTOF but present in QqQ)
P10	PI-COOH + glucosidation	7.5	C14H18NO2	394.1860	394.1858	-0.55	118, 130, 132, 144, 158, 186, 214, 232
P11	PI-COOH + hydroxylation	7.6	C14H18NO3	248.1281	248.1283	0.92	130, 174, 230
P12	Carboxylation + hydroxylation	7.7	C23H21N2O5	405.1445	405.1443	-0.51	144, 244
P13	Dihydroxylation	7.8	C23H23N2O4	391.1652	391.1654	0.41	144, 230
P14	Dihydrodiol formation + ketone formation	7.8	C23H23N2O5	407.1601	407.1604	0.58	144, 228
P15	Dihydroxylation	8.0	C23H23N2O4	391.1652	391.1655	0.58	144, 246
P16	Dihydroxylation	8.5	C23H23N2O4	391.1652	391.1653	0.27	144, 246
P17	Ketone formation + hydroxylation	8.5	C23H21N2O4	389.1496	389.1500	1.1	144, 228
P18	Ketone formation + dihydroxylation	8.6	C23H21N2O5	405.1445	405.1444	-0.17	260 (144 is missing in QTOF but present in QqQ)
P19	Dihydroxylation	8.7	C23H23N2O4	391.1652	391.1654	0.41	144, 246
P20	Ketone formation + hydroxylation	8.9	C23H21N2O4	389.1496	389.1498	0.55	144, 228
P21	Ketone formation + hydroxylation	9.8	C23H21N2O4	389.1496	389.1498	0.56	144, 244

ID	Metabolites	RT (min)	Elemental composition [M+H]	Exact mass	Accurate mass	Mass error (ppm)	Diagnostic product ions
P22	Ketone formation + hydroxylation	10.1	C23H21N2O4	389.1496	389.1493	-0.78	144, 228
P23	Ketone formation + hydroxylation	10.8	C23H21N2O4	389.1496	389.1494	-0.35	144, 244
P24	Carboxylation	11.1	C23H21N2O4	389.1496	389.1493	-0.84	144, 244
P25	Ketone formation + hydroxylation	11.3	C23H21N2O4	389.1496	389.1500	1.1	144, 228
P26	Hydroxylation	11.5	C23H23N2O3	375.1703	375.1706	0.66	144, 230
P27	Dihydrodiol formation	12.0	C23H25N2O4	393.1809	393.1812	0.72	144, 214
P28	Hydroxylation	13.2	C23H23N2O3	375.1703	375.1695	-2.06	130, 144, 158, 230
P29	Ketone formation	13.4	C23H21N2O3	373.1547	373.1547	0.11	144, 228
P30	Ketone formation	15.1	C23H21N2O3	373.1547	373.1547	0.06	144, 228
Parent	PB-22	21.7	C23H23N2O2	359.1754	359.1757	0.85	144, 214

Supplementary Table 3-3. XLR-11 metabolites with retention time, elemental composition, exact mass, accurate mass, mass error and diagnostic product ions.

ID	Metabolites	RT (min)	Elemental composition [M+H]	Exact mass	Accurate mass	Mass error (ppm)	Diagnostic product ions
X1	Oxidative defluorination to carboxylic acid + hydroxylation	7.5	C21H28NO4	358.2013	358.2012	-0.27	144, 244
X2	Oxidative defluorination + hydroxylation	7.7	C21H30NO3	344.2220	344.2203	-5.1	144, 230
X3	Dihydroxylation	7.8	C21H29FNO3	362.2126	362.2121	-1.49	144, 248
X4	Oxidative defluorination to carboxylic acid + hydroxylation	7.8	C21H28NO4	358.2013	358.2011	-0.38	144, 244
X5	Oxidative defluorination to carboxylic acid + carboxylation	7.9	C21H26NO5	372.1805	372.1807	0.35	144, 244, 354
X6	Dihydroxylation	8.0	C21H29FNO3	362.2126	362.2126	-0.13	144, 232
X7	Oxidative defluorination + hydroxylation	8.1	C21H30NO3	344.2220	344.2207	-3.79	144, 230
X8	Oxidative defluorination + carboxylation	8.1	C21H28NO4	358.2013	358.2008	-1.3	144, 230
X9	Dihydroxylation	8.1	C21H29FNO3	362.2126	362.2122	-1.22	144, 248
X10	Carboxylation + hydroxylation	8.4	C21H27FNO4	376.1919	376.1915	-1.01	130, 144, 248, 358
X11	Dihydroxylation	8.4	C21H29FNO3	362.2126	362.2123	-0.83	144, 248
X12	Dihydroxylation	8.5	C21H29FNO3	362.2126	362.2125	-0.19	144, 232
X13	Dihydroxylation	8.8	C21H29FNO3	362.2126	362.2124	-0.49	144, 232
X14	Carboxylation + glucosidation (in-source fragmentation)	8.9	C21H27FNO3	360.1969	360.1966	-0.99	144, 232, 342
X15	Oxidative defluorination to carboxylic acid + aldehyde formation	9.0	C21H26NO4	356.1856	356.1854	-0.7	144, 244
X16	Oxidative defluorination + aldehyde formation	9.4	C21H28NO3	342.2064	342.2061	-0.67	144, 230
X17	Oxidative defluorination to carboxylic acid + aldehyde formation	9.6	C21H26NO4	356.1856	356.1851	-1.55	144, 244
X18	Carboxylation + glucosidation (in-source fragmentation)	9.8	C21H27FNO3	360.1969	360.1965	-1.25	144, 232, 342
X19	Dihydroxylation	10.7	C21H29FNO3	362.2126	362.2124	-0.48	144, 232
X20	Dihydroxylation	11.0	C21H29FNO3	362.2126	362.2122	-0.98	144, 232

ID	Metabolites	RT (min)	Elemental composition [M+H]	Exact mass	Accurate mass	Mass error (ppm)	Diagnostic product ions
X21	Hydroxylation	11.6	C21H29FNO2	346.2177	346.2176	-0.28	144, 232
X22	Carboxylation	12.3	C21H27FNO3	360.1969	360.1967	-0.6	144, 232, 342
X23	Hydroxylation	12.8	C21H29FNO2	346.2177	346.2173	-1.01	144, 232
X24	Oxidative defluorination to carboxylic acid	13.3	C21H28NO3	342.2064	342.2059	-1.29	125, 144, 244
X25	Oxidative defluorination	14.2	C21H30NO2	328.2271	328.2265	-1.89	125, 144, 230
X26	Aldehyde formation	14.6	C21H27FNO2	344.2020	344.2017	-0.86	144, 232
Parent	XLR-11	20.9	C21H29FNO	330.2228	330.2223	-1.27	125, 144, 232

Supplementary Table 3-4. UR-144 metabolites with retention time, elemental composition, exact mass, accurate mass, mass error and diagnostic product ions.

ID	Metabolite	RT (min)	Elemental composition [M+H]	Exact mass	Accurate mass	Mass error (ppm)	Diagnostic product ions
U1	Trihydroxylation	6.2	C21H30NO4	360.2169	360.2165	-1.11	144, 230
U2	Trihydroxylation	6.5	C21H30NO4	360.2169	360.2166	-0.82	144, 230
U3	Trihydroxylation	7.3	C21H30NO4	360.2169	360.2165	-1.27	144, 230
U4	N-dealkylation + hydroxylation	7.5	C16H20NO2	258.1489	258.1487	-0.68	116, 144
U5	Trihydroxylation	7.6	C21H30NO4	360.2169	360.2163	-1.73	144, 230
U6	Carboxylation + hydroxylation	7.6	C21H28NO4	358.2013	358.2009	-1.15	144, 244
U7	Dihydroxylation	7.8	C21H30NO3	344.2220	344.2215	-1.6	144, 230
U8	Carboxylation + hydroxylation	7.9	C21H28NO4	358.2013	358.2009	-1.16	144, 244
U9	N-dealkylation + hydroxylation	7.9	C16H20NO2	258.1489	258.1490	0.43	116, 144
U10	Carboxylation + hydroxylation	8.2	C21H28NO4	358.2013	358.2007	-1.76	144, 230, 340
U11	Dihydroxylation	8.3	C21H30NO3	344.2220	344.2216	-1.25	144, 230
U12	Carboxylation + hydroxylation	8.5	C21H28NO4	358.2013	358.2014	0.28	144, 230, 340
U13	Dihydroxylation	8.6	C21H30NO3	344.2220	344.2218	-0.51	144, 230
U14	Ketone formation + hydroxylation	8.8	C21H28NO3	342.2064	342.2061	-0.78	144, 228
U15	Carboxylation + hydroxylation	9.2	C21H28NO4	358.2013	358.2007	-1.56	130, 144, 158, 230, 340
U16	Dihydroxylation	9.2	C21H30NO3	344.2220	344.2217	-0.95	144, 230
U17	Ketone formation + carboxylation	9.3	C21H26NO4	356.1856	356.1855	-0.24	144, 228, 338
U18	Ketone formation + hydroxylation	9.5	C21H28NO3	342.2064	342.2061	-0.76	144, 228
U19	Aldehyde formation + hydroxylation	9.6	C21H28NO3	342.2064	342.2059	-1.25	144, 230
U20	Ketone formation + carboxylation	10.3	C21H26NO4	356.1856	356.1854	-0.61	130, 144, 228, 338
U21	Aldehyde formation + ketone formation	11.1	C21H26NO3	340.1907	340.1910	0.82	144, 228
U22	Hydroxylation	14.4	C21H30NO2	328.2271	328.2264	-2.04	125, 144, 230
U23	Hydroxylation	14.7	C21H30NO2	328.2271	328.2268	-0.79	125, 144, 230
U24	Hydroxylation	15.3	C21H30NO2	328.2271	328.2268	-1.02	144, 214

ID	Metabolite	RT (min)	Elemental composition [M+H]	Exact mass	Accurate mass	Mass error (ppm)	Diagnostic product ions
U25	Hydroxylation	17.4	C21H30NO2	328.2271	328.2266	-1.5	144, 214
Parent	UR-144	26.1	C21H30NO	312.2322	312.2320	-0.72	125, 144, 214

Chapter 4: Structural elucidation of metabolites of synthetic cannabinoid UR-144 by *Cunninghamella elegans* using nuclear magnetic resonance spectroscopy

Chapter 4: Structural elucidation of metabolites of synthetic cannabinoid UR-144 by *Cunninghamella elegans* using nuclear magnetic resonance spectroscopy

4.1 Abstract

The number of new psychoactive substances keeps on rising despite the controlling efforts by law enforcement. Although metabolism of the newly emerging drugs are continuously studied to keep up with the new additions, the exact structures of the metabolites are often not identified due to the insufficient sample quantities for techniques such as nuclear magnetic resonance (NMR) spectroscopy. The aim of the study was to characterise several metabolites of the synthetic cannabinoid (1-pentyl-1H-indol-3-yl)(2,2,3,3-tetramethylcyclopropyl)methanone (UR-144) by NMR spectroscopy after the incubation with the fungus *Cunninghamella elegans*. UR-144 was incubated with *C. elegans* for 72 hours and the resulting metabolites were chromatographically separated. Six fractions were collected and analysed by NMR spectroscopy. UR-144 was also incubated with human liver microsomes (HLM) and the liquid chromatography – high resolution mass spectrometry analysis was performed on the HLM metabolites with the characterised fungal metabolites as reference standards. Ten metabolites were characterised by NMR analysis including dihydroxy metabolites, carboxy and hydroxy metabolites, a hydroxy and ketone metabolite, and a carboxy and ketone metabolite. Of these metabolites, dihydroxy metabolite, carboxy and hydroxy metabolites, and a hydroxy and ketone metabolite were identified in HLM incubation. The results indicate that the fungus is capable of producing human-relevant metabolites including the exact isomers. The capacity of the fungus *C. elegans* to allow for NMR structural characterisation by enabling production of large amounts of metabolites makes it an ideal model to complement metabolism studies.

Keywords: Synthetic cannabinoid, Metabolism, *Cunninghamella elegans*, UR-144, NMR

Abbreviations

C. elegans	*Cunninghamella elegans*
ESI	Electrospray ionisation
gCOSY	Gradient correlation spectroscopy
gHMBC	Gradient heteronuclear multiple bond correlation
gHSQC	Gradient heteronuclear single quantum correlation
HLM	Human liver microsomes
HPLC	High performance liquid chromatography
LC-QTOF-MS	Liquid chromatography-quadrupole time-of-flight mass spectrometry
MS	Mass spectrometry
NOESY	Nuclear overhauser effect spectroscopy
NMR	Nuclear magnetic resonance
NPS	New psychoactive substances
TMCP	Tetramethylcyclopropyl
UR-144	(1-pentyl-1H-indol-3-yl)(2,2,3,3-tetramethylcyclopropyl)methanone

4.2 Introduction

The emergence of new psychoactive substances (NPS) has been a worldwide problem for the last decade. In 2016, the rate of the emergence of new drugs has slowed down according to the European Monitoring Centre for Drugs and Drug Addiction [1]. The reporting of 66 new drugs in Europe during the year was the fewest within the last five years. Nevertheless, the introduction of more than 1 drug per week still poses a significant challenge especially when more than 620 NPS have to be monitored.

In an effort to keep up with the detection of NPS in drug testing, a number of metabolite identification studies has been conducted [2-6]. This is particularly important for drugs that are extensively metabolised such as synthetic cannabinoids, as the parent drugs may not be present in urine, giving a false negative result [7]. Identification of metabolites can also contribute to the more comprehensive determination of the drug safety, since some metabolites can retain significant pharmacological activities, complicating the adverse effects of the drugs [8].

Several *in vivo* and *in vitro* models are commonly used to identify metabolic profiles. Among the *in vivo* models, controlled self-administration of drugs is a rare strategy due to the health risks and ethical concerns, although it naturally gives the most reliable data [9]. Other *in vivo* models involve the use of animals such as rats and mice. These models offer the advantage of metabolism occurring within whole animal organisms similar to the human body, although they can be expensive and ethically undesirable, in addition to species differences [6, 10]. The most common *in vitro* model is human liver microsomes (HLM), which are relatively cheap and relevant to human metabolism. However, the lack of some enzymes present in cells can limit the ability to produce relevant *in vivo* metabolites including phase II metabolites. Also, the typical reaction condition, which contains excessive oxygen, may limit reductive transformation pathways, even when HLM has the appropriate enzyme for the reaction [6]. In contrast, human primary hepatocytes generally provide metabolite profiles that resemble *in vivo* human profiles more closely, as they are living cells with a closer environment to the human body than enzymes [11].

Although the aforementioned models provide invaluable metabolic data, they have one common limitation: production of small amounts of metabolites. With the recent advances in sensitivity of mass spectrometric techniques, the amounts obtained with these models generally suffice for mass spectrometric analysis. However, mass spectrometric analysis alone is often not adequate for unequivocal structural elucidation including the exact positions of modifications made, leading to the need for analysis by other techniques such as nuclear magnetic resonance (NMR) spectroscopy [11]. Unfortunately, NMR spectroscopy is still a relatively insensitive technique, for which the amount of metabolites obtained from the common models is usually insufficient. Therefore, currently for the unambiguous characterisation of metabolites using these models, it is vital to use reference standards to compare the retention time and mass fragmentation pattern in mass spectrometry.

The fungus *Cunninghamella elegans* (*C. elegans*) has been investigated for its capability to mimic human metabolism for decades and is suggested to provide the solution for producing sufficient quantities of metabolites [10]. *C. elegans* can produce a wide variety of metabolites in a similar manner to humans and incubation of *C. elegans* culture can easily be upscaled, allowing large production of metabolites. The advantage of large quantities of metabolites obtained from *C. elegans* has been proven useful in studies reporting structural characterisation of metabolites using NMR spectroscopy [12, 13].

In this chapter, we report, for the first time using NMR spectroscopy, the structural elucidation of several metabolites of the synthetic cannabinoid (1-pentyl-1H-indol-3-yl)(2,2,3,3-tetramethylcyclopropyl)methanone (UR-144), which was among the five most commonly seized synthetic cannabinoids in Europe in 2015 [1]. The structures of UR-144 and the metabolites are shown in Figure 4-1. In chapter 3, we demonstrated, using liquid chromatography – high resolution mass spectrometry, that *C. elegans* incubation of synthetic cannabinoids including UR-144 can result in similar metabolic profiles to human metabolism [14, 15]. This chapter further establishes the strength of the fungus, which allows more comprehensive metabolite characterisation by NMR spectroscopy. UR-144 was also incubated with HLM and the characterised fungal metabolites were used as reference standards to determine whether these fungal metabolites are produced in HLM incubation.

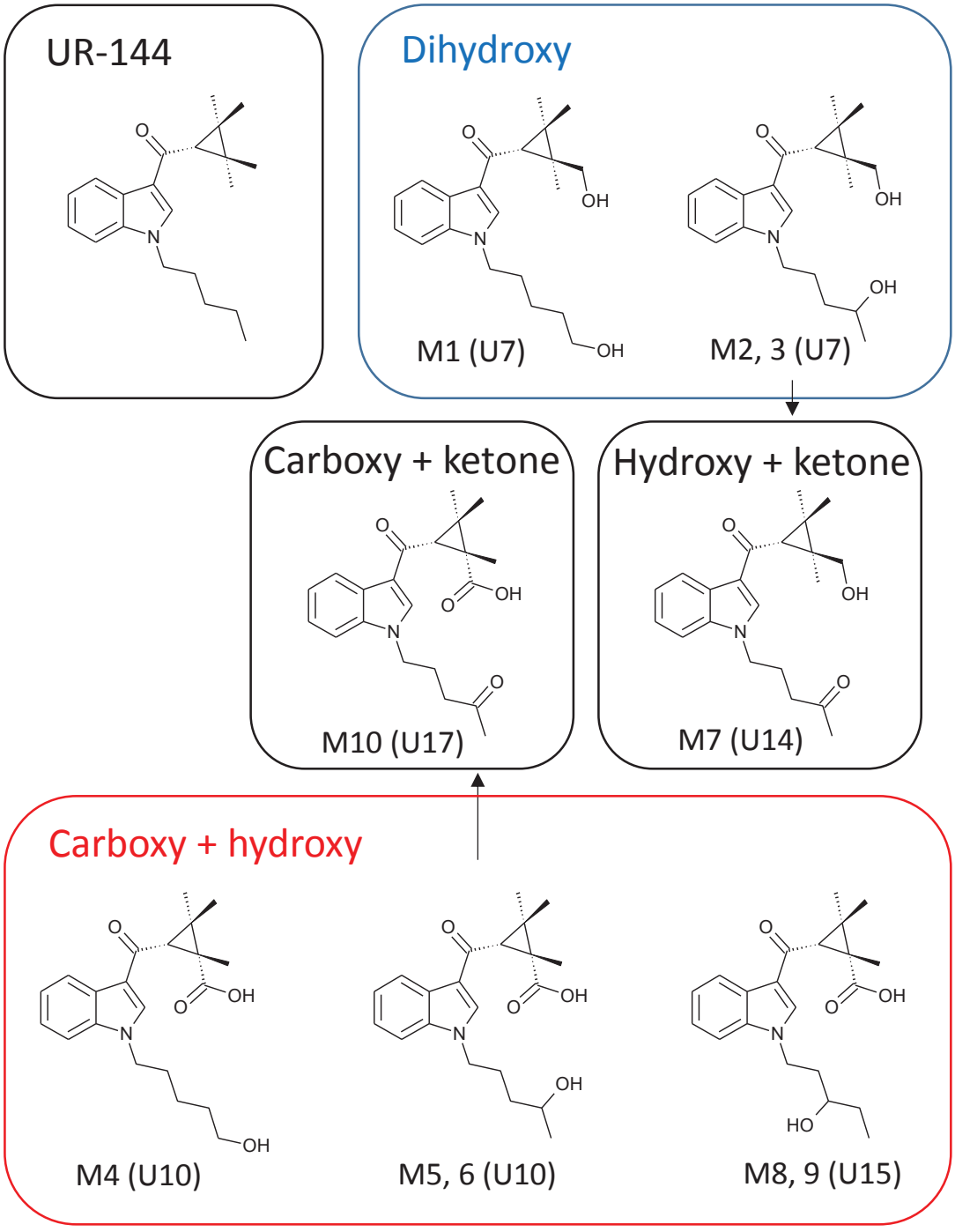

Figure 4-1. The structures of UR-144 and the metabolites analysed in this study. Brackets indicate the metabolite ID in chapter 3 [14]. Arrows indicate partial metabolic pathways. M2 and M3, M5 and M6, and M8 and M9 are diastereomers, respectively, and share the same structures apart from the spatial configurations at the stereo centres.

4.3 Materials and methods

4.3.1 Chemicals and reagents

UR-144 was synthesised in-house following previously reported methods and characterised by mass spectrometry (MS) and 1D, 2D NMR spectroscopy [16, 17]. LC-MS grade acetonitrile was obtained from Honeywell (Muskegon, MI, USA). Reagent grade dichloromethane and sodium chloride were from Chemsupply (Gilman, SA, Australia). LC-MS grade formic acid and deuterated chloroform (99.8 atom % D, containing 0.03 % (V/V) TMS) was purchased from Sigma–Aldrich (St. Louis, MO, USA). *C. elegans* ATCC 10028b was from Cryosite Ltd. (South Granville, NSW, Australia). Glycerol and potassium dihydrogen phosphate and dipotassium hydrogen phosphate were obtained from Ajax Chemicals (Auburn, NSW, Australia). Potato dextrose agar, glucose, peptone, and yeast extract were purchased from Oxoid Australia (Adelaide, SA, Australia). HLM 50-Doner pool, NADPH system solution A and NADPH system solution B were obtained from Corning (Corning, NY, USA).

4.3.2 Fungus metabolite characterisation

4.3.2.1 Fungus incubation

Incubation of UR-144 with *C. elegans* was performed as described in chapter 3 [14], with the following deviations. A total of 5 L growth media in multiple conical flasks were used to incubate 50 mg of UR-144. Following liquid-liquid extraction using dichloromethane, the combined extracts were evaporated to dryness and reconstituted in 14 mL of water:acetonitrile (55:45, v/v).

4.3.2.2 Preparative high performance liquid chromatography (HPLC)

HPLC system consisted of an Agilent 1290 LC system with an Agilent Zorbax Eclipse XDB-C18 semi-preparative column (250 mm × 9.4 mm, 5 μm) and an Agilent 1260 Infinity diode array detector. A hundred microliter of the sample was injected into HPLC to separate some UR-144 metabolites and six fractions were collected, after diode array

detection at 254 nm, to obtain purified metabolites. The mobile phase consisted of 0.1% formic acid in water (A) and 0.1% formic acid in acetonitrile (B) at a flow rate of 4.0 mL/min. A run was performed over 18 min in gradient mode with 45% B from 0 to 10 min, ramped to 95% B at 11 min and held till 14 min, and ramped back to 45% B at 15 min and held till 18 min. The column temperature was kept at 30°C. The procedure was repeated 100 times to obtain sufficient amount of metabolites for NMR analysis. The fractions were placed under a gentle stream of nitrogen gas to remove acetonitrile and then freeze-dried. The samples were redissolved in $CDCl_3$ and analysed by NMR.

4.3.2.3 NMR spectroscopy

NMR spectra were acquired at room temperature on an Agilent 500 MHz NMR spectrometer coupled with an Agilent 7510-AS automated NMR sample changer. UR-144 and its metabolites were characterised by ^{1}H NMR, ^{13}C NMR, gradient correlation spectroscopy (gCOSY), gradient heteronuclear single quantum correlation (gHSQC), gradient heteronuclear multiple bond correlation (gHMBC, jnxh = 8 Hz) and nuclear overhauser effect spectroscopy (NOESY) experiments. Acquisition was performed at the frequency of 499.86 MHz and 125.70 MHz for ^{1}H and ^{13}C NMR, respectively. Chemical shifts are reported in δ (ppm) and were measured relative to $CDCl_3$ (^{1}H δ = 7.26, ^{13}C δ = 77.0).

4.3.2.4 Liquid chromatography – quadrupole time-of-flight mass spectrometry (LC-QTOF-MS)

Each metabolite isolated by preparative HPLC was analysed by LC-QTOF-MS in the same manner as described in chapter 3 [14], to confirm the identity of the metabolites and compare with the results in the study.

4.3.3 HLM metabolite characterisation

4.3.3.1 HLM incubation

UR-144 solution in acetonitrile:water (40:60 v/v, 1 g/mL, 25 µL), phosphate buffer (0.1M, pH7.4, 855 µL), NADPH-A (50 µL) and NADPH-B (20 µL) were mixed in an Eppendorf tube, to which HLM (50 µL) was added. The final concentration of acetonitrile was 1%. The mixture was incubated at 37 °C in a shaking water bath for 3 h. Ice-cold acetonitrile (1 mL) was added to the mixture for quenching and the Eppendorf tube was centrifuged at 16,060 × g for 10 minutes. The supernatant was filtered with a 0.22 µm filter. Two microliter was injected into LC-QTOF-MS. A degradation control sample without HLM and a control without UR-144 were also incubated and analysed.

4.3.3.2 LC-QTOF-MS

LC-QTOF-MS experiments were performed as described above with the following exceptions. Some analyses were performed on an Agilent 6550A iFunnel Q-TOF with a Dual AJS ESI source in Auto MS/MS mode, operated with the same parameters as for the fungus analysis except for the following: gas temperature, 290 °C; gas flow, 11 L/min; sheath gas temperature, 350 °C; sheath gas flow, 11 L/min; max precursors per cycle, 5; static exclusion ranges, 100-300 and 500-1000.

4.4 Results

4.4.1 Fungus metabolite characterisation

After incubation of UR-144 with *C. elegans*, the metabolites were separated by HPLC. Based on the abundance and separation of the peaks, 6 fractions (labelled as fraction 1-fraction 6 below) containing one peak each were isolated and collected for further analysis, apart from fractions 2 and 3 where two peaks partially coeluted and could not be completely separated (Figure 4-2). LC-QTOF-MS analysis confirmed that fraction 1 contained a dihydroxy metabolite, labelled as U7 in chapter 3 [14]. Under the analytical conditions employed for LC- QTOF-MS analysis, the peaks in fractions 2 and 3 eluted as a single peak corresponding to a metabolite with carboxylation and hydroxylation (U10). Fraction 4 was a metabolite with hydroxylation and ketone formation (U14). Fraction 5 corresponded to U15, another metabolite with carboxylation and hydroxylation. Fraction 6 was a metabolite with carboxylation and ketone formation (U17).

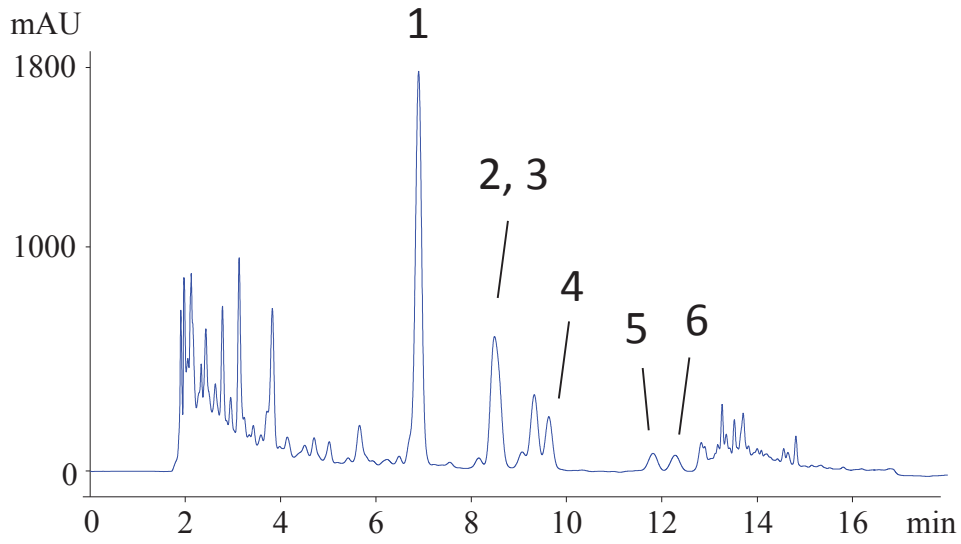

Figure 4-2. Preparative HPLC chromatogram showing separation of fractions 1-6. Fraction 2 and 3 partially coeluted.

4.4.1.1 NMR analysis

In total, 10 metabolites were characterised by NMR from 6 fractions as shown in Figure 4-1 (fraction 1 contained M1-3 (U7); fraction 2, M4 (U10); fraction 3, M5, 6 (U10); fraction 4, M7 (U14); fraction 5, M8, 9 (U15); fraction 6, M10 (U17)). The assigned ^{1}H and ^{13}C NMR data of UR-144 and the metabolites are presented in Tables 4-1—4-3. The gCOSY and gHMBC correlations, and selected NOE correlations are depicted in Figure 4-3 and were used to aid assignment of some overlapped ^{1}H and ^{13}C NMR signals in Tables 4-1—4-3.

4.4.2 HLM metabolite characterisation

Based on the comparison of retention time and fragmentation pattern in MS/MS scan with the fungal metabolites, dihydroxy metabolite (U7), carboxy and hydroxy metabolites (U10 and U15) and hydroxy and ketone metabolite (U14) were identified after HLM incubation.

Table 4-1. ^{1}H and ^{13}C NMR data for UR-144 and fraction 1 containing dihydroxy metabolites (M1-3) in $CDCl_3$.

Position No.	UR-144		Fraction 1			
			M1	M2/3	M1	M2/3
	^{13}C	^{1}H	^{13}C		^{1}H	
1	194.6		193.4			
2'	133.4	7.66 (s)	134.0	134.1, 134.4	7.83 (s)	7.87 (s), 7.88 (s)
3'	119.6		119.1, 119.2			
3'a	126.4		126.38, 126.42			
4'	122.7	8.39-8.41 (m)	122.7		8.38-8.40 (m)	
5'	122.0	7.23-7.29 (m), overlapped	122.26, 122.28		7.24-7.30 (m), overlapped	
6'	122.8	7.23-7.29 (m), overlapped	123.0, 123.1		7.24-7.30 (m), overlapped	
7'	109.6	7.33-7.35 (m)	109.60, 109.63		7.33-7.37 (m)	
7'a	136.6		136.6			
1"	47.0	4.14 (t, J = 7.3 Hz)	46.9	46.8	4.20 (t, J = 7.0 Hz)	4.20 (t, J = 7.0 Hz)
2"	29.6	1.89 (quintet, J= 7.5 Hz))	29.5	26.1, 26.2	1.93[a], overlapped	1.90-2.10 (m)
3"	29.0	1.36[a], overlapped	23.2	35.9, 36.0	1.44[a], overlapped	1.49 (quintet, J = 7.3 Hz)
4"	22.2	1.36[a], overlapped	31.9	67.6, 67.7	1.61[a], overlapped	3.84 (m), overlapped
5"	13.9	0.91 (t, J = 7.0 Hz)	62.5	23.8, 23.9	3.65 (td, J = 6.3, 4.3 Hz)	1.20 (d, 6.0 Hz)
1"'	41.6	1.94 (s)	38.76, 38.77		2.120 (s), 2.124 (s), 2.13 (s)	
2"'	31.5		36.0, 36.1			
3"'	31.5		30.0, 30.1, 30.2			
(*E*)-2"'-Me	24.0	1.31 (s)	69.3, 69.4, 69.5		3.766 (dd, J = 36.3, 11.3 Hz)	3.765 (dd, J = 19.5, 11.5 Hz), 3.769 (dd, J = 28.8, 11.3 Hz)
(*Z*)-2"'-Me	17.0	1.35 (s)	12.4, 12.5		1.40 (s), 1.42 (s), 1.43 (s)	
(*E*)-3"'-Me	24.0	1.31 (s)	17.52, 17.55, 17.57, or 23.5[b]		1.36 (s), 1.37 (s), 1.378 (s), 1.380 (s), 1.384 (s), 1.39 (s), overlapped	
(*Z*)-3"'-Me	17.0	1.35 (s)	17.52, 17.55, 17.57, or 23.5[b]		1.36 (s), 1.37 (s), 1.378 (s), 1.380 (s), 1.384 (s), 1.39 (s), overlapped	

[a] The chemical shifts were taken from HSQC data

[b] Based on the data, it could not be determined which chemical shifts correspond to (*E*)- and (*Z*)-methyl carbons

Table 4-2. ^{1}H and ^{13}C NMR data for carboxy and hydroxy metabolites (M4-6 and M8-9) in $CDCl_3$.

Position No.	M4		M5/6		M8/9	
	^{13}C	^{1}H	^{13}C	^{1}H	^{13}C	^{1}H
1	196.4		196.4		ND	
2'	136.2	7.80 (s)	136.3	7.82 (s), 7.83 (s)	136.8	7.85 (s), 7.88 (s)
3'	117.2		117.1[b]		117.2[b]	
3'a	126.1		126.1		126.1[b]	
4'	122.7	8.32-8.34 (m)	122.7	8.32-8.34 (m)	122.7	8.32-8.34 (m)
5'	123.7	7.35-7.38 (m), overlapped	123.7	7.35-7.38 (m), overlapped	123.7	7.35-7.38 (m), overlapped
6'	124.1	7.35-7.38 (m), overlapped	124.1	7.35-7.38 (m), overlapped	124.1	7.35-7.38 (m), overlapped
7'	110.2	7.40-7.44 (m)	110.3	7.40-7.44 (m)	110.3	7.45-7.47 (m)
7'a	136.9		136.9		136.9[b]	
1"	47.5	4.24 (td, J = 7.1, 3.8 Hz)	47.5	4.28 (t, J =7.3)	44.3	4.42 (t, J = 8.3 Hz)
2"	29.6	1.98 (quintet, 7.5 Hz)	26.2, 26.3	1.96-2.14 (m)	36.2	1.86-1.94 (m), 2.06-2.14 (m)
3"	23.2	1.48[a], overlapped	35.69, 35.72	1.51[a], overlapped	70.0	3.46-3.52 (m)
4"	31.9	1.63[a], overlapped	67.5, 67.6	3.85-3.90 (m)	30.8	1.52[a], overlapped
5"	62.3	3.67 (t, 6.3 Hz)	24.0, 24.1	1.22 (d, J = 6 Hz)	9.7	0.94 (t, J = 7.5 Hz)
1'"	44.0	2.38 (s)	44.0	2.38 (s)	44.0	2.38 (s)
2'"	40.4		40.4		40.4[b]	
3'"	33.2		33.2		33.2[b]	
(*E*)-2'"-Me	21.1	1.56 (s)	21.1	1.56 (s)	21.1	1.56[a], overlapped
(*Z*)-2'"-Me	173.6		173.6		173.6[b]	
(*E*)-3'"-Me	22.3	1.50 (s)	22.26, 22.29	1.50 (s)	22.3	1.49 (s)
(*Z*)-3'"-Me	17.6	1.26 (s)	17.61, 17.62	1.26 (s)	17.6	1.26 (s)

ND Not detected

[a] The chemical shifts were taken from HSQC data

[b] The chemical shifts were taken from HMBC data

Table 4-3. ^{1}H and ^{13}C NMR data for a hydroxy and ketone metabolite (M7) and a carboxy and ketone metabolite (M10) in $CDCl_3$.

Position No.	M7		M10	
	^{13}C	^{1}H	^{13}C	^{1}H
1	193.4		ND	
2'	133.9	7.78 (s)	136.2	7.79 (s)
3'	119.4		117.4[b]	
3'a	126.3		126.0	
4'	122.8	8.38-8.40 (m)	122.7	8.32-8.34 (m)
5'	122.4	7.26-7.30 (m), overlapped	123.7	7.35-7.39 (m), overlapped
6'	123.2	7.26-7.30 (m), overlapped	124.3	7.35-7.39 (m), overlapped
7'	109.6	7.35-7.37 (m)	110.3	7.44-7.47 (m)
7'a	136.6		136.9[b]	
1"	45.7	4.21 (t, J =7.3 Hz)	46.3	4.27 (t, J = 7.3 Hz)
2"	23.8	2.17 (quintet, J = 6.9 Hz)	23.8	2.19 (quintet, J = 6.9 Hz)
3"	39.6	2.43 (t, J = 6.8 Hz)	39.4	2.49 (td, J = 6.4, 2.8 Hz)
4"	207.5		207.2	
5"	30.0	2.11 (s), overlapped	30.1	2.15 (s)
1"'	38.8	2.11 (s), overlapped	44.0	2.37 (s)
2"'	36.3		40.5[b]	
3"'	30.4		33.4	
(*E*)-2"'-Me	69.5	3.77 (dd, J = 38.0, 11.0 Hz)	21.1	1.57[c], overlapped
(*Z*)-2"'-Me	12.4	1.44 (s)	173.5[b]	
(*E*)-3"'-Me	17.5 or	1.38 (s), overlapped	22.3	1.50 (s)
(*Z*)-3"'-Me	23.5[a]	1.38 (s), overlapped	17.6	1.26 (s)

ND Not detected

[a] Based on the data, it could not be determined which chemical shifts correspond to (*E*)- and (*Z*)-methyl carbons

[b] The chemical shifts were taken from HMBC data

[c] The chemical shifts were taken from HSQC data

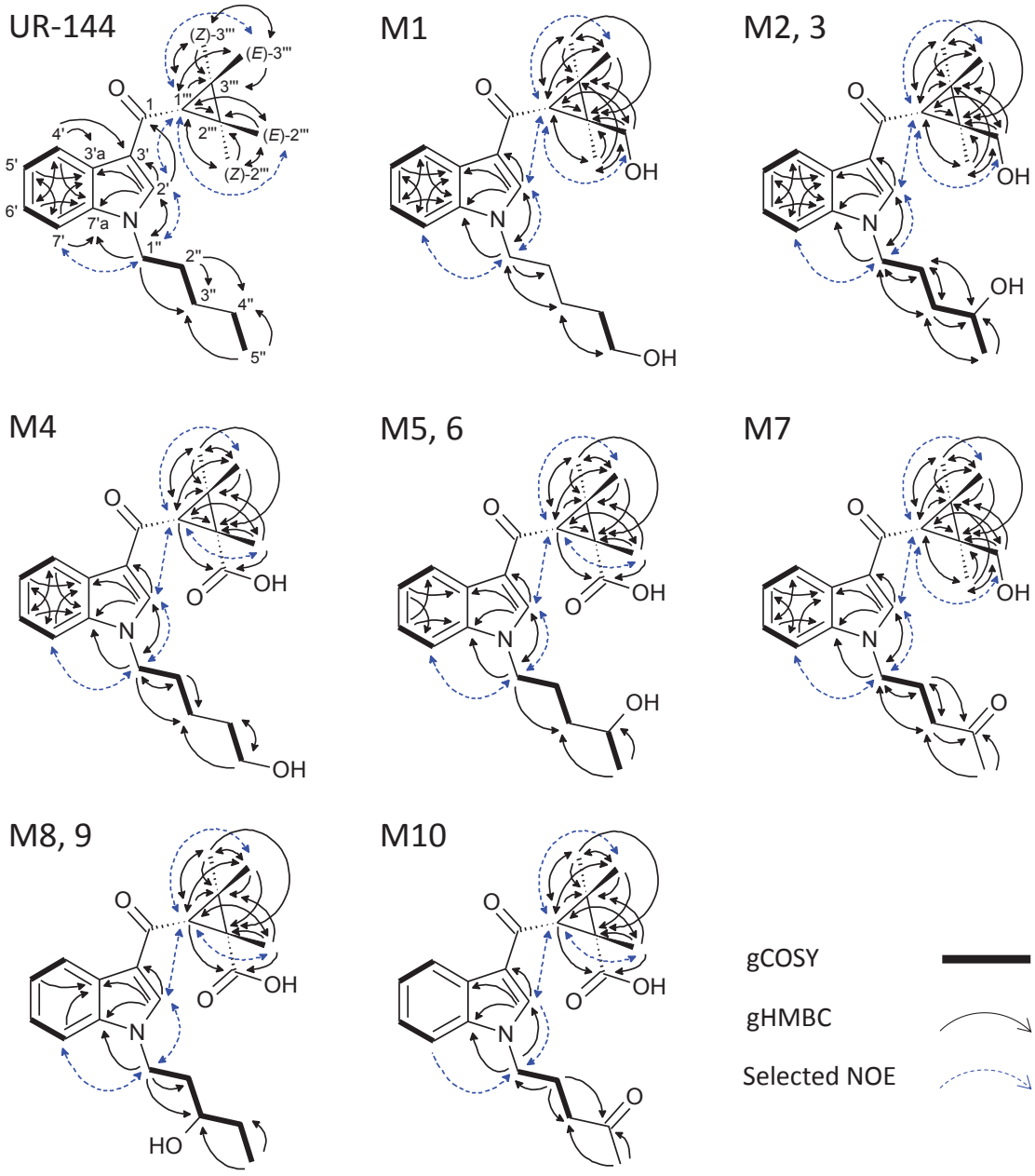

Figure 4-3. Gradient correlation spectroscopy (gCOSY), gradient heteronuclear multiple bond correlation (gHMBC) and selected nuclear overhauser effect (NOE) correlations of UR-144 and the metabolites analysed in the study.

4.5 Discussion

4.5.1 Fungus metabolite characterisation

According to the LC-QTOF-MS analysis in MS/MS mode, each fraction contained one metabolite each: a dihydroxy metabolite (U7) in fraction 1, carboxylation and hydroxylation metabolites (U10) in fraction 2 and 3 and (U15) in fraction 5, a hydroxylation and ketone formation metabolite (U14) in fraction 4, a carboxylation and ketone formation metabolite (U17) in fraction 6. To determine the exact positions of the modifications in these metabolites, 1D and 2D NMR data was obtained including ^{1}H, ^{13}C, gCOSY, gHSQC, gHMBC and NOESY spectra.

4.5.1.1 NMR analysis

4.5.1.1.1 UR-144

First, the parent drug UR-144 was analysed (Table 4-1). NMR data of UR-144 have been previously reported with some discrepancies in signal assignments among the studies [18-20]. Our results agree well with the assignments given by Langer *et al*. [18]. After the analysis of UR-144, each fraction containing metabolites was analysed. Since all the metabolites were determined to have the intact indole moiety based on LC-QTOF-MS, the signals related to the indole moiety are generally not discussed below.

4.5.1.1.2 Dihydroxy metabolites M1-3 (U7)

LC-QTOF-MS analysis of fraction 1 (U7) tentatively assigned the single peak (RT = 6.9 min, Fig. 4-2) as a dihydroxy metabolite, with one hydroxy group located at the tetramethylcyclopropyl (TMCP) ring and the other one at the pentyl side chain, as reported in the previous study [14]. NMR study has shown that this fraction in fact contained 3 isomers designated as M1, M2 and M3, respectively (Table 4-1). The NMR data shows that hydroxylation at the TMCP ring occurred at one of the four methyl groups instead of the C-1''' adjacent to the carbonyl group. This assignment was based on two observations. Firstly, the C-1''' was found to retain its hydrogen resonating around δ 2.12

ppm. Secondly, the appearance of the signals at δ 3.77 ppm as a doublet of doublets was attributable to the diastereotopic methylene protons following hydroxylation at one of the four methyl groups (2'''-Me, or 3'''-Me); the strong shift of the signal from around δ 1.30 ppm to the low magnetic field by approximately δ 2.45 ppm is in line with the electron withdrawing effect of the added hydroxyl group. NOESY cross peaks at δ 2.12-2.13 (H-1''')/δ 3.77 (HO-CH_2-(*E*)-2''') and δ 2.12-2.13 (H-1''')/δ 1.36-1.39 (CH_3-(*E*)-3''') suggests that the metabolites are *E*-isomers in that the hydroxy group is in an orientation *trans* to the adjacent carbonyl group (Fig. 4-3**,** M1-M3). Based on the results, the hydroxy group can be either at (*E*)-2'''-Me or (*E*)-3'''-Me. For simplicity, the hydroxy group is shown at (*E*)-2'''-Me only, as the ring structure is otherwise symmetrical. Similarly, hydroxylation and carboxylation for the subsequent metabolites will also be shown at 2'''-Me only rather than 2'''-Me and 3'''-Me.

In contrast to the TMCP ring, hydroxylation at the pentyl side chain occurred at two different positions. COSY and HMBC correlations showed two spin systems for the side chain as shown in Fig. 4-3 (M1-3). One of them is a 5-hydroxypentyl metabolite (M1), which is supported by C-5'' having two hydrogens instead of three as indicated by an HSQC cross peak (data not shown). The other one is a 4-hydroxypentyl metabolite, which is supported by H-5'' being a doublet. While 5-hydroxypentyl chain is achiral, 4-hydroxypentyl chain has a chiral centre. Therefore, 4-hydroxypentyl chain can exist as enantiomers with C-4'' having (*R*) or (*S*) configuration. In addition, the hydroxylated TMCP ring determined above also has a chiral carbon at (*E*)-2''' when (*E*)-2'''-Me is hydroxylated, i.e. (*S*)-isomer, whereas the metabolite with a hydroxy group at (*E*)-3'''-Me has the (*R*) configuration. Hence, there can be four stereoisomers for the dihydroxy metabolites containing 4-hydroxypentyl chain and a hydroxy group at (*E*)-2'''-Me or (*E*)-3'''-Me. Of the four stereoisomers, (4''*R*, 3'''*R*) and (4''*S*, 2'''*S*) are enantiomers as well as (4''*R*, 2'''*S*) and (4''*S*, 3'''*R*). Since enantiomers are not differentiated by NMR spectra, only the two diastereomers should appear in the spectra as observed in the study (M2 and M3). All three metabolites are similar in structure and account for the coelution in LC separation.

4.5.1.1.3 Hydroxy and ketone metabolite M7 (U14)

Fraction 4 (M7) showed proton and carbon signals almost identical to M2 and M3 for the TMCP ring indicating hydroxylation at (*E*)-2'''-Me (Table 4-3). The distinct carbon signal at δ 207.5 ppm suggested the presence of a ketone group, which is consistent with the MS findings. The proton signals for the pentyl side chain showed one singlet, two triplets and one quintet. A singlet can occur only when C-2" or C-4" has a ketone group. If C-2" had a ketone group, H-1" would become a singlet. However, there was a triplet at δ 4.21ppm corresponding to H-1" as seen for UR-144 and the dihydroxy metabolites, which concludes the position of the ketone group to be at C-4" of the pentyl side chain. The cross peaks in COSY and HMBC also supported the location of the ketone group to be C-4" (Fig. 4-3). The metabolite M7 is an oxidised metabolite of M2 and/or M3 (Fig. 4-1).

4.5.1.1.4 Carboxy and hydroxy metabolites M4-6 (U10) and M8-9 (U15)

Since fractions 2 and 3 were collected from the coeluting peaks in preparative HPLC, these fractions were expected to contain a few metabolites originating from the two coeluting peaks. Indeed, they contained signals from both peaks, but the relative abundance of the signals made it clear enough for assigning which signals were from fraction 2 or fraction 3. As expected from MS analysis, fraction 2 (M4) showed a carbon signal at δ 173.6 ppm for carboxylic acid in the TMCP ring (Table 4-2). Based on the structure of the TMCP ring, the possible position for carboxylation is at one of the four methyl groups, i.e., 2'''-Me or 3'''-Me. NOESY cross peaks at δ 2.38 (H-1''')/δ 1.56 (CH_3-(*E*)-2''') and δ 2.38 (H-1''')/δ 1.50 (CH_3-(*E*)-3''') indicated that the carboxy group is *cis* to the carbonyl group (Fig. 4-3). The hydroxy group at the pentyl side chain was assigned at H-5" based on the COSY and HMBC data (Fig. 4-3). The proton and carbon data for the side chain was analogous to those of M1, as M1 is also hydroxylated at H-5".

Having coeluted with a peak in fraction 2, a peak in fraction 3 is expected to have structurally similar compounds. In fact, fraction 1 displayed a similar case where 5-hydroxypentyl metabolite with another hydroxy group at the TMCP ring coeluted with two diastereomers of 4-hydroxypentyl metabolites having another hydroxy group at the TMCP ring. As expected, fraction 3 showed the presence of 4-hydroxypentyl metabolite with a carboxy group at the TMCP ring (M5 and M6); the carboxy group was found *cis*

to the carbonyl group in the TMCP ring as indicated by NOSEY cross peaks at δ 2.38 (H-1''')/δ 1.56 (CH_3-(*E*)-2''') and δ 2.38 (H-1''')/δ 1.50 (CH_3-(*E*)-3''') and the hydroxy group was assigned to H-4'' by COSY and HMBC cross peaks (Fig. 4-3) and the proton and carbon data was similar to that of M2 and M3. As was the case with M2 and M3, M5 and M6 can have two diastereomers due to the presence of two stereo centres and hence H-2' and some carbon atoms showed two signals corresponding to the presence of diastereomers.

Fraction 5 (M8 and M9) showed the proton and carbon signals for the TMCP ring, almost identical to those of M4-6, indicating the carboxy group is *cis* to the carbonyl group (Table 4-2, Fig. 4-3). Now that M4, and M5 and M6 were characterised as 5-hydroxypentyl and 4-hydroxypentyl metabolites, respectively, the position of the hydroxy group in the pentyl side chain for this fraction can only be at H-1'', H-2'' or H-3''. Regardless of the exact position, the metabolite would have two stereo centres, leading to two diastereomers as described above. Indeed, H-2' showed two signals resulting from the diastereomers. The cross peaks in COSY and HMBC revealed the position of hydroxylation to be at H-3'', which is supported by the fact that the proton peak at δ 4.42 (H-1'') is a triplet, which would be a doublet for a 2-hydroxypentyl metabolite, and the peak has two protons according to the HSQC data and hence cannot be hydroxylated at H-1''.

4.5.1.1.5 Carboxy and ketone metabolite M10 (U17)

Fraction 6 (M10) showed similar proton, carbon and 2D NMR data to M4, M5, M6, M8 and M9 for the TMCP ring, indicating carboxylation at a methyl group *cis* to the carbonyl group (Table 4-3, Fig. 4-3). For the pentyl side chain, the ketone carbon signal at δ 207.2 ppm together with proton and carbon data similar to M7 allowed the position of ketone formation to be C-4''. This metabolite M10 is considered to be derived from further oxidation of M5 and/or M6 (Fig. 4-1). It is interesting to note that the chemical shift of carbon signals at C-4', C-5' and C-6' in the indole moiety were in the order of C-4' < C-5' < C-6' for M10 and all the other metabolites with a carboxy group at the TMCP ring, whereas it was in the order of C-5' < C-4' < C-6' for UR-144 and the other metabolites.

4.5.2 HLM metabolite characterisation

Using the isolated and characterised fungal metabolites as reference standards, dihydroxy metabolite (U7/M1-3), carboxy and hydroxy metabolites (U10/M4-6 and U15/M8-9) and hydroxy and ketone metabolite (U14/M7) were able to be identified in the HLM sample. Under the chromatographic conditions employed, 5-hydroxypentyl and 4-hydroxypentyl metabolites (M1-3 and M4-6) coeluted and hence there can be both or either of the metabolites. The presence of these metabolites was previously reported in human metabolism as well as the fungal metabolism: dihydroxy metabolites and hydroxy and ketone metabolites in human urine; dihydroxy metabolites and carboxy and hydroxy metabolites in HLM; all the metabolites in the fungus [14, 21-24]. However, it was not possible to determine if the human metabolites were the same as the exact isomers found in the fungus without analysing them by the same LC-MS system. Given that the exact isomers of the fungal metabolites were identified after HLM incubation, the fungal metabolites can be a powerful tool to characterise human metabolites.

4.5.3 Advantages and disadvantages of the fungus metabolism

The main advantage of the fungus *C. elegans* is that experiments can easily be upscaled, which would allow NMR analysis of metabolites. As mentioned before, the NMR analysis of metabolites is imperative for comprehensive characterisation of most metabolites without using reference standards. This proves even more important for the metabolites which are not commercially available. As of now, there are only 6 metabolites available for UR-144 from Cayman Chemical; *N*-pentanoic acid metabolite, *N*-(5-hydroxypentyl) metabolite, (±)-*N*-(4-hydroxypentyl) metabolite, *N*-(2-hydroxypentyl) metabolite, *N*-(5-hydroxypentyl) β-D-glucuronide, UR-144 degradant *N*-pentanoic acid metabolite [25]. Also, the present study has demonstrated that NMR analysis can detect two or more isomers, which cannot be differentiated by MS, in a reasonably symmetrical peak in a chromatogram. Therefore, to fully characterise other metabolites including M1-10, analysis by NMR spectroscopy is essential and this could be provided by a large-scale fungus experiment. The limitations of the large-scale fungus experiment include the difficulty in separating closely-structured isomers using preparative HPLC and the amounts of metabolites obtained are still generally less than those obtained by synthesis,

making the NMR interpretation more challenging. However, chromatographic separations may be significantly improved by the use of different HPLC columns such as chiral columns and a larger column will make it easier to obtain larger amounts of metabolites. Unlike organic synthesis, several metabolites can be obtained in one incubation, in which the fungus "synthesises" the metabolites for us, including the metabolites which are difficult to synthesise chemically [10]. Hence, the fungus *C. elegans* can be an invaluable model for studying drug metabolism.

4.6 Conclusion

The synthetic cannabinoid UR-144 was incubated with the fungus *C. elegans* in a large scale and several metabolites were isolated by preparative HPLC. Ten metabolites were characterised by NMR analysis, including dihydroxy metabolites, carboxy and hydroxy metabolites, a hydroxy and ketone metabolite, and a carboxy and ketone metabolite. UR-144 was also incubated with HLM and the characterised fungal metabolites were used as reference standards to determine if these metabolites were generated by HLM. LC-QTOF-MS analysis identified dihydroxy metabolite (U7), carboxy and hydroxy metabolites (U10 and U15) and hydroxy and ketone metabolite (U14) after HLM incubation. These findings demonstrate the ability of the fungus to produce human-relevant metabolites of the synthetic cannabinoid in sufficient abundance for NMR analysis, indicating the potential for the fungus model as a tool to complement metabolism studies.

4.7 References

1. European Monitoring Centre for Drugs and Drug Addiction. European Drug Report 2017: Trends and Developments. Luxembourg: Publications Office of the European Union 2017.

2. Carlier J, Diao X, Sempio C, Huestis MA. Identification of New Synthetic Cannabinoid ADB-CHMINACA (MAB-CHMINACA) Metabolites in Human Hepatocytes. AAPS Journal. 2017:1-10. doi:10.1208/s12248-016-0037-5.

3. Grafinger KE, Hädener M, König S, Weinmann W. Study of the in vitro and in vivo metabolism of the tryptamine 5-MeO-MiPT using human liver microsomes and real case samples. Drug Test Anal.in press. doi:10.1002/dta.2245.

4. Meyer MR. New psychoactive substances: an overview on recent publications on their toxicodynamics and toxicokinetics. Arch Toxicol. 2016;90(10):2421-44. doi:10.1007/s00204-016-1812-x.

5. Watanabe S, Vikingsson S, Roman M, Green H, Kronstrand R, Wohlfarth A. In Vitro and In Vivo Metabolite Identification Studies for the New Synthetic Opioids Acetylfentanyl, Acrylfentanyl, Furanylfentanyl, and 4-Fluoro-Isobutyrylfentanyl. AAPS Journal. 2017;19(4):1102-22. doi:10.1208/s12248-017-0070-z.

6. Vikingsson S, Wohlfarth A, Andersson M, Gréen H, Roman M, Josefsson M, et al. Identifying Metabolites of Meclonazepam by High-Resolution Mass Spectrometry Using Human Liver Microsomes, Hepatocytes, a Mouse Model, and Authentic Urine Samples. AAPS Journal. 2017;19(3):736-42. doi:10.1208/s12248-016-0040-x.

7. Diao X, Scheidweiler KB, Wohlfarth A, Pang S, Kronstrand R, Huestis MA. In Vitro and In Vivo Human Metabolism of Synthetic Cannabinoids FDU-PB-22 and FUB-PB-22. AAPS Journal. 2016;18(2):455-64. doi:10.1208/s12248-016-9867-4.

8. Chimalakonda KC, Seely KA, Bratton SM, Brents LK, Moran CL, Endres GW, et al. Cytochrome P450-mediated oxidative metabolism of abused synthetic cannabinoids found in K2/Spice: identification of novel cannabinoid receptor ligands. Drug Metab Dispos. 2012;40(11):2174-84. doi:10.1124/dmd.112.047530.

9. Hutter M, Moosmann B, Kneisel S, Auwarter V. Characteristics of the designer drug and synthetic cannabinoid receptor agonist AM-2201 regarding its chemistry and metabolism. J Mass Spectrom. 2013;48(7):885-94. doi:10.1002/jms.3229.

10. Asha S, Vidyavathi M. Cunninghamella--a microbial model for drug metabolism studies--a review. Biotechnol Adv. 2009;27(1):16-29. doi:10.1016/j.biotechadv.2008.07.005.

11. Diao X, Huestis MA. Approaches, Challenges, and Advances in Metabolism of New Synthetic Cannabinoids and Identification of Optimal Urinary Marker Metabolites. Clin Pharmacol Ther. 2017;101(2):239-53. doi:10.1002/cpt.534.

12. Guddat S, Fußhöller G, Beuck S, Thomas A, Geyer H, Rydevik A, et al. Synthesis, characterization, and detection of new oxandrolone metabolites as long-term markers in sports drug testing. Anal Bioanal Chem. 2013;405(25):8285-94. doi:10.1007/s00216-013-7218-1.

13. Tian J-L, Chen Y, Wang Y-X, Huang X-X, Sun X, Liu K-C, et al. Microbial transformation of methyl cyperenoate by Cunninghamella elegans AS 3.2028 and the antithrombotic activities of its metabolites. RSC Adv. 2016;6(113):112712-20. doi:10.1039/c6ra24332k.

14. Watanabe S, Kuzhiumparambil U, Nguyen MA, Cameron J, Fu S. Metabolic Profile of Synthetic Cannabinoids 5F-PB-22, PB-22, XLR-11 and UR-144 by Cunninghamella elegans. AAPS Journal. 2017;19(4):1148-62. doi:10.1208/s12248-017-0078-4.

15. Watanabe S, Kuzhiumparambil U, Winiarski Z, Fu S. Biotransformation of synthetic cannabinoids JWH-018, JWH-073 and AM2201 by Cunninghamella elegans. Forensic Sci Int. 2016;261:33-42. doi:http://dx.doi.org/10.1016/j.forsciint.2015.12.023.

16. Nunomoto S, Kawakami Y, Yamashita Y, Takeuchi H, Eguchi S. Regioselectivity control in alkylation reactions of indolyl ambident anion. J Chem Soc, Perkin Trans 1. 1990(1):111-4. doi:10.1039/P19900000111.

17. Okauchi T, Itonaga M, Minami T, Owa T, Kitoh K, Yoshino H. A General Method for Acylation of Indoles at the 3-Position with Acyl Chlorides in the Presence of Dialkylaluminum Chloride. Org Lett. 2000;2(10):1485-7. doi:10.1021/ol005841p.

18. Langer N, Lindigkeit R, Schiebel H-M, Ernst L, Beuerle T. Identification and quantification of synthetic cannabinoids in 'spice-like' herbal mixtures: A snapshot of the German situation in the autumn of 2012. Drug Test Anal. 2014;6(1-2):59-71. doi:10.1002/dta.1499.

19. Kavanagh P, Grigoryev A, Savchuk S, Mikhura I, Formanovsky A. UR-144 in products sold via the Internet: Identification of related compounds and characterization of pyrolysis products. Drug Test Anal. 2013;5(8):683-92. doi:10.1002/dta.1456.

20. Shevyrin V, Melkozerov V, Nevero A, Eltsov O, Morzherin Y, Shafran Y. Identification and analytical properties of new synthetic cannabimimetics bearing 2,2,3,3-tetramethylcyclopropanecarbonyl moiety. Forensic Sci Int. 2013;226(1):62-73. doi:http://dx.doi.org/10.1016/j.forsciint.2012.12.009.

21. Sobolevsky T, Prasolov I, Rodchenkov G. Detection of urinary metabolites of AM-2201 and UR-144, two novel synthetic cannabinoids. Drug Test Anal. 2012;4(10):745-53. doi:10.1002/dta.1418.

22. Nielsen LM, Holm NB, Olsen L, Linnet K. Cytochrome P450-mediated metabolism of the synthetic cannabinoids UR-144 and XLR-11. Drug Test Anal. 2016;8(8):792-800. doi:10.1002/dta.1860.

23. Grigoryev A, Kavanagh P, Melnik A, Savchuk S, Simonov A. Gas and liquid chromatography-mass spectrometry detection of the urinary metabolites of UR-144 and its major pyrolysis product. J Anal Toxicol. 2013;37(5):265-76. doi:10.1093/jat/bkt028.

24. Adamowicz P, Zuba D, Sekula K. Analysis of UR-144 and its pyrolysis product in blood and their metabolites in urine. Forensic Sci Int. 2013;233(1-3):320-7. doi:10.1016/j.forsciint.2013.10.005.

25. Cayman Chemical. 2017. Available from: https://www.caymanchem.com/Search?q=ur-144. Accessed 27 July 2017.

Chapter 5: *In vitro* metabolism of synthetic cannabinoid AM1220 by human liver microsomes and *Cunninghamella elegans* using liquid chromatography coupled with high resolution mass spectrometry

Chapter 5: *In vitro* metabolism of synthetic cannabinoid AM1220 by human liver microsomes and *Cunninghamella elegans* using liquid chromatography coupled with high resolution mass spectrometry

5.1 Abstract

Identification of intake of synthetic cannabinoids generally requires the metabolism data of the drugs so that appropriate metabolite markers can be targeted in urine testing. However, the continuous appearance of new cannabinoids during the last decade has made it difficult to keep up with all the compounds including {1-[(1-methylpiperidin-2-yl)methyl]-1*H*-indol-3-yl}(naphthalen-1-yl)methanone (AM1220). In this study, metabolism of AM1220 was investigated with human liver microsomes and the fungus *Cunninghamella elegans*. Metabolic stability of AM1220 was analysed by liquid chromatography – tandem mass spectrometry in multiple reaction monitoring mode after 1 μM incubation in human liver microsomes for 30 min. Metabolite identification was performed on both human liver microsomes and fungal incubation samples using liquid chromatography – high-resolution mass spectrometry. Half-life of AM1220 was estimated to be 3.7 min, indicating a high clearance drug. Nine metabolites were detected after human liver microsomes incubation while seven were found after *Cunninghamella elegans* incubation, leading to eleven metabolites in total (five metabolites were common to both systems). Demethylation, dihydrodiol formation, combination of the two, hydroxylation and dihydroxylation were the observed biotransformations. Three most abundant metabolites in both human liver microsomes and *Cunninghamella elegans* were desmethyl, dihydrodiol and hydroxy metabolites, despite different isomers of dihydrodiol and hydroxy metabolites in each model. These abundant metabolites can potentially be useful biomarkers in urinalysis for AM1220 intake.

Keywords: AM1220, Synthetic cannabinoid, *In vitro* metabolism, Human liver microsomes, *Cunninghamella elegans*, High resolution mass spectrometry

Abbreviations

AM1220	[1-[(1-methyl-2-piperidinyl)methyl]-1H-indol-3-yl]-1-naphthalenylmethanone
CB_1	Cannabinoid receptor type 1
CB_2	Cannabinoid receptor type 2
C. elegans	*Cunninghamella elegans*
CYP	Cytochrome P450
CL_H	Hepatic clearance
CL_{int}	Intrinsic clearance
E_H	Hepatic extraction ratio
HLM	Human liver microsomes
LC-QTOF-MS	Liquid chromatography – quadrupole time-of-flight mass spectrometry
Q_H	Human hepatic blood flow
$t_{1/2}$	Half-life

5.2 Introduction

AM1220, or {1-[(1-methylpiperidin-2-yl)methyl]-1*H*-indol-3-yl}(naphthalen-1-yl)methanone, is a synthetic cannabinoid that was first synthesised in the 1990s for studying the structure activity relationship of cannabinoid receptors [1]. The cannabinoid was shown to have a binding affinity (Ki) of 3.88 nM and 73.4 nM to cannabinoid receptor type 1 (CB_1) and type 2 (CB_2) receptors, respectively [2]. Due to the high affinity to cannabinoid receptors, AM1220 began to be sold and abused as "herbal products" and "research chemicals" on the recreational drug market among the continuous emergence of a myriad of new psychoactive substances [3-8].

In these products, AM1220 is usually found together with its azepane isomer, [1-(1-Methyl-3-azepanyl)-1H-indol-3-yl](1-naphthyl)methanone [4, 5], which is suggested to be present as synthetic impurity [4] or due to a rearrangement that occurs over time [7]. The presence of the AM1220 azepane isomer may complicate interpretation of the pharmacological effects of AM1220, as the azepane isomer itself is shown to have binding affinities to CB_1 and CB_2 receptors [9].

For detection of synthetic cannabinoids in human, plasma samples are shown to be useful as the parent drugs can be found as they are without modifications [10]. However, there are some issues with detection in plasma samples. Firstly, the window of detection of the parent drugs in blood is short [10, 11]. Secondly, the concentrations of the parent drugs in plasma are reported to be lower than those of the major metabolites [11]. In addition, plasma samples are not always obtainable due to its invasiveness and urine samples are often the preferred choice for drug testing. Therefore, suitable methods for analysis of urine samples are desirable. Synthetic cannabinoids are extensively metabolised in human and are generally not excreted in urine in the parent drug form. Consequently, metabolites need to be monitored for detecting synthetic cannabinoids in urine specimens.

Metabolism studies of synthetic cannabinoids have been performed using several approaches. Human liver microsomes (HLM) incubation is the most common *in vitro* approach and even though not reflective of the metabolism in a whole human body, it can generate a wide variety of human metabolites with advantages such as low cost and larger

pools of donors [11-13]. Human hepatocytes provide the metabolic profiles closest to the *in vivo* human data [14-16] and animal models such as rats are valuable as a source of *in vivo* data, though not always consistent with human findings [17-19]. Incubation with the fungus *Cunninghamella elegans* (*C. elegans*) has been shown to produce similar metabolic profiles to the human system with the advantage of low cost and production of large quantity of metabolites, as shown in chapters 2, 3 and 4 [20-22]. The presence and abundance of the metabolites determined by these models may not be an accurate representation of *in vivo* metabolites. Thus, the *in vitro* metabolites should be confirmed in human urine, if available, by analysis of urine samples obtained from suspected users of synthetic cannabinoids, since analysis of human urine from controlled administration is difficult at this point without sufficient data to ensure safety [11].

To date, there has been no *in vitro* metabolism study of AM1220. There is one *in vivo* study by Zaitsu *et al.* reporting two metabolites of AM1220 and two more potential metabolites in postmortem human plasma and urine specimens, respectively, from a fatal intoxication case [10]. To complement the *in vivo* findings, which may have been affected by genotype and phenotype and/or inhibition of cytochrome P450 (CYP) enzymes by co-administration of drug, *in vitro* metabolism study will be useful [23].

In this study, we report the metabolic stability of AM1220 based on HLM incubation and identification of AM1220 metabolites obtained from HLM and *C. elegans* incubation. Suitable biomarkers for urinalysis are also suggested. Liquid chromatography – quadrupole time-of-flight mass spectrometry (LC-QTOF-MS) was used for analysis since high-resolution mass spectrometry has an advantage of providing accurate masses, enabling more confident characterisation of metabolites [24].

5.3 Materials and Methods

5.3.1 Chemicals and reagents

AM1220 was obtained from Cayman Chemical (Ann Arbor, MI, USA). 50-Doner HLM pool, NADPH system solution A and NADPH system solution B were from Corning (Corning, NY, USA). LC-MS grade acetonitrile was obtained from Honeywell (Muskegon, MI, USA). Reagent grade dichloromethane and sodium chloride were purchased from Chemsupply (Gilman, SA, Australia). LC-MS grade formic acid was obtained from Sigma–Aldrich (St. Louis, MO, USA). *C. elegans* ATCC 10028b was from Cryosite Ltd. (South Granville, NSW, Australia). Glycerol and potassium dihydrogen phosphate and dipotassium hydrogen phosphate were from Ajax Chemicals (Auburn, NSW, Australia). Potato dextrose agar, glucose, peptone, and yeast extract were purchased from Oxoid Australia (Adelaide, SA, Australia).

5.3.2 Metabolic stability

AM1220 solution in acetonitrile and phosphate buffer (40 µM, 25 µL), phosphate buffer (0.1M, pH7.4, 855 µL), NADPH-A (50 µL) and NADPH-B (20 µL) were mixed in an Eppendorf tube, to which HLM (50 µL) was added. The final concentration of AM1220 in the mixture was 1 µM with 0.003% acetonitrile. The mixture was incubated in triplicate at 37 °C in a shaking water bath. At time 0, 3, 8, 13, 20 and 30 min, a 100 µL aliquot was removed and placed into 100 µL ice-cold acetonitrile to quench the reaction. The mixture was centrifuged at 16,060 × g for 10 minutes and filtered with a 0.22 µm filter. 10 µL of the filtrate was diluted in 990 µL water:acetonitrile (70:30, v/v) and 10 µL was injected into liquid chromatography – triple quadrupole mass spectrometer in triplicate.

Chromatographic separation was performed on an Agilent 1290 LC system with an Agilent Zorbax Eclipse XDBC18 analytical column (150 mm × 4.6 mm, 5 µm). The mobile phase consisted of 0.1% formic acid in water (A) and 0.1% formic acid in acetonitrile (B). The gradient system was as follows: 30% B until 1 min, ramped to 40% B at 16 min, 95% B at 16.01 min and held until 19.1 min, ramped down to 30% B at 19.11

min and held until 23 min. The flow rate was 0.4 mL/min and the column temperature was kept at 30°C.

Mass spectrometry was run in multiple reaction monitoring mode on an Agilent 6490 Triple Quadrupole mass spectrometer with ESI source (positive ion mode). Two transitions (*m/z* 383 → 286 and *m/z* 383→ 98) were monitored with fragmentor voltage of 380 V and collision energy of 20 eV and 50 eV, respectively.

In vitro microsomal half-life ($t_{1/2}$) of AM1220 was calculated based on the plot of natural log of percentage of the drug remaining against time. Percentage of the drug remaining was calculated by dividing the peak area of the drug remaining at each time point by the peak area of the drug at time 0 min and multiplying by 100%. The slope of the line (-k) was used to give $t_{1/2}$ = ln2/k. Intrinsic clearance (CL_{int}) was calculated based on the following formula [25]:

$$CL_{int} = \frac{\ln 2}{t_{1/2}} \times \frac{\text{mL of incubation}}{\text{mg of microsomes}} \times \frac{\text{45 mg of microsomes}}{\text{g of liver}} \times \frac{\text{20 g of liver}}{\text{kg of body weight}}$$

Hepatic clearance (CL_H) and hepatic extraction ratio (E_H) were calculated based on the well-stirred model from the following formulae without considering blood protein and microsome binding [25, 26]. 21 mL/min/kg was used for human hepatic blood flow (Q_H) [25].

$$CL_H = \frac{Q_H \times CL_{int}}{Q_H + CL_{int}}$$

$$E_H = \frac{CL_H}{Q_H}$$

5.3.3 Metabolite identification

5.3.3.1 *Human liver microsomes incubation*

The incubation mixture was prepared as described for the metabolic stability study using 1 mg/mL AM1220 solution (final concentration of acetonitrile was 0.2%). The mixture was incubated at 37 °C in a shaking water bath for 1 h. The reaction was quenched by adding ice-cold acetonitrile (1 mL) to the mixture and it was centrifuged at 16,060 × g for 10 minutes. The sample was filtered (0.22 μm) and injected to LC-QTOF. A control sample without HLM, a control without AM1220 and a positive control using UR-144 were also incubated and analysed.

5.3.3.2 *Fungus incubation*

C. elegans was cultured on potato dextrose agar plates at 27 °C for 5 days. The mycelia of the fungus were mixed in sterile physiological saline solution (1 plate of mycelia/5 mL). Growth medium was prepared [27], and 1.5 mL of the fungus solution was added to 100 mL of medium in a conical flask. The culture was incubated for 48 h at 26 °C and 180 rpm on an Infors HT Multitron rotary shaker (In vitro Technologies, Noble Park North, VIC, Australia). AM1220 (1 mg in 0.5 mL acetonitrile) was added to the flask and incubated for another 72 h. The solution was filtered, extracted with dichloromethane (3 × 50 mL) and evaporated using a rotary evaporator and a vacuum pump. The sample was reconstituted in 2 mL acetonitrile, which was further diluted in acetonitrile by 10-fold. A control without fungus and a control without AM1220 were also incubated.

5.3.3.3 *LC-QTOF-MS*

Chromatographic equipment and conditions were the same as described for metabolic stability in the section 2.2., except for the following. The gradient started with 30% B and held until 1 min, ramped up to 40% B at 20 min, 90% B at 21 min and held till 24 min, and ramped down to 30% B at 25 min and held till 30 min for re-equilibration. Injection volume was 2 μL for MS scan and 10 μL for MS/MS scan.

Mass spectra were acquired on an Agilent 6510 Accurate Mass Q-TOF Mass Spectrometer, equipped with a Dual electrospray ionisation (ESI) source. The parameters were as follows: scanning mass range, m/z 100–1000 (MS), m/z 80–1000 (MS/MS); capillary voltage, 3500 V; nebulizer pressure, 30 psig; gas temperature, 325 °C; gas flow, 5 L/min; fragmentor voltage, 160 V; collision energy for MS/MS scan, 10, 20 and 40 eV; skimmer voltage, 65 V. Mass calibration was performed with the mixture provided by the manufacturer. Real-time mass calibration was enabled using the following reference masses: m/z 121.0509 and m/z 922.0098.

Additional MS analyses were performed on an Agilent 6550A iFunnel Q-TOF with a Dual AJS ESI source operated with the same parameters as above except for the following: gas temperature, 290 °C; gas flow, 11 L/min; sheath gas temperature, 350 °C; sheath gas flow, 11 L/min; injection volume for MS/MS scan, 2 μL.

Chromatograms and mass spectra were analysed using Agilent MassHunter Workstation Software Qualitative Analysis (version B.06.00). A PCDL library with known and potential metabolites of the drug was created with Agilent MassHunter PCDL Manager (version B.04.00) to search for the metabolites. Search parameters were as follows: mass tolerance, 20 ppm; maximum number of matches, 8; absolute peak area ≥ 5000. The criteria for metabolites were as follows: mass error of the protonated molecules ≤ 5 ppm; consistent fragmentation pattern with proposed structure; reasonable retention time relative to other biotransformations; absence of the metabolite in controls.

5.4 Results

5.4.1 Metabolic stability

In vitro $t_{1/2}$ of AM1220 was calculated to be 3.7 ± 0.4 min (mean ± SD, n = 3). From the calculated $t_{1/2}$ value, CL_{int}, CL_H and E_H were estimated to be 168.5 mL/min/kg, 18.7 mL/min/kg, and 0.89, respectively.

5.4.2 Metabolite identification

Chromatograms of AM1220 metabolites after HLM and *C. elegans* incubation are shown in Fig. 5-1. The MS/MS spectra and the suggested fragmentation patterns of the metabolites are shown in Fig. 5-2. The proposed metabolic pathway of AM1220 in HLM and *C. elegans* incubation is compared with the *in vivo* postmortem human data in the literature (Fig. 5-3). Table 5-1 lists all the metabolites with retention time, elemental composition, exact mass, accurate mass, mass error, diagnostic product ions and chromatographic peak area.

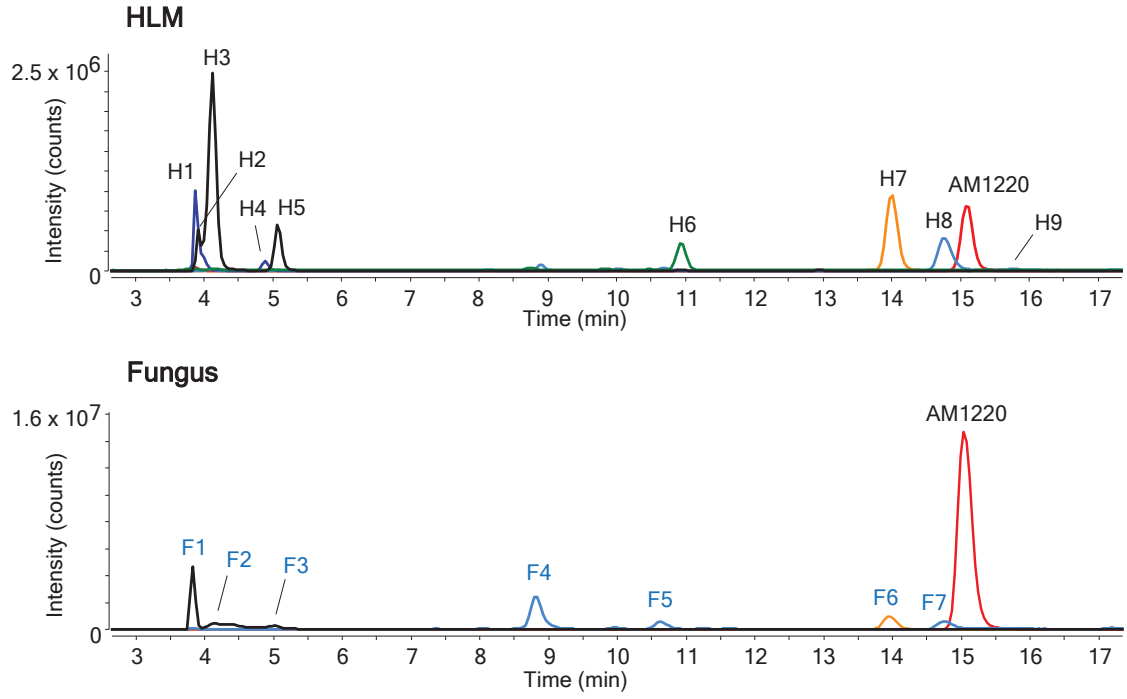

Figure 5-1. Combined extracted ion chromatograms of AM1220 and its metabolites in HLM and fungus incubation.

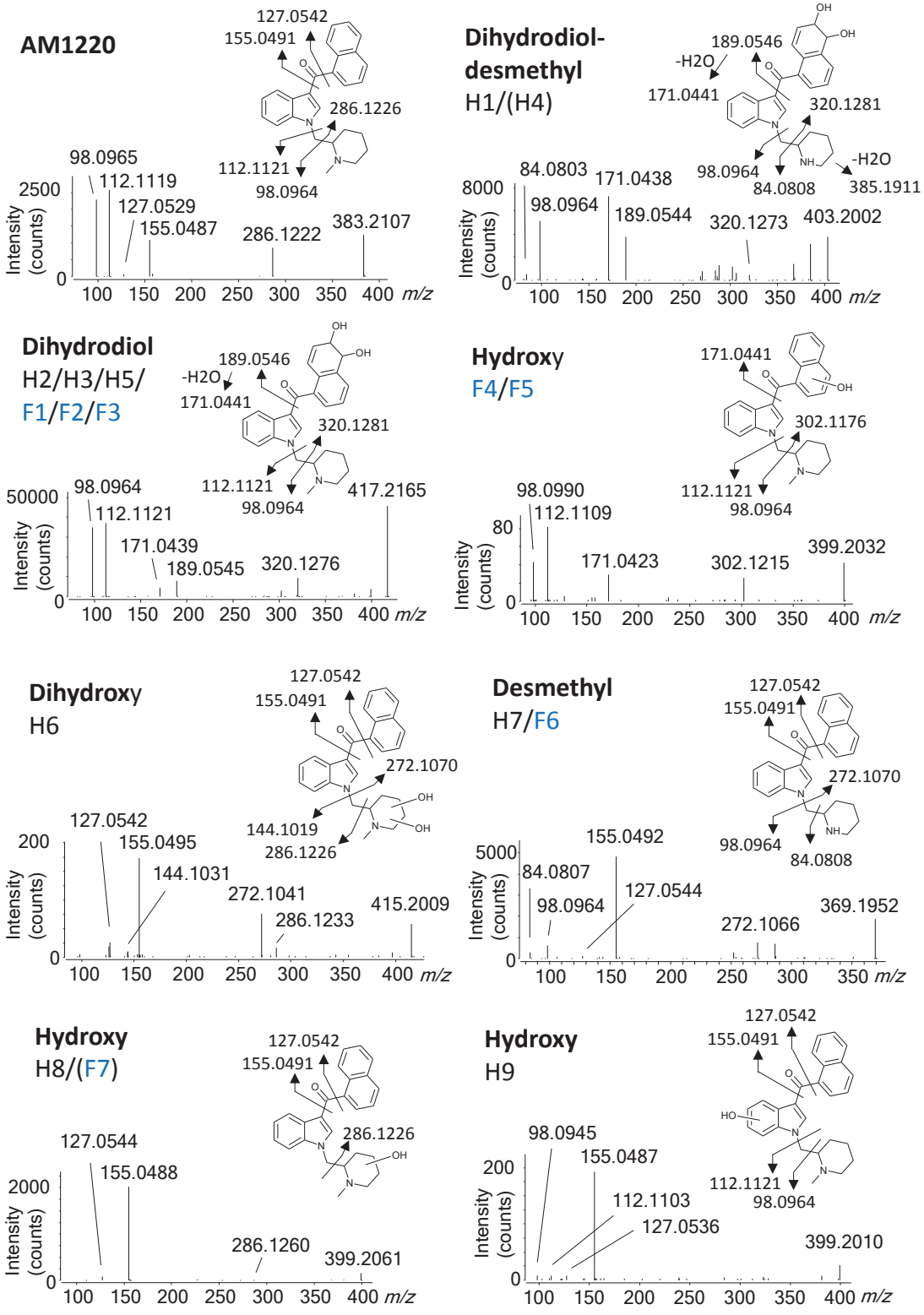

Figure 5-2. MS/MS spectra of AM1220 and its metabolites at collision energy of 20 eV, and proposed metabolite structures with exact masses of fragmentation. Metabolites in brackets did not show all the product ions. The exact location of dihydrodiol is not determined.

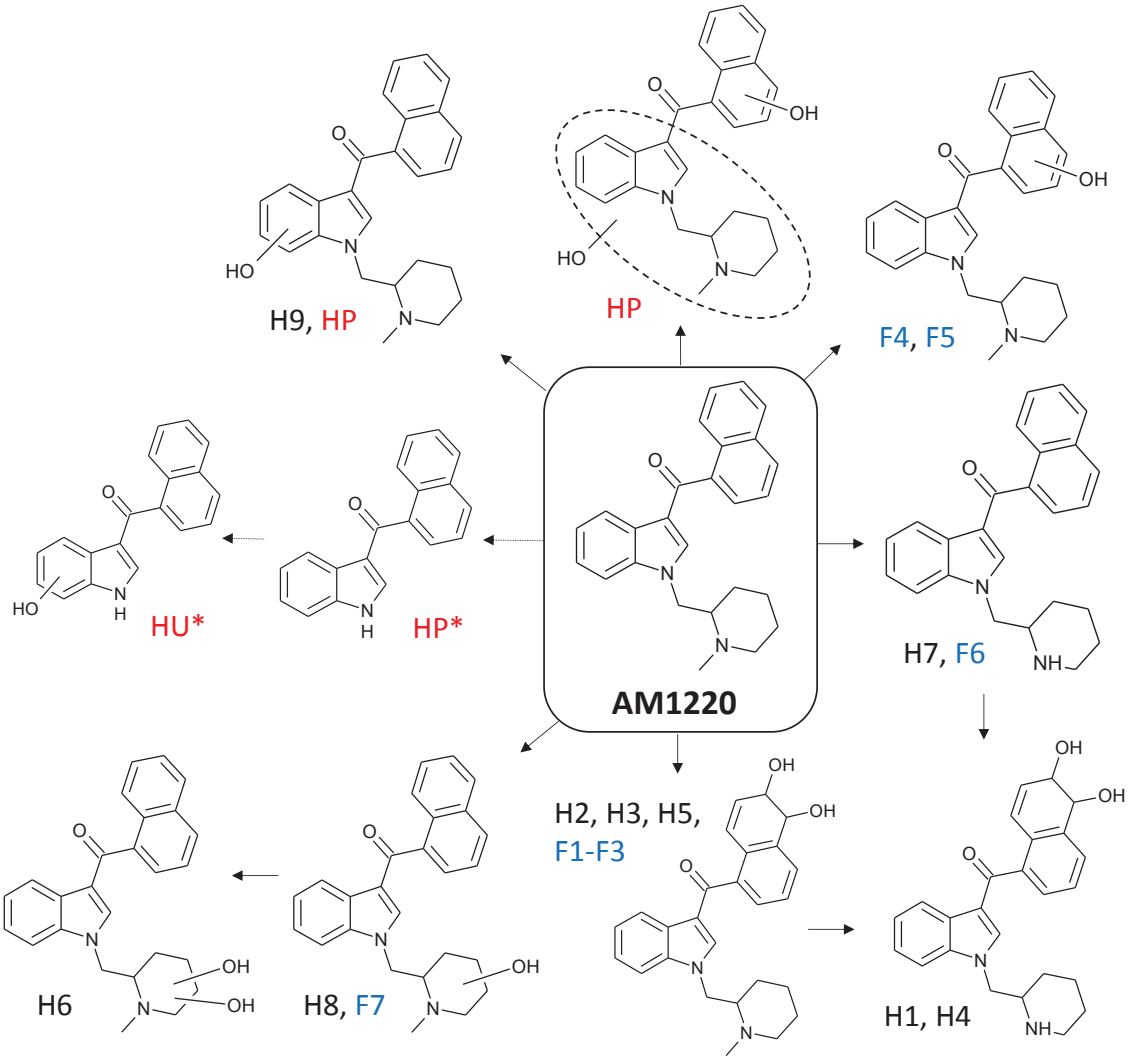

Figure 5-3. Proposed metabolic pathway of AM1220 in HLM and fungus *C. elegans* incubation in comparison with postmortem human data from the literature [10]. HP and HU refer to human plasma and human urine samples while asterisk indicates that the origin of the metabolite is not confirmed to be AM1220. The exact position of dihydrodiol is not determined.

5.4.2.1 *AM1220 identification by LC-QTOF-MS*

AM1220 eluted at 15.1 min (Fig. 5-1) and was fragmented to the product ions at *m/z* 98, 112, 127, 155 and 286 in MS/MS scan (Fig. 5-2). The accurate mass of the fragment ion at *m/z* 112 matched the (1-methyl-2-piperidinyl)methyl moiety resulting from *N*-dealkylation of the indole ring (Fig. 5-2). The fragment ion at *m/z* 98 was derived from further loss of a methylene group from the fragment at *m/z* 112. The cleavage that produced the fragment ion at *m/z* 98, also resulted in a product ion of 1-methyl-3-naphthoylindole moiety, matching the *m/z* 286. The product ions at *m/z* 127 and 155 are common fragments of synthetic cannabinoids with a naphthoyl group; the former ion is

Table 5-1. AM1220 metabolites after HLM and fungus *C. elegans* incubation.

ID		Metabolites	RT (min)	Elemental composition [M+H]	Exact mass	Accurate mass		Mass error (ppm)		Diagnostic product ions	Area	
HLM	Fungi					HLM	Fungi	HLM	Fungi		HLM	Fungi
H1		Dihydrodiol formation + demethylation	3.9	C25H27N2O3	403.2016	403.2015		0.17		84, 98, 171, 189, 320	5.55E+06	
H2	F1	Dihydrodiol formation	3.9	C26H29N2O3	417.2173	417.2173	417.2168	0.16	1.15	98, 112, 171, 189, 320	7.84E+05	2.54E+07
H3	F2	Dihydrodiol formation	4.1	C26H29N2O3	417.2173	417.2168	417.2171	-1.15	-0.84	98, 112, 171, 189, 320	1.93E+07	4.56E+06
H4		Dihydrodiol formation + demethylation	4.9	C25H27N2O3	403.2016	403.2012		-0.83		84, 98, 171, 385	9.72E+05	
H5	F3	Dihydrodiol formation	5.1	C26H29N2O3	417.2173	417.2168	417.2158	-1.06	1.08	98, 112, 171, 189, 320	4.41E+06	4.99E+06
	F4	Hydroxylation	8.8	C26H27N2O2	399.2067		399.2066		-0.34	98, 112, 171, 302		3.43E+07
	F5	Hydroxylation	10.6	C26H27N2O2	399.2067		399.2067		-0.83	98, 112, 171, 302		8.07E+06
H6		Dihydroxylation	10.9	C26H27N2O3	415.2016	415.2010		0.72		127, 144, 155, 272, 286	3.65E+06	
H7	F6	Demethylation	14.0	C25H25N2O	369.1961	369.1962	369.1961	0.25	0.16	84, 98, 127, 155, 272	1.19E+07	1.36E+07
H8	F7	Hydroxylation	14.8	C26H27N2O2	399.2067	399.2061	399.2067	0.27	0.35	127, 155, 286*	6.23E+06	1.14E+07
Parent		AM1220	15.1	C26H27N2O	383.2118	383.2118	383.2116	0.62	-0.22	98, 112, 127, 155, 286	1.03E+07	2.21E+08
H9		Hydroxylation	15.8	C26H27N2O2	399.2067	399.2058		-2.17		98, 112, 127, 155	5.57E+05	

*Not found in F7.

of a naphthalene moiety and the latter is of a naphthoyl moiety.

5.4.2.2 *Human liver microsomes*

Nine metabolites were detected in HLM incubation and assigned as H1-H9 in the order of retention time (Fig. 5-1). The following metabolites were detected; dihydrodiol (H2, H3, H5), dihydrodiol with demethylation (H1, H4), demethylation (H7), hydroxylation (H8, H9) and dihydroxylation (H6). The mass errors of the metabolites compared with the proposed elemental compositions were ≤ 2.17 ppm (Table 5-1). The top three abundant metabolites based on the peak area were dihydrodiol (H3), demethylation (H7) and hydroxylation (H8) metabolites.

5.4.2.3 *Fungus C. elegans*

Seven metabolites were found after *C. elegans* incubation and assigned as F1-F7 (Fig. 5-1). Dihydrodiol (F1-F3), demethylation (F6) and hydroxylation (F4, F5, F7) metabolites were identified. Five of them were the same metabolites as HLM metabolites (Table 5-1); dihydrodiol (H2 and F1, H3 and F2, H5 and F3), demethylation (H7 and F6) and hydroxylation (H8 and F7) were common metabolites between HLM and fungus metabolism. The mass errors were all ≤ 1.15 ppm. The three most abundant metabolites were hydroxylation (F4), dihydrodiol (F1) and demethylation (F6).

5.5 Discussion

5.5.1 Metabolic stability

In vitro $t_{1/2}$ of AM1220 was 3.7 min and this belongs to the class of high clearance compounds [28]. The estimated E_H of 0.89 also indicates high extraction, suggesting the compound to be highly susceptible to hepatic metabolism [29]. These findings are in line with other synthetic cannabinoids and account for the extensive metabolism of cannabinoids [15, 30, 31].

5.5.2 Metabolite identification

Nine and seven metabolites were detected after incubation of AM1220 with HLM and fungus, respectively. Based on the retention time and the fragmentation patterns of the metabolites, five of them were considered identical and hence a total of 11 metabolites were found from two *in vitro* models (Table 5-1). The identification of these metabolites is described below.

5.5.2.1 Hydroxylation

Four hydroxylated metabolites were detected at *m/z* 399. F4 and F5 showed product ions at *m/z* 171 and 302, which are 16 amu higher than the unchanged naphthoyl moiety and 1-methyl-3-naphthoylindole, respectively, indicating hydroxylation at the naphthalene moiety. Other product ions at *m/z* 98 and 112 confirmed the piperidine moiety to be unaltered. H8 was shown to be hydroxylated at the methylpiperidine moiety by the intact product ions at *m/z* 127, 155, and 286, indicative of the unmodified indole and naphthalene moieties. The absence of ions at *m/z* 98 and 112 also indicated the modification of the methylpiperidine ring. F7 eluted at the same retention time as H8 but only showed the fragment ions at *m/z* 127 and 155 without 286. Without the ion at *m/z* 286, hydroxylation could have occurred at either indole or piperidine moiety. However, it was considered to be the identical metabolite as H8 because of the retention time and the fact that the ions at *m/z* 98 and 112 were absent, which were seen for all the other metabolites without modification to the piperidine moiety and the parent drug. H9 was

characterised by the unchanged naphthalene (*m/z* 127, 155) and unchanged piperidine (*m/z* 98, 112), indicating the location of hydroxylation to be the indole ring.

5.5.2.2 Dihydroxylation

A dihydroxy metabolite (H6) was found at *m/z* 415, which resulted from further oxidation of H8. The fragment ions at *m/z* 127, 155 and 286 are in common with the parent drug, indicating the intact naphthoylindole moiety. The ion at *m/z* 144 indicated the (1-methyl-2-piperidinyl)methyl moiety to be the site of dihydroxylation. It is interesting to note that an abundant fragment ion at *m/z* 272 was observed. While the presence of the ion does not contradict the aforementioned position of dihydroxylation, this ion was formed from a different fragmentation pattern from the parent drug. This may be a proof to restrict the site of one of the hydroxylations to the methylene linker between the indole and piperidine rings, as a similar change in the fragmentation pattern of WIN 55,212-2 was reportedly caused by hydroxylation of its methylene linker [31].

5.5.2.3 Dihydrodiol formation

Three dihydrodiol metabolites (H2/F1, H3/F2 and H5/F3) were observed with *m/z* 417. All three metabolites showed the same fragment ions: *m/z* 98, 112, 171, 189 and 320. The ions at *m/z* 98 and 112 show the unchanged piperidine moiety while *m/z* 189 and 320 indicate dihydrodiol formation at naphthalene moiety with the former losing a water molecule to form *m/z* 171.

5.5.2.4 Demethylation

A metabolite demethylated at the piperidine nitrogen (H7/F6) was detected at *m/z* 369. The product ions at *m/z* 127 and 155 were retained as the naphthalene moiety is intact. The fragment ions at *m/z* 98 and 272 were generated by *N*-dealkylation of indole, corresponding to a demethylated piperidine moiety and the unaltered naphthoylindole, respectively (Fig. 5-2). The product ion at *m/z* 98 further lost a methylene moiety to form the ion at *m/z* 84. The lack of product ion at *m/z* 112 also supports demethylation of the methylpiperidine moiety.

5.5.2.5 Dihydrodiol formation and demethylation

Two metabolites at *m/z* 403 (H1, H4) were found to have undergone both dihydrodiol formation at the naphthalene ring and demethylation of the methylpiperidine moiety. For H1, the combination of the product ions at *m/z* 171, 189 and 320 indicates the formation of dihydrodiol at the naphthalene moiety, whereas the ions at *m/z* 84 and 98 without 112 reflect a demethylated piperidine ring. In fact, H4 did not show the fragment ion at *m/z* 189, but this is probably because the dihydrodiol at a particular position is less stable and easily loses a water molecule [32]. The hypothesis is supported by the observation that the fragment ion at *m/z* 385, resulting from water loss of the molecule, is prominent in H4.

5.5.3 Comparison of AM1220 metabolites in HLM and *C. elegans* with *in vivo* human metabolites

Out of 9 HLM and 7 fungal metabolites detected in this study, 5 metabolites were found to be identical, i.e. more than 50% of HLM and fungal metabolites were the same as each other. In terms of the biotransformations of AM1220, dihydrodiol formation, demethylation and hydroxylation were the common transformations between HLM and fungal metabolites. HLM additionally showed the transformations by dihydroxylation and combinations of dihydrodiol formation and demethylation. Overall, metabolism of AM1220 by HLM and *C. elegans* was highly consistent.

To date, the study by Zaitsu *et al*. is the only one reporting the *in vivo* human metabolites of AM1220 [10]. In the study, four metabolites were detected from a fatal case of intoxication; hydroxylation, dihydroxylation and *N*-dealkylation in plasma and *N*-dealkylation followed by hydroxylation in urine (Fig. 5-3). It should be noted, however, that metabolites of *N*-dealkylation and *N*-dealkylation followed by hydroxylation were not confirmed to have formed from AM1220 since AM-2232, which also contains a naphthoylindole moiety and hence another potential source of these metabolites, was also detected in plasma.

Out of the four metabolites, *N*-dealkylation and *N*-dealkylation followed by hydroxylation were not observed after either HLM or *C. elegans* incubation. Dihydroxylation was detected in HLM incubation (H6), yet the positions of hydroxy groups were different; dihydroxylation took place at the piperidine moiety in H6 while one hydroxylation at the naphthalene moiety and another at either the indole or piperidine moiety in the plasma metabolite. The hydroxylated metabolite is the only metabolite potentially in common with HLM incubation, as it may be identical to H9 based on the mass fragmentation pattern. The inconsistency between the *in vitro* and *in vivo* metabolites may be due to the genotype/phenotype and/or the co-administration of CYP enzyme inhibitor in this fatal case [23]. Another hypothesis is that AM1220 had not been sufficiently metabolised before the death, leading to less metabolites with an incomplete metabolic pattern. The higher concentration of AM1220 in plasma than its potential *N*-dealkylated metabolite is in line with this hypothesis (hydroxy and dihydroxy metabolites were not quantified), as well as the detection of hydroxy and dihydroxy metabolites in plasma despite their absence in urine [10]. For these reasons, it would be ideal to compare the *in vitro* metabolism data with multiple *in vivo* data.

5.5.4 Suggested biomarkers

The three most abundant metabolites in HLM and fungus incubations were dihydrodiol (H3), demethylation (H7) and hydroxylation at the piperidine moiety (H8), and hydroxylation at the naphthalene moiety (F4), dihydrodiol (F1) and demethylation (F6), respectively. Based on the high abundance observed *in vitro*, these metabolites could be potential *in vivo* markers of AM1220 intake. The desmethyl metabolite and hydroxy metabolite at the piperidine moiety are particularly interesting as the same transformation pathways were predominant for AM1241, an analogue of AM1220 with the naphthalene moiety replaced by 2-iodo-5-nitrophenyl group, in HLM and rat microsomes incubations [30]. The dihydrodiol metabolites are also promising, as dihydrodiol and hydroxy metabolites were the most abundant metabolites of AM2201 in authentic human urine samples, when excluding oxidative defluorination [32]. Since AM1220 does not undergo oxidative defluorination, dihydrodiol formation may be an abundant *in vivo* metabolic pathway.

5.6 Conclusion

A potent synthetic cannabinoid AM1220 was incubated in HLM and *C. elegans* to identify the *in vitro* metabolites. Metabolic stability of AM1220 was estimated from HLM incubation and the estimated *in vitro* half-life and hepatic extraction ratio indicated AM1220 to be a high clearance drug. LC-QTOF analysis of HLM and *C. elegans* samples resulted in detection of a total of 11 metabolites (9 and 7 metabolites in respective samples) and they consisted of hydroxy, dihydroxy, desmethyl, dihydrodiol, and dihydrodiol-desmethyl metabolites. The results did not match the *in vivo* metabolism previously reported, however it should be noted that the results in the study were based on a single postmortem sample. Based on the *in vitro* data, hydroxy, desmethyl and dihydrodiol metabolites are deemed suitable urinary markers of AM1220 intake. These data should help toxicological and clinical laboratories to identify AM1220 consumption from human urine samples.

5.7 References

1. D'Ambra TE, Eissenstat MA, Abt J, Ackerman JH, Bacon ER, Bell MR, et al. C-Attached aminoalkylindoles: potent cannabinoid mimetics. Bioorg Med Chem Lett. 1996;6(1):17-22. doi:http://dx.doi.org/10.1016/0960-894X(95)00560-G.

2. Makriyannis A, Deng H, inventorsCannabimimetic indole derivatives patent US 2008/0090871 A1. 2008.

3. Uchiyama N, Kawamura M, Kikura-Hanajiri R, Goda Y. Identification of two new-type synthetic cannabinoids, N-(1-adamantyl)-1-pentyl-1H-indole-3-carboxamide (APICA) and N-(1-adamantyl)-1-pentyl-1H-indazole-3-carboxamide (APINACA), and detection of five synthetic cannabinoids, AM-1220, AM-2233, AM-1241, CB-13 (CRA-13), and AM-1248, as designer drugs in illegal products. Forensic Toxicol. 2012;30(2):114-25. doi:10.1007/s11419-012-0136-7.

4. Kneisel S, Bisel P, Brecht V, Broecker S, Müller M, Auwärter V. Identification of the cannabimimetic AM-1220 and its azepane isomer (N-methylazepan-3-yl)-3-(1-naphthoyl)indole in a research chemical and several herbal mixtures. Forensic Toxicol. 2012;30(2):126-34. doi:10.1007/s11419-012-0137-6.

5. Nakajima Ji, Takahashi M, Seto T, Kanai C, Suzuki J, Yoshida M, et al. Analysis of azepane isomers of AM-2233 and AM-1220, and detection of an inhibitor of fatty acid amide hydrolase [3′-(aminocarbonyl)(1,1′-biphenyl)-3-yl]-cyclohexylcarbamate (URB597) obtained as designer drugs in the Tokyo area. Forensic Toxicol. 2013;31(1):76-85. doi:10.1007/s11419-012-0169-y.

6. Salomone A, Luciano C, Di Corcia D, Gerace E, Vincenti M. Hair analysis as a tool to evaluate the prevalence of synthetic cannabinoids in different populations of drug consumers. Drug Test Anal. 2014;6(1-2):126-34. doi:10.1002/dta.1556.

7. Langer N, Lindigkeit R, Schiebel H-M, Ernst L, Beuerle T. Identification and quantification of synthetic cannabinoids in 'spice-like' herbal mixtures: A snapshot of the German situation in the autumn of 2012. Drug Test Anal. 2014;6(1-2):59-71. doi:10.1002/dta.1499.

8. Blakey K, Boyd S, Atkinson S, Wolf J, Slottje PM, Goodchild K, et al. Identification of the novel synthetic cannabimimetic 8-quinolinyl 4-methyl-3-(1-

piperidinylsulfonyl)benzoate (QMPSB) and other designer drugs in herbal incense. Forensic Sci Int. 2016;260:40-53. doi:http://dx.doi.org/10.1016/j.forsciint.2015.12.001.

9. Nakajima Ji, Takahashi M, Uemura N, Seto T, Fukaya H, Suzuki J, et al. Identification of N,N-bis(1-pentylindol-3-yl-carboxy)naphthylamine (BiPICANA) found in an herbal blend product in the Tokyo metropolitan area and its cannabimimetic effects evaluated by in vitro [35S]GTPγS binding assays. Forensic Toxicol. 2015;33(1):84-92. doi:10.1007/s11419-014-0253-6.

10. Zaitsu K, Nakayama H, Yamanaka M, Hisatsune K, Taki K, Asano T, et al. High-resolution mass spectrometric determination of the synthetic cannabinoids MAM-2201, AM-2201, AM-2232, and their metabolites in postmortem plasma and urine by LC/Q-TOFMS. Int J Legal Med. 2015;129(6):1233-45. doi:10.1007/s00414-015-1257-4.

11. Diao X, Huestis MA. Approaches, Challenges, and Advances in Metabolism of New Synthetic Cannabinoids and Identification of Optimal Urinary Marker Metabolites. Clin Pharmacol Ther. 2017;101(2):239-53. doi:10.1002/cpt.534.

12. Kim U, Jin MJ, Lee J, Han SB, In MK, Yoo HH. Tentative identification of phase I metabolites of HU-210, a classical synthetic cannabinoid, by LC-MS/MS. J Pharm Biomed Anal. 2012;64-65:26-34. doi:10.1016/j.jpba.2012.02.007.

13. Kim JH, Kim HS, Kong TY, Lee JY, Kim JY, In MK, et al. In vitro metabolism of a novel synthetic cannabinoid, EAM-2201, in human liver microsomes and human recombinant cytochrome P450s. J Pharm Biomed Anal. 2016;119:50-8. doi:http://dx.doi.org/10.1016/j.jpba.2015.11.023.

14. Wohlfarth A, Castaneto MS, Zhu M, Pang S, Scheidweiler KB, Kronstrand R, et al. Pentylindole/Pentylindazole Synthetic Cannabinoids and Their 5-Fluoro Analogs Produce Different Primary Metabolites: Metabolite Profiling for AB-PINACA and 5F-AB-PINACA. AAPS Journal. 2015;17(3):660-77. doi:10.1208/s12248-015-9721-0.

15. Diao X, Scheidweiler KB, Wohlfarth A, Pang S, Kronstrand R, Huestis MA. In Vitro and In Vivo Human Metabolism of Synthetic Cannabinoids FDU-PB-22 and FUB-PB-22. AAPS Journal. 2016;18(2):455-64. doi:10.1208/s12248-016-9867-4.

16. Diao X, Carlier J, Zhu M, Pang S, Kronstrand R, Scheidweiler KB, et al. In vitro and in vivo human metabolism of a new synthetic cannabinoid NM-2201 (CBL-2201). Forensic Toxicol. 2017;35(1):20-32. doi:10.1007/s11419-016-0326-9.

17. Jang M, Yang W, Shin I, Choi H, Chang H, Kim E. Determination of AM-2201 metabolites in urine and comparison with JWH-018 abuse. Int J Legal Med. 2014;128(2):285-94. doi:10.1007/s00414-013-0884-x.

18. Grigoryev A, Melnik A, Savchuk S, Simonov A, Rozhanets V. Gas and liquid chromatography-mass spectrometry studies on the metabolism of the synthetic phenylacetylindole cannabimimetic JWH-250, the psychoactive component of smoking mixtures. J Chromatogr B Analyt Technol Biomed Life Sci. 2011;879(25):2519-26. doi:10.1016/j.jchromb.2011.07.004.

19. Kevin RC, Lefever TW, Snyder RW, Patel PR, Fennell TR, Wiley JL, et al. In vitro and in vivo pharmacokinetics and metabolism of synthetic cannabinoids CUMYL-PICA and 5F-CUMYL-PICA. Forensic Toxicol. 2017;35(2):333-47. doi:10.1007/s11419-017-0361-1.

20. Watanabe S, Kuzhiumparambil U, Winiarski Z, Fu S. Biotransformation of synthetic cannabinoids JWH-018, JWH-073 and AM2201 by Cunninghamella elegans. Forensic Sci Int. 2016;261:33-42. doi:http://dx.doi.org/10.1016/j.forsciint.2015.12.023.

21. Watanabe S, Kuzhiumparambil U, Winiarski Z, Fu S. Data on individual metabolites of synthetic cannabinoids JWH-018, JWH-073 and AM2201 by Cunninghamella elegans. Data Brief. 2016;7:332-40. doi:10.1016/j.dib.2016.02.039.

22. Watanabe S, Kuzhiumparambil U, Nguyen MA, Cameron J, Fu S. Metabolic Profile of Synthetic Cannabinoids 5F-PB-22, PB-22, XLR-11 and UR-144 by Cunninghamella elegans. AAPS Journal. 2017;19(4):1148-62. doi:10.1208/s12248-017-0078-4.

23. Steuer AE, Williner E, Staeheli S, Kraemer T. Studies on the metabolism of the fentanyl-derived designer drug butyrfentanyl in human in vitro liver preparations and authentic human samples using liquid chromatography-high resolution mass spectrometry (LC-HRMS). Drug Test Anal. 2016:(in press). doi:10.1002/dta.2111.

24. Pasin D, Cawley A, Bidny S, Fu S. Current applications of high-resolution mass spectrometry for the analysis of new psychoactive substances: a critical review. Anal Bioanal Chem. 2017. doi:10.1007/s00216-017-0441-4.

25. Obach RS. Prediction of Human Clearance of Twenty-Nine Drugs from Hepatic Microsomal Intrinsic Clearance Data: An Examination of In Vitro Half-Life Approach and Nonspecific Binding to Microsomes. Drug Metab Dispos. 1999;27(11):1350-9.

26. Naritomi Y, Terashita S, Kimura S, Suzuki A, Kagayama A, Sugiyama Y. Prediction of Human Hepatic Clearance from in Vivo Animal Experiments and in Vitro Metabolic Studies with Liver Microsomes from Animals and Humans. Drug Metab Dispos. 2001;29(10):1316-24.

27. Choudhary MI, Khan NT, Musharraf SG, Anjum S, Atta ur R. Biotransformation of adrenosterone by filamentous fungus, Cunninghamella elegans. Steroids. 2007;72(14):923-9. doi:http://dx.doi.org/10.1016/j.steroids.2007.08.002.

28. McNaney CA, Drexler DM, Hnatyshyn SY, Zvyaga TA, Knipe JO, Belcastro JV, et al. An Automated Liquid Chromatography-Mass Spectrometry Process to Determine Metabolic Stability Half-Life and Intrinsic Clearance of Drug Candidates by Substrate Depletion. Assay Drug Dev Technol. 2008;6(1):121-9. doi:10.1089/adt.2007.103.

29. Lavé T, Dupin S, Schmitt C, Valles B, Ubeaud G, Chou RC, et al. The Use of Human Hepatocytes to Select Compounds Based on Their Expected Hepatic Extraction Ratios in Humans. Pharm Res. 1997;14(2):152-5. doi:10.1023/a:1012036324237.

30. Wood JT, Smith DM, Janero DR, Zvonok AM, Makriyannis A. Therapeutic modulation of cannabinoid lipid signaling: Metabolic profiling of a novel antinociceptive cannabinoid-2 receptor agonist. Life Sci. 2013;92(8):482-91. doi:http://dx.doi.org/10.1016/j.lfs.2012.06.019.

31. Mardal M, Gracia-Lor E, Leibnitz S, Castiglioni S, Meyer MR. Toxicokinetics of new psychoactive substances: plasma protein binding, metabolic stability, and human phase I metabolism of the synthetic cannabinoid WIN 55,212-2 studied using in vitro tools and LC-HR-MS/MS. Drug Test Anal. 2016;8(10):1039-48. doi:10.1002/dta.1938.

32. Sobolevsky T, Prasolov I, Rodchenkov G. Detection of urinary metabolites of AM-2201 and UR-144, two novel synthetic cannabinoids. Drug Test Anal. 2012;4(10):745-53. doi:10.1002/dta.1418.

Chapter 6: *In vitro* and *in vivo* metabolite identification studies for the new synthetic opioids acetylfentanyl, acrylfentanyl, furanylfentanyl, and 4-fluoro-isobutyrylfentanyl

Chapter 6: *In vitro* and *in vivo* metabolite identification studies for the new synthetic opioids acetylfentanyl, acrylfentanyl, furanylfentanyl, and 4-fluoro-isobutyrylfentanyl

This work was performed in collaboration with the Swedish National Board of Forensic Medicine and my contribution includes conducting *in vivo* and *in vitro* experiments of acrylfentanyl and furanylfentanyl, interpretation of the experimental results, and writing a manuscript.

6.1 Abstract

New fentanyl analogues have recently emerged as new psychoactive substances and have caused numerous fatalities worldwide. To determine if the new analogues follow the same metabolic pathways elucidated for fentanyl and known fentanyl analogues, we performed *in vitro* and *in vivo* metabolite identification studies for acetylfentanyl, acrylfentanyl, 4-fluoro-isobutyrylfentanyl and furanylfentanyl. All compounds were incubated at 10 μM with pooled human hepatocytes for up to 5 h. For each compound, four or five authentic human urine samples from autopsy cases with and without enzymatic hydrolysis were analysed. Data acquisition was performed in data-dependent acquisition mode during liquid-chromatography high-resolution mass spectrometry analyses. Data was analysed (1) manually based on predicted biotransformations and (2) with MetaSense software using data-driven search algorithms. Acetylfentanyl, acrylfentanyl, and 4-fluoroisobutyrylfentanyl were predominantly metabolised by *N*-dealkylation, cleaving off the phenethyl moiety, monohydroxylation at the ethyl linker and piperidine ring, as well as hydroxylation/methoxylation at the phenyl ring. In contrast, furanylfentanyl's major metabolites were generated by amide hydrolysis and dihydrodiol formation while the nor-metabolite was minor or not detected in case samples at all. In general, *in vitro* results matched the *in vivo* findings well, showing identical biotransformations in each system. Phase II conjugation was observed, particularly for acetylfentanyl. Based on our results, we suggest the following specific and abundant metabolites as analytical targets in urine: a hydroxymethoxy and monohydroxylated metabolite for acetylfentanyl, a

monohydroxy and dihydroxy metabolite for acrylfentanyl, two monohydroxy metabolites and a hydroxymethoxy metabolite for 4-fluoro-isobutyrylfentanyl, and a dihydrodiol metabolite and the amide hydrolysis metabolite for furanylfentanyl.

Keywords: Authentic human urine samples, Fentanyl analogues, Human hepatocytes, LC-HRMS, Metabolite identification

Abbreviations

KHB	Krebs–Henseleit buffer
LC-HRMS	Liquid chromatography high-resolution mass spectrometry
LC-QTOF	Liquid chromatography-quadrupole time-of-flight mass spectrometer
NPS	New psychoactive substances
RT	Retention time

6.2 Introduction

Synthetic opioids are a class of new psychoactive substances (NPS) mostly consisting of analogues of the prescription drug fentanyl. Since 2012, they have caused an alarming number of fatalities worldwide [1]. Fentanyl itself is a potent μ-opioid receptor agonist [2] and is estimated to be at least 50 times more potent than morphine [3]. Although therapeutically prescribed as an analgesic since the 1960s, fentanyl has also been abused for its euphoric effects with fatalities occurring due to respiratory depression followed by apnea [4, 5].

A plethora of fentanyl analogues have been developed over the last decades [6], some examples are shown in Figure 6-1. Approved medications are e.g. alfentanil, sufentanil and remifentanil for use in humans and carfentanil for use in animals. "Older" fentanyl analogues abused recreationally are 3-methylfentanyl, α-methylfentanyl, and ß-hydroxyfentanyl [7]. The analogues that recently appeared as NPS are usually generated by modification or replacement of fentanyl's propionyl chain (acetylfentanyl, acrylfentanyl, butyrylfentanyl, isobutyrylfentanyl, furanylfentanyl, ocfentanil) or replacement of the ethylphenyl moiety (isofentanyl, ß-hydroxythiofentanyl). Existing variants are further substituted with fluoro, chloro, or methoxy substituents at the *N*-phenyl ring [8, 9]. Not only are the fentanyl analogues highly potent, their potencies are also variable, making it difficult for the users to dose the drugs correctly and increasing the risk of accidental overdoses.

To understand and monitor the abuse of fentanyl analogues, reliable analytical methods are needed in clinical and forensic laboratories. Urine is still the matrix of choice for drug testing due to the non-invasive nature of sampling, well-established procedure, and admissibility. Less than 8% of fentanyl is excreted unchanged. Approximately 85% is excreted within 72 h in faeces and urine, the majority as metabolites [10] mainly as norfentanyl generated by *N*-dealkylation at the piperidine nitrogen. Minor metabolites are despropionylfentanyl, which is formed by carboxamide hydrolysis, and hydroxyfentanyl and hydroxynorfentanyl metabolites, both hydroxylated at the propionyl moiety [11, 12].

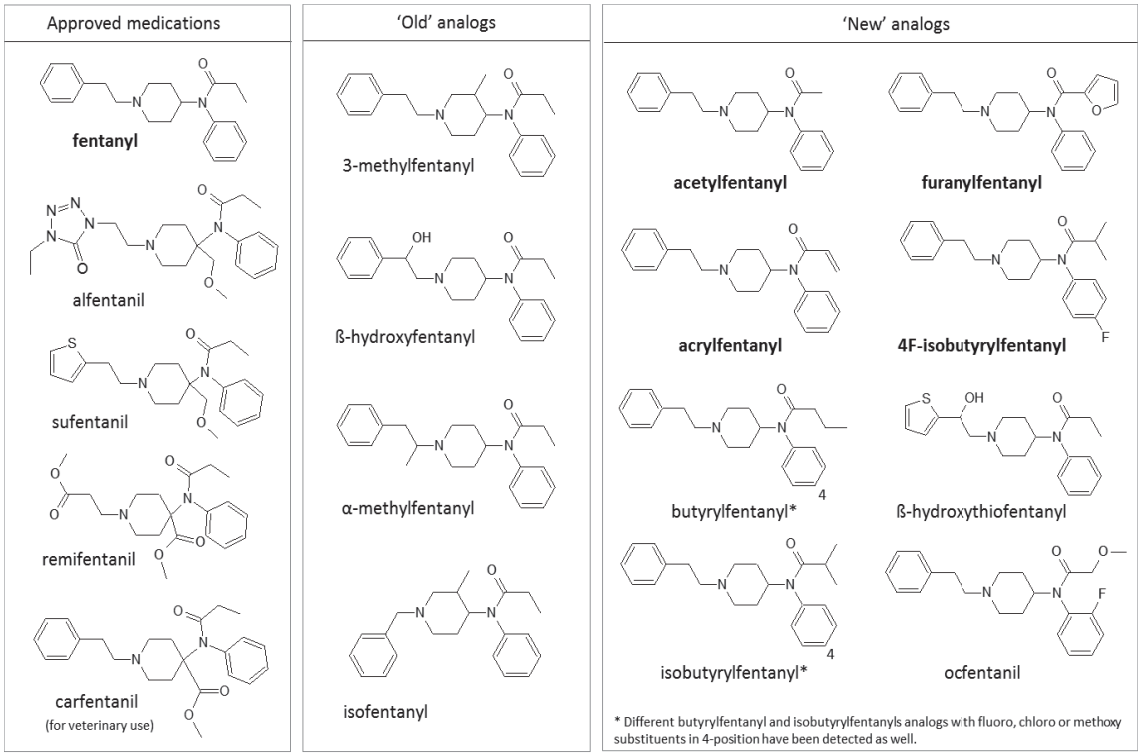

Figure 6-1. Structures of fentanyl and analogues that have approved medicinal use, others that have been abused for several decades, and those that appeared recently on the illicit drug market.

To date, information about metabolism of fentanyl analogues, which have been found as drugs of abuse, is limited to a few studies: So far, metabolism of α-methylfentanyl in rat urine [13], 3-methylfentanyl in rat urine [14], isofentanyl in rat urine [14], butyrylfentanyl in human blood, tissues and urine [15] and acetylfentanyl in human liver microsomes and rat urine [16] and human urine [17] has been investigated. Some analogues, such as α-methylfentanyl, 3-methylfentanyl, isofentanyl and acetylfentanyl, were metabolised to the nor-metabolite, similar to fentanyl. Minor metabolites were produced by hydroxylation, dihydroxylation and carboxylation, often in combination with *N*-dealkylation. For acetylfentanyl, however, hydroxylation and hydroxylation/methoxylation at the phenethyl moiety dominated over *N*-dealkylation. For butyrylfentanyl, hydroxylation and carboxylation dominated, while the nor-metabolite and desbutyryl metabolite were minor.

Based on the current state of knowledge, we hypothesise that suitable analytical targets in urine for new fentanyl analogues can often, but not always, be predicted based on fentanyl's metabolic pathway demonstrating the need to perform individual metabolism studies. Therefore, the aims of this study were to perform metabolism studies for four

new fentanyl analogues: acetylfentanyl, acrylfentanyl, 4-fluoro-isobutyrylfentanyl, and furanylfentanyl. We analysed authentic human urine samples that were available from casework and also incubated the drugs with human hepatocytes. Sample analysis was performed under identical conditions with liquid chromatography high-resolution mass spectrometry (LC-HRMS) allowing for direct comparison between hepatocyte and urine samples and producing accurate mass measurements for metabolite molecules and fragment ions. Incubation with human hepatocytes provides *in vitro* metabolite profiles that are often similar to what is found in humans [18, 19]. Individual incubation under controlled conditions eliminates analogues as potential source of metabolites. However, *in vitro* models are inherently limited running the risk of missing metabolites or misinterpreting their relevance. Conversely, authentic human urine samples contain the real human metabolites formed from the whole organism. They usually come, however, with limited information about the intake itself, e.g. time before sampling, identity, and purity of the drug or co-consumption of other compounds. A combination of both systems, complementing advantages and compensating for disadvantages, seems to be the road forward.

6.3 Materials and Methods

6.3.1 Chemicals and reagents

Acetylfentanyl, acrylfentanyl, furanylfentanyl, and 4-fluoro-isobutyrylfentanyl were purchased as powders from Cayman Chemical (Ann Arbor, USA), diclofenac from Sigma (Stockholm, Sweden). Cryopreserved hepatocytes LiverPool (10-donor-pool), InVitro Gro HT, and InVitro Gro KHB media were obtained from Bioreclamation IVT (Brussels, Belgium). Liquid chromatography mass spectrometry grade acetonitrile, water, methanol and formic acid were from Fisher Scientific (Gothenburg, Sweden), ammonium formate from Fluka (Sigma-Aldrich, Stockholm, Sweden), and ammonium acetate and acetic acid from Merck (Darmstadt, Germany). The β-glucuronidase/sulfatase mixture (Helix pomatia) was purchased from Roche (Mannheim, Germany). Ultra-pure water was prepared in-house using a MilliQ Gradient 10 production unit (Millipore, Billerica, USA).

6.3.2 Incubation with human hepatocytes and sample preparation

Cryopreserved human hepatocytes were thawed at 37 °C and transferred into InVitro Gro HT medium. The solution was centrifuged at 100×g for 4 min, the supernatant aspirated, and the hepatocyte pellet suspended in Krebs–Henseleit buffer (KHB). After centrifugation at 60×*g* for 4 min and aspiration of the supernatant the pellet was re-suspended in KHB. Using Trypan blue (0.4% v/v) dye exclusion method, cell viability was determined as 100%. Drugs were incubated at 10 µmol/L with human hepatocytes (125,000 cells/125 µL total volume/well) in a 96-well plate at 37 °C for 1, 3, and 5 h. The reaction was quenched by 125 µL ice-cold acetonitrile. Organic solvent content was ≤0.4%. A positive control with diclofenac, a negative control without drugs, and degradation controls without hepatocytes were included. After centrifugation, the supernatant was stored at –20 °C. Samples were injected undiluted onto the liquid chromatography-quadrupole time-of-flight mass spectrometer (LC-QTOF); injection volume was 1 µL.

6.3.3 Authentic human urine specimens and sample preparation

Four or five human urine specimens for each fentanyl analogue from fatal overdose cases were used for metabolite profiling. A corresponding blood sample had always confirmed positive for the respective parent compound in the routine TOF screening [20] without showing the presence of other fentanyl analogues. For all cases, the cause of death was ruled to be an overdose with the respective fentanyl analogue, except in four cases, which were ruled intoxication with the fentanyl analogue in combination with oxycodone (4-fluoro-isobutyrylfentanyl case sample #2), alcohol (4-fluoro-isobutyryl fentanyl case sample #4), pregabalin (furanylfentanyl case sample #1), or fentanyl (furanylfentanyl case sample #4). Each urine sample was analysed with and without enzymatic hydrolysis: To cleave phase II conjugates, 100 µL urine was incubated with 10 µL β-glucuronidase/sulfatase (4.5 and 14 U/mL, respectively) in 300 µL ammonium acetate buffer (pH 5.0) at 40 °C for 2 h. The non-hydrolysed set of samples was diluted with 310 µL ammonium acetate buffer only. One microliter of each sample was injected onto the LC-QTOF system.

6.3.4 LC-QTOF analysis

Chromatographic separation was performed on an Agilent 1290 Infinity UHPLC system with an Acquity HSS T3 column (150 mm x 2.1 mm, 1.8 μm) fitted with an Acquity VanGuard precolumn, both from Waters (Sollentuna, Sweden), at 60 °C. Mobile phases were 10 mM ammonium formate in 0.05% formic acid (A) and 0.05% formic acid in acetonitrile (B) and were run in gradient at a flow rate of 0.5 mL/min starting at 1% B until 0.6 min, ramped to 5% B at 0.7 min, 50% B at 13 min, 95% B at 15 min until 18 min, then ramped down to 1% B at 18.1 min and re-equilibration until 19 min.

Mass spectrometric data was obtained with an Agilent 6550 iFunnel QTOF mass spectrometer with a Dual Agilent Jet Stream electrospray ionisation source. Auto MS/MS acquisition was performed in positive ion mode with the following conditions: scan range, 100–950 *m/z* (MS) and 50–950 *m/z* (MS/MS); precursor intensity threshold, 5000 counts; precursor number per cycle, 5; fragmentor voltage, 380 V; collision energy, 3 eV at 0 *m/z* ramped up by 8 eV per 100 *m/z*; gas temperature, 150°C; nebulizer gas pressure, 50 psig; and sheath gas temperature, 375°C. Automated calibration was in place during data acquisition.

6.3.5 Manual and software-assisted data analysis

Full scan MS and MS/MS data sets were analysed by Agilent MassHunter Qualitative Analysis (version B.07.00) using a PCDL library that contained known biotransformations of fentanyl and fentanyl analogues as well as reactions predicted by MetaSite™ (v.5, Molecular Discovery, Pinner, UK). Searching parameters were as follows: mass error 15 ppm, absolute peak area >10,000 counts, maximum number of matches 5, chromatogram extraction window 100 ppm. Metabolites were evaluated based on the following criteria: mass error for protonated molecule being less than 5 ppm, consistent isotopic pattern, MS/MS product ions consistent with proposed structure, retention time plausible for the proposed structure, appropriate peak shape, and absence of identical peaks in negative controls.

All *in vitro* and *in vivo* samples were also processed with MetaSense™ software (version 1.0, in combination with Spectrus Processor 2016.1.3 and DB Enterprise 2016.1.3, Advanced Chemistry Development, Inc., Toronto, ON, Canada). Processing options were as follows: MS accuracy 0.005 Da, three metabolite generations, minimum metabolite mass 150 Da, human specific and phase II metabolites included, and minimum metabolite >0.01% of the parent.

6.4 Results

Hydroxydiclofenac was observed in the diclofenac positive control confirming hepatocyte metabolic activity. Any peaks that appeared either in the negative or degradation control were not considered as metabolites.

6.4.1 Metabolic profile of acetylfentanyl

In total, 32 acetylfentanyl metabolites (A1 to A32, in increasing order of retention time (RT)) were identified, all of them with mass error ≤4.22 ppm. The parent drug was found in high abundance in all samples. Metabolites were formed via *N*-dealkylation (A3) followed by hydroxylation (A1, A2), monohydroxylation (A24, A25, A28, A30) – preferably at the ethyl linker – followed by glucuronidation (A6, A11, A20) or sulfation (A17, A23), dihydroxylation (A8, A13, A14, A19) followed by glucuronidation (A5, A10) or sulfation (A22), monohydroxylation and carbonylation (A15, A18), dihydrodiol formation (A4, A7), dihydroxylation with methylation at the phenyl ring (A26, A27, A29) followed by glucuronidation (A9, A12) or sulfation (A21) as well as amide hydrolysis (A32) followed by hydroxylation (A16, A31). Retention times were between 2.77 and 9.09 min, with A32 eluting after the parent (RT 7.92 min). The three sample sets showed different numbers of metabolites with different signal intensities: Specifically, in hepatocytes, seven metabolites were detected (A3, A4, A6, A18, A24, A26, and A30). Based on MS peak areas in the 5-h sample, the nor-metabolite A3 was most abundant followed by the monohydroxylated metabolite A24 and the dihydrodiol metabolite A4. In hydrolysed urine, 24 metabolites were found showing a wider spectrum of first-generation and second-generation metabolites and including all hepatocyte metabolites. Ranking MS peak areas, the most dominant metabolite was the hydroxymethoxy metabolite A26, followed by A3 and A24. These findings are in general agreement with Melent'ev *et al*.'s study [17]. Finally, in non-hydrolysed urine samples, many additional phase II metabolites were detected; out of 32 metabolites, 7 were glucuronides and 4 were sulfates. Generally, hydrolysis led to complete cleavage of the conjugates; exceptions occurred for A17 and A20. Table 6-1 lists all 32 metabolites with retention time, accurate mass of the protonated molecule, proposed metabolic transformation, elemental composition, mass error, diagnostic product ions, and chromatographic peak areas in

Table 6-1. Acetylfentanyl metabolites with proposed biotransformation, retention time, elemental composition, accurate mass of protonated molecule, mass error of proposed metabolite, MS peak areas in hepatocyte samples (0h, 1h, 3h and 5h) and in five urine samples (hydrolysed and non-hydrolysed), and diagnostic product ions (masses and mass errors taken from sample #3, and #5 in case of saturation).

ID	Biotransformation	RT (min)	Elemental composition	*m/z*	mass error (ppm)	Peak areas in the hepatocyte samples				Peak areas in the urine samples					Diagnostic ions
						0h	1h	3h	5h	#1 HYD	#2 HYD	#3 HYD	#4 HYD	#5 HYD	
										NON-HYD	NON-HYD	NON-HYD	NON-HYD	NON-HYD	
	Blood acetylfentanyl concentration (in µg/g)									0.77	0.17	0.18	0.04	0.02	
A1	*N*-dealkylation + hydroxylation	2.77	$C_{13}H_{18}N_2O_2$	235.1441	0.08	ND	ND	ND	ND	1.0E+06	ND	1.9E+05	ND	ND	84.0809
										ND	ND	1.7E+05	ND	ND	
A2	*N*-dealkylation + hydroxylation	2.93	$C_{13}H_{18}N_2O_2$	235.1444	2.24	ND	ND	ND	ND	3.6E+05	ND	1.1E+05	ND	ND	84.0803
										2.7E+05	ND	6.9E+04	ND	ND	
A3	*N*-dealkylation (yielding nor-metabolite)	4.19	$C_{13}H_{18}N_2O$	219.1490	-0.89	4.6E+05	2.1E+06	4.4E+06	5.6E+06	2.5E+07	2.9E+06	1.8E+07	2.3E+05	2.3E+06	84.0805, 94.0645, 136.0750
										2.4E+07	3.0E+06	1.7E+07	2.3E+05	2.4E+06	
A4	Dihydrodiol formation (ethylphenyl)	4.66	$C_{21}H_{28}N_2O_3$	357.2195	4.22	ND	7.1E+05	1.2E+06	1.7E+06	1.7E+07	4.6E+05	1.0E+07	5.1E+04	3.7E+05	121.0644, 146.0962, 158.0952, 188.1071, 204.1374, 222.1462
										1.6E+07	4.4E+05	9.5E+06	ND	3.2E+05	
A5	Dihydroxylation + Glucuronidation	4.74	$C_{27}H_{34}N_2O_9$	531.2339	0.15	ND	ND	ND	ND	ND	ND	ND	ND	ND	91.0532, 119.0475, 137.0595, 220.1317, 355.2043
										1.8E+06	ND	3.6E+05	ND	3.4E+04	

ID	Biotransformation	RT (min)	Elemental composition	*m/z*	mass error (ppm)	Peak areas in the hepatocyte samples				Peak areas in the urine samples					Diagnostic ions
						0h	1h	3h	5h	#1 HYD	#2 HYD	#3 HYD	#4 HYD	#5 HYD	
										NON-HYD	NON-HYD	NON-HYD	NON-HYD	NON-HYD	
A6	Hydroxylation + Glucuronidation	4.79	$C_{27}H_{34}N_2O_8$	515.2380	-2.04	ND	ND	ND	1.0E+04	2.9E+06	ND	2.2E+04	ND	ND	84.0808, 121.0641, 204.1379
										2.8E+07	7.4E+05	1.7E+07	7.1E+04	1.3E+06	
A7	Dihydrodiol formation (*N*-phenyl)	4.85	$C_{21}H_{28}N_2O_3$	357.2170	-0.94	ND	ND	ND	ND	1.8E+06	ND	3.5E+05	ND	ND	105.0697, 188.1436
										2.1E+06	ND	3.9E+05	ND	ND	
A8	Dihydroxylation	4.92	$C_{21}H_{26}N_2O_3$	355.2013	-3.27	ND	ND	ND	ND	8.6E+05	ND	1.9E+05	ND	4.1E+04	84.0806, 121.0648, 204.0378
										1.9E+05	ND	5.1E+04	ND	ND	
A9	Dihydroxylation + Methylation + Glucuronidation	4.97	$C_{28}H_{36}N_2O_9$	545.2526	3.87	ND	ND	ND	ND	ND	ND	ND	ND	ND	84.0808, 119.0486, 151.0749, 234.1486
										2.6E+07	5.6E+05	1.5E+07	1.7E+05	1.8E+06	
A10	Dihydroxylation + Glucuronidation	5.10	$C_{27}H_{34}N_2O_9$	531.2333	-0.4	ND	ND	ND	ND	ND	ND	ND	ND	ND	84.0802, 119.0473, 137.0586, 220.1319, 355.1995
										3.7E+06	ND	1.1E+06	ND	8.6E+04	
A11	Hydroxylation + Glucuronidation	5.17	$C_{27}H_{34}N_2O_8$	515.2383	-0.65	ND	ND	ND	ND	ND	ND	ND	ND	ND	121.0644, 204.1379, 339.2073
										4.0E+06	6.7E+04	8.9E+05	ND	3.6E+04	

ID	Biotransformation	RT (min)	Elemental composition	*m/z*	mass error (ppm)	Peak areas in the hepatocyte samples				Peak areas in the urine samples					Diagnostic ions
						0h	1h	3h	5h	#1	#2	#3	#4	#5	
										HYD	HYD	HYD	HYD	HYD	
										NON-HYD	NON-HYD	NON-HYD	NON-HYD	NON-HYD	
A12	Dihydroxylation + Methylation + Glucuronidation	5.55	$C_{28}H_{36}N_2O_9$	545.249	-0.52	ND	ND	ND	ND	ND	ND	ND	ND	ND	119.0487, 151.0752, 192.0989, 234.1476
										2.4E+06	1.6E+04	5.9E+05	ND	5.6E+04	
A13	Dihydroxylation	5.60	$C_{21}H_{26}N_2O_3$	355.2018	0.46	ND	ND	ND	ND	1.2E+06	ND	2.7E+05	ND	ND	107.0491, 121.0630, 188.1064, 202.1230, 337.1857
										6.6E+05	ND	9.7E+04	ND	ND	
A14	Dihydroxylation	5.72	$C_{21}H_{26}N_2O_3$	355.2012	-1.12	ND	ND	ND	ND	2.1E+07	6.5E+05	1.6E+07	1.5E+05	2.5E+06	91.0539, 119.0488, 137.0595, 220.1330
										5.3E+06	1.4E+05	7.4E+06	ND	2.5E+05	
A15	Carbonylation + Hydroxylation	5.74	$C_{21}H_{24}N_2O_3$	353.1854	-1.11	ND	ND	ND	ND	7.3E+06	3.6E+04	9.8E+05	ND	1.9E+05	118.0647 132.0806, 164.0705, 202.1221, 218.1167
										8.1E+06	4.2E+04	1.1E+06	ND	2.4E+05	
A16	Hydroxylation + Amide hydrolysis	5.75	$C_{19}H_{24}N_2O$	297.1959	-1.05	ND	ND	ND	ND	ND	ND	3.8E+05	ND	5.1E+04	105.0689, 188.1416
										ND	ND	ND	ND	ND	
A17	Hydroxylation + Sulfation	5.87	$C_{21}H_{26}N_2O_5S$	419.1634	-0.78	ND	ND	ND	ND	1.2E+06	ND	2.5E+05	ND	ND	103.0530, 121.0650, 204.1380

ID	Biotransformation	RT (min)	Elemental composition	*m/z*	mass error (ppm)	Peak areas in the hepatocyte samples				Peak areas in the urine samples					Diagnostic ions
						0h	1h	3h	5h	#1 HYD	#2 HYD	#3 HYD	#4 HYD	#5 HYD	
										NON-HYD	NON-HYD	NON-HYD	NON-HYD	NON-HYD	
										1.2E+06	ND	2.5E+05	ND	ND	
A18	Carbonylation + Hydroxylation	5.88	$C_{21}H_{24}N_2O_3$	353.1852	-1.94	ND	2.4E+04	2.8E+04	2.5E+04	7.1E+06	2.3E+04	8.8E+05	ND	1.9E+05	118.0651, 132.0806, 164.0704, 202.1215
										8.0E+06	2.5E+04	1.1E+06	ND	2.1E+05	
A19	Dihydroxylation	5.89	$C_{21}H_{26}N_2O_3$	355.2010	-2.56	ND	ND	ND	ND	3.2E+06	ND	1.3E+06	ND	5.5E+04	91.0540, 105.0694, 188.1433
										6.4E+05	ND	3.0E+05	ND	ND	
A20	Hydroxylation + Glucuronidation	5.90	$C_{27}H_{34}N_2O_8$	515.2380	-1.85	ND	ND	ND	ND	7.4E+05	ND	7.9E+04	ND	ND	186.1280, 321.1947
										1.1E+06	ND	7.9E+04	ND	ND	
A21	Dihydroxylation + Methylation + Sulfation	5.93	$C_{22}H_{28}N_2O_6S$	449.1741	0.14	ND	ND	ND	ND	ND	ND	ND	ND	ND	84.0806, 119.0483, 151.0748, 234.1476
										6.0E+06	4.5E+04	8.6E+05	ND	1.2E+05	
A22	Dihydroxylation + Sulfation	6.12	$C_{21}H_{26}N_2O_6S$	435.1582	-0.21	ND	ND	ND	ND	ND	ND	ND	ND	ND	84.0809, 137.0581, 220.1336
										7.7E+05	ND	1.3E+05	ND	5.0E+04	
A23	Hydroxylation + sulfation	6.26	$C_{21}H_{26}N_2O_5S$	419.1629	-1.41	ND	ND	ND	ND	ND	ND	ND	ND	ND	84.0805, 121.0636, 186.9208, 204.1377, 339.2067

ID	Biotransformation	RT (min)	Elemental composition	*m/z*	mass error (ppm)	Peak areas in the hepatocyte samples				Peak areas in the urine samples					Diagnostic ions
						0h	1h	3h	5h	#1 HYD	#1 NON-HYD	#2 HYD	#2 NON-HYD	#3 HYD	#3 NON-HYD	#4 HYD	#4 NON-HYD	#5 HYD	#5 NON-HYD	
										2.5E+05	ND	1.0E+05	ND	ND					
A24	Hydroxylation	6.30	$C_{21}H_{26}N_2O_2$	339.2071	0.56	ND	1.4E+06	2.5E+06	2.9E+06	2.4E+07	4.1E+06	2.1E+07	2.2E+05	6.2E+06	84.0806, 103.0535, 121.0643, 204.1385
										1.9E+07	8.5E+05	1.4E+07	ND	1.3E+06	
A25	Hydroxylation	6.46	$C_{21}H_{26}N_2O_2$	339.2063	-1.05	ND	ND	ND	ND	5.7E+06	3.2E+04	8.4E+05	ND	ND	105.0696, 188.1428
										2.4E+06	ND	3.1E+05	ND	ND	
A26	Dihydroxylation + Methylation	6.60	$C_{22}H_{28}N_2O_3$	369.2189	3.1	ND	1.1E+05	1.5E+05	1.7E+05	2.4E+07	3.9E+06	2.1E+07	8.6E+05	8.6E+06	91.0542, 119.0490, 151.0758, 234.1487
										1.5E+07	4.3E+05	1.1E+07	9.5E+04	1.1E+06	
A27	Dihydroxylation + Methylation	6.72	$C_{22}H_{28}N_2O_3$	369.2168	-1.28	ND	ND	ND	ND	2.5E+06	ND	4.4E+05	ND	4.8E+04	84.0807, 105.0698, 188.1426
										2.6E+05	ND	5.8E+04	ND	ND	
A28	Hydroxylation	6.74	$C_{21}H_{26}N_2O_2$	339.2063	-0.81	ND	ND	ND	ND	4.9E+06	3.5E+04	7.7E+05	ND	ND	105.0697, 188.1430
										9.2E+05	ND	ND	ND	ND	
A29	Dihydroxylation + Methylation	6.87	$C_{22}H_{28}N_2O_3$	369.2183	1.91	ND	ND	ND	ND	1.2E+07	2.2E+05	7.9E+06	7.2E+04	7.9E+05	91.0540, 119.0488, 151.0750, 234.1477
										2.8E+05	ND	1.5E+05	ND	ND	

ID	Biotransformation	RT (min)	Elemental composition	*m/z*	mass error (ppm)	Peak areas in the hepatocyte samples				Peak areas in the urine samples					Diagnostic ions
						0h	1h	3h	5h	#1 HYD	#2 HYD	#3 HYD	#4 HYD	#5 HYD	
										NON-HYD	NON-HYD	NON-HYD	NON-HYD	NON-HYD	
A30	Hydroxylation	7.00	$C_{21}H_{26}N_2O_2$	339.2063	-1.21	ND	2.9E+05	5.9E+05	7.3E+05	1.2E+07	1.1E+05	2.7E+06	ND	ND	91.0537, 105.0691, 132.0806, 186.1278, 204.1392
										1.1E+07	9.8E+04	1.5E+06	ND	ND	
A31	Hydroxylation + Amide hydrolysis	7.24	$C_{19}H_{24}N_2O$	297.1954	-3.92	ND	ND	ND	ND	9.8E+04	ND	6.9E+04	ND	4.7E+04	103.0545, 121.0637
										8.5E+04	ND	4.6E+04	ND	3.8E+04	
P	Acetylfentanyl	7.92	$C_{21}H_{26}N_2O$	323.2120	0.49	2.5E+07	2.4E+07	2.2E+07	2.1E+07	2.5E+07	1.7E+07	2.1E+07	6.7E+05	4.3E+06	105.0697, 132.0801, 188.1434
										2.6E+07	1.7E+07	2.1E+07	7.3E+05	4.8E+06	
A32	Amide hydrolysis	9.09	$C_{19}H_{24}N_2$	281.2009	-1.19	ND	ND	ND	ND	3.8E+05	ND	2.7E+06	ND	4.9E+05	105.0696, 134.0955, 188.1423
										4.0E+04	ND	2.9E+06	ND	5.5E+05	

HYD: hydrolysed; NON-HYD: non-hydrolysed; ND: Not detected; RT: retention time, P: parent compound

hepatocyte, hydrolysed, and non-hydrolysed urine samples, while Figure 6-2 shows the proposed metabolic pathway of acetylfentanyl and Supplementary Figure 6-1, in the appendix to this chapter, shows the MS/MS spectra of selected metabolites and their proposed fragment pattern.

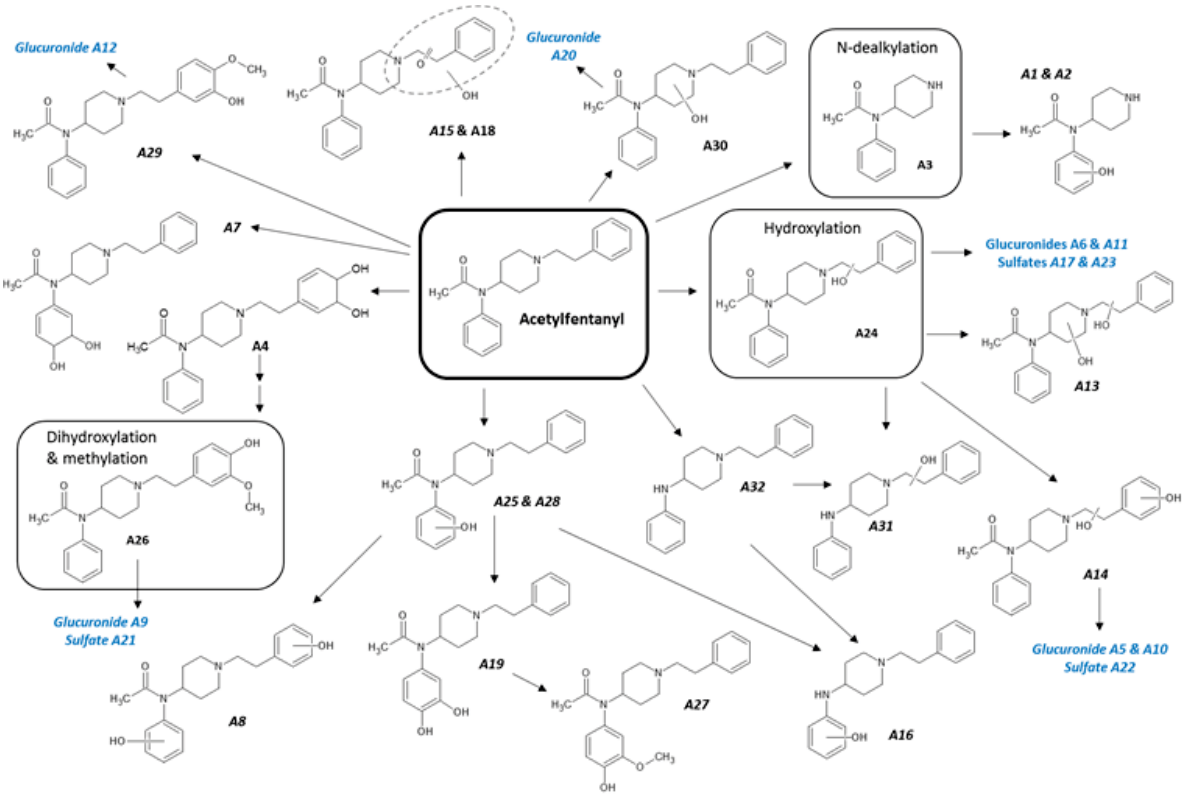

Figure 6-2. Proposed metabolic pathway of acetylfentanyl combining both human hepatocyte and human urine metabolites. Markush structures are used where the exact position of functional groups cannot be determined. Enclosed metabolites are the major metabolites detected in hydrolysed human urine samples; metabolites in italics were only found in either the *in vitro* or *in vivo* experiment.

6.4.2 Metabolic profile of acrylfentanyl

For acrylfentanyl, a total of 14 metabolites were identified with mass error ≤4.48 ppm (B1 to B14). The observed biotransformations were *N*-dealkylation (B1), monohydroxylation (B9, B10, B13) followed by glucuronidation (B3), dihydroxylation (B7, B8) followed by glucuronidation (B5), dihydrodiol formation (B2, B6), dihydroxylation with methylation (B11, B12) followed by glucuronidation (B4) or amide hydrolysis (B14). Acrylfentanyl was present in high abundance in all samples. Metabolite retention times were between 5.25 and 9.06 min; the parent eluted at 8.85 min. Preferred

molecular site of hydroxylation was the ethylphenyl moiety. In hepatocytes, eight metabolites were observed (B1, B2, B6, B9, B10, B11, B13, and B14), of which the nor-metabolite B1 and the monohydroxylated metabolites B13 and B9 were the most abundant metabolites after 5 h incubation. In hydrolysed urine samples, 12 metabolites were detected with B1 being the major metabolite followed by B9 and B8. In total, three glucuronides B3, B4, and B5 were identified, which could be successfully hydrolysed by the enzyme mixture, notably increasing the peak areas of the corresponding aglycones B9, B11, and B8. Table 6-2 provides an overview on all acrylfentanyl metabolites; Figure 6-3 depicts the proposed metabolic pathway, and Supplementary Figure 6-2, in the appendix to this chapter, shows MS/MS spectra of metabolites and their proposed fragmentation pattern.

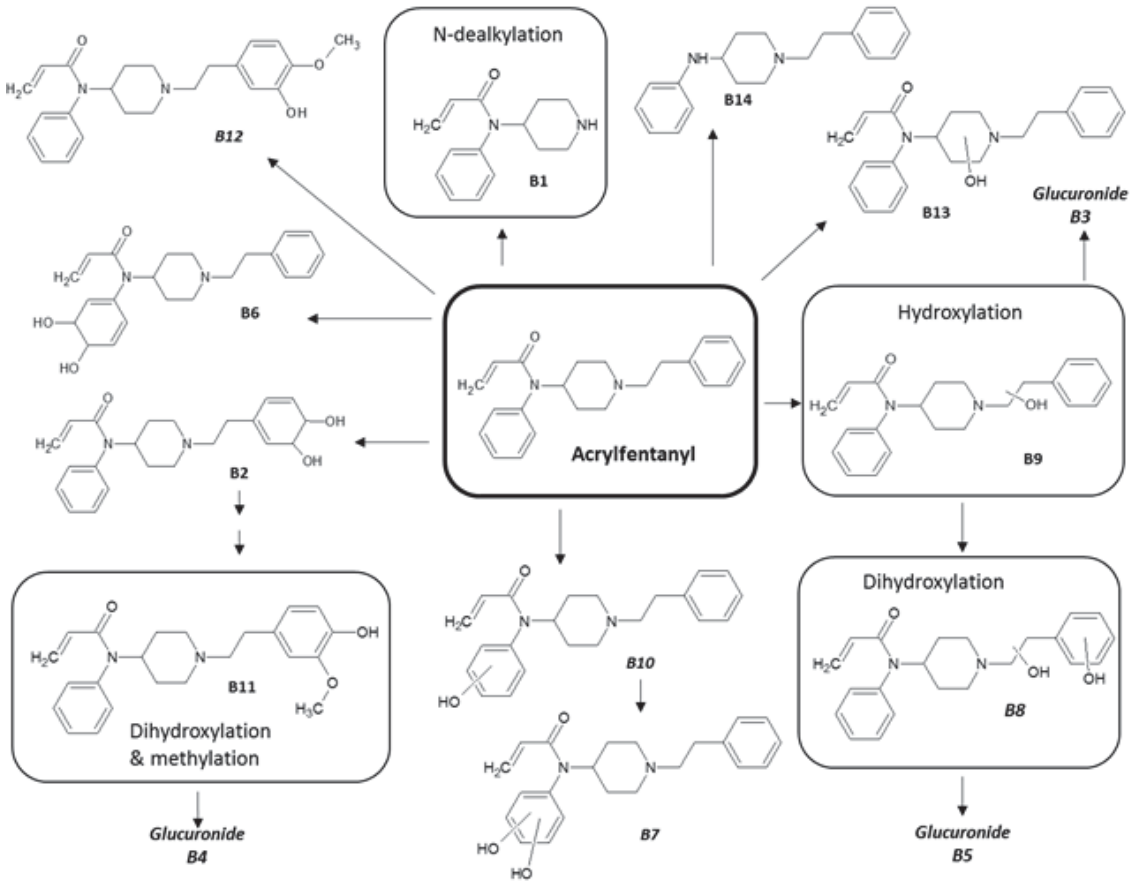

Figure 6-3. Proposed metabolic pathway of acrylfentanyl combining both human hepatocyte and human urine metabolites. Markush structures are used where the exact position of functional groups cannot be determined. Enclosed metabolites are the major metabolites detected in hydrolysed human urine samples, metabolites in italics were only found in either the *in vitro* or *in vivo* experiment.

Table 6-2. Acrylfentanyl metabolites with proposed biotransformation, retention time, elemental composition, accurate mass of protonated molecule, mass error of proposed metabolite, MS peak areas in hepatocyte samples (0h, 1h, 3h and 5h) and in five urine samples (hydrolysed and non-hydrolysed), and diagnostic product ions (masses and mass errors generally taken from sample #3, except for B12 (#2), B1 and B14 (#5) and B10 (hepatocytes).

ID	Biotransformation	RT (min)	Elemental composition	*m/z*	Mass error (ppm)	Peak areas in the hepatocyte samples				Peak areas in the urine samples					Diagnostic ions
						0h	1h	3h	5h	#1 HYD	#2 HYD	#3 HYD	#4 HYD	#5 HYD	
										NON-HYD	NON-HYD	NON-HYD	NON-HYD	NON-HYD	
	Blood acrylfentanyl concentration (in ng/g)									0.06	1.20	0.10	0.05	0.11	
B1	*N*-Dealkylation (yielding nor-metabolite)	5.25	$C_{14}H_{18}N_2O$	231.1503	4.48	5.0E+04	3.5E+06	6.5E+06	8.2E+06	2.0E+06	3.2E+05	1.3E+07	2.1E+06	5.1E+06	84.0804
										1.5E+06	2.1E+05	1.1E+07	1.2E+06	3.4E+06	
B2	Dihydrodiol formation (at ethylphenyl)	5.65	$C_{22}H_{28}N_2O_3$	369.2172	-0.09	ND	1.3E+05	2.2E+05	2.6E+05	7.2E+05	3.5E+05	2.4E+06	1.2E+05	6.2E+05	121.0648, 146.0966, 158.0957, 200.1067
										3.4E+05	ND	4.9E+05	3.7E+04	1.3E+05	
B3	Hydroxylation (at ethyl) + Glucuronidation	5.78	$C_{28}H_{34}N_2O_8$	527.2381	-0.93	ND	ND	ND	ND	ND	ND	3.4E+05	ND	ND	103.0546, 121.0646, 204.1361, 351.2007
										1.3E+05	1.3E+05	7.9E+05	2.4E+04	3.0E+05	
B4	Dihydroxylation + Methylation + Glucuronidation	5.92	$C_{29}H_{36}N_2O_9$	557.2497	0.97	ND	ND	ND	ND	ND	ND	2.1E+05	ND	ND	91.0559, 151.0762, 234.1470
										6.5E+04	1.2E+05	4.5E+05	ND	9.6E+04	
B5	Dihydroxylation (at ethylphenyl) + Glucuronidation	6.01	$C_{28}H_{34}N_2O_9$	543.2338	0.29	ND	ND	ND	ND	ND	ND	ND	ND	ND	84.0813, 137.0599, 220.1343
										1.9E+04	ND	1.4E+05	ND	3.7E+04	

ID	Biotransformation	RT (min)	Elemental composition	*m/z*	Mass error (ppm)	Peak areas in the hepatocyte samples				Peak areas in the urine samples					Diagnostic ions
						0h	1h	3h	5h	#1 HYD	#2 HYD	#3 HYD	#4 HYD	#5 HYD	
										NON-HYD	NON-HYD	NON-HYD	NON-HYD	NON-HYD	
B6	Dihydrodiol formation (*N*-phenyl ring)	6.01	$C_{22}H_{28}N_2O_3$	369.2175	0.55	ND	1.9E+05	4.8E+05	7.3E+05	3.5E+05	7.4E+05	3.0E+06	7.4E+05	2.6E+06	105.0696, 188.1428
										2.3E+05	ND	1.3E+06	2.9E+05	1.1E+06	
B7	Dihydroxylation (at *N*-phenyl or acryl moiety)	6.53	$C_{22}H_{26}N_2O_3$	367.2022	1.6	ND	ND	ND	ND	ND	ND	1.7E+05	ND	ND	105.0695, 188.1441
										ND	ND	ND	ND	ND	
B8	Dihydroxylation (at phenethyl moiety)	6.72	$C_{22}H_{26}N_2O_3$	367.2028	2.54	ND	ND	ND	ND	8.1E+05	3.3E+05	5.6E+06	1.3E+05	1.5E+06	84.0807, 91.0541, 119.0485, 137.0597, 220.1330
										7.8E+04	6.8E+04	9.9E+05	ND	5.9E+04	
B9	Hydroxylation (at ethyl)	7.28	$C_{22}H_{26}N_2O_2$	351.2075	1.8	ND	4.2E+05	6.6E+05	8.6E+05	1.1E+06	1.3E+06	5.4E+06	3.8E+05	3.5E+06	103.0541, 121.0646, 204.1384
										1.1E+05	1.5E+05	3.3E+05	4.9E+04	2.6E+05	
B10	Hydroxylation (at *N*-phenyl or acryl moiety)	7.47	$C_{22}H_{26}N_2O_2$	351.2072	1.13	ND	1.6E+05	1.8E+05	1.9E+05	ND	ND	ND	ND	ND	105.0696, 188.1370
										ND	ND	ND	ND	ND	
B11	Dihydroxylation + Methylation (both at phenyl moiety)	7.54	$C_{23}H_{28}N_2O_3$	381.2174	0.33	ND	1.7E+04	2.6E+04	3.3E+04	4.6E+05	1.0E+06	2.9E+06	1.1E+05	8.1E+05	91.0542, 119.0493, 151.0755
										ND	7.0E+04	1.0E+05	ND	ND	
B12	Dihydroxylation + Methylation (both at phenyl moiety)	7.8	$C_{23}H_{28}N_2O_3$	381.2179	1.3	ND	ND	ND	ND	ND	7.2E+04	7.9E+04	ND	2.7E+04	91.0532, 119.0879, 151.0736
										ND	ND	ND	ND	ND	

ID	Biotransformation	RT (min)	Elemental composition	*m/z*	Mass error (ppm)	Peak areas in the hepatocyte samples				Peak areas in the urine samples					Diagnostic ions
						0h	1h	3h	5h	#1 HYD	#1 NON-HYD	#2 HYD	#2 NON-HYD	#3 HYD	#3 NON-HYD	#4 HYD	#4 NON-HYD	#5 HYD	#5 NON-HYD	
B13	Hydroxylation (at piperidinyl)	7.94	$C_{22}H_{26}N_2O_2$	351.2071	1.18	ND	3.9E+05	7.5E+05	9.8E+05	ND	ND	2.8E+04	ND	3.5E+05	1.3E+05	8.1E+04	ND	2.1E+05	7.4E+04	91.0533, 105.0688, 186.1282
P	Acrylfentanyl	8.85	$C_{22}H_{26}N_2O$	335.213	2.99	2.6E+07	2.4E+07	2.3E+07	2.1E+07	8.8E+05	7.0E+05	1.3E+06	9.2E+05	6.6E+06	5.4E+06	2.7E+06	1.7E+06	7.1E+06	5.3E+06	105.0697, 188.1441
B14	Amide hydrolysis	9.06	$C_{19}H_{24}N_2$	281.2015	1.09	ND	3.1E+04	6.4E+04	7.2E+04	ND	ND	1.6E+04	ND	ND	2.2E+04	ND	ND	9.8E+04	5.6E+04	105.0687, 188.1433

HYD hydrolysed, *NON-HYD* non-hydrolysed, *ND* Not detected, *RT* retention time, *P* parent compound

6.4.3 Metabolic profile of 4-fluoro-isobutyrylfentanyl

For 4-fluoro-isobutyrylfentanyl, 17 metabolites were identified (C1 to C17) with mass error ≤5.09 ppm. The metabolites were generated by *N*-dealkylation (C3), hydroxylation (C7, C8, C10, C11, C15, C17) followed by glucuronidation (C5), dihydroxylation (C9), dihydrodiol formation (C4), dihydroxylation with methylation (C12, C13) followed by glucuronidation (C6), amide hydrolysis (C14), oxidative *N*-dealkylation and further reduction of the keto group (C1), carboxylation (C2), and carbonylation (C16). Retention times were between 4.08 and 11.48 min; the *N*-oxide metabolite C17 eluted after the parent (RT 10.38 min). The parent drug was the most or second most abundant peak in hepatocyte and urine samples. In hepatocytes, nine metabolites were observed (C3, C8, C10, C12, C14–C17), of which the nor-metabolite C3 was the major metabolite in the 5-h sample, followed by the monohydroxylated metabolites C15 and C10. In hydrolysed urine, 11 metabolites were detected (C1, C2, C3, C4, C7, C9–C13, C15), and although the subset was different from the one in hepatocytes, the major metabolites were almost identical with the only difference that hydroxymethoxy 4-fluoro-isobutyrylfentanyl (C12) was also abundant. In non-hydrolysed urine, two additional glucuronides C5 and C6 were found. They were completely cleaved by hydrolysis, which was reflected in a significant peak area increase of C15 and C12, respectively. Table 6-3 provides an overview on all 4-fluoro-isobutyrylfentanyl metabolites; Figure 6-4 depicts the proposed metabolic pathway, and Supplementary Figure 6-3, in the appendix to this chapter, shows MS/MS spectra of metabolites and their proposed fragmentation patterns.

6.4.4 Metabolic profile of furanylfentanyl

Finally, for furanylfentanyl, 14 metabolites (D1 to D14) were identified with mass error ≤3.11 ppm. With retention times between 3.56 and 9.05 min, all of them eluted before the parent (9.38 min). Metabolites were formed via *N*-dealkylation (D6), hydroxylation (D11, D13), amide hydrolysis (D14) followed by hydroxylation (D4, D8, D12) with glucuronidation (D3) or sulfation (D5), dihydrodiol formation (D10) followed by hydroxylation (D7) or *N*-dealkylation (D1), oxidative *N*-dealkylation and reduction of the keto group (D2), and furanyl ring opening and carboxylation (D9). In contrast to the other three fentanyls, amide hydrolysis and dihydrodiol formation led to the most abundant

Table 6-3. 4-Fluoro-isobutyrylfentanyl metabolites with proposed biotransformation, retention time, elemental composition, accurate mass of protonated molecule, mass error of proposed metabolite, MS peak areas in hepatocyte samples (0h, 1h, 3h and 5h) and in five urine samples (hydrolysed and non-hydrolysed), and diagnostic product ions (masses and mass errors generally taken from sample #3, except for C2 (#1) and C8, C14, C16 and C17 (hepatocytes).

ID	Biotransformation	RT (min)	Elemental composition	*m/z*	Mass error (ppm)	Peak areas in hepatocytes				Peak areas in urine samples				Diagnostic ions
						0h	1h	3h	5h	#1 HYD	#2 HYD	#3 HYD	#4 HYD	
										NON-HYD	NON-HYD	NON-HYD	NON-HYD	
	Blood 4-fluoro-isobutyrylfentanyl concentration (in ng/g)									78	3.2	102	46	
C1	Oxidative *N*-dealkylation + reduction	4.08	$C_{13}H_{19}NO$	206.1543	-0.57	ND	ND	ND	ND	1.2E+06	ND	2.3E+04	ND	105.0698
										1.1E+06	ND	2.2E+04	ND	
C2	Carboxylation	6.64	$C_{23}H_{27}FN_2O_3$	399.2101	5.09	ND	ND	ND	ND	1.3E+05	ND	ND	ND	105.0689, 188.1443
										ND	ND	ND	ND	
C3	*N*-dealkylation	7.23	$C_{15}H_{21}FN_2O$	265.1710	-0.38	4.9E+04	5.0E+06	8.1E+06	9.2E+06	1.5E+07	3.8E+06	1.2E+07	3.0E+06	84.0806
										1.5E+07	3.8E+06	1.2E+07	3.3E+06	
C4	Dihydrodiol formation (at ethylphenyl)	7.46	$C_{23}H_{31}FN_2O_3$	403.2387	-0.51	ND	4.6E+04	8.0E+04	9.8E+04	2.3E+05	2.9E+04	6.9E+05	1.6E+05	121.0639, 150.0701, 164.0874, 207.1286, 234.1250
C5	Hydroxylation + glucuronidation	7.51	$C_{29}H_{37}FN_2O_8$	561.2607	-0.11	ND	ND	ND	ND	2.3E+05	3.0E+04	7.6E+05	1.9E+05	103.0512, 121.0644, 204.1406
										ND	ND	ND	ND	
										4.2E+04	1.2E+04	1.7E+05	1.5E+04	
C6	Di-hydroxylation & methylation & glucuronidation	7.6	$C_{30}H_{39}FN_2O_9$	591.2714	-0.28	ND	ND	ND	ND	ND	ND	ND	ND	84.0808, 119.0486, 151.0747, 234.1486, 415.2304

ID	Biotransformation	RT (min)	Elemental composition	*m/z*	Mass error (ppm)	Peak areas in hepatocytes				Peak areas in urine samples				Diagnostic ions
						0h	1h	3h	5h	#1	#2	#3	#4	
										HYD	HYD	HYD	HYD	
										NON-HYD	NON-HYD	NON-HYD	NON-HYD	
										2.9E+04	2.8E+04	2.0E+05	1.2E+04	
C7	Hydroxylation	7.97	$C_{23}H_{29}FN_2O_2$	385.2283	-1.02	ND	ND	ND	ND	7.1E+04	ND	1.0E+05	1.9E+04	105.0693, 188.1407
										5.7E+04	ND	5.9E+04	ND	
C8	Hydroxylation	8.28	$C_{23}H_{29}FN_2O_2$	385.2294	1.67	ND	7.9E+04	1.5E+05	2.0E+05	ND	ND	ND	ND	105.0698, 188.1434
										ND	ND	ND	ND	
C9	Dihydroxylation	8.44	$C_{23}H_{29}FN_2O_3$	401.2231	-0.66	ND	ND	ND	ND	9.1E+04	3.7E+04	1.5E+06	5.0E+04	84.0805, 91.0534, 119.0484, 137.0590, 220.1323
										ND	ND	6.9E+04	1.9E+04	
C10	Hydroxylation	8.95	$C_{23}H_{29}FN_2O_2$	385.2284	-0.65	ND	1.7E+05	2.9E+05	4.0E+05	1.0E+06	1.9E+05	3.1E+06	1.7E+05	103.0543, 121.0645, 204.1368
										3.7E+05	4.2E+04	6.3E+05	6.2E+04	
C11	Hydroxylation	9.15	$C_{23}H_{29}FN_2O_2$	385.2282	-0.40	ND	ND	ND	ND	8.1E+04	ND	9.2E+04	2.5E+04	84.0804, 121.0642, 204.1368
										ND	ND	ND	ND	
C12	Di-hydroxylation & methylation	9.17	$C_{24}H_{31}FN_2O_3$	415.2395	0.62	ND	1.8E+04	3.1E+04	5.3E+04	5.6E+05	4.6E+05	3.5E+06	1.6E+05	84.0810, 91.0537, 119.0493, 151.0751, 234.1474

ID	Biotransformation	RT (min)	Elemental composition	*m/z*	Mass error (ppm)	Peak areas in hepatocytes				Peak areas in urine samples				Diagnostic ions
						0h	1h	3h	5h	#1 HYD	#1 NON-HYD	#2 HYD	#2 NON-HYD	#3 HYD	#3 NON-HYD	#4 HYD	#4 NON-HYD	
										8.3E+04		3.3E+04		3.6E+05		3.7E+04		
C13	Di-hydroxylation & methylation	9.37	$C_{24}H_{31}FN_2O_4$	415.2393	0.34	ND	ND	ND	ND	ND		ND		7.3E+04		1.3E+04		84.0801, 91.0523, 119.0473, 151.0744, 234.1421
										ND		ND		ND		ND		
C14	Amide hydrolysis	9.40	$C_{19}H_{23}FN_2$	299.1923	1.71	ND	2.7E+04	3.4E+04	8.9E+04	ND		ND		ND		ND		105.0699, 132.0808, 164.0870, 188.1431
										ND		ND		ND		ND		
C15	Hydroxylation	9.56	$C_{23}H_{29}FN_2O_2$	385.2280	-1.04	ND	1.7E+06	2.7E+06	3.8E+06	4.0E+06		1.8E+05		1.2E+06		1.6E+05		91.0547, 105.0701, 132.0810, 150.0709, 174.1281, 186.1275, 204.1365
										1.9E+06		1.2E+05		7.9E+05		7.7E+04		
C16	Carbonylation	10.16	$C_{23}H_{27}FN_2O_2$	383.2125	-1.12	ND	2.1E+04	2.5E+04	3.3E+04	ND		ND		ND		ND		91.0532, 148.0752, 174.0921, 202.1201
										ND		ND		ND		ND		
P	4-fluoro-isobutyrylfentanyl	10.38	$C_{23}H_{29}FN_2O$	369.2343	1.10	2.6E+07	2.4E+07	2.2E+07	2.2E+07	1.2E+07		3.6E+05		6.8E+06		1.9E+06		105.0698, 188.1434

ID	Biotransformation	RT (min)	Elemental composition	*m/z*	Mass error (ppm)	Peak areas in hepatocytes				Peak areas in urine samples				Diagnostic ions
						0h	1h	3h	5h	#1 HYD	#2 HYD	#3 HYD	#4 HYD	
										NON-HYD	NON-HYD	NON-HYD	NON-HYD	
										1.2E+07	3.8E+05	7.0E+06	2.2E+06	
C17	Hydroxylation	11.48	$C_{23}H_{29}FN_2O_2$	385.2296	2.43	ND	2.0E+05	3.1E+05	3.1E+05	ND	ND	ND	ND	105.0700, 164.0869
										ND	ND	ND	ND	

HYD hydrolysed, *NON-HYD* non-hydrolysed, *ND* Not detected, *RT* retention time, *P* parent compound

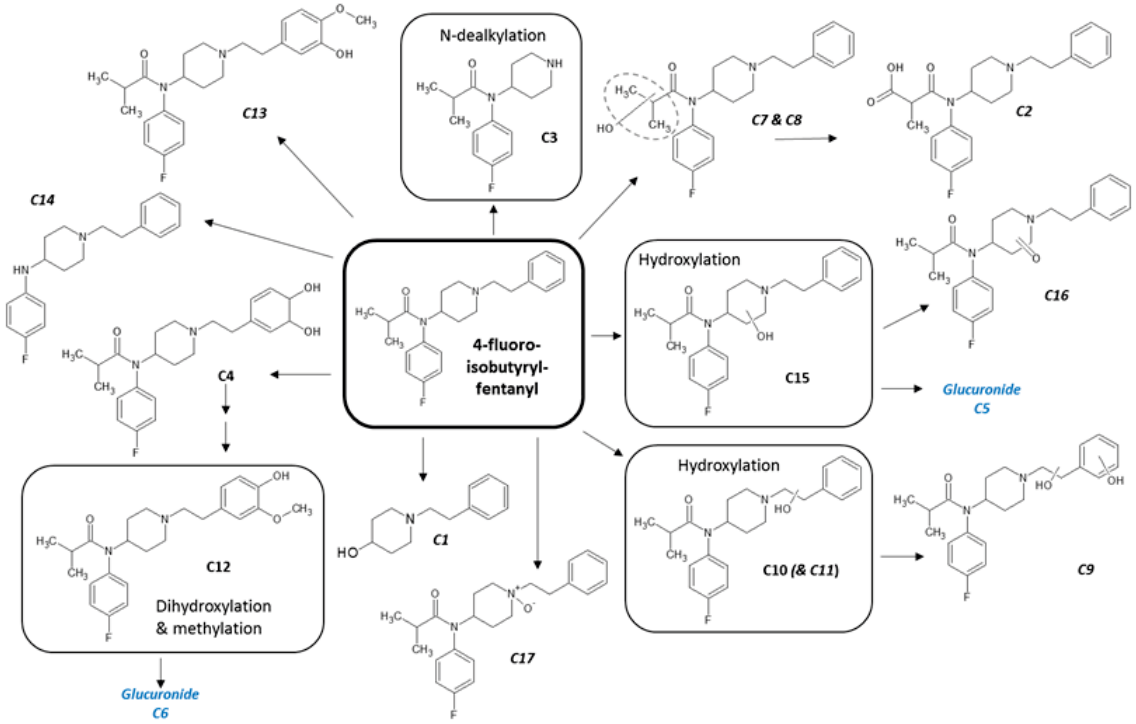

Figure 6-4. Proposed metabolic pathway of 4-fluoro-isobutyrylfentanyl combining both human hepatocyte and human urine metabolites. Markush structures are used where the exact position of functional groups cannot be determined. Enclosed metabolites are the major metabolites detected in hydrolysed human urine samples, metabolite in italics were only found in either the *in vitro* or *in vivo* experiment.

phase I metabolites in urine samples, and although *N*-dealkylation was the second most common reaction in hepatocytes, the nor-metabolite D6 was only minor in urine. Furanylfentanyl was abundant in hepatocytes over the whole incubation time, but showed less intense signals compared to the other fentanyl analogue parents in the five urine samples. In hepatocytes, all metabolites but D3 were found. The amide hydrolysis metabolite D14 was the major metabolite; the nor-metabolite D6 and the dihydrodiol metabolite D10 ranked #2 and #3. In hydrolysed urine samples, nine metabolites were detected (D1, D2, D4–D8, D10, D14) with D14 being the most abundant peak followed by D10, then D5. In non-hydrolysed urine samples, one glucuronide (D3) and one sulfate (D5) were found as phase II metabolites. Enzymatic cleavage was successful for the glucuronide resulting in the appearance of D4, but failed for the sulfate. Table 6-4 provides an overview on all furanylfentanyl metabolites; Figure 6-5 depicts the proposed metabolic pathway, and Supplementary Figure 6-4, in the appendix to this chapter, shows MS/MS spectra of metabolites and their proposed fragmentation patterns.

Table 6-4. Furanylfentanyl metabolites with proposed biotransformation, retention time, elemental composition, accurate mass of protonated molecule, mass error of proposed metabolite, MS peak areas in hepatocyte samples (0h, 1h, 3h and 5h) and in five urine samples (hydrolysed and non-hydrolysed), and diagnostic product ions (masses and mass errors generally taken from sample #5, except for D6, D9, D11, D12 and D13 (hepatocytes).

ID	Biotransformation	RT (min)	Elemental composition	*m/z*	Mass error (ppm)	Peak areas in hepatocytes				Peak areas in urine samples				Diagnostic ions
						0h	1h	3h	5h	#1 HYD NON-HYD	#2 HYD NON-HYD	#3 HYD NON-HYD	#4* HYD NON-HYD	
	Blood furanylfentanyl concentration (in ng/g)									0.90 0.90	0.41 0.41	1.10 1.10	0.38 0.38	
D1	*N*-dealkylation + Dihydrodiol formation	3.56	$C_{16}H_{20}N_2O_4$	305.15	-0.98	ND	ND	2.3E+04	3.2E+04	ND ND	ND ND	9.6E+04 7.1E+04	1.1E+05 9.5E+04	84.0789, 146.0595
D2	Oxidative *N*-dealkylation + reduction	4.05	$C_{13}H_{19}NO$	206.155	3.11	ND	1.5E+04	2.2E+04	2.3E+04	ND ND	1.9E+04 ND	7.2E+05 5.0E+05	1.5E+05 9.5E+04	105.0703, 188.1438
D3	Amide hydrolysis + Hydroxylation (*N*-phenyl) + Glucuronidation	4.42	$C_{25}H_{32}N_2O_7$	473.229	1.25	ND	ND	ND	ND	ND ND	ND ND	ND 6.5E+04	ND 2.0E+05	105.0699, 188.1405
D4	Amide hydrolysis + Hydroxylation (*N*-phenyl)	5.65	$C_{19}H_{24}N_2O$	297.196	0.99	ND	1.4E+05	9.8E+05	2.4E+06	ND ND	2.9E+04 ND	5.9E+04 ND	3.9E+05 ND	105.0698, 188.1435
D5	Amide hydrolysis + Hydroxylation (*N*-phenyl) + sulfation	5.77	$C_{19}H_{24}N_2O_4S$	377.153	-0.05	ND	ND	ND	1.2E+04	ND ND	1.6E+05 1.4E+05	6.2E+05 5.3E+05	1.3E+06 1.1E+06	105.0698, 188.1438

ID	Biotransformation	RT (min)	Elemental composition	*m/z*	Mass error (ppm)	Peak areas in hepatocytes				Peak areas in urine samples				Diagnostic ions
						0h	1h	3h	5h	#1 HYD NON-HYD	#2 HYD NON-HYD	#3 HYD NON-HYD	#4* HYD NON-HYD	
D6	*N*-dealkylation (yielding nor-metabolite)	5.79	$C_{16}H_{18}N_2O_2$	271.144	0.52	ND	2.8E+06	4.9E+06	4.0E+06	ND ND	ND ND	3.5E+04 2.6E+04	ND ND	84.0810, 95.0128, 188.0694
D7	Dihydrodiol formation + Hydroxylation (ethyl)	5.82	$C_{24}H_{28}N_2O_5$	425.207	0.82	ND	1.9E+04	3.8E+04	2.7E+04	ND ND	2.3E+05 1.4E+05	1.6E+05 7.9E+04	4.6E+05 2.8E+05	103.0562, 121.0649
D8	Amide hydrolysis + Hydroxylation (ethyl)	7.19	$C_{19}H_{24}N_2O$	297.196	-0.03	ND	6.5E+04	2.0E+05	2.6E+05	ND ND	4.1E+04 ND	1.2E+05 7.4E+04	2.6E+05 1.6E+05	103.0529, 121.0646
D9	Furan ring opening + Carboxylation	7.38	$C_{24}H_{28}N_2O_3$	393.2175	0.25	ND	ND	ND	3.0E+04	ND ND	ND ND	ND ND	ND ND	105.0693, 188.1448
D10	Dihydrodiol formation	7.5	$C_{24}H_{28}N_2O_4$	409.212	-0.34	ND	1.8E+06	3.5E+06	2.9E+06	ND ND	4.8E+05 3.0E+05	2.3E+05 1.8E+05	1.3E+06 9.5E+05	105.0698, 188.1440
D11	Hydroxylation (ethyl)	7.86	$C_{24}H_{26}N_2O_3$	391.2018	0.99	ND	4.6E+04	3.7E+04	1.4E+04	ND ND	ND ND	ND ND	ND ND	121.0649
D12	Amide hydrolysis + Hydroxylation (piperidine)	7.99	$C_{19}H_{24}N_2O$	297.1963	0.96	ND	3.3E+05	1.1E+06	1.3E+06	ND ND	ND ND	ND ND	ND ND	91.0539, 105.0690, 132.0818

ID	Biotransformation	RT (min)	Elemental composition	*m/z*	Mass error (ppm)	Peak areas in hepatocytes				Peak areas in urine samples				Diagnostic ions
						0h	1h	3h	5h	#1	#2	#3	#4*	
										HYD	HYD	HYD	HYD	
										NON-HYD	NON-HYD	NON-HYD	NON-HYD	
D13	Hydroxylation (probably at piperidine)	8.52	$C_{24}H_{26}N_2O_3$	391.2024	1.65	ND	4.1E+05	4.3E+05	1.8E+05	ND	ND	ND	ND	91.0538, 132.0792
										ND	ND	ND	ND	
D14	Amide hydrolysis	9.05	$C_{19}H_{24}N_2$	281.202	1.22	2.0E+04	1.0E+07	1.7E+07	1.8E+07	5.9E+04	4.9E+05	5.4E+05	3.8E+06	105.0697, 188.1433
										ND	3.5E+05	3.8E+05	2.9E+06	
P	Furanylfentanyl	9.38	$C_{24}H_{26}N_2O_2$	375.207	0.62	2.5E+07	2.1E+07	1.6E+07	1.0E+07	1.6E+04	3.8E+05	6.7E+04	2.2E+06	105.0699, 188.1433
										1.5E+04	2.9E+05	1.8E+05	1.6E+06	

HYD hydrolysed, *NON-HYD* non-hydrolysed, *ND* Not detected, *RT* retention time, *P* parent compound
* The corresponding blood sample of urine #4 contained 1.2 ng/g fentanyl.

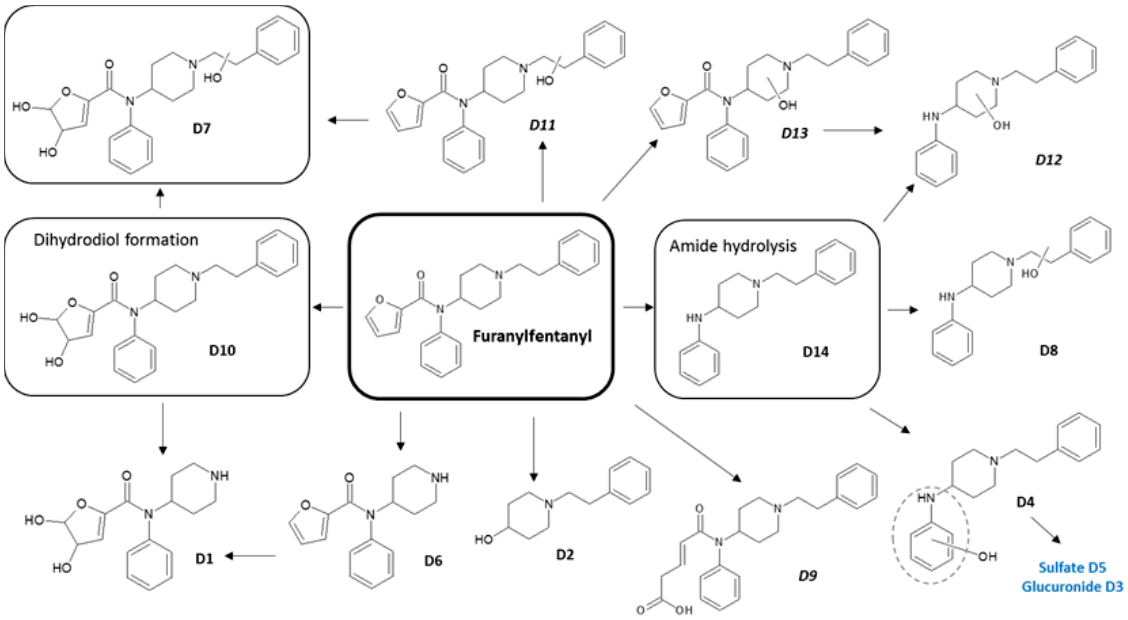

Figure 6-5. Proposed metabolic pathway of furanylfentanyl combining both human hepatocyte and human urine metabolites. Markush structures are used where the exact position of functional groups cannot be determined. Enclosed metabolites are the major metabolites detected in hydrolysed human urine samples, metabolite in italics were only found in either the *in vitro* or *in vivo* experiment.

6.5 Discussion

6.5.1 Structural elucidation of metabolites

All four fentanyl analogues investigated in this study shared the phenethylpiperidine substructure. Upon collision-induced dissociation, several characteristic fragments can be derived from it, which were used to determine the type of biotransformation and where it could have occurred: If the phenethylpiperidine structure is unchanged, as is the case in all parent molecules and many metabolites, two major signals are usually found in the MS/MS spectrum: one at *m/z* 105.0699, associated with the phenethyl moiety, and one at *m/z* 188.1434, corresponding to the complete structure. Depending on the compound's peak intensity and preferred fragmentation behaviour, also minor fragments at *m/z* 84.0808 (unchanged piperidine ring) or 132.0808 (phenethyliminomethylium ion) can be detectable.

6.5.1.1 Acetylfentanyl metabolites

The MS/MS spectrum of acetylfentanyl showed the three aforementioned peaks at *m/z* 105.0697, 132.0801, and 188.1434. The most abundant metabolite A3 was the nor-metabolite, which is generated by *N*-dealkylation at the piperidine nitrogen resulting in a loss of the phenethyl moiety. The MS/MS spectrum showed one intense fragment ion at *m/z* 84.0805 but lacked *m/z* 105.0699 and 188.1434. Minor fragment ions were observed at *m/z* 94.0645 (anilinyl moiety) and 136.0750 (*N*-phenylacetamide moiety). Hydroxylation of A3 yielded A1 and A2 with the major fragment ion at *m/z* 84.0809 and 84.0803, respectively, suggesting the position of hydroxylation at the acetyl moiety or *N*-phenyl ring.

Monohydroxylated metabolites were identified by the addition of 15.9949 u (+O) to the mass of acetylfentanyl: The most abundant hydroxy metabolite A24 was hydroxylated at the ethyl linker as indicated by *m/z* 121.0643 (hydroxyphenethyl) and *m/z* 103.0535, its water loss fragment ion. An aliphatic hydroxy group is likely, because water loss is uncommon at aromatic rings [21]. A25 and A28 were either hydroxylated at the *N*-phenyl ring or the acetyl moiety (*m/z* 188.1428/188.1430). A30 is generated by hydroxylation at

the piperidine ring, which is supported by the fragment ions at *m/z* 105.0691, 204.1392 (hydroxyphenethylpiperidinyl) and the corresponding water loss peak at *m/z* 186.1279.

The four dihydroxylated metabolites were identified by a mass shift of 31.9898 u (+2O) compared to the parent. The most dominant dihydroxylated metabolite was A14, which was hydroxylated once at the ethyl linker and once at the adjacent phenyl ring. The fragment ions at *m/z* 220.1330 and 137.0595 can be associated with dihydroxyphenethylpiperidine and dihydroxyphenethyl, respectively, while *m/z* 119.0488 represents the corresponding water loss ion from *m/z* 137.0595. A8 is suggested to be hydroxylated once on each phenyl ring; the presence of *m/z* 121.0648 and the absence of *m/z* 103.0542 indicate aromatic hydroxylation, and *m/z* 84.0806 and 204.0378 exclude the possibility of a second hydroxy group at the piperidine ring. A13's MS/MS spectrum showed fragment ions at *m/z* 107.0491 (hydroxytoluene) and *m/z* 202.1230 (water loss ion from *m/z* 220.1332 indicating two hydroxy groups at the phenethylpiperidine moiety). A19 is likely hydroxylated twice at the *N*-phenyl ring (*m/z* 105.0694 and 188.1433) serving as the precursor for A27.

Interestingly, three metabolites generated by dihydroxylation and methylation of one of the hydroxy groups were also observed, one of them (A26) in high abundance: A26 and A29 showed similar characteristic fragment ions. The ions at *m/z* 151.0758 suggest the presence of a hydroxy and a methoxy group at the phenethyl moiety. A loss of methanol will then generate the fragment ion at *m/z* 119.0490. The methylation reaction is probably catalysed by catechol-O-methyltransferase, an enzyme that is involved in the metabolism of catecholic neurotransmitters, such as adrenaline, noradrenaline, and dopamine [22], and xenobiotics like MDMA, MDEA, and MBDB [23]. The literature shows that the hydroxy group in *meta* position is preferred for methylation, suggesting that A26 is methylated there. In contrast, A27 was dihydroxylated and methylated at the *N*-phenyl ring as the phenethyl and piperidinyl moiety remained intact (*m/z* 188.1426).

Two dihydrodiol metabolites (A4 and A7) are formed via the epoxide-diol pathway, which has been described for other phenyl ring-containing drugs as well, such as ethotoin, phenytoin, oxazepam, and rofecoxib [24], as well as benzene [25]. A4, the intense isomer, is modified at the ethylphenyl ring. The fragment ion at *m/z* 222.1489 corresponds to the

ethylphenylpiperidine substructure with dihydrodiol; *m/z* 188.1070 (≠ *m/z* 188.1434) indicates that the *N*-phenyl ring remained unchanged. As a water loss from one of the dihydrodiol hydroxy groups leads to re-aromatization, we suggest that this reaction is extremely favourable explaining the presence of *m/z* 121.1559, but the absence of expected *m/z* 139.0754. A similar phenomenon was observed for a dihydrodiol metabolite of AM2201 [26]. Notably, the dihydrodiol can be further metabolised by dihydrodiol dehydrogenase yielding a catechol – this reaction could produce the intermediate catechol of the two hydroxy methoxy metabolites A26 and A29. A7, only a minor metabolite, is modified at the *N*-phenyl ring (*m/z* 105.0699, 188.1434) and is probably the precursor of A27.

Carbonylation, probably at the ethyl linker (*m/z* 202.1221/202.1215), and hydroxylation, probably at the phenyl or piperidine ring (*m/z* 164.0707/164.0704 and 218.1134/218.1199), produced two almost equally intense metabolites A15 and A18. The fragment ions at m/z 118.0647/118.0651 and *m/z* 132.0806 indicate an unchanged *N*-phenyl ring.

A32 is formed by hydrolysis of the amide functional group cleaving off the acetyl moiety and leaving phenethylpiperidine unchanged (*m/z* 188.1423). Further hydroxylation leads to A16 hydroxylated at *N*-phenyl (*m/z* 188.1416) and A31 hydroxylated at the ethyl linker (*m/z* 121.0637, 103.0545).

In the non-hydrolysed samples, several glucuronides (A5, A6, A9, A10, A11, A12, A20) and sulfates (A17, A21, A22, A23) were detected. Phase II metabolites were assigned to their respective phase I metabolites based on shared fragment ions, consistent elution behaviour, matching relative intensities and increasing peak areas of the phase I metabolite after hydrolysis. Figure 6-2 shows the proposed individual assignments. Surprisingly, two glucuronides (A6 and A11) and two sulfates (A17 and A23), all clearly baseline-separated, were identified as possible conjugates of the abundant monohydroxylated metabolite A24. A possible explanation to explain the occurrence of two distinct glucuronide signals for one phase I metabolite is the formation of diastereomers. If the phase I metabolite has a stereogenic centre (A24 does), the conjugation with another chiral molecule such as glucuronic acid will lead to

diastereomers, which can be separated on non-chiral LC columns [27]. However, this hypothesis does not stand up to the fact that there are also two sulfates formed from A24. Possibly, the broad and intense A24 peak consists of two co-eluting isomers, both hydroxylated at the ethyl linker, but at different positions. The same phenomenon was observed for the dihydroxylated metabolite A14, to which two glucuronides (A5 and A10) could be assigned.

6.5.1.2 Acrylfentanyl metabolites

As expected, acrylfentanyl fragmented to the two major product ions at *m/z* 105.0697 and 188.1441. Similarly to acetylfentanyl, acrylfentanyl underwent *N*-dealkylation at the piperidine nitrogen producing the major nor-metabolite B1 (*m/z* 84.0804 without *m/z* 105.0699 and 188.1434). Monohydroxylated metabolites were either hydroxylated at the ethyl linker in B9 (*m/z* 121.0646, 103.0541), the *N*-phenyl ring or acryl moiety in B10 (*m/z* 105.0696, 188.1370), or the piperidine ring in B13 (*m/z* 105.0688, 186.1261). One of the two dihydroxy metabolites, B7, was dihydroxylated at the *N*-phenyl ring or the acryl moiety (*m/z* 105.0695, 188.1441), while the other one, B8, was hydroxylated once each at the ethyl liker and the adjacent phenyl group as indicated by *m/z* 137.0597 and its water loss fragment at *m/z* 119.0485. In analogy to acetylfentanyl, we detected two dihydrodiol metabolites (B2, B6): one carrying the two hydroxy groups at the ethylphenyl ring (*m/z* 121.0648) and the other one on the *N*-phenyl ring (*m/z* 105.0696, *m/z* 188.1428). Both dihydroxylated/methylated metabolites B11 and B12 carried the hydroxy and methoxy group at the phenyl ring of the phenethyl moiety (*m/z* 151.0755 and 151.0736; *m/z* 119.0493 and 119.0879, the methanol loss fragment ions) and probably originate from B2. In view of strikingly different intensities for both isomers, we suggest that B11 is methylated at the preferred *meta* position and B12 at the less favoured *para* position. Finally, the desacrylated metabolite B14, which is generated by amide hydrolysis, is characterised by the intact phenethylpiperidine moiety (*m/z* 105.0687, 188.1433) and is, in fact, identical to A32. The three glucuronides that were identified in non-hydrolysed urine samples were assigned to the following aglycones based on shared fragment ions: B3 is the glucuronide of monohydroxy metabolite B9, B4 the glucuronide of the abundant dihydroxylated/methylated metabolite B11, and B5 the glucuronide of the most intense dihydroxylated metabolite B8.

6.5.1.3 4-Fluoro-isobutyrylfentanyl metabolites

The MS/MS spectrum of 4-fluoro-isobutyrylfentanyl also showed the major fragment ions at *m/z* 105.0698 and 188.1434. The nor-metabolite C3 was characterised by one single intense product ion at *m/z* 84.0806. Six monohydroxy metabolites were detected: C7 and C8 had an unchanged phenethylpiperidine moiety (*m/z* 105.0693 and 105.0698, 188.1407 and 188.1434, respectively); their relatively early retention time suggests aliphatic hydroxylation at the isobutyryl chain rather than aromatic hydroxylation. The abundant metabolite C10 was hydroxylated at the ethyl linker (*m/z* 103.0543, 121.0645). C11, in contrast, showed an ion at *m/z* 121.0642 but lacked the water loss fragment at *m/z* 103.0542 and hence can be hydroxylated at either the ethyl linker or the adjacent phenyl group. C15, one of the major metabolites, is hydroxylated at the piperidine ring (*m/z* 105.0701, 204.1365). C17 showed product ions at *m/z* 105.0700 and 164.0869 indicating that phenethyl moiety and *N*-phenyl ring are unchanged and leaving the site of modification to the piperidine ring. Interestingly, C17 eluted after the parent drug, which is rather uncommon for the supposedly more polar hydroxy metabolites. This phenomenon has been frequently observed for *N*-oxides; thus, C17 is probably an *N*-oxide [28-30]. The dihydroxylated metabolite C9 was hydroxylated once each at the ethyl linker and at the adjacent phenyl ring (*m/z* 119.0482, 137.0590). Only one dihydrodiol metabolite (C4) was identified, which carried the dihydrodiol substructure at the ethylphenyl ring (*m/z* 121.0639, 234.1250) and likely is the precursor for C12 and C13. Interestingly, the fluoro substituent seems to have blocked dihydrodiol formation at the *N*-phenyl ring. The dihydroxylated/methylated metabolites C12 and C13, similar to acetylfentanyl and acrylfentanyl, were modified at the phenyl ring (*m/z* 119.0493 and 119.0473, 151.0751 and 151.0744, respectively), with the more abundant isomer C12 proposed to be methylated at *meta* position. Amide hydrolysis generated C14 with phenethylpiperidine moiety intact (*m/z* 105.0699, 188.1431) and the isobutyryl chain lost. We also observed oxidative *N*-dealkylation with further reduction of the formed keto group, which generated C1. The whole *N*-fluorophenylisobutamide moiety is cleaved off during this process; the phenethyl moiety remains intact (*m/z* 105.0698). Carboxylation to generate C2 occurred at the isobutyryl chain, the only plausible site (*m/z* 105.0689, 188.1443). C16's MS/MS spectrum displayed a fragment ion at *m/z* 202.1201 indicating a carbonylated phenethylpiperidine moiety. The carbonyl group is proposed to be next to

the piperidine nitrogen, as this would facilitate the formation of *m/z* 148.0751. Further evidence derives from the absence of *m/z* 119.0491, which would be expected, if the carbonyl group was on the phenethyl moiety. In the non-hydrolysed samples, the glucuronides C5 and C6, phase II conjugates of C15 and C12, were detected.

6.5.1.4 Furanylfentanyl metabolites

While acetylfentanyl, acrylfentanyl and 4-fluoro-isobutyrylfentanyl differ only slightly in respect to the substituent at the amide group, furanylfentanyl contains a substantially different structure. Furan is an aromatic, heterocyclic system known to undergo characteristic bioactivation reactions, such as epoxidation and ring scission [31, 32], and the dominance of these reactions significantly affected furanylfentanyl's metabolic profile. Besides, the different structure seemed to favour an otherwise less important reaction, the amide hydrolysis.

Identical to the other analogues, furanylfentanyl generated the common two major fragment ions *m/z* 105.0699 and 188.1425. Amide hydrolysis produced the most abundant metabolite, D14, which showed an intact phenethylpiperidine moiety (*m/z* 105.0697, 188.1433) and could be further metabolised by hydroxylation either at the *N*-phenyl to yield D4 (*m/z* 105.0698, 188.1435), at the ethyl linker to form D8 (*m/z* 103.0529, 121.0646) or at the piperidine ring to generate D12 (*m/z* 105.0690, 186.1269). The second most dominant biotransformation was epoxidation of furan followed by hydration, which yielded the dihydrodiol metabolite D10 (*m/z* 105.0698, 188.1440). Although the MS/MS spectrum does not exclude the possibility of dihydrodiol formation at the *N*-phenyl ring, we suggest that the furan ring is the more probable target [31]. Notably, furan epoxidation or ring opening to an α,β-unsaturated carbonyl intermediate can lead to reactive metabolites as shown for other furan-containing compounds like aflatoxin B1, ipomeanol, and furosemide, which are known to cause hepatic and renal necrosis [31]. D10 was further hydroxylated at the piperidine ring to form D7 (*m/z* 103.0562, 121.0649) or *N*-dealkylated to form the nor-metabolite D1 (*m/z* 84.0789). The nor-metabolite D6, abundant in hepatocytes but minor in human urine, showed the typical fragment ion at *m/z* 84.0810 and also fragment ions at *m/z* 188.0694 (resulting from the loss of piperidine) and *m/z* 95.0128 (further loss of phenylamine). D2 was formed by oxidative *N*-

dealkylation and reduction of the keto group retaining the intact phenethyl moiety (*m/z* 105.0698, 188.1434). D11 and D13 were hydroxylated at the ethyl linker (*m/z* 103.0533, 121.0649) and the piperidine ring (*m/z* 105.0685, 186.1274), respectively. Furanyl ring opening and subsequent carboxylation are proposed to generate D9 with *m/z* 105.0693 and 188.1448. In non-hydrolysed samples, we identified D3 and D5, glucuronide (D3) and sulfate conjugate of D4.

6.5.2 How well did hepatocyte study results correlate with the findings in human urine samples?

In general, major hepatocyte metabolites were in good agreement with major urine metabolites adding to the finding of previous hepatocytes studies that human metabolism can be well predicted by *in vitro* hepatocyte experiments [18, 27, 33]. The same biotransformations were observed, and for each drug, two out of the three major urine metabolites also ranked among the top three metabolites in hepatocytes (three out of four for 4-fluoro-isobutyrylfentanyl). Many deviations between hepatocytes and urine metabolites can be explained by the different time allowed for metabolism, which leads to fewer metabolites in general and a lower prevalence of second-generation or third-generation metabolites in hepatocytes. Another possible reason is the enrichment of polar and conjugated metabolites in urine. Different genotypes and phenotypes of the drug-metabolizing enzymes could be another factor for different metabolic profiles. However, such variance was expected to be reduced, at least partially, in the hepatocyte incubation since a pool from 10 donors was used in this study. For acetylfentanyl, the three most abundant urinary metabolites (#1 hydroxymethoxy metabolite A26, #2 hydroxy metabolite A24, #3 nor-metabolite A3) were also generated by hepatocytes and ranked #4, #2, #1 in terms of abundance in the 5h sample. Similarly, for acrylfentanyl, three out of the four most abundant urinary metabolites (#1 nor-metabolite B1, #2 hydroxy metabolite B9, #3 dihydroxy metabolite B8 and #4 hydroxymethoxy metabolite B11) were also observed in hepatocytes ranking #1, #3 and #8. B8 was not detected, probably due to the relatively short incubation time. For the same reason, i.e. increased prevalence of second-generation and third-generation metabolites in urine, the second most abundant metabolite in hepatocyte B13 only ranked #7 in the case samples. For 4-fluoro-isobutyrylfentanyl, the three most abundant metabolites (#1 nor-metabolite C3, #2

monohydroxy metabolites C10 and C15) were identical for hepatocytes and urine samples. The hydroxymethoxy metabolite C12, #3 in urine samples, ranked #8 in hepatocytes. For furanylfentanyl, the two major urinary metabolites (#1 hydrolysed metabolite D14, #2 dihydrodiol metabolite D10) were detected after hepatocyte incubation ranking #1 and #3. However, the third most abundant metabolite in urine, D7, only ranked #10 and would have never been predicted as an abundant *in vivo* metabolite. In fact, the hepatocyte experiment also suggested high prevalence for the nor-metabolite D6 (#2 in hepatocytes), which strikingly mismatched the actual findings in the urine samples, illustrating the need to analyse *in vivo* human samples. Most likely, the nor-metabolite was further metabolised *in vivo*: We checked the data for second-generation nor-metabolites and found intense signals for a potential nordesfuranyl metabolite at 0.92 min, albeit without MS/MS spectral information. Steuer *et al*. observed a similar phenomenon with butyrylfentanyl, where the nor-metabolite was major in human liver microsome incubations but insignificant in a postmortem human urine and blood sample [34].

It should be noted that phase II conjugation can affect the availability of the phase I metabolite biomarkers. Particularly in acetylfentanyl urine samples, a several-fold increase (up to 50×) in phase I metabolite peak area was not uncommon after hydrolysis. Ten out of 32 metabolites were conjugates. While major metabolites, e.g. A24, A26, and A14, could be both glucuronidated and sulfated, less abundant metabolites, e.g. A29 and A30, were only glucuronidated. Phase II conjugation seemed to play a smaller role in acrylfentanyl, 4-fluoro-isobutyrylfentanyl, and furanylfentanyl metabolism, as we identified only three, two, and two phase II metabolites, respectively. Nevertheless, a hydrolysis step should always be included in the sample preparation.

6.5.3 Which metabolites are suitable analytical targets for urine analysis?

The studied fentanyl analogues were generally highly abundant in urine, indicating that parent drugs are one of the most suitable targets nonetheless. However, all urine samples were from fatal overdose cases; consequently, parent drugs might be less abundant in non-overdose samples. As the window of detection of metabolites is usually longer than for the parent drugs and as the additional presence of metabolites increases the plausibility

of the results, it is useful to target not only one but two or three compounds including metabolites.

Target metabolites should generally be abundant, specific of the parent drug, and prevalent in most, if not all, case samples. As routine analysis usually involves a hydrolysis step and as reference standards usually become available earlier, phase I metabolites are preferred. With this in mind, the nor-metabolite, although commonly abundant and prevalent, is a less suitable target because it has lost substantial parts of the molecule and consequently can be formed from similar drugs. The same is true for metabolites generated by oxidative *N*-dealkylation and amide hydrolysis. Both are reactions that cleave off the specific moiety to distinguish between different analogues. As a result of that, in our study, metabolites were shared across the different metabolic profiles and none of them represents a suitable analytical target: hydrolysed metabolites (A32 = B14 = D14, RT 9.07 min), hydrolysed/hydroxylated metabolites (A16 = D4, RT 5.70 min as well as A31 = D8, RT 7.22 min), and the metabolites generated by oxidative *N*-dealkylation and reduction (C1 = D2, RT 4.06 min).

Based on the aforementioned criteria, we suggest the following analytical targets: the hydroxymethoxy metabolite A26 and the monohydroxylated metabolite A24 for acetylfentanyl, the monohydroxy metabolite B9 and the dihydroxy metabolite B8 for acrylfentanyl, and the monohydroxy metabolites C15 and C10 and the hydroxymethoxy metabolite C12 for 4-fluoro-isobutyrylfentanyl. Regarding furanylfentanyl, none of the metabolites satisfied all criteria. The dihydrodiol metabolite D10 was not prevalent in all tested samples, but due to its abundance and specificity it should be considered the best target. In the absence of D10, e.g. in urine sample #1 and #3, the amide hydrolysis metabolite D14 may be targeted, although it does not prove furanylfentanyl consumption beyond doubt. As mentioned above, the abundance of major metabolites can be affected by different phenotypes of the metabolising enzymes due to not only different genotypes but also co-administered drugs [34].

6.5.4 Is the metabolism of the new fentanyl analogues consistent with previous findings?

In general, metabolism of fentanyl analogues follows similar pathways. Three of our four analogues, acetylfentanyl, acrylfentanyl, and 4-fluoro-isobutyrylfentanyl, produced large amounts of the nor-metabolite, a hydroxyethyl metabolite and a hydroxymethoxy metabolite. This is consistent with previous findings that the nor-metabolite is a major metabolite of fentanyl [11] and other fentanyl analogues [13, 14] and that hydroxy metabolites are commonly observed for fentanyl and analogues [11, 13, 14, 34]. Notably, the hydroxymethoxy metabolite has not been reported for fentanyl itself but was observed for other analogues, e.g. 3-methylfentanyl, isofentanyl [14] and butyrylfentanyl [34]. The discrepancy might indicate that this metabolite was not searched for fentanyl in the previous studies.

In contrast, furanylfentanyl's major metabolites were generated by amide hydrolysis with/without hydroxylation and dihydrodiol formation while the nor-metabolite was not even detected in most of the urine samples. The aromatic furan ring, which has different reactivity from the side chains in the other three analogues, is considered to be the reason for the preference of other biotransformations. Another fentanyl analogue with different major metabolites is butyrylfentanyl, which is mainly metabolised *in vivo* by hydroxylation and carboxylation on the butyryl side chain [34]. Surprisingly, this side chain, which is only one carbon atom longer than fentanyl's, seems to have changed the metabolic profile.

6.6 Conclusion

Given the great number of possible structural variations and the current phenomenon of constantly emerging new psychoactive substances, more "new" fentanyl analogues are likely to appear. Taken together our results, we consider it legitimate to—initially—predict metabolites of newly emerged fentanyl analogues based on current knowledge about the metabolism of known fentanyl analogues. Likely, the nor-metabolite, one or several hydroxy metabolites, and/or a hydroxymethoxy metabolite will be prevalent. However, as some analogues can show a significantly different metabolism, we consider it crucial to confirm the predictions with comprehensive metabolite identification studies, if possible with both *in vitro* and *in vivo* studies.

6.7 References

1. European Monitoring Centre for Drugs and Drug Addiction. EMCDDA–Europol 2015 Annual Report on the implementation of Council Decision 2005/387/JHA. 2016. Available from: http://www.emcdda.europa.eu/publications/implementation-reports/2015. Accessed 26 September 2016.

2. Chen JC, Smith ER, Cahill M, Cohen R, Fishman JB. The opioid receptor binding of dezocine, morphine, fentanyl, butorphanol and nalbuphine. Life Sci. 1993;52(4):389-96. doi:http://dx.doi.org/10.1016/0024-3205(93)90152-S.

3. Higashikawa Y, Suzuki S. Studies on 1-(2-phenethyl)-4-(N-propionylanilino)piperidine (fentanyl) and its related compounds. VI. Structure-analgesic activity relationship for fentanyl, methyl-substituted fentanyls and other analogues. Forensic Toxicol. 2008;26(1):1-5. doi:10.1007/s11419-007-0039-1.

4. Nelson L, Schwaner R. Transdermal fentanyl: Pharmacology and toxicology. J Med Toxicol. 2009;5(4):230-41. doi:10.1007/bf03178274.

5. Kronstrand R, Druid H, Holmgren P, Rajs J. A cluster of fentanyl-related deaths among drug addicts in Sweden. Forensic Sci Int. 1997;88(3):185-95. doi:http://dx.doi.org/10.1016/S0379-0738(97)00068-6.

6. Vardanyan RS, Hruby VJ. Fentanyl-related compounds and derivatives: current status and future prospects for pharmaceutical applications. Future Med Chem. 2014;6(4):385-412. doi:10.4155/fmc.13.215.

7. Henderson G. Designer Drugs: Past History and Future Prospects. J Forensic Sci. 1988;33(2):569-75. doi: https://doi.org/10.1520/JFS11976J.

8. Helander A, Backberg M, Beck O. Intoxications involving the fentanyl analogs acetylfentanyl, 4-methoxybutyrfentanyl and furanylfentanyl: results from the Swedish STRIDA project. Clin Toxicol (Phila). 2016;54(4):324-32. doi:10.3109/15563650.2016.1139715.

9. Backberg M, Beck O, Jonsson KH, Helander A. Opioid intoxications involving butyrfentanyl, 4-fluorobutyrfentanyl, and fentanyl from the Swedish STRIDA project. Clin Toxicol (Phila). 2015;53(7):609-17. doi:10.3109/15563650.2015.1054505.

10. McClain DA, Hug CC. Intravenous fentanyl kinetics. Clin Pharmacol Ther. 1980;28(1):106-14. doi:10.1038/clpt.1980.138.

11. Goromaru T, Matsuura H, Yoshimura N, Miyawaki T, Sameshima T, Miyao J, et al. Identification and Quantitative Determination of Fentanyl Metabolites in Patients by Gas Chromatography-Mass Spectrometry. Anesthesiology. 1984;61(1):73-7.

12. Mahlke NS, Ziesenitz V, Mikus G, Skopp G. Quantitative low-volume assay for simultaneous determination of fentanyl, norfentanyl, and minor metabolites in human plasma and urine by liquid chromatography-tandem mass spectrometry (LC-MS/MS). Int J Legal Med. 2014;128(5):771-8. doi:10.1007/s00414-014-1040-y.

13. Higashikawa Y, Suzuki S. Studies on 1-(2-Phenethyl)-4-(N-Propionylanilino)Piperidine (Fentanyl) and Its Related Compounds: Novel Metabolites in Rat Urine Following Injection of & alpha-Methylfentanyl, One of the Most Abused Typical Designer Drugs. J Health Sci. 2008;54(6):629-37. doi:10.1248/jhs.54.629.

14. Meyer MR, Dinger J, Schwaninger AE, Wissenbach DK, Zapp J, Fritschi G, et al. Qualitative studies on the metabolism and the toxicological detection of the fentanyl-derived designer drugs 3-methylfentanyl and isofentanyl in rats using liquid chromatography–linear ion trap–mass spectrometry (LC-MSn). Anal Bioanal Chem. 2012;402(3):1249-55. doi:10.1007/s00216-011-5528-8.

15. Staeheli SN, Baumgartner MR, Gauthier S, Gascho D, Jarmer J, Kraemer T, et al. Time-dependent postmortem redistribution of butyrfentanyl and its metabolites in blood and alternative matrices in a case of butyrfentanyl intoxication. Forensic Sci Int. 2016;266:170-7. doi:10.1016/j.forsciint.2016.05.034.

16. Patton AL, Seely KA, Pulla S, Rusch NJ, Moran CL, Fantegrossi WE, et al. Quantitative measurement of acetyl fentanyl and acetyl norfentanyl in human urine by LC-MS/MS. Anal Chem. 2014;86(3):1760-6. doi:10.1021/ac4036197.

17. Melent'ev AB, Kataev SS, Dvorskaya ON. Identification and analytical properties of acetyl fentanyl metabolites. J Anal Chem. 2015;70(2):240-8. doi:10.1134/s1061934815020124.

18. Wohlfarth A, Scheidweiler KB, Pang S, Zhu M, Castaneto M, Kronstrand R, et al. Metabolic characterization of AH-7921, a synthetic opioid designer drug: in vitro

metabolic stability assessment and metabolite identification, evaluation of in silico prediction, and in vivo confirmation. Drug Test Anal. 2016;8(8):779-91. doi:10.1002/dta.1856.

19. Castaneto MS, Wohlfarth A, Desrosiers NA, Hartman RL, Gorelick DA, Huestis MA. Synthetic cannabinoids pharmacokinetics and detection methods in biological matrices. Drug Metab Rev. 2015;47(2):124-74. doi:10.3109/03602532.2015.1029635.

20. Roman M, Strom L, Tell H, Josefsson M. Liquid chromatography/time-of-flight mass spectrometry analysis of postmortem blood samples for targeted toxicological screening. Anal Bioanal Chem. 2013;405(12):4107-25. doi:10.1007/s00216-013-6798-0.

21. Holcapek M, Jirasko R, Lisa M. Basic rules for the interpretation of atmospheric pressure ionization mass spectra of small molecules. J Chromatogr A. 2010;1217(25):3908-21. doi:10.1016/j.chroma.2010.02.049.

22. Guldberg HC, Marsden CA. Catechol-O-Methyl Transferase: Pharmacological Aspects and Physiological Role. Pharmacol Rev. 1975;27(2):135-206.

23. Meyer MR, Maurer HH. Enantioselectivity in the Methylation of the Catecholic Phase I Metabolites of Methylenedioxy Designer Drugs and Their Capability To Inhibit Catechol-O-methyltransferase-Catalyzed Dopamine 3-Methylation. Chem Res Toxicol. 2009;22(6):1205-11. doi:10.1021/tx900134e.

24. Testa B, Mayer JM. The Hydration of Epoxides. Hydrolysis in Drug and Prodrug Metabolism: Verlag Helvetica Chimica Acta; 2006. p. 591-661.

25. Nebert DW, Roe AL, Vandale SE, Bingham E, Oakley GG. NAD(P)H:quinone oxidoreductase (NQO1) polymorphism, exposure to benzene, and predisposition to disease: A HuGE review. Genet Med. 2002;4(2):62-70.

26. Sobolevsky T, Prasolov I, Rodchenkov G. Detection of urinary metabolites of AM-2201 and UR-144, two novel synthetic cannabinoids. Drug Test Anal. 2012;4(10):745-53. doi:10.1002/dta.1418.

27. Wohlfarth A, Pang S, Zhu M, Gandhi AS, Scheidweiler KB, Liu HF, et al. First metabolic profile of XLR-11, a novel synthetic cannabinoid, obtained by using human

hepatocytes and high-resolution mass spectrometry. Clin Chem. 2013;59(11):1638-48. doi:10.1373/clinchem.2013.209965.

28. Feasel MG, Wohlfarth A, Nilles JM, Pang S, Kristovich RL, Huestis MA. Metabolism of Carfentanil, an Ultra-Potent Opioid, in Human Liver Microsomes and Human Hepatocytes by High-Resolution Mass Spectrometry. AAPS J. 2016:1-11. doi:10.1208/s12248-016-9963-5.

29. Cashman JR, Park SB, Yang ZC, Wrighton SA, Jacob P, Benowitz NL. Metabolism of nicotine by human liver microsomes: stereoselective formation of trans-nicotine N'-oxide. Chem Res Toxicol. 1992;5(5):639-46. doi:10.1021/tx00029a008.

30. Pirmohamed M, Williams D, Madden S, Templeton E, Park BK. Metabolism and bioactivation of clozapine by human liver in vitro. J Pharmacol Exp Ther. 1995;272(3):984-90.

31. Peterson LA. Reactive metabolites in the biotransformation of molecules containing a furan ring. Chem Res Toxicol. 2013;26(1):6-25. doi:10.1021/tx3003824.

32. Kalgutkar AS, Gardner I, Obach RS, Shaffer CL, Callegari E, Henne KR, et al. A Comprehensive Listing of Bioactivation Pathways of Organic Functional Groups. Curr Drug Metab. 2005;6(3):161-225. doi:http://dx.doi.org/10.2174/1389200054021799.

33. Diao X, Wohlfarth A, Pang S, Scheidweiler KB, Huestis MA. High-Resolution Mass Spectrometry for Characterizing the Metabolism of Synthetic Cannabinoid THJ-018 and Its 5-Fluoro Analog THJ-2201 after Incubation in Human Hepatocytes. Clin Chem. 2016;62(1):157-69. doi:10.1373/clinchem.2015.243535.

34. Steuer AE, Williner E, Staeheli S, Kraemer T. Studies on the metabolism of the fentanyl-derived designer drug butyrfentanyl in human in vitro liver preparations and authentic human samples using liquid chromatography-high resolution mass spectrometry (LC-HRMS). Drug Test Anal. 2016:(in press). doi:10.1002/dta.2111.

6.8 Appendices

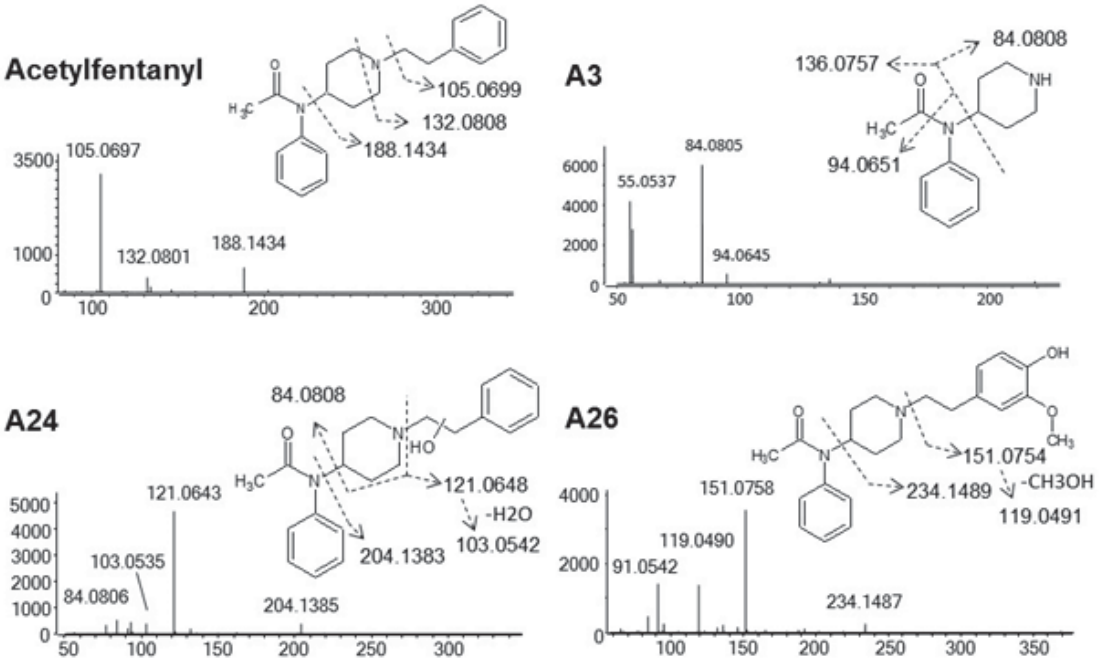

Supplementary Figure 6-1. MS/MS spectra and proposed fragmentation pattern of acetylfentanyl and its major metabolites in hydrolysed human urine samples.

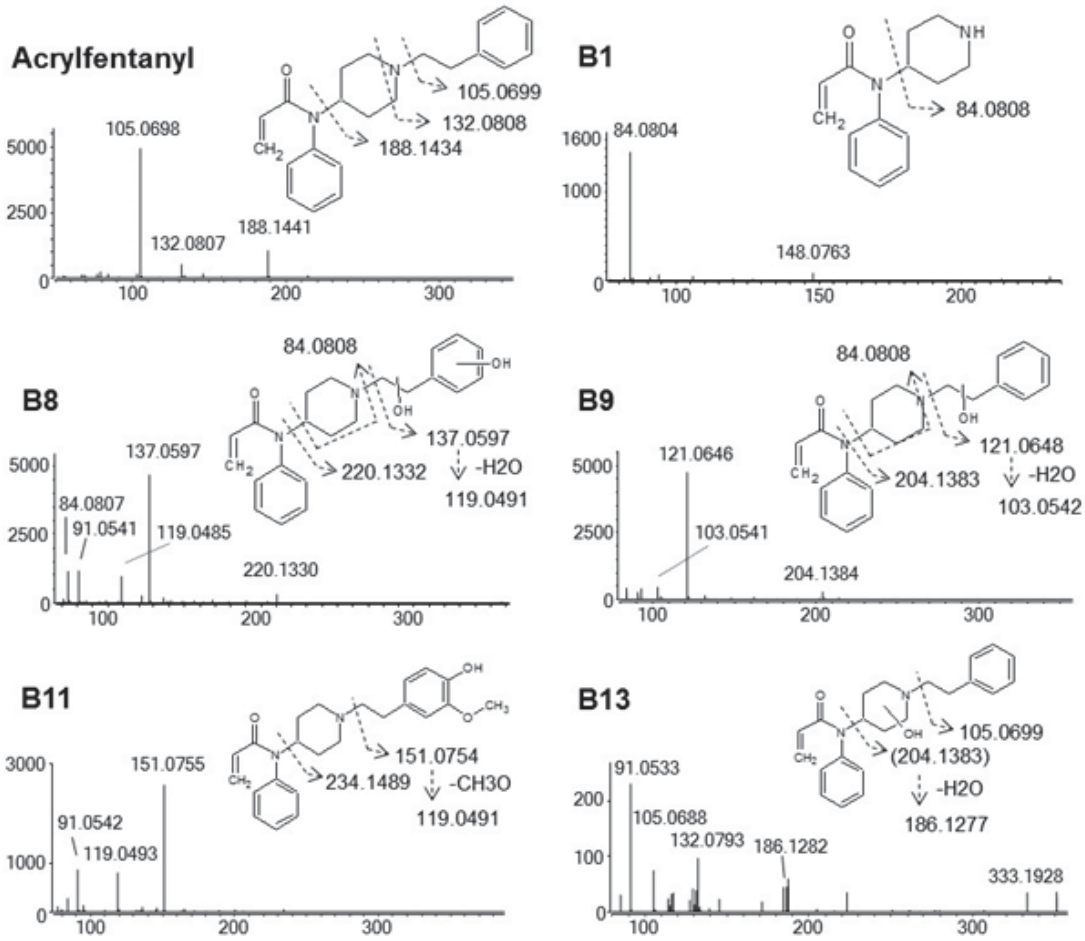

Supplementary Figure 6-2. MS/MS spectra and proposed fragmentation pattern of acrylfentanyl and its major metabolites in hydrolysed human urine samples.

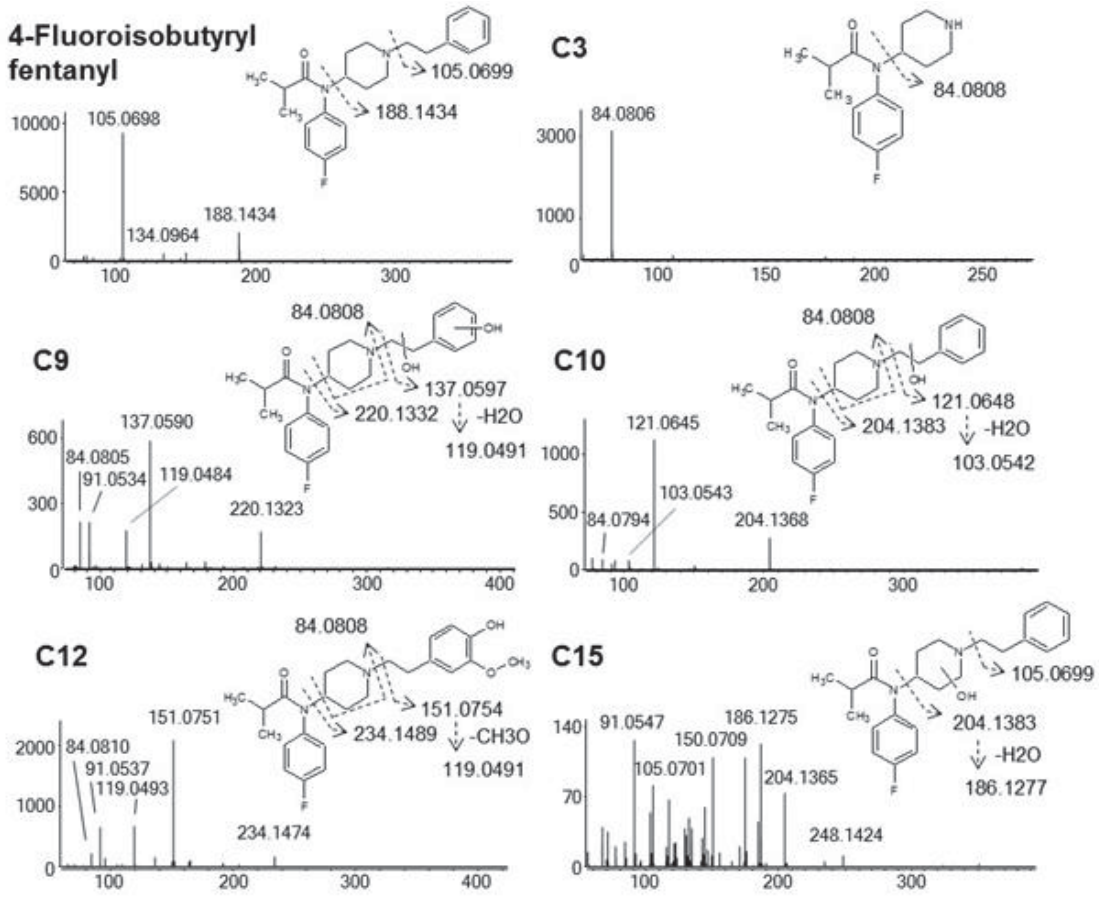

Supplementary Figure 6-3. MS/MS spectra and proposed fragmentation pattern of 4-fluoroisobutyryllfentanyl and its major metabolites in hydrolysed human urine samples.

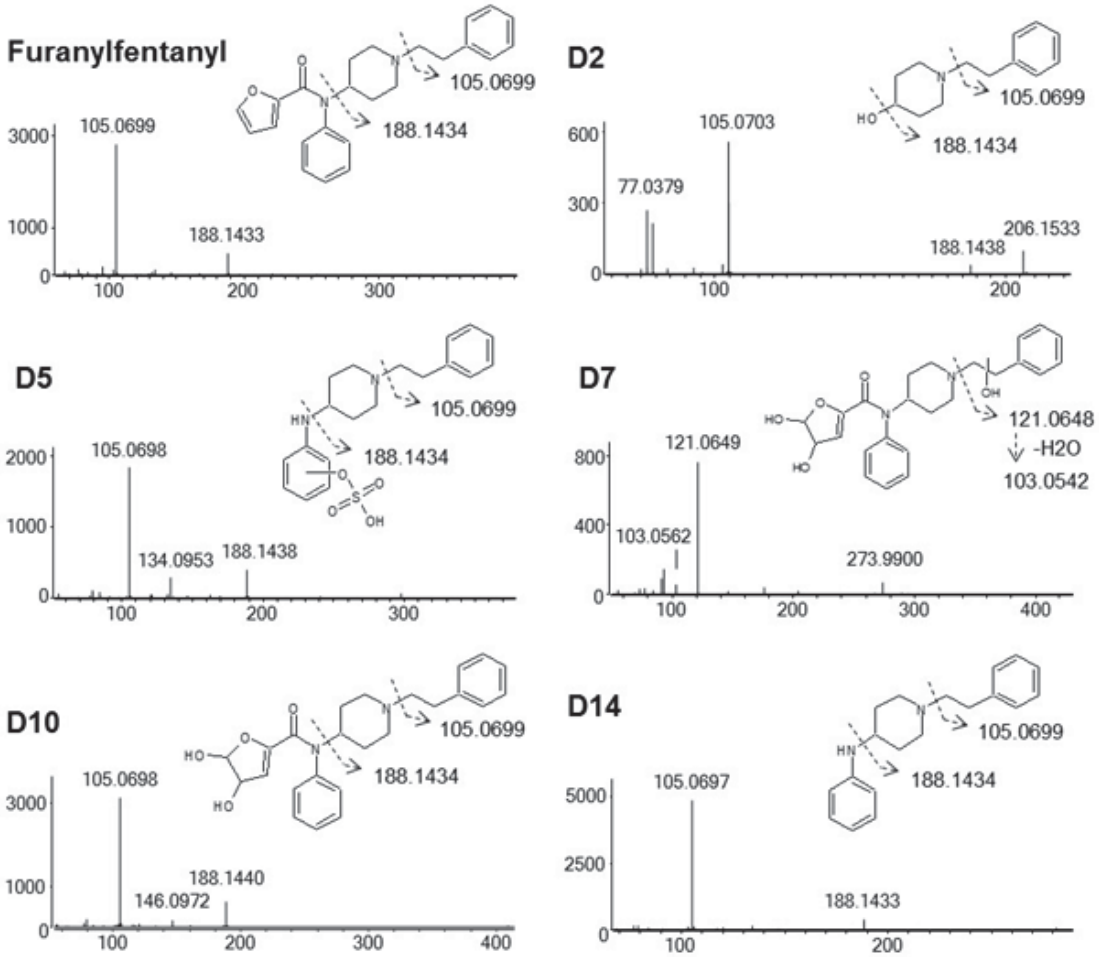

Supplementary Figure 6-4. MS/MS spectra and proposed fragmentation pattern of furanylfentanyl and its major metabolites in hydrolysed human urine samples.

Chapter 7: Conclusions and recommendations for further work

Chapter 7: Conclusions and recommendations for further work

Incubation of several synthetic cannabinoids, namely JWH-018, JWH-073, AM2201, 5F-PB-22, PB-22, XLR-11 and UR-144, with the fungus *Cunninghamella elegans* successfully produced a number of metabolites. The analysis by LC-MS/MS, particularly the use of high resolution mass spectrometry, enabled the identification of the obtained metabolites. The majority of the metabolites identified were phase I metabolites. The observed biotransformations include, either alone or in combination, carboxylation, defluorination, dehydrogenation, demethylation, dihydrodiol formation, dihydroxylation, ester hydrolysis, hydroxylation, ketone formation, *N*-dealkylation, oxidative defluorination, oxidative defluorination to carboxylic acid, and trihydroxylation as phase I reactions. The major phase II biotransformation identified was glucosidation while sulfation was detected as a minor metabolic pathway.

Comparison with the metabolites of these synthetic cannabinoids in authentic human urine and/or other metabolism models such as human hepatocytes and human liver microsomes reported in literature, revealed that the types of fungal metabolites obtained were generally in good agreement with human related metabolites. The common metabolites between the fungus and human models include, but are not limited to, carboxylation, dihydroxylation, hydroxylation for cannabinoids in general; dihydrodiol formation for cannabinoids with naphthalene or quinoline moiety; oxidative defluorination and oxidative defluorination to carboxylic acid for fluorinated cannabinoids; ester hydrolysis for cannabinoids with ester group.

The major difference between the fungal and human metabolism observed was that phase II metabolites were not commonly detected for the fungal metabolites and that the fungal phase II metabolites were mostly glucosides whereas the human phase II metabolites are usually glucuronides. Also, the ratio of the fungal metabolite abundance was not always reflective of the human metabolism data. These variances may be due to the difference in the type and/or the abundance of the enzymes inherent in the fungus and human models. In order to determine whether phase II metabolites were generally not present in the fungus samples or simply not detected, a hydrolysis step can be included in the sample

preparation procedure to compare with non-hydrolysed samples. If phase II metabolites are not present in large abundance, the abundance of phase I metabolites detected by LC-MS/MS should be similar for hydrolysed and non-hydrolysed samples. As for the prevalence of metabolites, it varies over time according to the duration of incubation. Therefore, it will be useful to study the change in prevalence of metabolites at different time points of incubation. The optimised incubation time may be different for different drugs depending on the metabolic stability of the drugs. Nevertheless, the study should give an indication of the suitable incubation time. Overall, *C. elegans* demonstrated its ability to produce human-relevant metabolites, showing the potential for metabolism studies.

In order to demonstrate that *C. elegans* is capable of production of large amounts of metabolites enabling NMR analysis of the metabolites, the synthetic cannabinoid UR-144 was incubated with the fungus in a large scale. The obtained metabolite sample was subsequently isolated by preparative HPLC and analysed by NMR spectroscopy including 1D and 2D NMR. Ten metabolites were characterised, including three pairs of diastereomers, and they were dihydroxy metabolites, carboxy and hydroxy metabolites, a hydroxy and ketone metabolite, and a carboxy and ketone metabolite. HLM incubation of UR-144 was also conducted so that the fungal metabolites characterised by NMR could be used as reference standards for the analysis of the HLM metabolite sample by LC-MS/MS. Under the chromatographic conditions employed, some metabolites that are constitutional isomers eluted at the same retention time and therefore were not unequivocally identified. However, dihydroxy metabolite, carboxy and hydroxy metabolites, and a hydroxy and ketone metabolite were successfully identified in the HLM sample. This indicates that *C. elegans* has the ability to generate the human-relevant metabolite isomers for synthetic cannabinoids and therefore can be used to produce reference standards. With the common metabolism models such as human hepatocytes, it is difficult to achieve an NMR analysis of metabolites due to small quantities and hence the fungus can be a valuable complementary model for metabolism studies. It will be especially useful for the metabolites which are not provided by the commercial suppliers.

Since this study provided the proof of concept, it would be desirable to perform a large scale incubation of other newer synthetic cannabinoids followed by NMR analysis to

further establish the feasibility of the concept. In this work, the separation of closely-structured isomers by preparative HPLC was a major issue. Accordingly, it would be important to optimise the separation potentially by trying different columns such as chiral columns. In theory, the use of *C. elegans* to obtain large quantities of metabolites should also be applicable to drugs of other class. Thus, it would be interesting to investigate the potential of the fungus with drugs of other class as well. Additionally, the fungal metabolites of a drug that are isolated and characterised can be used not only as reference standards to confirm the presence of the metabolites in biological samples, but also as standards for developing a chromatographic method for simultaneous detection of a number of drugs as well as for assessing toxicity of the metabolites to gain a more complete understanding of the drug toxicity.

Having established the relevance of *C. elegans* to human metabolism, the metabolism of the synthetic cannabinoid AM1220 was investigated by the fungus as well as HLM. The half-life of AM1220 by HLM incubation was estimated to be 3.7 min, indicating the drug to be a high clearance compound. A total of 11 metabolites were identified (9 from HLM and 7 from the fungus) and included demethylation, dihydrodiol formation, dihydroxylation, hydroxylation and combinations thereof. Three most abundant metabolites were desmethyl, dihydrodiol and hydroxy metabolites in both models although the abundant dihydrodiol and hydroxy metabolites were different isomers for both models. These metabolites are likely to be suitable biomarkers for urine drug testing.

As a side project, metabolites of four fentanyl analogues, acetylfentanyl, acrylfentanyl, 4-fluoro-isobutyrylfentanyl, and furanylfentanyl were identified in authentic human urine and human hepatocytes samples. The biotransformations included amide hydrolysis, carbonylation, carboxylation, dihydrodiol formation, dihydroxylation, furan ring opening, hydroxylation, methylation, *N*-dealkylation, *N*-oxidation and reduction for phase I, and glucuronidation and sulfation for phase II metabolism. Generally, *in vitro* and *in vivo* metabolites were in good agreement. Acetylfentanyl, acrylfentanyl, and 4-fluoro-isobutyrylfentany shared the major metabolic transformations: *N*-dealkylation, hydroxylation, and hydroxylation and methoxylation. On the other hand, furanylfentanyl mainly underwent amide hydrolysis and dihydrodiol formation. These findings indicate that metabolism of structurally related compounds generally undergo similar metabolic

pathways. However, a significantly different metabolism pattern can be observed as was the case with furanylfentanyl. This illustrates the importance of investigating the metabolism of each new drug as they emerge, since their metabolism is not always predictable.

Overall, these projects demonstrated the potential of the fungus *C. elegans* and the value of the existing *in vitro* models and authentic urine specimens. *C. elegans* can provide more comprehensive characterisation of metabolites, filling the gaps in the metabolic profiles provided by *in vitro* human models and authentic urine specimens. Therefore, the fungus can be a suitable complementary model for metabolism studies and appears to be ideal to be used together with *in vitro* human models and authentic urine specimens.